Multiscale characterization and modeling of the mechanical behavior of the artery

Witold Krasny

N°d'ordre NNT : 2017LYSEM035

THESE de DOCTORAT DE L'UNIVERSITE DE LYON
opérée au sein de
l'Ecole des Mines de Saint-Etienne

Ecole Doctorale N° 488
Sciences, Ingénierie, Santé

Spécialité de doctorat :
Discipline : Mécanique et ingénierie

Soutenue publiquement le 15/11/2017, par :
Witold Krasny

Caractérisation et modélisation multi-échelle du comportement mécanique de l'artère

---

Devant le jury composé de :

Nikolaos Stergiopulos, Professeur, EPFL (Suisse)	Président du jury
Jean-Marc Allain, Professeur, Ecole Polytechnique, Palaiseau	Rapporteur
Karine Bruyère-Garnier, Directrice de recherche IFFSTAR, Univ.Lyon 1	Rapporteure
Christian Hellmich, Professeur, TU Wien (Autriche)	Examinateur
Katherine Yanhang Zhang, Professeur, Boston University (USA)	Examinatrice
Stéphane Avril, Professeur, Mines Saint Etienne	Directeur de thèse
Hélène Magoariec, Maître de conférences, Ecole Centrale Lyon	Encadrante de thèse
Claire Morin, Enseignant-Chercheur, Mines Saint Etienne	Encadrante de thèse

Spécialités doctorales	Responsables :	Spécialités doctorales	Responsables
SCIENCES ET GENIE DES MATERIAUX	K. Wolski Directeur de recherche	MATHEMATIQUES APPLIQUEES	O. Roustant, Maître-assistant
MECANIQUE ET INGENIERIE	S. Drapier, professeur	INFORMATIQUE	O. Boissier, Professeur
GENIE DES PROCEDES	F. Gruy, Maître de recherche	SCIENCES DES IMAGES ET DES FORMES	JC. Pinoli, Professeur
SCIENCES DE LA TERRE	B. Guy, Directeur de recherche	GENIE INDUSTRIEL	X. Delorme, Maître assistant
SCIENCES ET GENIE DE L'ENVIRONNEMENT	D. Graillot, Directeur de recherche	MICROELECTRONIQUE	Ph. Lalevée, Professeur

EMSE : Enseignants-chercheurs et chercheurs autorisés à diriger des thèses de doctorat (titulaires d'un doctorat d'Etat ou d'une HDR)

ABSI	Nabil	CR	Génie industriel	CMP
AUGUSTO	Vincent	CR	Image, Vision, Signal	CIS
AVRIL	Stéphane	PR2	Mécanique et ingénierie	CIS
BADEL	Pierre	MA(MDC)	Mécanique et ingénierie	CIS
BALBO	Flavien	PR2	Informatique	FAYOL
BASSEREAU	Jean-François	PR	Sciences et génie des matériaux	SMS
BATTON-HUBERT	Mireille	PR2	Sciences et génie de l'environnement	FAYOL
BEIGBEDER	Michel	MA(MDC)	Informatique	FAYOL
BLAYAC	Sylvain	MA(MDC)	Microélectronique	CMP
BOISSIER	Olivier	PR1	Informatique	FAYOL
BONNEFOY	Olivier	MA(MDC)	Génie des Procédés	SPIN
BORBELY	Andras	MR(DR2)	Sciences et génie des matériaux	SMS
BOUCHER	Xavier	PR2	Génie Industriel	FAYOL
BRODHAG	Christian	DR	Sciences et génie de l'environnement	FAYOL
BRUCHON	Julien	MA(MDC)	Mécanique et ingénierie	SMS
CAMEIRAO	Ana	MA(MDC)	Génie des Procédés	SPIN
CHRISTIEN	Frédéric	PR	Science et génie des matériaux	SMS
DAUZERE-PERES	Stéphane	PR1	Génie Industriel	CMP
DEBAYLE	Johan	CR	Sciences des Images et des Formes	SPIN
DEGEORGE	Jean-Michel	MA(MDC)	Génie industriel	Fayol
DELAFOSSE	David	PR0	Sciences et génie des matériaux	SMS
DELORME	Xavier	MA(MDC)	Génie industriel	FAYOL
DESRAYAUD	Christophe	PR1	Mécanique et ingénierie	SMS
DJENIZIAN	Thierry	PR	Science et génie des matériaux	CMP
DOUCE	Sandrine	PR2	Sciences de gestion	FAYOL
DRAPIER	Sylvain	PR1	Mécanique et ingénierie	SMS
FAUCHEU	Jenny	MA(MDC)	Sciences et génie des matériaux	SMS
FAVERGEON	Loïc	CR	Génie des Procédés	SPIN
FEILLET	Dominique	PR1	Génie Industriel	CMP
FOREST	Valérie	MA(MDC)	Génie des Procédés	CIS
FOURNIER	Jacques	Ingénieur chercheur CEA	Microélectronique	CMP
FRACZKIEWICZ	Anna	DR	Sciences et génie des matériaux	SMS
GARCIA	Daniel	MR(DR2)	Sciences de la Terre	SPIN
GAVET	Yann	MA(MDC)	Sciences des Images et des Formes	SPIN
GERINGER	Jean	MA(MDC)	Sciences et génie des matériaux	CIS
GOEURIOT	Dominique	DR	Sciences et génie des matériaux	SMS
GONDRAN	Natacha	MA(MDC)	Sciences et génie de l'environnement	FAYOL
GRAILLOT	Didier	DR	Sciences et génie de l'environnement	SPIN
GROSSEAU	Philippe	DR	Génie des Procédés	SPIN
GRUY	Frédéric	PR1	Génie des Procédés	SPIN
GUY	Bernard	DR	Sciences de la Terre	SPIN
HAN	Woo-Suck	MR	Mécanique et ingénierie	SMS
HERRI	Jean Michel	PR1	Génie des Procédés	SPIN
KERMOUCHE	Guillaume	PR2	Mécanique et Ingénierie	SMS
KLOCKER	Helmut	DR	Sciences et génie des matériaux	SMS
LAFOREST	Valérie	MR(DR2)	Sciences et génie de l'environnement	FAYOL
LERICHE	Rodolphe	CR	Mécanique et ingénierie	FAYOL
MALLIARAS	Georges	PR1	Microélectronique	CMP
MOLIMARD	Jérôme	PR2	Mécanique et ingénierie	CIS
MOUTTE	Jacques	CR	Génie des Procédés	SPIN
NIKOLOVSKI	Jean-Pierre	Ingénieur de recherche	Mécanique et ingénierie	CMP
NORTIER	Patrice	PR1	Génie des Procédés	SPIN
O CONNOR	Rodney Philip	MA(MDC)	Microélectronique	CMP
OWENS	Rosin	MA(MDC)	Microélectronique	CMP
PERES	Véronique	MR	Génie des Procédés	SPIN
PICARD	Gauthier	MA(MDC)	Informatique	FAYOL
PIJOLAT	Christophe	PR0	Génie des Procédés	SPIN
PINOLI	Jean Charles	PR0	Sciences des Images et des Formes	SPIN
POURCHEZ	Jérémy	MR	Génie des Procédés	CIS
ROBISSON	Bruno	Ingénieur de recherche	Microélectronique	CMP
ROUSSY	Agnès	MA(MDC)	Microélectronique	CMP
ROUSTANT	Olivier	MA(MDC)	Mathématiques appliquées	FAYOL
SANAUR	Sébastien	MA(MDC)	Microélectronique	CMP
STOLARZ	Jacques	CR	Sciences et génie des matériaux	SMS
TRIA	Assia	Ingénieur de recherche	Microélectronique	CMP
VALDIVIESO	François	PR2	Sciences et génie des matériaux	SMS
VIRICELLE	Jean Paul	DR	Génie des Procédés	SPIN
WOLSKI	Krzystof	DR	Sciences et génie des matériaux	SMS
XIE	Xiaolan	PR1	Génie industriel	CIS
YUGMA	Gallian	CR	Génie industriel	CMP

Mise à jour : 12/12/2016

Acknowledgments - *Remerciements*

Because a doctoral research project is a collective venture in many ways, I wish here to acknowledge all direct and indirect contributors and helpers. Starting from those who, during my studies at EPFL and Ecole Polytechnique, inspired me through their communicative enthusiasm for science, I would like to thank Prof. François Gallaire (EPFL) and Prof. Abdul Barakat (Ecole Polytechnique). Regarding transmitting the curiosity spark for cardiovascular science, I am very grateful to Dr. Franz Bozsak (Sensome) and Dr. David Gonzalez-Rodriguez (University of Lorraine).

My greatest gratitude goes to my PhD supervisors, Prof. Stéphane Avril (Mines Saint Etienne), Dr. Claire Morin (Mines Saint Etienne) and Dr. Hélène Magoariec (Ecole Centrale Lyon) who trusted and accompanied me throughout the experimental and theoretical activities of the thesis, including protocol discussion, results analysis, brainstorming, improvement of publications and oral presentations... Through their scientific know-how and rigor, they have made this PhD a learning experience of immense value for my future. I also thank Prof. Thierry Hoc for welcoming me in the MMV research group at Ecole Centrale Lyon and providing access to the IVTV Equipex Platform (Ingénierie et Vieillissement des Tissus Vivants, ANR-10-EQPX-06-01).

Concerning research funding, I would like to acknowledge the ARC 2 program of the Auvergne Rhônes-Alpes region, managed by Dr. Pascale Michalon, which supported this project through a doctoral grant. I would also like to thank all additional financial contributors. Research Group MMV - Mécanique des Matériaux du Vivant (LTDS, UMR CNRS 5513), Institut Carnot Ingénierie@Lyon, and BQR LTDS enabled carrying out all experimental campaigns; while Mines Saint Etienne, Armines, Sainbiose Laboratory (INSERM, U1059) and the ERC "Biolochanics" grant provided complementary support for scientific activities.

I sincerely thank this doctoral work's reviewers ("rapporteurs") for their acute and detailed scientific feedback: Prof. Karine Bruyère-Garnier (IFFSTAR - Université Lyon 1) and Prof. Jean Marc Allain (Ecole Polytechnique). I am also very grateful to the other members of my defense committee, its president Prof. Nikos Stergiopulos (EPFL), but also Prof. Katherine Zhang (University of Boston) and Prof Christian Hellmich (TU Wien). Through their presence

and broad scientific experience, they raised fascinating questions during the defense discussion. In particular, I am truly thankful to Prof. Hellmich and to all members of the IMWS laboratory for welcoming me at Technische Uniwersität Wien during an enriching doctoral academic visit. This two-months long stay was financially supported by the Amadeus program of Campus France, that should also be acknowledged.

I am also grateful to Dr. Caroline Boulocher (VetAgro Sup) and Fabrice Desplanches (Centre Lago) for enabling the supply of animal samples needed for experimental campaigns, and also to Prof. Eric Viguier (VetAgro Sup) for the time he devoted to train me in sample excision. I also thank warmly Guillaume Fargier, Benoit Ponsard, Ophélie Pollet and Catherine Bosser for their help and training on the mechanical and optical facilities of the IVTV research platform. As for technical assistance in the manufacturing and design of my setup's components, I would like to acknowledge Damien Constant and Lionel Charles from Ecole Centrale Lyon.

A deeper level of gratitude, not the least important, is dedicated to all colleagues of both labs that hosted me: Sainbiose at Mines Saint Etienne and LTDS-MMV at Ecole Centrale de Lyon. I am truly thankful to all, interns, PhD students, junior and senior scientists, administrative staff, whose kindness and sympathy made this doctoral thesis a fun and pleasant time.

My final acknowledgement words go to those who endorse the fundamental "you can do it" role. A huge thank to my wife Rafaele who gives me the confidence to undertake any new project, thumbs up to my daughter Maxime for reminding me always that being a father is yet another kind of fantastic venture, and cheers to my parents for their unconditional and reassuring support.

Contents

List of Figures

List of Tables

Chapter 1

Introduction Générale - *General Introduction*

1.1 Eléments d'histoire en biomécanique cardiovasculaire

Bien qu'initiée de manière rudimentaire, la biomécanique peut être considérée comme une discipline millénaire, remontant au premier homme qui utilisa un bâton en bois en guise de béquille, et ainsi guérir une jambe blessée ou malade [Humphrey 10].

Cependant l'intérêt des scientifiques, médecins ou ingénieurs, pour le système cardiovasculaire est plus récent. En la matière, un pionnier emblématique fut Leonard de Vinci (1452-1519), qui parmi ses nombreux dessins et schémas élaborés sur la base de dissections d'animaux et d'humains, produisit une description saisissante de précision du réseau vasculaire abdominal (Figure 1.1). Ces dessins ont à l'époque révélé la complexité d'un réseau vasculaire caractérisé par une multitude de bifurcations, chevauchements, et composé de vaisseaux de diamètres très variables.

D'autres scientifiques s'intéressèrent par la suite aux artères. En particulier, Galilée (1564-1642) qui utilisa son invention, l'horloge à pendule, afin de quantifier le pulse cardiaque humain [Humphrey 10]. Quant à Euler (1707-1783), il étudia la physiologie à laquelle il appliqua ses connaissances en mécanique, l'amenant à écrire pour la première fois un article sur la propagation des ondes de pression dans les artères en 1775 [Fung 93]. Peu de temps plus tard, Young apporta sa contribution à la compréhension empirique du système cardiovasculaire d'un point de vue fonctionnel, par la publication d'un article dans lequel il discute des contributions musculaires et élastiques à la réponse mécanique de l'artère et de la manière dont ces contributions régulent le flux sanguin [Young 08]. Dans cet article, Young suggère que la compréhension de la physiologie et des pathologies vasculaires implique la nécessaire combinaison de méthodologies issues des mathématiques, de la physique et de la biologie.

Ce n'est qu'à partir de la deuxième moitié du XIXe siècle que le tissu artériel fut caractérisé en termes de relation "force-déplacement", avec notamment les contributions pionnières de [Wertheim 47] et [Roy 81], illustrant le fait que le tissu artériel n'obéit pas à la loi de Hooke, qui caractérise les matériaux présentant une réponse mécanique élastique linéaire. Les travaux cités ci-dessus constituent, en guise d'introduction, un aperçu des premiers éléments

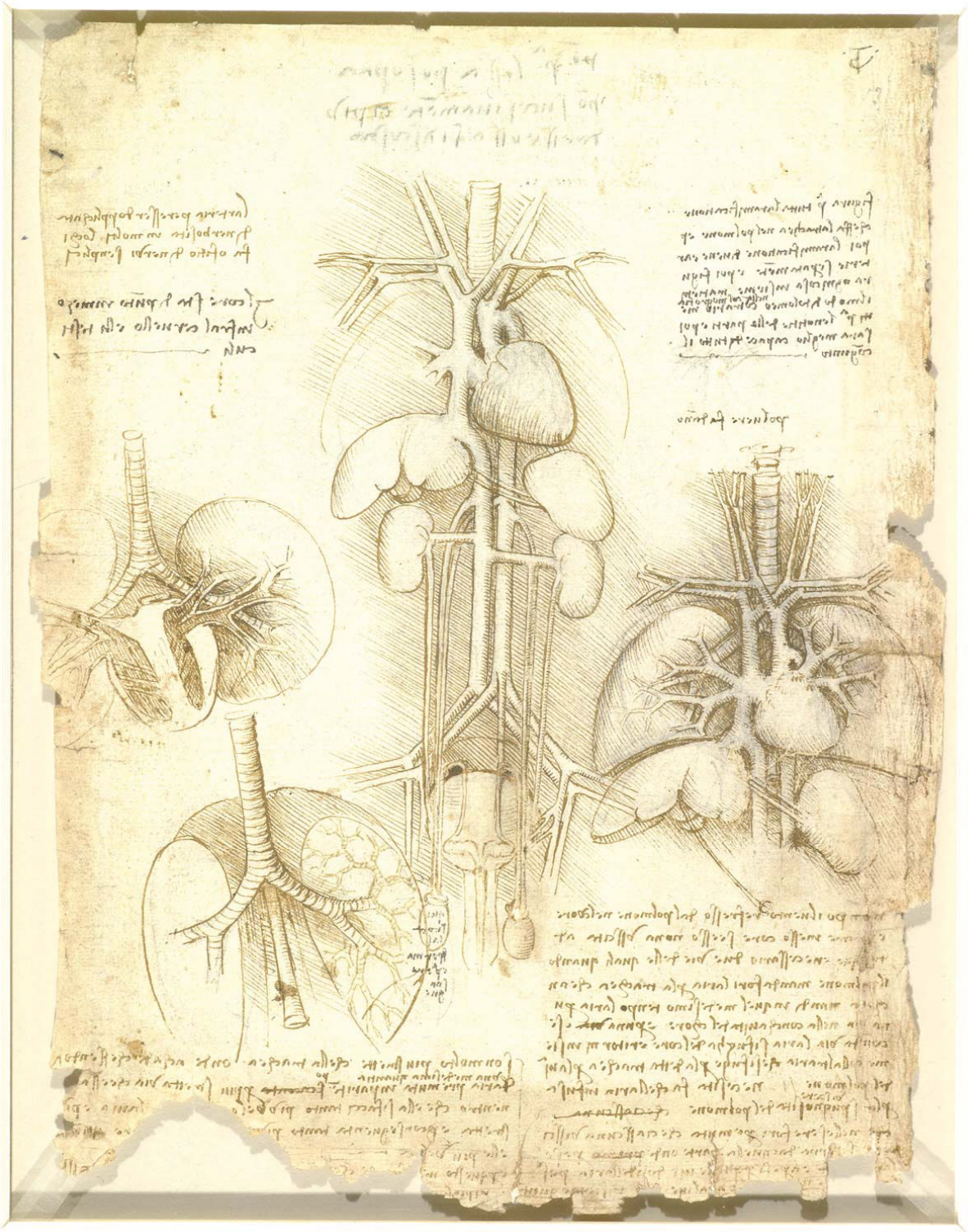

Figure 1.1 – Internal organs of the chest and abdomen with special attention to the heart, the vascular system and the lungs. C.1513; Windsor, RL19104v. Auteur: Leonard de Vinci. Source : gallery.nen.gov.uk

de compréhension de la biomécanique du système cardiovasculaire, apportés par des savants et scientifiques qui ont marqué leur temps. De nos jours, les outils expérimentaux et outils

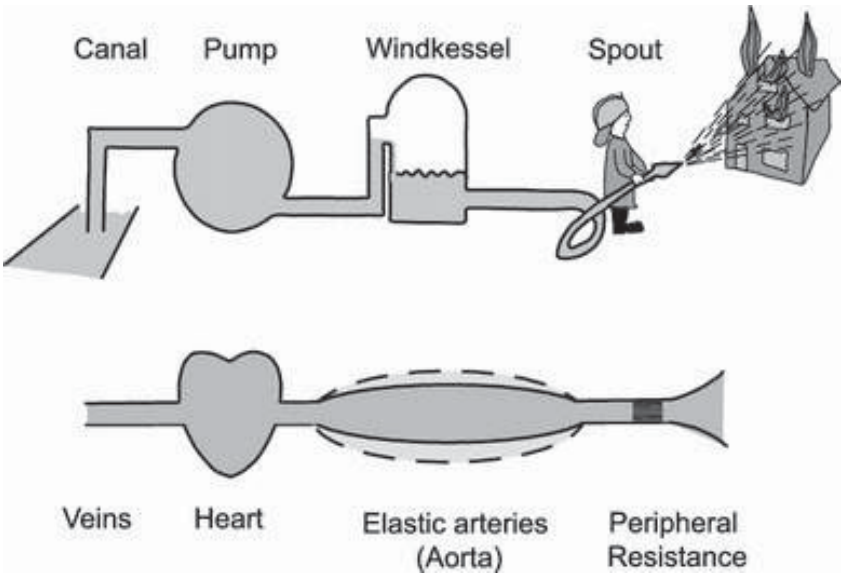

Figure 1.2 – Le concept du Windkessel [Westhoff 09]. Le réservoir d'air est le Windkessel réel, et les grandes artères jouent le rôle de Windkessel.

de calculs ont fait basculer la science cardiovasculaire vers une tout autre dimension. Dans le Chapitre 2, un état-de-l'art actualisé est présenté, détaillant les dispositifs mécaniques, les moyens d'imagerie, et les méthodes de modélisation mis à disposition des chercheurs évoluant au sein de cette discipline.

1.2 L'artère : rôle et fonction

Dans le système cardiovasculaire, le rôle des artères est d'assurer la circulation du sang du coeur vers les capillaires périphériques afin de fournir de l'oxygène et des nutriments à tous les tissus et organes du corps, mais également réguler l'équilibre acido-basique ainsi que la température du corps. Dans le corps humain, le sang est mis en circulation par pulsations successives exercées par le ventricule gauche du coeur. A la sortie du ventricule (phase systolique), la pression sanguine peut atteindre 170 mmHg, et elle est susceptible de générer des pics de flux importants de l'ordre de 400 ml/s [Reymond 12]. Or, afin que les échanges biologiques aient lieu selon une cinétique appropriée, les pulsations sanguines doivent être amorties et converties en écoulement régulier dans les capillaires périphériques. Le rôle fonctionnel du réseau vasculaire est donc de confiner les pulsations d'écoulement et de pression aux plus grandes artères (principalement l'aorte, les artères carotides et les artères fémorales). De par leur dilatation et leur repli élastique, ces grandes artères agissent comme de véritables amortisseurs mécaniques atténuant le front de pression exercé par le ventricule [O'Rourke 07]. Cette propriété mécanique est généralement appelée effet Windkessel [Wagner 52, Westhoff 09], (Figure 1.2). Par conséquent le flux sanguin dans les artères périphériques est considérablement amorti comme par exemple dans l'artère temporale [Reymond 12].

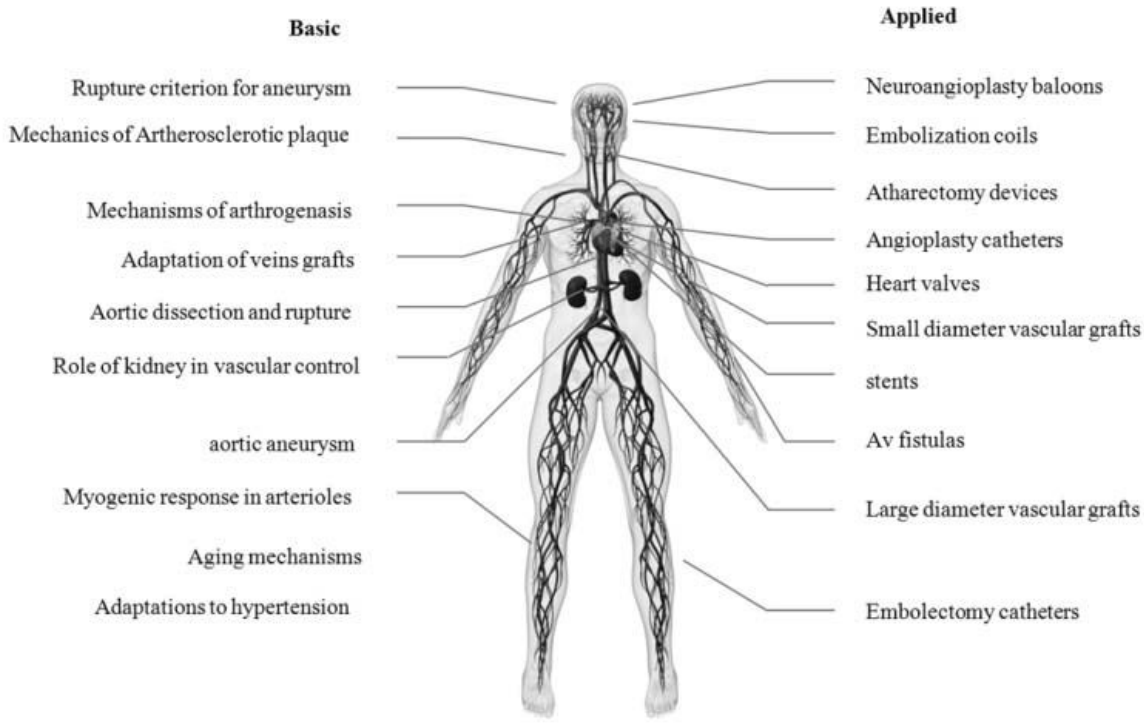

Figure 1.3 – Problématiques cliniques fondamentales et appliquées en biomécanique artérielle [Saitta-Rezakhaniha 10].

1.3 Pathologies vasculaires et défis cliniques

L'occurrence de pathologies affectant les artères naît de l'interaction complexe de facteurs génétiques, d'environnement et de mode de vie. L'Organisation Mondiale de la Santé (OMS) rapporte (via des données collectées en 2012) que les maladies cardiovasculaires sont la première cause de décès dans le monde, puisqu'elles sont liées à 17,5 millions de décès chaque année (soit 31% de la mortalité totale), engendrant des dépenses de santé publique considérables.

Parmi les nombreuses pathologies possibles (Figure 1.3, Figure 1.4) figure l'anévrisme de l'aorte abdominale, un nom provenant du grec "$\alpha\nu\epsilon\rho\upsilon\sigma\mu\alpha$", désignant une dilatation ou élargissement de l'artère. L'anévrisme se caractérise par une microstructure artérielle altérée et généralement endommagée ainsi que par un environnement de sollicitation mécanique fortement modifié. Aujourd'hui la définition la plus répandue d'un anévrisme de l'aorte abdominale est basée sur son diamètre. Ainsi, on considère que lorsque celui-ci mesure localement 3 cm ou plus (correspondant à une augmentation de deux fois la déviation standart, par rapport au diamètre moyen de l'aorte chez les hommes et les femmes), l'aorte est atteinte d'un anévrisme [Moll 11]. L'étude de [Moll 11] précise que les facteurs de risques principaux sont l'âge, le genre masculin et le tabac.

La détection précoce d'un anévrisme de l'aorte abdominale est un enjeu important. Dans de nombreux cas un cardiologue peut détecter la pulsation anormale des plus gros anévrismes par palpation de la partie supérieure de l'abdomen. Des examens additionnels révèlent ultérieure-

ment et de manière fiable la présence d'un anévrisme grâce à l'échographie (Figure 1.4), l'imagerie par résonance magnétique (IRM) ou la tomodensitométrie (TDM). Lors de la détection d'un anévrisme, un clinicien est confronté à la possibilité d'une intervention chirurgicale visant à remplacer la partie anévrismale par une prothèse vasculaire. Étant donné que la mortalité associée à ce genre d'intervention varie entre 3% et 5%, la qualité du critère de décision chirurgicale est primordiale. Actuellement, cet acte chirurgical est préconisé selon un critère géométrique qui combine (i) des seuils de diamètre de l'anévrisme et (ii) son taux de croissance, ce qui établit un compromis pour le patient entre d'une part le risque du rupture de l'anévrisme et d'autre part le risque de complications liées à la chirurgie [Davies 02, Fillinger 07]. En revanche, ce choix clinique entre la réparation invasive que constitue la chirurgie et le traitement préventif du tissu aortique anévrismal ne prend en compte aucun critère pouvant véritablement prédire le risque de rupture [Gasser 10].
D'autres pathologies artérielles sont également répandues. Citons notamment l'athérosclérose, qui est un épaississement avec durcissement localisé de l'artère, dont la caractéristique principale est la formation d'une plaque rigide et graisseuse dans la couche interne de la paroi artérielle. Cette plaque d'athérome obstrue progressivement la lumière de l'artère, provoquant l'apparition d'une sténose et détériorant la qualité de distribution de l'oxygène vers les organes en avals. L'athérosclérose peut toucher une grande variété d'artères allant de l'artère coronaire à l'artère carotide, et est traitée par l'apposition de stents vasculaires (Figure 1.3) [Serruys 94].
Les pathologies vasculaires sont diverses mais ont pour dénominateur commun la perte d'intégrité mécanique de la structure artérielle. Lorsqu'elles affectent les grandes artères élastiques, la fonction d'amortissement peut s'en trouver menacée via une dégradation des propriétés d'élasticité, de résistance à la rupture ou d'épaisseur de la paroi (conférant la lumière pour l'écoulement sanguin).

1.4 Défis scientifiques pour le biomécanicien cardiovasculaire

L'évaluation de l'intégrité mécanique de l'artère à un moment donné, et plus encore la prédiction de l'évolution de cette intégrité, impliquent une démarche systémique, transdisciplinaire. En effet, l'artère est le siège de stimuli complexes, de nature biologique, chimique, électrique, mécanique et thermique. Les mécanismes de couplage entre ces stimuli, intervenant à différentes échelles, mobilisent actuellement de nombreux chercheurs, rapprochant progressivement des disciplines scientifiques qui encore récemment évoluaient de manière cloisonnée.
En particulier, il est aujourd'hui connu que les propriétés mécaniques de l'artère sont directement liées à l'organisation de sa microstructure. Or la microstructure, dotée de mécanismes pouvant interpréter son environnement mécanique, est en constant remodelage adaptatif selon des processus biochimiques dédiés. L'artère est dès lors caractérisée par une relation "structure-propriété" [Humphrey 09] qui gouverne son intégrité mécanique, au regard des conditions de chargement propres à son environnement mécanique. La prise en compte de cette relation "structure propriété" apparait dès lors essentielle afin d'améliorer, à terme, la prise en charge

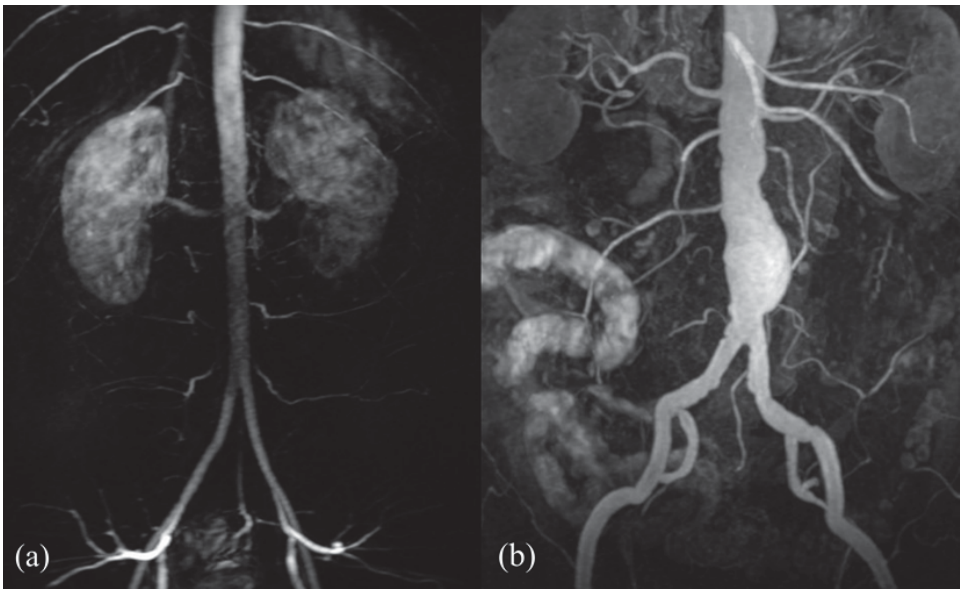

Figure 1.4 – (a) Aorte abdominale saine (sujet masculin agé de 25 ans, contributeur à l'étude de cas : Prof. Frank Gaillard, Source : https://radiopaedia.org) ; (b) aorte abdominale présentant un anévrisme au dessus de la bifurcation des artères fémorales, (sujet masculin de 65 ans, contributeur à l'étude de cas : Dr. Roberto Schubert, Source : https://radiopaedia.org).

des troubles cardiovasculaires.

Le présent travail doctoral s'inscrit dans cette démarche transdisciplinaire visant à comprendre et prédire les mécanismes de couplage qui existent dans l'artère, et qui régissent en continu, d'une part la composition et l'arrangement spatial des constituants biologiques de sa microstructure, et d'autre part sa réponse mécanique. Il s'articule autour d'une double approche complémentaire "observation-modélisation". En effet après un aperçu de l'état-de-l'art en biomécanique vasculaire (Chapitre 2) établissant les principales problématiques qui constitue le fil directeur du présent travail doctoral, deux campagnes expérimentales de caractérisation du comportement multi-échelle de l'artère sont décrites (Chapitres 3 et 4), comprenant les discussions des résultats obtenus. Ensuite, un modèle multi-échelle de l'artère est présenté, et les résultats commentés (Chapitre 5). Pour finir, une discussion générale des résultats sera proposée (Chapitre 6), comprenant des éléments d'ouverture et de perspective, en lien avec les avancées scientifiques énoncées. En guise de complément, une annexe est également fournie reprenant plus en détail les méthodologies expérimentales conçues et appliquées dans le cadre de ce travail doctoral.

Chapter 2

State-of-the-art - *Etat de l'art*

Contribution: This chapter is largely inspired from the article: "Multiscale Mechanical Behavior of Large Arteries" authored by Claire Morin, Witold Krasny, and Stéphane Avril, accepted for publication in the Reference Module in Biomedical Research, published by Elsevier. For this article, Witold Krasny reviewed the literature on arterial microstructure organization, on the related exploration techniques, as well as on the load-induced rearrangements of the arterial microstructure. He prepared the text and the corresponding figures. The present chapter is an extension of this review article.

Contents

Résumé

L'état de l'art concernant la compréhension du système vasculaire s'étend sur une large gamme de domaines scientifiques. En particulier, il est aujourd'hui admis que l'intégrité des propriétés mécaniques des artères est essentielle pour la bonne distribution de l'oxygène et des nutriments aux divers organes du corps [Humphrey 10]. Parmi ces propriétés, la grande élasticité à faible contrainte, suivie d'une rigidification passé un certain seuil de déformation [Roy 81, Burton 54], joue un rôle important. Dans la première partie de ce chapitre, nous examinons ces propriétés et décrivons les dispositifs mécaniques qui les ont mises en évidence expérimentalement, à savoir les dispositifs de traction uniaxiale [Hill 12], de tension biaxiale [Humphrey 08b] ou les dispositifs de gonflement conçus pour tester des échantillons artériels de diverses natures [Romo 14, Schrauwen 12]. Ces propriétés mécaniques sont conférées par la microstructure hiérarchique complexe du tissu artériel. En effet, l'artère est une structure composite composée de trois couches concentriques appelées "tuniques" : l'intima, la media et l'adventice, partant de la couche interne vers la couche périphérique [Humphrey 10]. En distinguant la composition biologique de chaque couche, nous décrivons qualitativement les morphologies des différents composants constituant la microstructure artérielle [O'Connell 08, Dingemans 00, Ushiki 02], révélée par diverses techniques d'imagerie dont les principes physiques sont également rappelés. Les morphologies de l'élastine et du collagène, qui sont les principaux contributeurs aux propriétés mécaniques de l'artère et à sa résistance à la rupture, sont particulièrement détaillées. La microstructure de l'artère, de par sa configuration morphologique, mais aussi par ses réarrangements induits par la déformation, assure au tissu une souplesse suffisante sous de faibles contraintes et permet une rigidification significative sous contraintes élevées, favorisant ainsi l'amortissement des pulses de pression tout en empêchant une distension excessive du tissu. La connaissance actuelle de ces mécanismes microscopiques est présentée [Roy 11, Hill 12, Chen 13, Schrauwen 12], ainsi que les méthodes automatiques qui ont été développées pour quantifier l'évolution de la morphologie des réseaux fibreux [Rezakhaniha 12, Schriefl 12, Koch 14]. En particulier, de nombreuses contributions scientifiques concernent la quantification de la réorientation des fibres au cours de la déformation du tissu. Les résultats suggèrent une cinématique potentiellement non-affine des fibres de collagène [Billiar 97, Chandran 06, Lake 12]. Cet état de l'art nous amène à une première problématique de ce travail de thèse : la cinématique non-affine des fibres concerne-t-elle tous les réseaux fibreux de la microstructure de l'artère; et est-elle associée à des scenarii de déformation particuliers ? Ces deux questions constituent un premier fil directeur du présent travail doctoral, guidant particulièrement les campagnes expérimentales dont les méthodes sont présentées aux Chapitres 3 et 4, détaillées en Annexe, et dont les résultats sont discutés au chapitre 6.

Dans une deuxième partie, nous présentons les stratégies de modélisation existantes appliquées à la prédiction du comportement mécanique de l'artère. Après la présentation des principaux modèles hyperélastiques [Holzapfel 01, Gasser 07], approches phénoménologiques permettant de re-

produire la réponse mécanique non linéaire du tissu artériel à partir de la définition de l'énergie de déformation du tissu, nous mentionnons les avantages mais aussi les limites de ces stratégies de modélisation et justifions l'intérêt grandissant de la communauté scientifique pour les stratégies multi-échelles. Un descriptif synthétique des modèles mécaniques multi-échelles existant est proposé [Stylianopoulos 07, Marino 13, Fan 14, Zhang 13]. Cependant, de nombreux défis sont encore ouverts pour déterminer le comportement mécanique de l'artère à partir des évolutions de sa microstructure en utilisant un schéma multi-échelle. Nous choisissons particulièrement de nous intéresser à la question suivante : dans quelle mesure les réarrangements de la microstructure de l'artère sont-ils à l'origine de sa réponse mécanique, quels mécanismes peuvent expliquer la cinématique complexe des fibres ? Ces questions constituent le second fil directeur de ce travail doctoral, motivant l'implémentation et la campagne de tests de ce modèle micromécanique dont la formulation et les résultats sont présentés au Chapitre 5.

Principaux résultats de l'état de l'art

- *Les différences de cinématiques des réseaux fibreux, selon la localisation dans les différentes couches de l'artère, ne sont pas caractérisées ;*
- *L'analyse de la dépendance des cinématiques de fibres au type de chargement est marginale;*
- *De récentes observations expérimentales remettent en question l'hypothèse affine régissant la cinématique des fibres ;*
- *Le défi de la détermination des propriétés mécaniques de l'artère à partir de sa microstructure évolutive, via un schéma de modélisation muli-échelle, demeure ouvert.*

Questions soulevées

- *Pour chaque constituant de la microstructure vasculaire (réseau de collagène, réseau d'élastine), les changements de morphologie, consécutifs à un chargement, sont-ils identiques dans chaque couche de la structure composite (media et adventice) ?*
- *La cinématique des fibres est-elle exclusivement régie par la règle de cinématique affine ?*
- *Certains scenarii de chargement, se traduisant par des conditions aux limites différentes, peuvent-ils provoquer ou accentuer une cinématique non-affine des fibres ?*
- *Dans quelle mesure la réponse mécanique non linéaire de l'artère peut-elle être la conséquence du réalignement progressif des fibres ?*
- *Un modèle micromécanique peut-il suggérer de nouveaux mécanismes microscopiques qui régissent du mouvement des fibres ?*

Abstract

It is nowadays known that the mechanical integrity of arteries is essential for the proper delivery of oxygen and nutrients to all organs. In the first part of this Chapter, we review these properties, and describe the mechanical setups that revealed them, namely monitored *in situ* uniaxial tension, biaxial tension or inflation setups designed for the testing of arterial samples. The oxygen and nutriments dispatching function of healthy arteries is optimally fulfilled thanks to the aforementioned mechanical properties, which originate in the tissue's complex hierarchical microstructure. In fact, the artery is a composite structure made of three concentric layers: the intima, the media and the adventitia. We describe qualitatively the layer-specific morphologies of the various components making-up the arterial microstructure, revealed by various imaging techniques, whose physical principles are also recalled. The contributions of elastin and collagen, which are the artery's major load-bearing biological components, are particularly emphasized. The arterial microstructure, through its load-free morphological configuration but also its load-induced rearrangements, ensures a sufficient compliance at low stresses and allows stiffening at higher stresses, preventing over-distension. The knowledge associated with these microscopic mechanisms is discussed, along with the automatic methods that were developed to quantify the evolving morphology of the fiber networks. In particular, numerous contributions have focused on quantifying the fiber reorientations during the tissue's deformation, suggesting potential non-affine fiber kinematics. The question of the conditions under which non-affine fiber behavior occurs, is raised: may non-affine fiber kinematics concern any fibrous network of the artery's microstructure; and is it enhanced under particular deformation scenarii ? In a second part of this state-of-the-art Chapter, we present existing modeling strategies that are applied to the prediction of the artery's mechanical behavior. After presenting the dominant hyperelastic models which render the characteristic nonlinear mechanical response of the tissue through variously designed strain energy functions, we mention the benefits but also the limits of these modeling strategies and justify the growing interest of the scientific community to multiscale strategies. A review of existing multiscale mechanical models is presented, leading to the conclusion that despite their interesting outcomes, determining the mechanical behavior of the artery from its evolving microstrucure under a multiscale scheme, remains an open challenge. We raise from this observation the following questions: can a model based on continuum micromechanics predict the coupling between the artery's microstructure rearrangements and its mechanical response, and can it shed a new light on underlying mechanisms behind complex fiber motion?

Outcomes of the state-of-the-art

- The inter-layer differences in fiber kinematics are not characterized;
- The load dependence of fiber kinematics is marginally commented;
- The affine assumption for fiber kinematics is challenged by recent experimental findings;

– The determination of the mechanical behavior of the artery from its evolving microstrucure, through multiscale modeling, remains unsettled.

Questions raised

– For each constituent of the vascular microstructure (collagen network, elastin network), are the morphological changes under load identical in each layer of the composite structure (media and adventitia)?

– Is fiber kinematics in the artery governed exclusively by the affine rule?

– May particular loading scenarii, hence particular boundary conditions, provoke or enhance non-affine fiber kinematics?

– To which extent can the arterial nonlinear mechanical response be a consequence of the progressive fiber rearrangements?

– Can a micromechanical model shed a new light on underlying mechanisms behind complex fiber motion?

2.1 Research challenges

The arteries are responsible for different functions in the body. In particular, large elastic arteries as the aorta, the femoral or carotid arteries fulfill a mechanical function essential to the proper functioning of the organism, namely damping of the pulsatile pressure coming from the left ventricule of the heart. This damping contributes to maintaining a steady flow in capillaries, which host the biological processes essential to nutriments and oxygen delivery. This function can be sustained if the mechanical integrity of the tissue is assured, meaning its sufficient resistance to the undergone loading, and its adequate elasticity. In order to fulfill this function, the arteries' composite microstructure made of concentric layers of fiber networks is particularly suitable. However, the advent of vascular pathologies can degrade the ability of the arteries to satisfy their mechanical function, and it is essential to be able to estimate the mechanical integrity of the arterial tissue with respect to the loadings to which it is subjected. It is recognized that changes in the arterial microstructure (in terms of composition, mechanical integrity of the constituents, or their spatial arrangement) directly affect the overall mechanical response of the artery. On the other hand, the variations in mechanical loading seen by the artery generate changes in the microstructure, which seeks to adapt in order to best respond to mechanical stresses. In order to estimate the mechanical and strength properties of the arterial tissue, it is therefore essential to take into account this strong coupling between biological adaptation of the microstructure, composition and arrangement of the microstructure, and overall mechanical properties in order to minimize the clinical risk for the patient.

In the challenging scientific context of arterial biomechanics, numerous strategies have been initiated in order to understand and predict the mechanical behavior of arteries, both at the macroscopic scale and at the microscopic scale (Figure 2.1). While biomechanicians have characterized the mechanical behavior of the arterial material, by submitting it to a variety of loadings [Wertheim 47, Roy 81, Burton 54, Wolinsky 67, Holzapfel 05, Choudhury 09] (Figure 2.1 red color), biologists and microscopy experts developed a thorough description of the arterial microstructure [Wolinsky 67, Eisenstein 75, Wasano 83, Ushiki 02, Dingemans 00, O'Connell 08] (Figure 2.1 blue color). Initially, these mechanical and microstructural investigations were carried out separately and the bridges between the two communities remained scarce. However the development of a new generation of microscopy techniques (e.g. confocal microscopy, multiphoton microscopy, X-ray tomography) allowed imaging without prior fixation and staining, and a new approach to experimental arterial mechanics arose, which consists in coupling microscopy to mechanical deformation setups, and analyzing not exclusively the unloaded morphology of the vascular microstructure, but its response to the applied loading, rearrangements, and specific fiber kinematics occurring during the deformation [Voytik-Harbin 03, Gleason 04a, Roy 11, Hill 12, Schrauwen 12, Chen 11] (Figure 2.1, purple color). Subsequently, this new approach confirmed the link between the nonlinear mechanical response and microstructural rearrangements. This stressed the need to include microscopic phenomena into the exist-

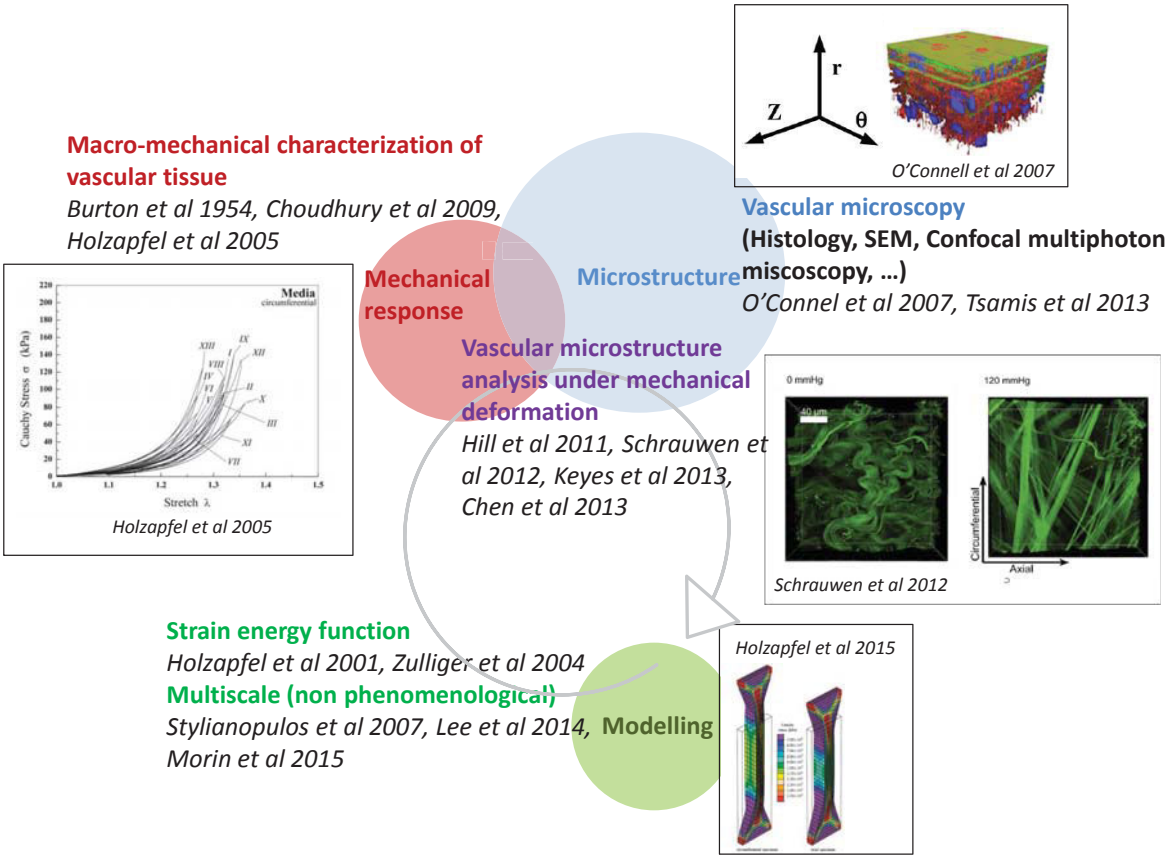

Figure 2.1 – Research paths in vascular biomechanics.

ing models and pushed forward a new category of multiscale constitutive models that downscale the macroscopic loading at the microstructural scale and upscale the subsequent biological and mechanical events occurring in the microstructure, to the macrostructural scale (Figure 2.1, green color). In more details, multiscale models offer new tools to investigate the microscopic mechanisms that enter into play during the deformation of the artery, such as the microscopic stress and strain felt individually by the cells and fibers of the arterial microstructure, tissue remodeling processes, extracellular constituent's damage mechanisms, non-affine fiber kinematics, as well as the effects of all these mechanisms on the macroscopic mechanical behavior.

In the following sections, a state-of-the-art of arterial biomechanics is proposed, presenting the existing mechanical characterization of the tissue, the characterization of the arterial tissue's structure, the analysis of load-induced rearrangements of this microstructure and finally reviewing modeling strategies. To conclude this state-of-the-art review, a set of open questions is presented as the motivation to the experimental and modeling research strategies adopted in the present research work.

2.2 Characterization of the arterial tissue's macroscopic mechanical behavior

A common approach to vascular biomechanics consists in submitting samples of arterial tissue to mechanical bench tests in order to characterize their macroscopic mechanical properties. The following subsection presents the existing setups as well as the already identified macro-mechanical properties of the vascular tissue.

2.2.1 Setups for *ex vivo* testing of arterial samples

Mechanical characterization setups for arterial material have been inspired by the classical tests developed for inert materials (composites, metallic materials) [Hooke 31]. It consists first in uniaxial tests on strips of arterial tissues, and second in various types of biaxial loading setups. The tests are carried out in humid atmosphere by keeping the sample in a saline solution, in order to prevent the tissue from drying and therefore altering its mechanical properties.

2.2.1.1 Uniaxial testing

Uniaxial tensile tests are the simplest tests for the characterization of the mechanical response of tissues, and were therefore widely applied [Roy 81, Burton 54, Holzapfel 05, Choudhury 09, Richardson 89, Duprey 10]. In such a setup, arterial samples are prepared from cylindrical portions of aortas, carotids or coronary arteries, and opened longitudinally [Choudhury 09]. Eventually a dogbone shape is conferred to the flat strip in order to create a homogeneous stress distribution in the cross-sectional area [Hill 12] (Figure 2.2(a)). Usually, the arterial sample is fixed using screwed clamps and a special care is given to prevent the slipping of the sample in the direction of the tension. In order to capture a possible anisotropy of the tissue, uniaxial tensile tests may be performed independently in the axial and circumferential directions [Okamoto 02, Choudhury 09, Kao 11], and separately to the different layers of the composite structure of the arterial wall [Holzapfel 05, Teng 09].

2.2.1.2 Biaxial testing

More complex loading scenarii and related stress states can be achieved from various biaxial testing setups.

1. **Flat biaxial setups**
   In this setup, the arterial sample is prepared from a longitudinally opened portion of the artery, and the flat square or cross shaped sample is usually fixed using hooked suture wire to the clamps (Figure 2.2(b)). This setup allows sequenced biaxial tension or equibiaxial tension [Fridez 01, Choudhury 09, Keyes 13, Lally 04, Geest 06, Zeinali-Davarani 15].

2. **Tension-inflation setups**
   Uniaxial and biaxial mechanical setups applied on flat arterial samples do not allow re-

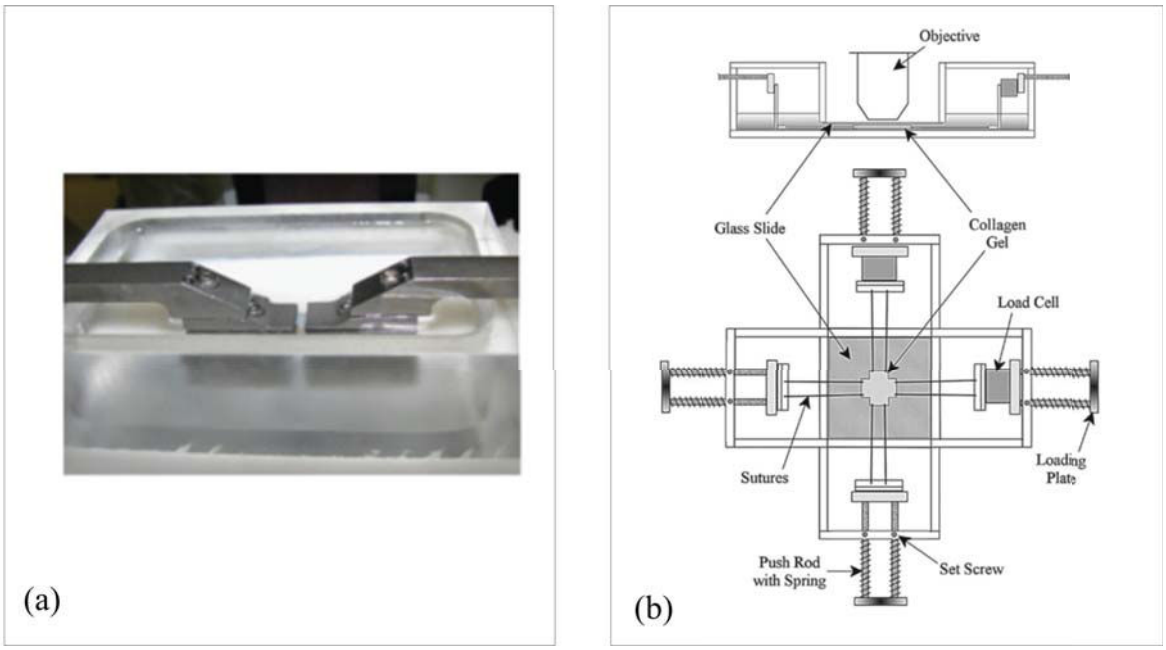

Figure 2.2 – (a) Uniaxial tension on flat longitudinally opened arterial samples [Hill 12]; (b) Equibiaxial tension on flat longitudinally opened tissue samples [Humphrey 08b].

producing the native mechanical loading environment, namely the physiological answer to inflation caused by the blood pulse. To overcome this drawback, inflation tests were developed, in which the arterial sample is either inflated equibiaxially (bulge tests, Figure 2.3(a)) [Romo 14, Luo 08, Cavinato 17] or submitted to tension-inflation in cylindrical form [Cox 75, Weizsacker 88, Dobrin 86, Schrauwen 12, Genovese 13] (Figure 2.3(b)), using pressurized air or pressurized saline solution. Noticeably, digital image correlation methods recently allowed retrieving strain and stress fields in the tissue during the deformation [Wang 13, Genovese 13, Cavinato 17]. Concerning tension-inflation tests, the arterial response is characterized by the variations of the arterial diameter as a function of the applied pressure or applied axial stretch, as well as by the variations of the axial reaction force.

3. Characterizing the *in vivo* configuration
   Arteries are subjected *in vivo* to pre-stress and pre-stretch, as evidenced by [Bergel 61, Vaishnav 87, Fung 93]. This *in vivo* stress-strain state originates from the growth and remodeling processes occurring in the vascular tissue. It allows achieving a homeostatic stress state, being nearly uniform and equibiaxial across the arterial wall thickness [Humphrey 09]. As a consequence, excising and longitudinally opening arterial segments partially release this existing *in vivo* stress-strain state, but there is no certainty that this excised and flat configuration corresponds to a stress-free configuration.

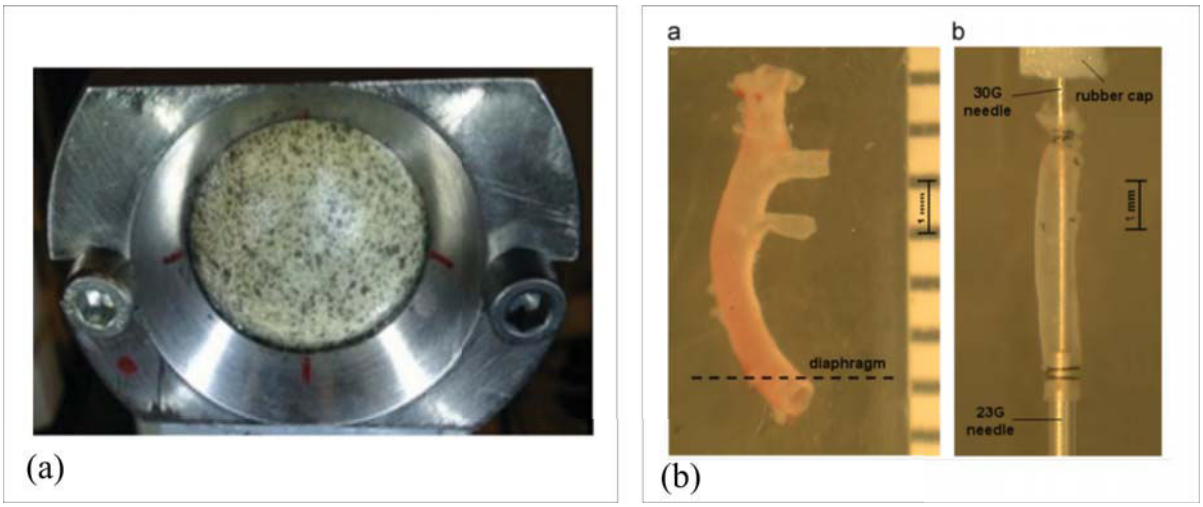

Figure 2.3 – (a) Pictures of a human aorta tested under bulge inflation [Romo 14]; (b) Pictures of the excised mouse suprarenal aorta tested under tension-inflation [Genovese 13].

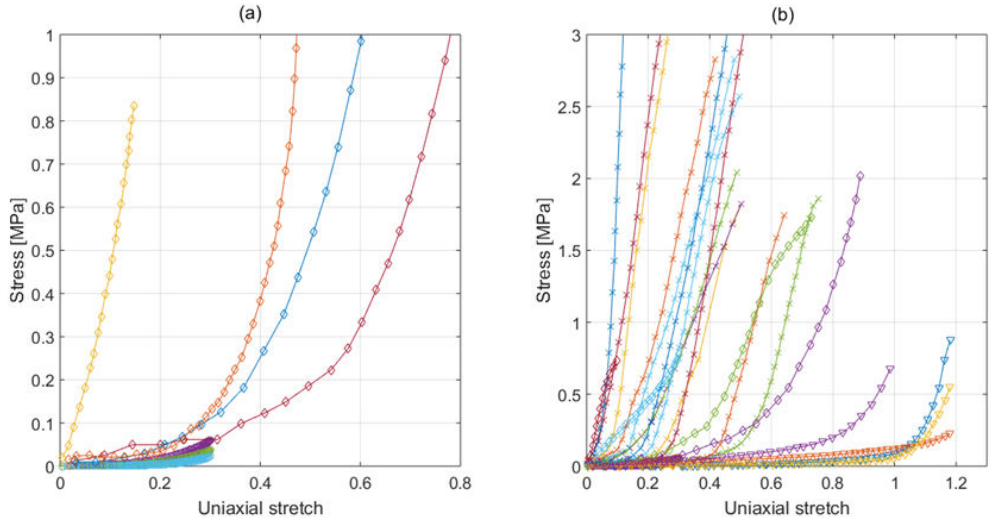

Figure 2.4 – Mechanical response of different arterial tissues subjected to uniaxial tension in the (a) circumferential and (b) longitudinal directions: porcine coronary arteries (crosses [Lally 04]), human ascending aorta (circles [Choudhury 09]), human mid-thoracic descending aortas (diamonds [Mohan 82]), and rabbit and pig aortas (triangles, [Sokolis 02, Sokolis 06]). Data published in [Morin 17].

2.2.2 Macroscopic mechanical properties of the arterial wall

The aforementioned setups have generated extensive macroscopic characterizations of the arterial tissue's mechanical response, whose observations and conclusions are summarized thereafter.

2.2.2.1 Non linear constitutive response

The arterial wall exhibits a highly nonlinear mechanical response (Figure 2.4), which was already described in the 1880s [Roy 81]: while, at low applied stresses, arteries are highly com-

pliant, the arterial response becomes much stiffer at higher applied stresses. This nonlinear response occurs in any load direction [Choudhury 09]. In order to characterize the mechanical response of arterial samples, it is important to account for the existence of a transient mechanical response: after a long term resting of the tissue (absence of externally applied load), its mechanical response exhibits an important but transient hysteresis which is reduced after several load cycles; the steady state mechanical response barely shows any hysteresis. Experimental biomechanicians usually get rid of this transient response by performing several preconditioning cycles [Hill 12]. The number of preconditioning cycles varies with the precise protocol, and the loading path and maximum load generally coincide with the further applied loading. The microstructural underlying mechanisms occurring during preconditioning are not yet elucidated. The mechanisms are probably related to viscous effects, liquid diffusion, and crosslinks reconfiguration between fibers.

The presence of fiber networks within the arterial tissue may induce a mechanical anisotropy. However, although this anisotropy has been investigated by means of the previsouly mentioned experimental setups [Lally 04, Holzapfel 05], no general conclusion can be drawn. Still, carotid arteries are found stiffer in the circumferential direction [Cox 75, Patel 70], while coronary arteries are stiffer in the longitudinal direction [Papageorgiou 88, Patel 70]. It is however remarkable that there is no statistical difference in the mechanical responses of arteries whether tested in the circumferential or in the longitudinal directions, when the tests are performed in conditions close to the physiological ones: this was observed e.g. by [Sato 79] on dog abdominal aortas, by [Dobrin 86] on dog carotid arteries, and by [Sommer 10] on human carotid arteries. Another much debated feature is the strain rate dependence of the arterial mechanical response. It is now admitted that at low strain rates, the mechanical response of arteries does not vary with the strain rate [Sato 79, Zemánek 09, Tanaka 74]. The viscous character of arteries is also a complex question, since also creep and relaxation tests should be investigated.

2.2.2.2 Existence of a pre-stretch in arteries *in vivo*

When inflating cylindrical samples under constant axial stretch, the axial reaction force can be measured as a function of the applied pressure. Figure 2.5 presents the variation of the axial reaction force as a function of the applied luminal pressure for different magnitudes of imposed axial stretches. These tests evidence the salient feature of the *in vivo* axial stretch level; indeed, for axial stretches being smaller (resp. larger) than the *in vivo* axial stretch, the axial reaction force decreases (resp. increases), when the pressure increases. But, when the axial stretch is equal to the *in vivo* stretch, the axial reaction force does not depend on the applied inner pressure [Weizsacker 88, Sommer 10] and remains constant during the pressure cycle (Figure 2.5, 4th curve from above). Accordingly, finding the longitudinal stretch which keeps the axial force unchanged during inflation provides an accurate estimation of the *in vivo* axial stretch.

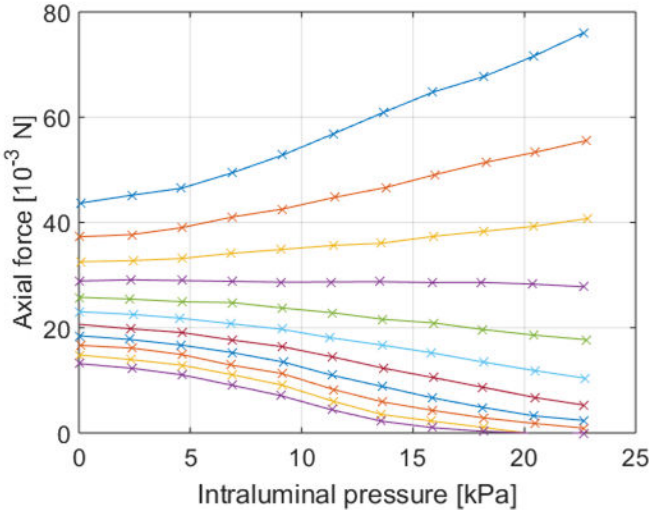

Figure 2.5 – Variation of the axial reaction force as a function of the applied luminal pressure, for different prescribed axial stretches. Experimental data from [Weizsacker 88].

2.2.2.3 Incompressibility hypothesis

Finally, these macroscopic mechanical tests also allow checking the widely accepted assumption of incompressibility of arterial tissues. Incompressibility implies that the changes in sample thickness can be deduced from the changes in the circumferential and axial dimensions. To our best knowledge, [Carew 68] was the only study that experimentally checked this assumption, by evaluating the ratio between bulk and shear moduli based on a tension-inflation test. As a result, the arterial bulk modulus was about three times larger than the Young's modulus determined by [Bergel 61], while the hydrostatic and deviatoric stresses were of the same order of magnitude. They could therefore conclude that arteries are only slightly compressible.

2.2.2.4 Characterization of the mechanical behavior of arterial layers

As further detailed in section 2.3.2, arteries as composite structures made of three distinct layers names intima (innermost layer), media, and adventitia (outermost layer) (Figure 2.8(b)). They exhibit a layer-specific mechanical response, which depends on the layer morphology as proven by tensile tests that could be performed independently on each of the composite layers of the artery. Mechanical tests on the separate layers were performed by [Holzapfel 05, Weisbecker 12], and showed that:

- The intima exhibits a stiffer mechanical response when loaded in the longitudinal direction than in the circumferential one. However, it is generally agreed on, that the intima layer barely contributes to the mechanical response of arteries, due to its relatively small thickness (except for atherosclerotic arteries);

- In the media layer, the circumferential direction shows a stiffer uniaxial response than the longitudinal direction;

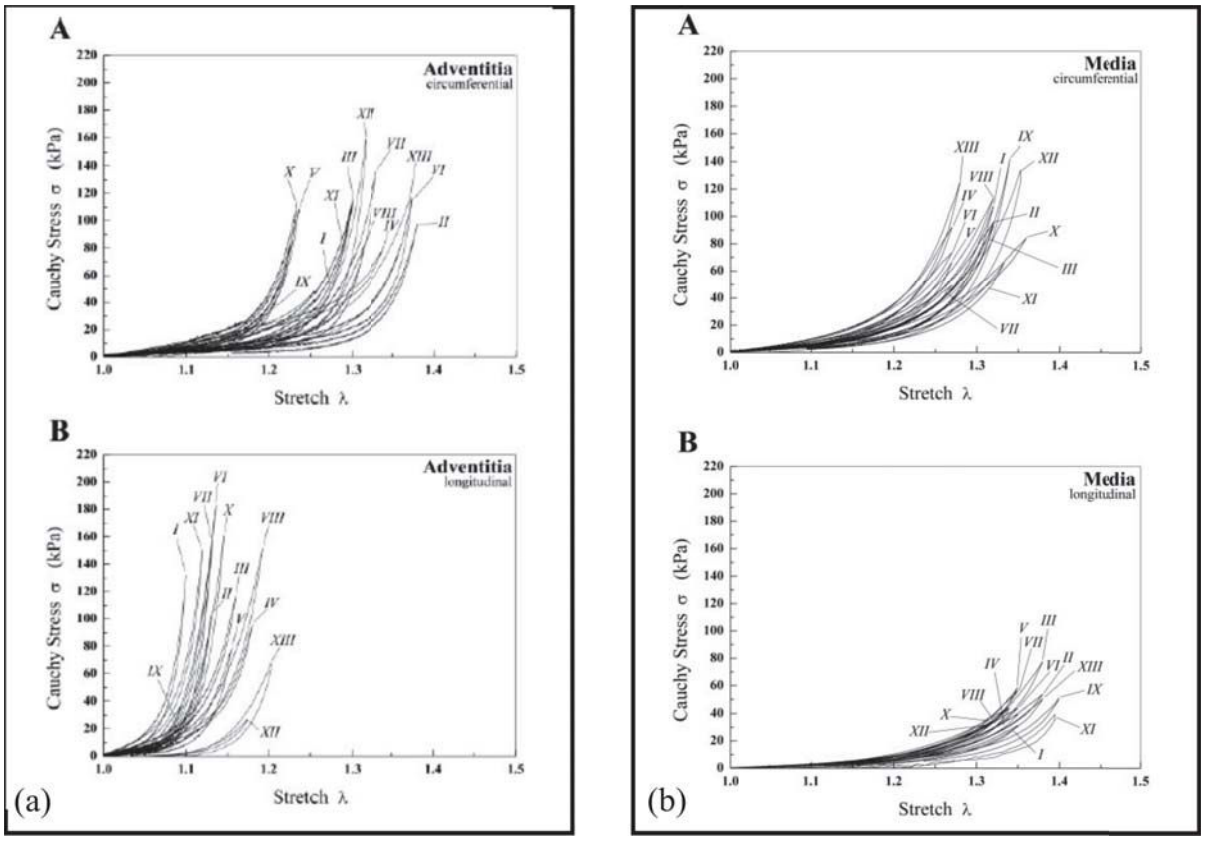

Figure 2.6 – (a) Uniaxial tensile stress-stretch responses for adventitia samples in circumferential (A) and longitudinal (B) directions [Holzapfel 05]; (b) uniaxial tensile stress-stretch responses for media samples in circumferential (A) and longitudinal (B) directions [Holzapfel 05].

– In the adventitia layer, the uniaxial mechanical response is stiffer in the longitudinal direction than in the circumferential one.

Finally, these layer specific tests have revealed that the media is more compliant, while the adventitia resists to larger loads.

2.2.2.5 Variability of mechanical behaviors

As documented in the current literature, the mechanical properties of arteries appear as very scattered and were shown to vary during aging or due to pathologies, but also across the considered organs or species [Lally 04, Weizsacker 88, Holzapfel 05]. However, the aforementioned variability of mechanical properties may mainly be governed by the variability of the related microstructural and compositional properties of the tested tissues [Holzapfel 05] (see the section 2.3 for a detailed review of the arterial microstructure).

2.3 Characterization of the arterial tissue's structure

Depending on the species or on their location in the organism (aorta, femoral artery, carotid artery, etc), arteries have to sustain and regulate different levels of blood pressure, resulting in

an important variability in microstructure morphologies. Still, the global hierarchical structure of the arterial wall remains unchanged among the vertebrate kingdom. The arterial tissue is made up by cells (endothelial cells, smooth muscle cells, and fibroblasts) and an extracellular matrix (ECM) composed of three main elementary constituents, namely elastin (Figure 2.8(j)), collagen (Figure 2.8(h)), and water. The ECM is also composed of different other organic molecules such as glycosaminoglycans (GAGs) and proteoglycans. All these elementary constituents are arranged in morphological hierarchical structures occurring in most of the large arteries of vertebrates, and described by means of the following three levels:

- At a characteristic length of several millimeters, the macrostructure of the arterial wall is characterized by varying thicknesses and mechanical properties depending on the precise biological function of the considered arterial wall (Figure 2.8(a)). This arterial macrostructure is composed of three concentric tunicae: the intima, media, and adventitia, see Figure 2.8(b). Each of these layers has a specific morphology as well as a specific function within the arterial wall. This scale will be referred to as the macrostructure of the arterial wall (Figure 2.7, length L, here the example of the aortic diameter).

- At a characteristic length of some tens of micrometers to some hundreds of micrometers, the layers are made up by an arrangement of cells embedded in different imbricated fibrous elastin and collagenous networks (Figure 2.8(c-f)). This will be referred to as the arterial microstructure (Figure 2.7, length l).

- Zooming at these fibrous networks reveals the ultrastructure of the fibers (Figure 2.7, length d corresponding to the mean fiber diameter), made of an arrangement of crosslinked fibrils, at a hundred of nanometers to several micrometers scale, Figure 2.8(g, i).

Understanding the arrangement of the different constituents within the arterial wall has been the source of an impressive amount of scientific publications; and the emergence in the last fifteen years of multiphoton microscopy has led to a better understanding of the constituent arrangement and of the relation to their mechanical function. After a brief overview of the diverse observation techniques, the multiscale description of the arterial wall microstructure will be reviewed in details.

2.3.1 Multiscale observation techniques of the arterial structure

The hierarchical character of arteries has been revealed by the use of different microscopy techniques, offering a wide range of resolutions, as well as different imaging characteristics (in-depth resolution, need for prior staining, etc.).

2.3.1.1 Macrostructure (1-10 mm)

The composite structure of the artery has been originally revealed by histology studies using optical microscopy. The latter analysis technique is dedicated to the study of the microscopic

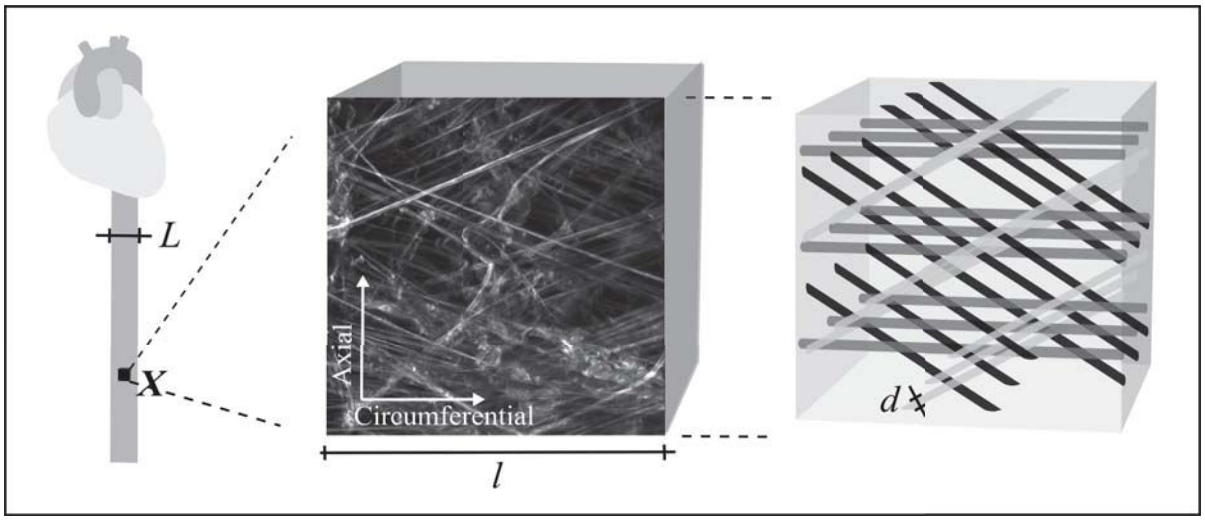

Figure 2.7 – Characteristic lengthscales of analysis in arterial biomechanics. Left: the example of the aortic diameter D providing the scale of the macrostructure; middle: the characteristic size of a Representative Volume Element l providing the scale of the microstructure; right: mean fiber diameter d providing the scale of the ultrastructure.

anatomy of cells and tissues. It uses visible light and a system of lenses to magnify images of biological samples. The specimens are previously sectioned (cut into a thin cross-section with a microtome), stained, and mounted on a microscope slide (Figure 2.8(b)).

2.3.1.2 Microstructure (10-100 µm)

Different microscopy techniques may be used to visualize the arrangement of the vascular microstructure.

- **Confocal and multiphoton microscopy:**
  One common optical sectioning method allowing in-depth imaging is called confocal microscopy or confocal laser scanning [Voytik-Harbin 03]. It consists in the installation of a spatial pinhole at the confocal plane of the lens, which acts as a spatial filter and allows only the in-focus portion of the light to be imaged. Confocal microscopy is characterized by an increased spatial resolution but decreased signal intensity, hence requiring long exposure times of the biological samples to the imaging beam and the use of photomultipliers. More recently, multiphoton microscopy, also called nonlinear or two-photon microscopy, has been developed in order to increase axial resolution and penetration depth [Van Zandvoort 04]. Under a multiphoton microscope, the sample is illuminated at twice its normal excitation wavelength by a high-energy short-pulsed laser beam, allowing fluorescence to be precisely localized at the illumination region. When imaging biological tissues, the signal of collagen is generated from the second harmonic generation, while the elastin signal on the other hand is recovered by auto fluorescence, before being collected by two bandpass filters. Multiphoton microscopy can also reveal vascular cells such as fibroblasts or smooth muscle cells [O'Connell 08] upon prior staining for flu-

orescence. Both aforementioned techniques provide high optical resolution and contrast while eliminating out-of-focus light. Eventually, they enable the reconstruction of three-dimensional structures from the obtained images by collecting sets of images at different depths, with imaging penetration depths reaching several hundreds of microns.

- **Diffusion tensor imaging:**
  Diffusion tensor imaging [Vilanova 06, Ghazanfari 12] relies on a different technology: it uses the diffusion of water molecules to generate contrast in magnetic resonance images. As the molecular diffusion of water in tissues is constrained, it can reflect interactions with many obstacles when tracked, such as macromolecules, fibers, and membranes. This tracking provides a mapping of diffusion patterns therefore revealing microscopic details about the tissue architecture.

- **Tomography:**
  Tomographic imaging of biological tissues provides section views of organic components through the use of various penetrating waves (e.g. X-ray). Tomographic slices can be reconstructed into 3D views by means of specific reconstruction techniques [Fujimoto 99, Acosta 17].

- **Polarized light microscopy:**
  Finally, the vascular microstructure can also be imaged using polarized light microscopy [Gasser 12]. Polarized light is obtained by means of a polarizer oriented at 90° for blockage of directly transmitted light. When imaging biological tissues under polarized light, previously stained collagen expresses different interference colors influenced by the fiber thickness but also by the packing of the collagen fibers.

2.3.1.3 Ultrastructure (10-100 nm)

At the scale of a few tens to hundreds of nanometers, the resolved structure of the different fiber networks can be revealed by means of scanning electron microscopy [Ushiki 02, Raspanti 06, O'Connell 08]. This technique uses a beam of accelerated electrons as a source of illumination. The higher resolving power of scanning electron microscopes originates in the wavelength of electrons being up to 100,000 times shorter than that of visible light photons used in optical microscopy. The tissue can undergo acid and elastase digestion before microscopy in order to expose particular cells [Ushiki 02].

2.3.2 Hierarchical organization of the arterial structure

Use of these different microscopy techniques allowed revealing the hierarchical structure of arteries.

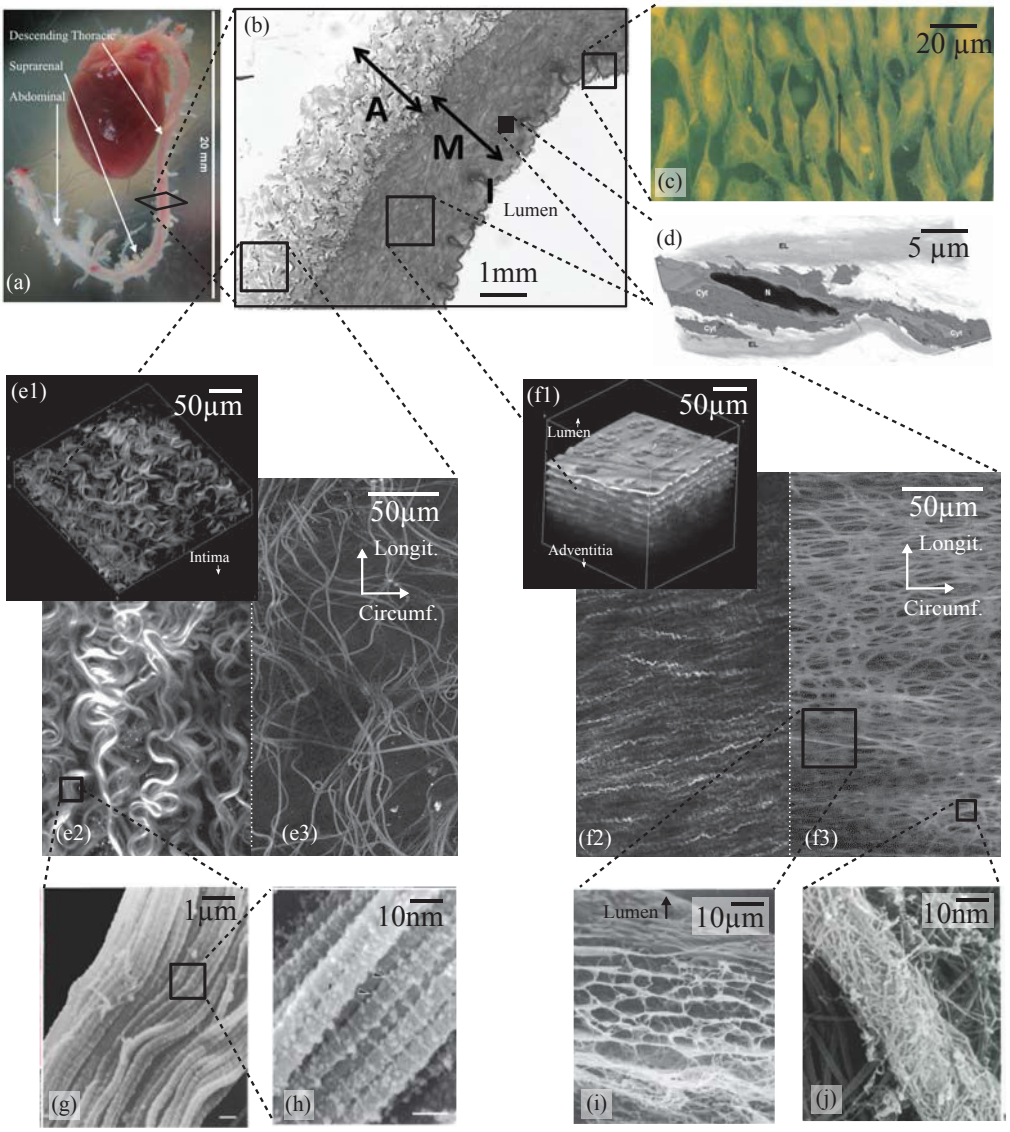

Figure 2.8 – Hierarchical structure of large elastic arteries: (a) macroscopic view of large arteries, taken from [Keyes 11]; (b) at the millimeter scale, the arterial wall is made of three concentric layers, the adventitia tunica (A), the tunica media (M) and the intima tunica (I); electron micrograph from [Ratz 16]; (c) at the micrometer scale, the intima is made of a continuous layer of endothelial cells (inverted phase microscope image from [Ives 86]); the media is made of an arrangement of medial lamellar units, as seen on (d) by means of scanning electron microscopy (taken from [O'Connell 08]), and (f1) from multiphoton microscopy stack of images; zooming further on the lamellar unit, multiphoton microscopy allows distinguishing (f2) the collagen fibers and (f3) the elastin network; the adventitia is made of (e1) an arrangement of collagen bundles (also e2) and elastin fibers (also e3); finally, the collagen fibers are made of a (g) staggered arrangement of collagen fibrils (scanning electron microscope image taken from [Ushiki 02], themselves made of (h) an arrangement of crosslinked collagen molecules (scanning electron microscope image taken from [Ushiki 02]); while the elastin network is made of (i) elastic fibers, lamellae, and struts, themselves made of an (j) arrangement of elastin and crosslinking molecules (scanning electron microscope image taken from [Ushiki 02]). Images (e1)-(e3), (f1)-(f3) were obtained by a confocal bi-photon microscope (IVTV Platform, ANR-10-EQPX-06-01, FR) imaging a rabbit carotid artery.

2.3.2.1 Macrostructure (1-10 mm)

As introduced in section 2.2.2.4, at the macroscopic scale, the artery is a composite cylindrical structure made of three concentric layers: the adventitia, the media, and the intima, as seen on Figure 2.8(b), an electron micrograph obtained by [Ratz 16]. Each of these layers is characterized by specific microstructures, specific thicknesses [Wolinsky 67], different mechanical properties [Holzapfel 05], and different structural and biological functions [O'Connell 08]. The relative proportions of layer thicknesses differ in particular between proximal and distal regions [Canham 89].

1. **Macrostructure of the tunica intima**
   This innermost layer is made of the endothelium and of an internal elastic lamina. The endothelium is a monolayer of endothelial cells, lining the luminal surface of blood vessels, as seen on Figure 2.8(c), obtained from [Ives 86] by means of an inverted phase optical microscope. It plays the role of an interface between blood vessel walls and the blood flow [Ives 86], being therefore subjected to both fluid shear stress and pressure-induced strain components of the flow [Ives 86]. In particular, the effect of shear stress on endothelial cell morphology and functions has been exclusively studied, highlighting that the endothelium shows a tendency toward parallel alignment of the cells with the principal axis of strain, and that endothelial cell morphology is closely related to its cytoskeletal structure [Ohashi 05]. Moreover, the mechanical forces coming from blood flow have been proposed as causative factors in cardiovascular diseases, such as the atherosclerosis, and have been implicated in modulating endothelial cell morphology and function [Ives 86]. The internal elastic lamina (not shown on Figure 2.8) lies between the endothelium and the media and is known to provide structural cohesion and support for axial pre-tension [Farand 07, Timmins 10].

2. **Macrostructure of the tunica media**
   This layer is a concentric set of superimposed medial lamellar units, as reconstructed in Figure 2.8(f1) from a stack of multiphoton microscopy images. A single medial lamellar unit, as shown on Figure 2.8(d) obtained from [O'Connell 08] by means of scanning electron microscopy, consists in a row of overlapping smooth muscle cells surrounded on the upper and lower sides by two concentric elastic lamellae. The overlapping muscle cells lie parallel to orthoradial-axial planes. The number of lamellar units in the media of adult mammalian aortas has been shown to be nearly proportional to the aortic radius regardless of species or of variations in measured wall thickness [Wolinsky 67]. The tunica media is therefore, from a morphological point of view, a composite material organized periodically.

3. **Macrostructure of the tunica adventitia**
   This outermost concentric layer of the arterial wall is made of fibroblasts embedded in a matrix made of an arrangement of collagen bundles and few elastic fibers, as seen on

Figure 2.8(e1) obtained from reconstruction of a stack of multiphoton microscopy images in the framework of this thesis.

2.3.2.2 Microstructure (10-100 µm)

At the tens to hundreds of micrometers scale, microscopy techniques reveal the precise morphology of the different fiber networks that exist in each arterial layer.

1. **Microstructure of the tunica intima**
   Lying against the axially oriented endothelial cells, a continuous sheet of elastin, called the internal elastic lamina [Farand 07, Timmins 10] marks a separation between the endothelium and the tunica media. It takes the form of a dense elastin sheet which comprises a longitudinal network of elastic fibers coated on its continuous surface.

2. **Microstructure of the tunica media**
   As already mentioned in section 2.3.2.1, the medial lamellar unit is made of an arrangement of elastic fibers, vascular smooth muscle cells, and collagen fibers, which are hereafter successively described. From a morphological point of view at the micrometer scale, medial elastin takes three different forms:

   - Firstly, lamellae, composed of a dense meshwork of elastic fibers oriented circumferentially [Farand 07, Timmins 10]. They form a periodical concentric separation between medial lamellar units containing the vascular smooth muscles cells (Figure 2.8(f1) and Figure 2.9(E1)). These lamellae show large, round, reinforced fenestrations (Figure 2.9(E2), also visible on the upper lamella of Figure 2.8(f1)), and harbor the superior and inferior anchorages of smooth muscle cells, allowing them to weave through the tunica media [Dingemans 00];
   - Secondly, thick radial elastin struts provide structural cohesion to the overall medial lamellar unit, while preserving an angular 20° tilt with regards to smooth muscle cell orientation (Figure 2.9(E3)) [Dingemans 00, Koch 14, Tsamis 13];
   - Finally, thin elastic radial fibers take the form of ridges [Dingemans 00] or protruding ribs [Raspanti 06], connecting the smooth muscle cells to both lamellae, Figure 2.9(E4).

   Moreover, through their actively adaptive behavior, the vascular smooth muscle cells are responsible for the regulation and maintenance of blood flow and for the regulation of stress across the arterial wall thickness. For this reason, vascular smooth muscle cells harbor actin-myosin filaments (myofilament) that permit rapid stress-development, sustain stress-maintenance and vessel constriction [Ratz 15]. The relaxed smooth muscle cell is a very long and thin (fusiform) structure [Ratz 15] with a large surface area, and an ellipsoidal shape of its nucleus [O'Connell 08]. Upon contraction, the vascular muscle cells can undergo dramatic shortening accompanied by shape change, surface rearrangements,

and a loss of volume that is regained upon relengthening. As for their spatial positioning among the constituents of the medial lamellar unit, the cells weave diagonally throughout the interlamellar elastin framework [O'Connell 08]. Smooth muscle cells do not contribute at rest to the mechanical properties of arteries, due to a high (up to 150%) distensibility [Faury 01, Nagayama 04]. Their functional role is however of prime importance, since they are responsible for the regulation and maintenance of blood flow, enabling a more constant peripheral blood flow [Ratz 15, Faury 01].

Collagen is also organized in different morphologies within the tunica media. Firstly, interlaced bundles made of type IV collagen microfibrils (oxytalan fibers) in the immediate pericellular matrix contribute, along with elastin radial struts and interlamellar elastin protrusions, to smooth muscle cell cohesion and fixation on the lamellae (Figure 2.9(C2)) [Clark 85,Dingemans 00]. It is understood that the smooth muscle cells preferentially adhere to these ill-defined streaks rather than directly to the solid lamellae (Figure 2.9(SMC)) [Dingemans 00]; secondly, wavy collagen bundles run parallel to the elastic lamella, between the lamella and the smooth muscle cells (Figure 2.9(C1) and Figure 7(f2)) [Clark 85]. These collagen fibers are oriented circumferentially [O'Connell 08, Timmins 10,Roy 11,Hill 12] and are closely associated with the elastic lamellae [Dingemans 00] but not with the smooth muscle cells. Upon pressure, these medial collagen fibers decrimp and stretch to prevent over distension of the vessel. Collagen takes also the form of membranes enveloping the smooth muscle cells (Figure 2.9(C3)).

3. **Microstructure of the tunica adventitia**
   Finally, the outermost arterial layer, the tunica adventitia, is made of coexiting networks of elastin and collagen with embedded fibroblasts. In the adventitia, elastin takes the form of a low density meshwork made of variously oriented fibers showing bifurcations (transversely oriented segments), with a dominant longitudinal direction [Chen 11, Chen 13] (Figure 2.8(e3)). Conversely, collagen fibers pack into thick bundles of 10 to 30 fibers, folded (crimped) under the *in vivo* pre-stress and pre-stretch conditions. These wavy bundles are oriented helicoidally making a 45° angle with respect to the longitudinal and circumferential directions, and show a negligible transmurality [Rezakhaniha 12, Schrauwen 12] (Figure 2.8(e1) and (e3)). For an excised cut open tissue, the crimping at rest appears considerably more important than in the excised cylindrical configuration, and the bundles are oriented closer to the axial direction [Tsamis 13, Koch 14, D'Amore 10]. The adventitial collagen network is capable of undergoing important morphology rearrangements under mechanical load. These rearrangements are further detailed in section 2.4.2. The adventitial microstructure is also composed of fibroblasts (not shown on Figure 2.8), which are mechanosensitive cells, responsible for arterial remodeling and arranged circumferentially about collagen bundles [Esterly 68].

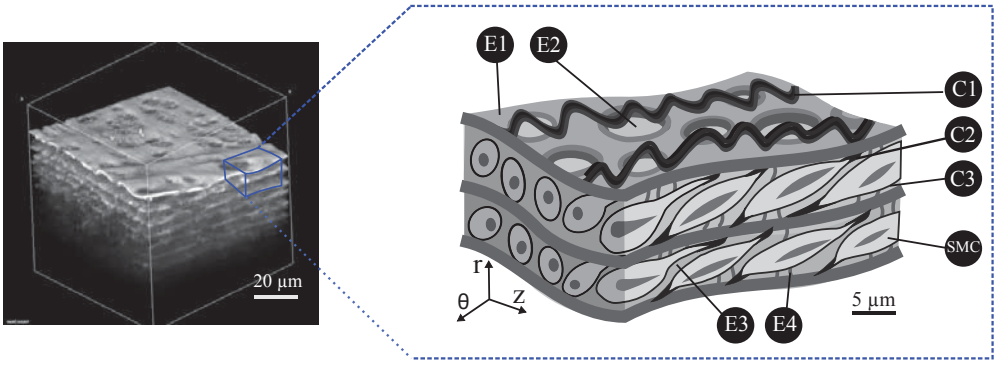

Figure 2.9 – Left: multiphoton 3D image of medial elastin organized in concentric units; right: Schematic representation of one medial lamellar unit morphology. (E1) elastin lamella, (E2) fenestration of the elastin lamella, (E3) elastin interlamellar struts, (E4) elastin surface ridges, (SMC) smooth muscle cells, (C1) collagen fibers, (C2) cohesive collagen microfibril bundles, (C3) collagen envelope of SMCs. Inspired from illustrations by [Dingemans 00, O'Connell 08].

2.3.2.3 Ultrastructure (10-100 nm)

Starting from the arterial lumen, in the endothelium, the actin filaments (F-actin) are one of the major cytoskeletal structures of the endothelial cells [Ookawa 92]; this actin network also exists in the smooth muscle cells. They are organized in bundles and are usually grouped in the central part of the cells. Noticeably, the redistribution of F-actin filaments within the cells is one of the early cellular responses to the onset of shear stress: when experiencing low-shear forces coming from the blood flow, F-actin filaments localize at the periphery of the endothelial cells [Ookawa 92]; whereas when experiencing high shear forces, F-actin bundles are observed in the central part of the elongated cells. In parallel, the cells orient in the direction of the applied flow.

Remaining at the hundreds of nanometers scale, the structure of elastic and collagen fibers is revealed, as well as the existence of crosslinks between and within these fibers. The morphology of the elastic lamellae presents a fibrous texture suggestive of a "criss-crossed", delicate filamentous scaffold [Ushiki 02, Raspanti 06]. The elastic fiber and elastin meshwork however are made of elastin fibrils and microfibrils that run in various directions (Figure 2.8(i) and (j)). Those microfibrils are coated together within an elastic fiber by proteoglycans and glycosaminoglycans [Ushiki 02]. At the same scale, collagen bundles are made of closely packed, parallel, thin collagen fibrils, with a characteristic diameter of 30-100 nm, with altering number of coated fibrils depending on the region in the bundle [Ushiki 02, Raspanti 06]. In the adventitia, these bundles are thicker than in the media due to a higher number of constituting fibrils (Figure 2.8(g)). The fibrils present a regular, orthogonal lattice of surface-bound proteoglycans [Raspanti 06, Berillis 13] (Figure 2.8(h)). Finally, at the nanometer scale, the cohesion between fibrils constituting elastic or collagen fibers is realized by crosslinking proteoglycans, formed by covalent bonding between acid glycosaminoglycans and proteins [Eisenstein 75]. At

	Intima	**Media**	**Adventitia**	**References**
Macrostructure (1-10 mm)	Endothelium	Periodic lamellar units	Collagenous medium	[Wolinski 67] [Ives 86] [Farand 07]
Microstructure (10-100 µm)	Endothelial cells Elastin lamina	Elastin lamellae Interlamellar elastin struts Smooth muscle cells Collagen fibers	Collagen wavy bundles Elastin network Fibroblasts	[Dingemans 00] [O'Connell 07] [Rezakhaniha 12] [Chen 13]
Ultrastructure (10-100 nm)	Actin filaments Elastin microfibrils	Actin filaments Myosin Elastin microfibrils Proteoglycans Glycosaminoglycans (GAGs) Collagen fibrils	Elastin microfibrils Proteoglycans GAGs Collagen fibrils	[Eyre 84] [Ushiki 02] [Raspenti 06] [Berillis 13] [Ratz 15]

Table 2.1 – Summary of the multiscale hierarchical structure of the artery.

the microfibrillar level, collagen and elastin are crosslinked by a unique mechanism based on aldehyde formation from lysine or hydroxylysine side chains [Eyre 84, Sáez 16].

At the scale of the ultrastructure also, several proteins are considered as influential to vascular smooth muscle cells mechanics, namely: (i) the motor protein, called myosin II, assembled into thick filaments; (ii) filamentous actin, which can be seen as a truss on which myosin heads bind and can "walk" on [Ratz 16]; and (iii) smooth muscle titin and microtubules of the cytoskeleton. Actin filaments weave through the smooth muscle cell and are part of its contractile apparatus. They consist in semi-flexible polymers that can, in conjunction with myosin, act as biological active springs able to exert or resist against force in a cellular environment [Blanchoin 14]. They therefore participate in arterial acute adaptive plasticity [Bednarek 11]. It has also been shown that smooth muscle cell filamentous actin is in a continuous state of remodeling [Bursac 07]. Other studies about myosin thick filaments of muscle cells have revealed their partial dissociation and reformation during, respectively, relaxation and contraction [Smolensky 05].

Table 2.1 summarises the multiscale hierarchical structure of the artery described in this section, with related literature references.

2.3.3 Universal pattern for arterial composition

Along with qualitative descriptions of arterial microstructure, past studies have attempted to quantify structural parameters that characterize the various configurations of the complex and heterogeneous arterial microstructure. Those quantifications were usually realized for modeling purposes. We here focus on the characterization of the arterial composition: whether

chemical or optical methods were applied, the vascular microstructure was analyzed in order to quantify the mass fractions of the different biological constituents. [Morin 17] collected the mass fractions of elastin and collagen in various large elastic arteries (from the abdominal to the carotid arteries), from a great variety of species (from rats to human) and ages, and evidenced a general composition rule. Noticeably, since important modifications in the arterial composition occur in the perinatal and early childhood periods [Bendeck 91], as well as in aging organisms [Schlatmann 77, Tsamis 13], the data selection was restricted to adult organs with no aging effects. The resulting relationship illustrates that collagen and elastin contents strongly correlate mutually, and that the thoracic aortas are characterized by a larger content in elastin as compared to the abdominal aortas, which contain more collagen. Also, as a general rule, the elastin content decreases from proximal to distal regions. In parallel, it was observed that the number of lamellar units also decreases in more distal aortas [Wolinsky 67, Sokolis 02].

2.4 Load-driven microstructural rearrangements of the arterial microstructure

At the scale of the fiber networks, the microstructural origin of the nonlinear mechanical behavior has been evidenced by means of confocal and multiphoton microscopy: namely, in the course of the mechanical loading, the fiber networks making up the microstructure tend to rearrange to better resist the loading. *In situ* mechanical testing showed the ability of the different fiber networks to resist the applied mechanical loading by progressively aligning, with various rotation amplitudes, with the strain direction [Chen 13, Tower 02, Keyes 13, Sugita 17], and the related kinematics of the fibers are currently under investigation. To this aim, the fiber network geometrical configurations have been investigated: applying custom image processing algorithms, fiber networks were analyzed in terms of fiber orientation densities and other morphological characteristics such as fiber diameter, waviness, tortuosity, or node connectivity. The following subsection summarizes these quantification methods, before discussing rearrangement properties of the fibrous networks, in the context of uniaxial tension experiments.

2.4.1 Quantitative characterization of the fiber network arrangement

The characterization of a fibrous network requires the accurate extraction of descriptive structural parameters from imaging data, including fiber dispersion and mean fiber orientation. Two methods are widely applied in the existing literature: structure tensor methods and Fast Fourier Transform (FFT) methods (with a band-pass filter, the most accurate method according to [Morrill 16])(Figure 2.10).

1. **Structure tensors**
   Using the gradient-based structure tensor method [Jähne 93, Bigun 04, Rezakhaniha 12], the sequence of steps is the following:

   – A structure tensor is calculated for each pixel in the spatial domain by computing

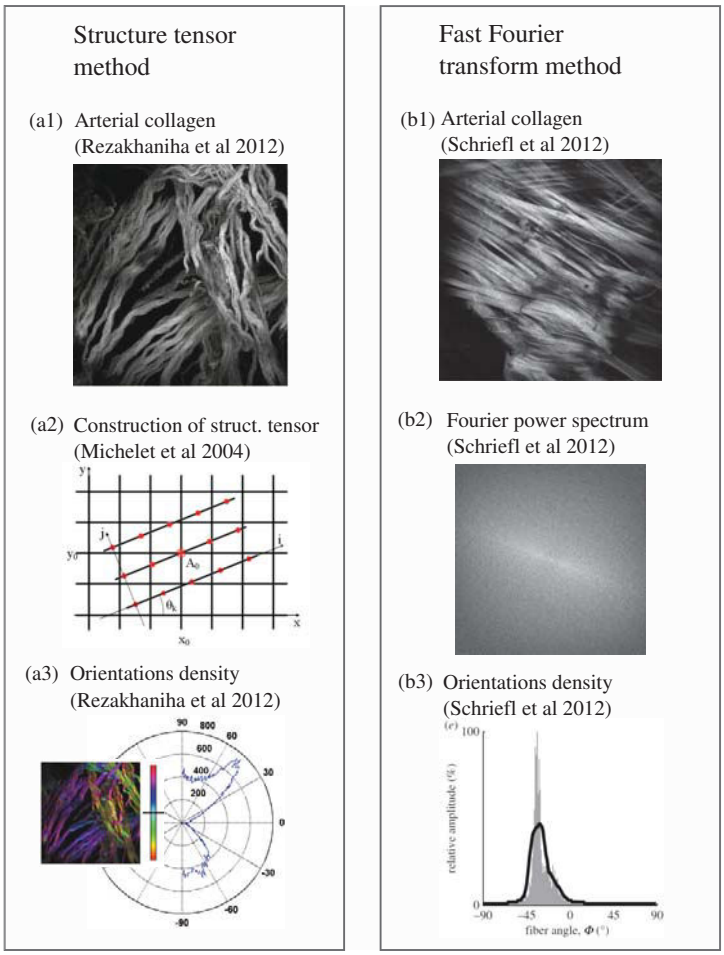

Figure 2.10 – Quantification of fiber orientation densities with the structure tensor method (left) and with the Fast Fourier transform method (right).

the pixel intensity gradients in the two spatial directions within a user-specified Gaussian-shaped window;

- The local fiber orientation at each pixel is defined by the eigenvector corresponding to the smallest eigenvalue of the structure tensor;
- The fiber orientation distribution is built from pixel orientations that are weighted by coherency values, so that elongated structures are emphasized [Jähne 93, Rezakhaniha 12].

The gradient-based structure tensor method is available in the "Directionality" plug-in and OrientationJ plugin of ImageJ® software [Rezakhaniha 12].

2. **Fast Fourier Transform**
   Using FFT 2D [Polzer 13, Ayres 06, Morrill 16, Sander 09, Schriefl 12], the sequence of processing steps is the following:

   - Images are converted to the frequency domain by means of a 2D discrete Fourier transform (frequencies are representative of changes in pixel intensity [Gonzalez 02]);

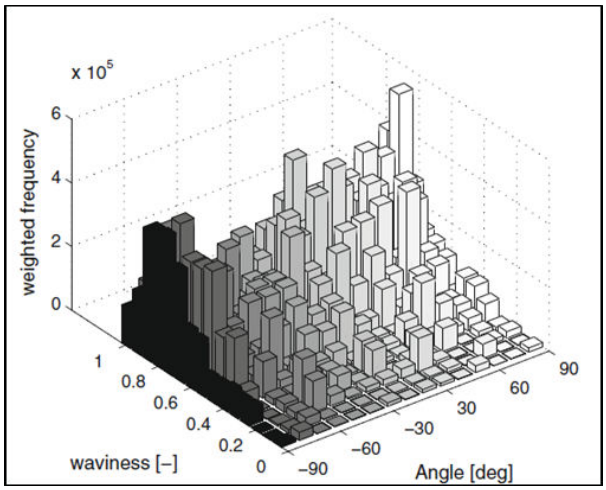

Figure 2.11 – Bivariate histogram of straightness parameter (i.e. waviness) and global angles with respect to the axial direction of the artery based on the entire weighted dataset [Rezakhaniha 12]. The authors realized the measurements on load-free rabbit carotid arteries.

- The transform contains both real and imaginary parts; therefore, the Fourier transform is converted to a power spectrum with no imaginary part (the imaginary part does not include information about texture orientation);
- The power spectrum intensities are intergrated, and a wedge-shape sum approach is used to determine total intensity for each 1° wedge to create a fiber orientation distribution of the fiber network [Ayres 08, Schriefl 12].

The FFT 2D method is usually implemented and customized in Matlab® but is also encapsulated and available in "Oval Profile Plot" and "Directionality", which are plugins for ImageJ® and Fiji®, respectively [Schneider 12, O'Connell 08].

Both methods allow extracting orientation densities but most importantly allow quantifying the reorientation amplitudes of the fibers undergoing a macroscopic deformation.

The measurement of fiber waviness or fiber straightness can, in turn, be achieved by means of manual fiber tracking methods [Chen 11, Rezakhaniha 12, Wang 13, Sugita 17, Chow 14, Hill 12]. After a selection of representative fibers on the images (5-10 fibers), their length is measured and divided by the distance between the fiber tips in order to extract the fiber's waviness parameter. This measure provides an insight into the degree of engagement of the fibers, given that above a certain waviness threshold, the fibers are considered to be fully engaged and sustain tension (Figure 2.11).

Along with a detailed assessment of the fiber network's statistical orientations, or of the vascular biological composition, many studies have focused on the extraction of other geometrical characteristics of the microstructure. Non exhaustively, custom image analysis methods focused on the analysis of the fiber diameters [D'Amore 10, Phillippi 14], the fiber

	Quantification technique	Applicability	Software tool	References
Fiber angle densities	Structure tensor method	All fiber networks	Custom or OrientationJ (ImageJ)	[Jahne 93, Bigun 04]
	Fast Fourier Transform	All fiber networks	Custom (Matlab, Fortran); "Oval Profile Plot and Directionality" plugin (ImageJ)	[Ayres 06, Schriefl 12]
Fiber waviness	Semi automatic tracking	Wavy fibers (crimped collagen)	Custom, NeuronJ (ImageJ)	[Chow 05, Hill 11]
Fiber diameter	Custom image skeletonization	All fiber networks	Custom	[D'Amore 10, Phillippi 14]
Fiber lengths	Custom image skeletonization	All fiber networks	Custom	[D'Amore 10; Rezakhaniha 11]
Fiber volume fractions	Image thresholding	All fiber networks	Custom ImageJ	[Tonar 03, O'Connell 08]
Fiber tortuosity	Custom image skeletonization	Medial elastin, medial collagen	Custom (Matlab)	[Koch 14]
Node connectivity	Custom image skeletonization	Medial elastin, medial collagen	Custom (Matlab)	[D'Amore 10; Koch 14]
Density of transversely oriented segments	Custom image skeletonization	Medial elastin, medial collagen	Custom (Matlab)	[Koch 14]

Table 2.2 – Summary of quantification methods applied to the analysis of the arterial microstructure.

lengths [D'Amore 10, Rezakhaniha 12, Hill 12, Tsamis 13, Phillippi 14, Cicchi 14], or fiber volume fractions [Tonar 03, Hayashi 74, O'Connell 08]. More recently, for modeling purposes, more complex morphological features were quantified, such as fiber tortuosity [Koch 14], node connectivity and spatial intersections density [D'Amore 10, Koch 14], or density of transversely oriented segments [Koch 14]. Table 2.2 summarizes the above mentioned quantification techniques with related litterature references.

While evaluating the reorientation of fibers in the deforming microstructure of arteries, another possible characterization of fiber kinematics consists in comparing the measured reorientations to reorientations predicted by affine kinematics. A fiber reorients in an "affine" manner if it is considered firmly embedded in its surrounding matrix, and therefore follows the shape change of the representative volume element in which it is embedded. The hyperelastic arterial models assume an affine reorientation during deformation [Holzapfel 05], which was later evidenced by the observation of an affine behavior of the fibers [Sacks 03a, Wan 12], although recent measurements of the fiber kinematics under different load protocols question this evidence. In fact, several studies analyzed fiber kinematics in different collageneous tissues, such as tendon [Lake 12], collagenous constructs [Chandran 06], bovine pericardium [Billiar 97], the liver capsule [Jayyosi 16] or the skin [Jayyosi 17]. These studies revealed non-affine collagen kinematics, in turn evidencing that other mechanisms are active in the reorientation process.

2.4.2 Rearrangement of the adventitial collagen bundles

As previously described, in the unloaded configuration, the adventitial collagen network exhibits randomly distributed orientations and a high degree of crimping [Dingemans 00, O'Connell 08, Rezakhaniha 12]. Upon mechanical loading, the collagen bundles progressively unfold [Canham 92, Greenwald 97], coinciding with the progressive stiffening of the arterial material (as long as collagen fibers are not straight, they cannot sustain load and the softer constituents making up the arterial tissue sustain the applied load). The measurement of fiber wavi-

ness [Chen 11, Schrauwen 12, Wang 13, Sugita 17] revealed in particular that recruitment, or engagement of collagen fibers, is gradual (unsynchronized among fibers) and starts at a finite strain [Hill 12, Chow 14]. The process can differ whether the observed vascular region is close or remote from the heart (distal regions vs. proximal regions) [Zeinali-Davarani 15]. In particular, past studies showed that recruitment starts, in the case of porcine aortic tissue, after 20% strain [Chow 14] and that only 6-7% of collagen fibers are engaged at physiological pressures, when testing rabbit carotid arteries [Greenwald 97].

Adventitial collagen fiber bundles may also undergo a progressive realignment in response to the application of a macroscopic deformation [Chow 14, Keyes 13, Chen 11]. This realignment has been observed to take place after recruitment in order for the artery to continue deforming without damaging the engaged fibers [Wang 13], as shown by tracking the collagen bundle deformation, either by means of fluorescent microspheres [Chen 11], or by means of X-ray diffraction [Schmid 05]. The post engagement fiber realignment showed discrepancies in fiber realignment amplitudes, depending on the initial fiber angle and on the type of deformation [Wan 12, Chen 13]. The fiber bundles are finally stretched upon further mechanical loading. Consequently, a correct assessment of the mechanical fields within the adventitia relies on a correct description of the collagen network and of its evolution during loading.

2.4.3 Rearrangement of other fiber networks

Collagen bundle recruitment is driven by the presence of the elastin network: in the adventitia, the elastin network is, at rest, aligned with the collagen network [Chen 11]. It tends to reorient and align by application of a mechanical loading. Still, the realignment of the adventitial elastin network is less pronounced than the collagen realignment [Chen 13]. In the media, elastin lamellae, collagen fibers, and smooth muscle cells also undergo load-induced reorientation. Under uniaxial and biaxial load cases, the medial fiber networks and the collagen network tend to align with the load direction [Timmins 10]. Also, the engagement of collagen fibers occurs first in the media, and starts later in the adventitia [Chow 14, Zeinali-Davarani 15]. Other observations, focusing on medial collagen, concerned changes in fiber waviness during pressurization, showing that collagen fibers around the smooth muscle cells become straight at lower intraluminal pressures than those in elastic lamellae, indicating that smooth muscle cells stretch more than elastic lamellae [Sugita 17].

At a larger scale, the elastic lamellae progressively unfold with the load application and then stretch, as observed by means of polarized light microscopy by [Sokolis 06] and represented in Figure 2.12 (see blue line denoting the section of the internal lamellae) based on microscopy performed during this thesis which confirmed previous literature results. The cohesive pericellular interlaced fibrils (Figure 2.9 - C2) also straighten and reorient by application of a load [Sokolis 06], and this recruitment process was shown to be faster than the recruitment of the circumferentially oriented, parallel collagen bundles covering the elastic lamellae [Sugita 17].

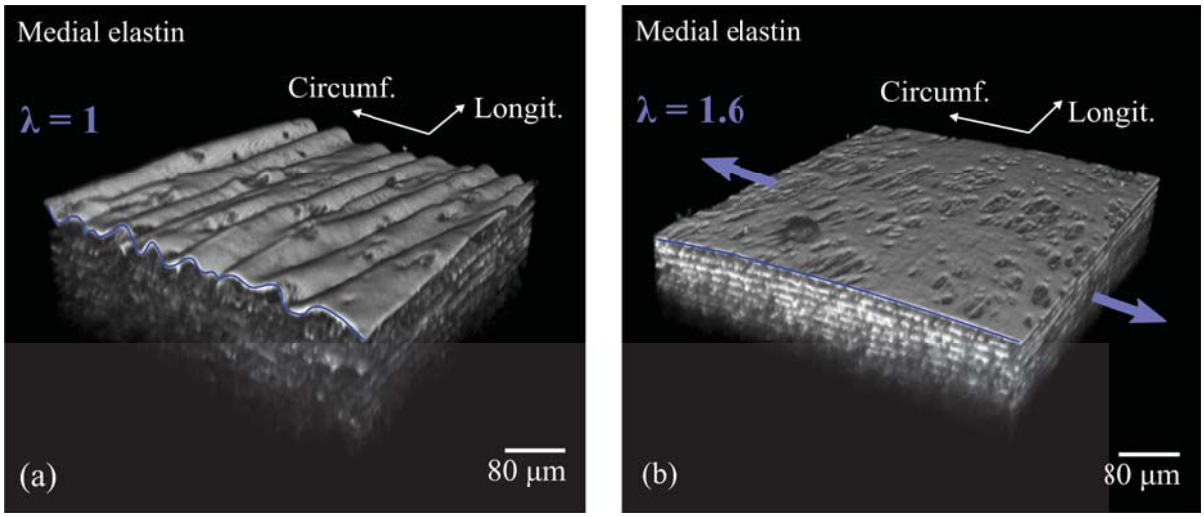

Figure 2.12 – Unfolding of elastic lamellae imaged under multiphoton microscopy (IVTV Platform, Ecole Centrale Lyon, FR) on rabbit carotid arteries submitted to circumferentially oriented uniaxial tension. (a) Unloaded configuration (uniaxial circumferential stretch λ=1), (b) loaded configuration (uniaxial circumferential stretch λ=1.6).

The latter authors propose the stiffness difference between elastin and smooth muscle cells as the possible explanation, the more compliant surrounding medium allowing faster recruitment of the initially crimped fibers.

2.4.4 Underlying mechanisms governing the observed rearrangements

While non-affine fiber kinematics are experimentally evidenced by the aforementioned studies, their interpretations mostly rely on assumptions. For example, non-affine fiber kinematics are attributed either to the decrimping process itself [Lee 15], to fiber-fiber interactions [Chow 14] or to fiber-matrix interactions [Billiar 97, Thorpe 13]. Indeed the microstructural and micromechanical origin of non-affine fiber kinematics has not yet been experimentally documented nor understood, which constitutes a limit for further refined multiscale formulations.
Despite an absence of experimental evidence, several models proposed micromechanical mechanisms that may explain the non-affine fiber kinematics. Among them [Stylianopoulos 07] built an arterial model in which a RVE was made up by fibers attached to each other by freely rotating crosslinks. This model results in a non-affine fiber kinematics, which is a consequence of minimizing fiber stretch during reorientation under load. In fact, the affine assumption for fiber motion maximizes fiber stretch, whereas freely rotating fibers may reorient in the direction of the macroscopic strain while limiting inner fiber stretching.

Moreover, several studies investigated the nature of fiber-fiber and fiber-matrix bindings, attributing a binding role between the fibers and the matrix to proteoglycans and glycosaminoglycan side chains [Sáez 14, Thorpe 13]. Results suggest that these molecules govern interactions that may provide an anchoring network for cells within the extracellular matrix [Ritty 03]. Proteoglycans and glycosaminoglycans are also considered to play an important role in the stretch-

ing of the collagen bundles, by enabling an inner sliding of the fibrils [Lynch 17]. Fibulin-5 has also been shown to play an important role in the bindings between elastin fibers and cells [Yanagisawa 02]. Although an increasing focus is devoted to these binding proteins, the understanding of underlying mechanisms governing fiber rearrangements remains limited.

2.5 Modelling approaches

Constitutive modeling of soft biological tissues has generated an abundant literature over the last thirty years, trying to capture their complex mechanical behavior. As discussed previously, their anisotropic mechanical response to solicitations is characterized by large recoverable deformations together with progressive stiffening of the mechanical response with increased stretching of the tissue, resulting in a complex, highly non-linear response. Stiffening is correlated to the progressive recruitment and realignment of collagen fibers, which are the main load-bearing contributors in the large strain regime. There exists nowadays various macroscopic and multiscale approaches to the modeling of the constitutive behavior of soft tissues, which are presented in the following section.

2.5.1 Hyperelastic models

Historical hyperelastic models were developed within the finite-strain theory, based on the definition of a strain-energy function: considering soft tissues as fiber-reinforced composites and using an energy superposition principle, the contribution of each constituent is taken into account by one term in the strain energy function. These models define a neo-Hookean matrix and several (from 2 to 6) fiber families with various orientations, and with polynomial or exponential contributions to the strain energy function [Holzapfel 01, Holzapfel 07]. Several models propose also to take into account the statistical dispersion of fiber angles for better capturing the stress-strain response [Gasser 07, Zulliger 04]. These phenomenological models account for the anisotropic character of the tissue mechanical response, and usually reproduce the experimental data with very good accuracy. This accuracy was further improved along with the addition of a fiber activation stretch or of a probability distribution function, accounting for gradual recruitment of collagen fibers at finite strain [Roy 11, Hill 12, Weisbecker 12]. More recent trends in the development of these hyperelastic models concern the addition of a collagen crosslinking parameter [Sáez 14, Sáez 16] into the strain energy function, accounting for the presence of transversely oriented crosslinking proteoglycans [Raspanti 06] in the undulated collagen bundles. In fact these attachments between the main fibers were shown to provide compliance in the transverse direction of the main fibers [Sáez 14]. Another trend in the context of strain-energy function models consists in using an angular integration approach for 2D and 3D fiber dispersions. These developments allowed to account for the much greater dispersion of fiber orientations in the tangential plane, than out of plane, and allowed the exclusion of fibers under compression [Holzapfel 15a, Holzapfel 15b, Li 16]. All these models assume an affine rearrangement of the collagen network. This assumption was experimentally evidenced

by several contributions [Sacks 03a, Wan 12], i.e. the fibers are assigned to follow the overall material deformation. Given their phenomenological formulation which implies parameter fitting to meet experimental results, they do not incorporate the physical relations that govern the mechanics of the microstructure at the fibers' scale. Moreover, another drawback is that they introduce a large set of parameters, which are not necessarily related to measureable quantities. Nevertheless, their remarkable computational potential allows current simulations to be pushed towards translation into (applied) biomedicine, with the development of computer assisted software tools for surgeons (for instance Predisurge™Software, http://www.predisurge.com/, Saint Etienne, FR, currently under development).

2.5.2 Multiscale models

The previously described phenomenological models are not aimed at modeling the microstructural mechanisms (whether fiber reorientations or remodeling) introduced in section 2.1, which lead to changes in the mechanical response. Noticeably, although the constrained mixture model proposed by [Humphrey 02, Gleason 04b] accounts successfully for changes in the 3-D distribution of stress within the arterial wall through a multiscale mechanobiological scheme, it still incorporates affine fiber kinematics given that it is coupled to hyperelastic models [Holzapfel 01, Gasser 07]. Consequently, different relevant multiscale studies arose. The multiscale approach to arterial modeling consists of the geometrical and physical descriptions of the heterogeneous arterial microstructure (matrix and fibers) making up a microscopic Representative Volume Element (RVE), in order to retrieve the constitutive behavior of each and every point of the macroscopic structure made by these RVEs.

A simple method to represent the constitutive behavior of the hierarchically organized substructure of the arterial tissue is to approximate the collagen fiber crimp by a cylindrical helix, considered as a three dimensional spring [Freed 05, Grytz 09]. Then, the nonlinear axial force-stretch relationship of the extensible helical spring governs the mechanical response, including the full extension of the spring as a limit case. Such models only require one material parameter (the spring's elastic modulus) and two geometrical parameters to be determined from experiments (the dimensions of the helix) [Grytz 09]. In particular, when the length of the spring (the sinusoid if the configuration is reduced to a bidimensional problem) is kept constant during deformation, fiber kinematics is non-affine. On the contrary, [Fan 14] proposed to model the adventitial collagen network with decrimping fibers under load, via assumptions of affine kinematics. In more details, while stochastically modifying the individual fiber strain in order to account for their crimped structure, [Fan 14] conferred an affine behavior to homogenized fiber ensembles characterized by common spatial orientations, and showed that the model could then correctly reproduce the mechanical behavior of the artery.

Most of the models limit the fiber rotation phenomena to the decrimping mechanisms [Fan 14, Lee 15]. However, the multisale model developed by [Nierenberger 13] considers, through suc-

cessive scale transitions applied to undulated collagen fibers, reorientations of fibers both at fibril scale (intra-bundle reconfiguration) and at fiber bundle scale (global realignements). In this model, both rotation mechanisms are governed by the affine assumption for fiber kinematics. Another approach to fiber rotation allows going beyond affine rotations (although it remains empirical) by defining a bijective map which asymptotically aligns the fibers with the loading direction [Raina 13].

Fiber realignement can also be governed by a specific description of the collagenous network, namely a three dimensional cross-linked network embedded in a matrix [Stylianopoulos 07, Zhang 13]. [Stylianopoulos 07] proposed a coupling of the contributions of the collagenous network and of the non-collagenous matrix. Accordingly, neo-Hookean relations describe the mechanical properties of the non-collagenous matrix, which plays a significant role in the overall mechanical response of the tissue. It introduces a non-affine rotation of the collagen considering straight fibers interacting with each other via freely rotating crosslinks. The model however neglects the potential fiber decrimping, as well as the interaction between fibers and the surrounding matrix. Using a similar description of cross-linked fibers, [Zhang 13] described the collagenous network with linear elastic fibers which store energy only in the tensile deformation mode, and commented the affinity of fiber kinematics as being directly linked to the modulus of the matrix: when the modulus of the matrix increases, the fiber network reorientation is closer to the affine model, leading to internal forces acting between the network and the matrix. Alternatively, the multiscale model of [Morin 15] uses random homogenization and load-induced fiber rotation. The details about this pioneering modeling approach to the artery are provided in Chapter 5, as the development and application of this model is one of the objectives of this thesis.

The previously mentioned models can be extended through an incremental upscaling of elastic properties, in order to account, through strains and stresses averaging procedures over the material's constituents, for several scales of heterogeneities and at which physical mechanisms take place, and physical phenomena scales [Nierenberger 13, Marino 13, Maceri 10].

2.6 Governing questions

The current knowledge about the mechanical response of the arterial tissue has been summarized, as well as the state-of-the-art concerning the arterial microstructure, its load-induced rearrangements, and modeling strategies. This review reveals several knowledge limitations. Namely, the explanations about the underlying microscopic mechanisms governing the load-induced microstructure rearrangements are scarce, and the inter-layer differences in the rearrangements of the collagen and the elastin networks have not been quantitatively characterized and compared to affine kinematics.
The Chapter 3 of this thesis is devoted to address these questions:

- **Are the well-known morphological changes of the vascular tissue under load (decrimping, realignment) different depending on the direction of the load?**
- **For each constituent of the vascular microstructure (collagen network, elastin network), are the morphological changes under load identical in each layer of the composite structure (media and adventitia)?**
- **Are these morphology changes governed exclusively by the rule of affine transformations [Chandran 06, Jayyosi 16]?**

To this aim, a uniaxial setup was developed and used allowing mechanical testing of flat samples of carotid arteries in three distinct directions (circumferential, longitudinal, and diagonal) while analyzing the rearrangements of the various networks of the tissue's multi-layered microstructure by means of multiphoton microscopy.

Moreover, while non-affine collagen kinematics is currently taken into account in a novel generation of multiscale and micromechanical modeling approaches [Stylianopoulos 07, Zhang 13], few studies investigate the dependence of fiber kinematics on the loading type [Wan 12, Chen 13], and to the author's knowledge, none have characterized fiber rotations for the same tracked fibers undergoing different loading scenarii, while comparing them to affine predicted reorientations. Yet the lack in understanding the influence of the loading type (hence of boundary conditions) on the fiber kinematics constitutes a limit for further refined multiscale model formulations. In Chapter 4, we bridge this gap by answering the following questions:

- **Do particular deformation scenarii or conditions challenge affinity of fiber motion?**
- **Is the fibers' behavior dependent on boundary conditions, i.e. dependent on loading scenarii?**

To this aim, a tension-inflation setup was developed and used, allowing the application of diverse biaxial loading scenarii while analyzing the rearrangements of the vascular microstructure by means of multiphoton microscopy.

Finally, current approaches in arterial modeling, with regards to clinical challenges facing towards personalized medicine and microstructure driven assessment of vascular integrity, show jointly the importance of the multiscale approach, even though strain energy based models have shown a good computational potential. In particular, further questioning microstructural mechanisms governing the macroscopic mechanical behavior of the artery brings:

- **To which extent does the load-induced rotation of the fibers predict the behavior of the arterial tissue on both macroscopic and microscopic scales?**
- **What is the effect of the mechanical interactions between constituents of the microstructure on the amplitude of fiber rotation?**

In the Chapter 5 of this thesis, we present a modeling strategy based on continuum micromechanics which investigates these questions using a random homogenization scheme and load-induced fiber rotation. We simulate a series of loadings by adapting and applying the micromechanical model currently developed by [Morin 15].

Chapter 3

A comprehensive study of layer-specific morphological changes in the microstructure of carotid arteries under uniaxial load

Authored by: Witold Krasny, Claire Morin, Hélène Magoariec and Stéphane Avril

Published in: Acta Biomaterialia, Volume 57, 15 July 2017, Pages 342-351,
DOI: 10.1016/j.actbio.2017.04.033.

Contribution: Witold Krasny designed the experimental setup according to the state-of-the-art and preliminary studies prepared at the Laboratory of Tribology and Dynamics of Systems (Ecole Centrale Lyon). He performed all experiments, from carotid excision to image processing and analysis.

Contents

Résumé

Comme précisé dans la revue de l'état de l'art (Chapitre 2), les propriétés mécaniques des grandes artères élastiques (aorte, artère fémorale, artère carotide, etc) sont principalement conférées par les réseaux de collagène et d'élastine, dont l'organisation micro-structurelle joue un rôle important dans l'évolution de diverses pathologies artérielles. En particulier, ces réseaux fibreux sont capables de se réorganiser et se réorienter dans l'espace lors des déformations mécaniques. Dans ce chapitre, ces réarrangements sont étudiés en investiguant en particulier si les réarrangements morphologiques déjà connus, tels que la rotation des fibres vers l'axe de la déformation, sont les mêmes dans toute l'épaisseur de la paroi artérielle et, par la suite, si les mécanismes qui régissent ces réarrangements peuvent être prédits en utilisant le principe de la cinématique affine [Chandran 06]. Pour ce faire, des échantillons de carotide de lapin ont été soumis à des essais de traction uniaxiale selon trois directions de déformation distinctes et des images de la microstructure 3D ont été acquises simultanément via microscopie multiphoton. Les résultats montrent que les réalignements observés du collagène et de l'élastine dans la couche media, ainsi que de l'élastine de la couche adventice, sont restés faibles en termes d'amplitudes de rotation. Ces rotations ont pu être prédites par la cinématique affine. Par contre les réseaux de collagène de la couche adventice se sont comportés de manière sensiblement différente: ils ont révélé une capacité remarquable à se réorienter dans la direction du chargement, quelle que soit la direction de la tension appliquée à l'échantillon. Les angles de réorientation des fibres étaient par ailleurs significativement plus élevés que ceux relatifs aux prévisions affines. Cette propriété particulière des réseaux de collagène dans l'adventice n'a jamais été observée auparavant au sein de l'artère, elle montre que le collagène qui compose la couche externe de la paroi artérielle subit des déformations complexes qui remettent en cause les modèles hyperélastiques traditionnels basés sur la théorie des mélanges.

Originalités des méthodes appliquées :

- *Variété des scenarii de chargement : l'artère a été testée selon trois directions de traction uniaxiale différentes ;*
- *Caractérisation de la cinématique des fibres : les réorientations affines ont été calculées et comparées directement aux réorientations mesurées expérimentalement.*

Résultats à retenir :

- *Les réseaux d'élastine et le collagène de la media, ainsi que ceux d'élastine de l'adventice, se sont comportés de manière affine ;*
- *Le collagène de l'adventice a subit d'importants réalignements dans la direction du chargement, quelle que soit la direction de ce chargement ;*
- *Concernant les fibres de collagène de l'adventice, les angles de réorientation mesurés se sont révélés significativement plus élevés que les prévisions affines.*

Abstract

The load bearing properties of large blood vessels are principally conferred by collagen and elastin networks and their microstructural organization plays an important role in the outcomes of various arterial pathologies. In particular, these fibrous networks are able to rearrange and reorient spatially during mechanical deformations. In this study, we investigate for the first time whether these well-known morphological rearrangements are the same across the whole thickness of blood vessels, and subsequently if the underlying mechanisms that govern these rearrangements can be predicted using affine kinematics. To this aim, we submitted rabbit carotid samples to uniaxial load in three distinct deformation directions, while recording live images of the 3D microstructure using multiphoton microscopy. Our results show that the observed realignment of collagen and elastin in the media layer, along with elastin of the adventitia layer, remained limited to small angles that can be predicted by affine kinematics. We show also that collagen bundles of fibers in the adventitia layer behaved in significantly different fashion. They showed a remarkable capacity to realign in the direction of the load, whatever the loading direction. Measured reorientation angles of the fibers were significantly higher than affine predictions. This remarkable property of collagen bundles in the adventitia was never observed before, it shows that the medium surrounding collagen in the adventitia undergoes complex deformations challenging traditional hyperelastic models based on mixture theories.

Originality of the developed methods:

- Variety of loading scenarii: the artery was tested under three different uniaxial tensile directions;
- Characterization of fiber kinematics: affine reorientations were computed and directly compared to experimentally measured reorientations.

Main results:

- Medial elastin and collagen, as well as adventitial elastin networks behaved in an affine manner;
- Adventitia collagen was able to realign in the direction of the load, whatever the loading direction;
- Measured reorientation angles of the adventitial collagen fibers were significantly higher than affine predictions.

3.1 Introduction

Cardiovascular disorders are a significant public health issue affecting ageing populations globally and causing considerable public health expenses (31% of total mortality in 2012 - source: World Health Organization). In numerous cases, the disorder involves significant changes in the vascular mechanical properties, generating extensive studies about arterial biomechanics and mechanobiology. In this respect, a common approach to vascular biomechanics consists in submitting samples of arterial tissue to mechanical bench tests in order to characterize their macroscopic mechanical properties. Existing investigations [Burton 54, Richardson 89, Duprey 10] consisted in applying a tensile loading on flat samples of arterial material, revealing in particular the material's ability to undergo large strains and a characteristic stiffening occurring above a given tensile stress. In order to capture this complex mechanical behavior and a potential anisotropy of the response, uniaxial tensile tests have been performed independently in the axial and circumferential directions [Okamoto 02, Choudhury 09], and separately to the different layers of the composite structure of the arterial wall [Holzapfel 05, Teng 09].

In parallel to this macroscopic characterization of the mechanical properties, the microstructure of the vascular wall has been extensively analyzed by different microscopy techniques. In particular scanning electron microscopy allowed a morphological analysis of the arterial microstructure at the micron scale [Gross 49, Wasano 83, Denk 04, Raspanti 06]. As for dynamic 2nd harmonic microscopy, it enabled simultaneous image acquisition and optical analysis of collagen fiber orientation, by means of the collagen's optical property of second harmonic generation in the presence of an intense laser beam coupled to a polarizer [Stoller 02, Tower 02, Kabir 13]. Confocal microscopy and multiphoton microscopy enabled live imaging with independent emissions signals corresponding to elastin and collagen [Van Zandvoort 04] providing a 3D point of view on morphological characteristics of the vascular wall, and allowing the evaluation of volume fractions of the different components of the microstructure [O'Connell 08]. These techniques revealed the morphology of each concentric layer (intima, media, adventitia). Concerning the intima, it is composed of endothelial cells, oriented longitudinally [Richardson 89]. As for the media, it is composed principally of circumferentially oriented smooth muscle cells and collagen fibers embedded in an elastin network [Wolinsky 70, Clark 85, Walker-Caprioglio 92, Dingemans 00, Farand 07]. Finally, the adventitia is composed of thick collagen bundles and of a net of helically oriented elastic fibers [Chen 11].

Recently, a special attention has been dedicated to further characterize collagen and elastin fibers, for instance by measuring the waviness of adventitial collagen [Rezakhaniha 12], fiber segment length and the radially-connecting fiber density in the media [Tsamis 13, Koch 14]. Also, several studies started investigating the link between the arterial tissue's macroscopic mechanical response and the associated rearrangements of its microstructure, by coupling mechanical testing with live microscopy. The latter studies confirmed the load-bearing properties

of collagen fibers and revealed a progressive morphological rearrangement under load, namely decrimping and reorientation of the collagen fibers in the direction of the load, as well as the subsequent stiffening of the material's response [Tower 02, Sutton 08, Genovese 13, Wang 13]. Those tests consisted in the application of uniaxial tension on flat samples [Voytik-Harbin 03, Hill 12,Roy 11], biaxial tension on flat samples [Sacks 03b,Humphrey 08a,Timmins 10,Keyes 11, Keyes 13, Chen 13], or tension-inflation on cylindrical samples [Gleason 04a, Zoumi 04, Ferruzzi 11]. The observed morphological rearrangements concerned in particular bundle waviness and orientation [Chen 11, Schrauwen 12, Keyes 13, Wang 13].

As a conclusion, extensive characterizations of both the mechanical layer-specific anisotropic behavior of the arterial wall, and the load-free microstructure morphology exist. Moreover, studies aiming at the characterization of load-induced microstructure rearrangements also exist and come up with advanced insights into the coupling between macro-mechanical response and tissue microstructure rearrangements. However neither the underlying microscopic mechanisms governing the load-induced microstructure rearrangements nor the inter-layer differences in the rearrangements of the collagen and elastin networks have been characterized. This paper is devoted to bridge these gaps in knowledge, by answering the following questions: are the well-known morphological changes of the vascular tissue under load (uncrimping, realignment) dependent on the direction of the load, on the vascular layer, and on the constituent under consideration? Are these morphological changes governed exclusively by the rule of affine transformations [Chandran 06, Jayyosi 16]?

3.2 Materials and methods

The materials and methods presented hereafter are further detailed in the Appendix "Experimental methodology".

3.2.1 Sample preparation

Seven carotid arteries (Figure 3.1(a)) were harvested from healthy male New Zealand White rabbits, weighing 3 kg approximately. Excisions were realized at the Veterinary Campus of the Université de Lyon (VetAgro Sup, Marcy l'Étoile, FR). Rabbit cadavers, previously sacrificed under compliance with the NIH Guide for Care and Use of Laboratory Animals, were kindly provided by Centre Lago (Vonnas, FR). The length of each carotid was measured *in vivo* and *ex vivo*, i.e. immediately after harvesting (Table 3.1 - columns 2 and 3), in order to evaluate the *in vivo* pre-stretch condition (computed as the ratio of the *ex vivo* length to the *in vivo* length, Table 3.1 - column 4). The arteries were immediately frozen at -20 °C until the day of the experimental tests and unfrozen in a bath of phosphate-buffered saline (10x PBS, pH 7.1) at ambient temperature (24 °C). 10 mm long cylindrical portions were excised from the arteries and longitudinally cut open, with a resulting width of approximately 5 mm. For each artery, a 0.5 mm long ring (Figure 3.1(b)) was also extracted for optical measurement of the arterial

thickness (Table 3.1 - last column). This resulted in a cross-sectional area of 0.5±0.1 mm^2. The rectangular strips were cut into dogbone shapes [Hill 12] aligned along the three following in-plane directions: circumferential, longitudinal, and an intermediate direction making a 45° angle with respect to the longitudinal direction (see Figure 3.2(a) for a sketch of the sample preparation). In the following, this intermediate direction will be referred to as the diagonal direction. Twelve samples (four in each orientation group) were dedicated to mechanical testing coupled to multiphoton microscopy, while 6 additional samples (two in each orientation group) were dedicated to mechanical testing alone.

3.2.2 Tensile test

A screw-driven high precision tensile machine (Deben® Microtest tensile/compression stage) was used for uniaxial tensile tests, with a 150 N capacity load cell (Figure 3.1(c)). The load cell signal provided a 0.01 N precision with satisfactory stability. The two heads of the tensile device moved in opposite directions, while the force and the displacement were recorded. Particular care was taken to ensure that the protocol for sample fixation limited the risk of inducing any pre-strain or pre-stress in the sample. Each sample underwent quasi static triangular preconditionning. According to the choice made by [Hill 12], a displacement-speed control was applied a rate of 0.5 mm·min^{-1}, corresponding to a relative elongation speed of 0.2 min^{-1}, with fixed target tensile force equal to 1N. During the mechanical test, the sample was continuously immerged in PBS at a constant ambient temperature of 24 °C. After preconditioning, four measures of the sample width in the unloaded configuration were recorded using a caliper and averaged [Hill 12]. An image of the harvested ring of the artery was taken using a macro optic objective (Nikon D7200® optical camera equipped with Nikon AF-S VR Micro-Nikkor® optical 105 mm f/2.8G IF-ED lens). The caliper in 0.5 mm opening position was placed next to the sample ring in order to caliber the pixel size and subsequently measure the thickness of the arterial wall. The measures of the sample width and thickness allowed the computation of the reference cross-sectional area A_0 (under zero load, after preconditioning) and of the first Piola-Kirchhoff (engineering) stress [Hill 12] $\sigma_{PK} = F/A_0$, where F is the displacement-dependent measure of the tensile force. The stretch was computed from the actual and reference interclamp length of the strip (respectively l and l_0) as: $\lambda = l/l_0$. The reference length of the strip was defined as the interclamp length of the strip after preconditioning.

3.2.3 Multiphoton Microscopy

A multiphoton microscope (NIKON, A1R MP PLUS®) of the IVTV platform (Engineering and Ageing of Living Tissues Platform, ANR-10-EQPX-06-01) was used to image the collagen and elastin networks of the samples (Figure 3.2(b)). Setting the excitation wavelength to 870 nm [Hill 12] allowed collecting autofluorescence and collagen second harmonic generation (SHG) signals through 500-550 nm and 400-492 nm band-pass filters respectively [Jayyosi 16], without any staining or fixation. The imaging resolution was set to 0.5 µm in all directions [Hill 12, Schrauwen 12] with a 512 µm^2 imaging window. This setting resulted in stacks

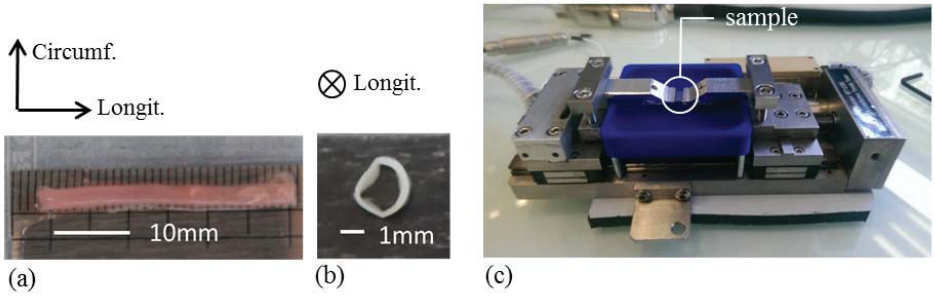

Figure 3.1 – (a) Excised carotid artery from a New Zealand White rabbit; (b) Cross-sectional ring of the artery for optical thickness measurement; (c) Tensile machine.

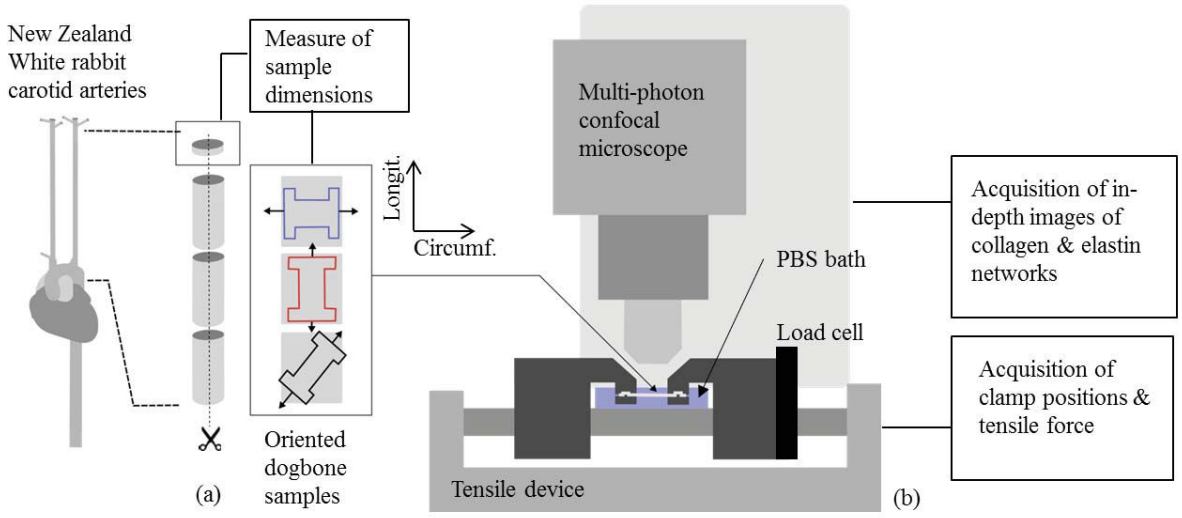

Figure 3.2 – (a) Schematic representation of the vascular tissue samples, prepared from cut-open cylindrical portions of New Zealand White rabbit carotid arteries; (b) schematic representation of the experimental setup composed of a tensile machine coupled to a multiphoton microscope.

of images characterized by 60 to 90 µm thicknesses, depending on the quality of the signal at in-depth focal position. In order to achieve an optimal compromise between image quality and acquisition time, the scan speed was set to 0.25 frames per second, with two-frame averaging. This setting resulted in acquisition times of approximately 20 to 30 minutes for a given elongation configuration. Each arterial tissue sample underwent two imaging sequences: one sequence with the adventitial side facing the objective of the microscope after five preconditioning cycles [Hill 12]; and the other sequence with the intimal side facing the objective after two additional stabilizing preconditioning cycles. Images were taken in the unloaded configuration and in three gradually loaded configurations, respectively at 0.2 N, 0.5 N, and 0.8 N. Before imaging, a period of 10 to 15 minutes was observed in order to stabilize the tissue after initial material creep. Creep dynamics were previously analyzed and it was shown that 10 minutes were sufficient to avoid an important creeping. It was also observed by live imaging that possible further creep did not modify noticeably the microstructure morphology.

3.2.4 Image analysis

The image stacks representing collagen and elastin were analyzed in terms of spatial orientation of the fibrous networks. Previous studies have investigated the transmural angle (radial direction) of the fibers and showed that it is negligible in comparison to the in-plane angle [Roy 11, Rezakhaniha 12, Schrauwen 12]. They have also showed that the most relevant morphological changes in the microstructure occur in the circumferential and longitudinal directions. Subsequently, we focused in the following on the analysis of the in-plane angles of the fibrous networks. Prior to the analysis of relative angle densities, the image stacks were pre-processed so that they could represent the true tissue morphology on two-dimensional images while enabling liable angle density extraction. To this aim, the stack portion representing the adventitial layer of the vascular wall was subdivided into three equally thick sublayers (20-30 µm) and each sublayer was projected orthogonally onto a single image using a maximum intensity projection algorithm. The choice of three sublayers allowed to achieve an optimum between image pixel density and fiber trans-mural continuity (due to non-zero transmural angles which could cause bias in the angle density analysis). Pre-processing of the media stack consisted in a projection in the thickness of one representative lamella (5-10 µm), after verification of the equivalent morphologies of the different lamellae. The resulting set of 2D images used for the analysis of the fiber angle density consisted in three images of the adventitial collagen, three images of the adventitial elastin, one image of the medial collagen and one image of the medial elastin (Figure 3.3(a)). The relative angle densities of the fibrous networks seen on each of these images were analyzed by combining wedge-shape integration of the Fourier power spectrum [Ayres 08, Schriefl 12, Schriefl 13] (Figure 3.3(b)) and a custom method for the extraction of local density maxima with their associated dispersions (Figure 3.3(c)). Local density maxima were determined by a standard peak detection algorithm. The associated dispersions were evaluated by first determining an arbitrary density threshold that represented a cumulative percentile of total fiber angles extracted from the image, and secondly by reading out angle values corresponding to this threshold. Explicitly, let θ represent a local orientation angle, and $d(\theta)$ the angle density of the analyzed image; the angle density threshold p is the angle density below which the fraction $\alpha_p = 0.8$ of the total fibers is counted, i.e. the solution of the following equation:

$$\alpha_p = \frac{\int_0^\pi \min(d(\theta), p) d\theta}{\int_0^\pi d(\theta) d\theta} = 0.8. \tag{3.1}$$

We evaluated corresponding angles about each detected local maximum in order to extract related relative dispersions (Figure 3.3(c)).

3.2.5 Predicting the amplitude of fiber rotation by affine reorientation

The assumption of affine reorientation considers that the fibers are continuously embedded in their surrounding matrix and are therefore constrained to the same deformation gradient as the matrix [Billiar 97, Chandran 06, Jayyosi 16]. For a uniaxial tensile loading, the fiber orientations θ can be computed as a function of the initial angle θ_0 and deformation stretch λ

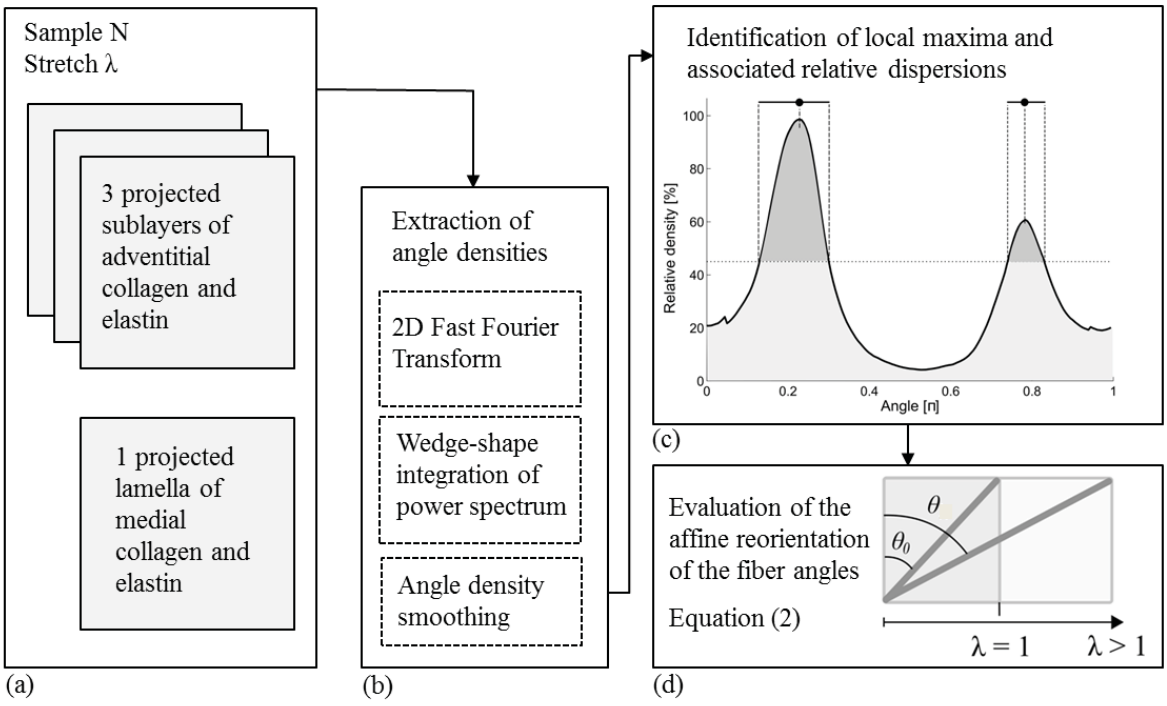

Figure 3.3 – Summary of the image analysis method. (a) Partial z-projections of adventitial and medial microstructure image stacks; (b) Fast Fourier 2D analysis of microstructure images; (c) local maxima dectection and associated relative dispersions evaluation on smoothed fiber angles density function; (d) analytical computation of affine fiber reorientation.

(Figure 3.3(d)) by:

$$\theta = \arctan(\lambda \tan \theta_0). \tag{3.2}$$

The angle values predicted by Equation (3.2) are compared to the experimentally measured angles in order to analyze to which extent this affine reorientation can predict true fiber network reorientations. In particular, the adventitial collagen bundles showed, in the load-free state, a dense crimped configuration for which it was difficult to extract global orientations of the bundles using traditional image processing techniques (Fourier analysis, local gradients, etc). In order to avoid a subsequent imprecision of the analysis, a specific method was designed to isolate the global fiber rotation mechanism from the uncrimping mechanism, and to test the hypothesis of affine kinematics only on the global reorientation of the fibers. To this aim, we considered a deformation scenario which starts in the diagonally deformed state and reaches the circumferentially and longitudinally deformed states in two sequenced steps: diagonal unloading followed by circumferential or longitudinal loading. Accordingly, only deformed configurations with straight collagen bundles needed to be processed for fiber angle analysis. Prediction errors were computed by dividing the difference between experimental and predicted fiber angles by the experimental fiber angle.

Specimen	***Ex vivo* length** [mm]	***In vivo* length** [mm]	***In vivo* stretch** [-]	**Thickness** [mm]
1	4.3	7.1	1.6	0.18
2	4.1	6.9	1.6	0.17
3	4.3	7.0	1.6	0.19
4	4.2	6.9	1.6	0.16
5	4.3	7.5	1.7	0.18
6	4.0	6.5	1.6	0.18
7	3.9	6.6	1.7	0.19

Table 3.1 – Geometrical measurements of the harvested carotid arteries.

3.3 Results

3.3.1 Macromechanical response of the arterial tissue

Engineering stress evaluated against stretch revealed a macroscopic anisotropy of the material's mechanical response, as shown by (i) the characteristic stiffening of the samples starting at different stretch values depending on the direction of the load (Figure 3.4(a)); (ii) the estimated elastic moduli in the final loading regime (Figure 3.4(b)-middle), and (iii) the stretch values when reaching 0.5 MPa (Figure 3.4(b)-right). In particular, the mean estimated elastic moduli in the final loading regime was 50% higher in the circumferential direction than in the longitudinal direction; and 20% higher in the circumferential direction than in the diagonal direction. Accordingly, the mean stretch when reaching 0.5 MPa was 20% lower in the circumferential direction than in the longitudinal direction; and 15% lower than in the diagonal direction. Concerning the estimated elastic moduli in the initial loading regime (Figure 3.4(b)-left), the comparison of mean values showed lower differences between the sample families as their standard deviation amounts to 8%. Comparing the measured *in vivo* stretches to the longitudinal mechanical response (Table 3.1), the carotid were subjected *in vivo* to a longitudinal stress of about 0.1 MPa, in the soft region of the curve (Figure 3.4(a) - red curves).

3.3.2 Microstructure morphological rearrangements under uniaxial load

Fibrous networks of the arterial microstructure revealed varying morphologies depending on the biological constituent (elastin, collagen), on the considered arterial layer (adventitia, media), and on the direction of the applied uniaxial load (Figure 3.5). Figure 3.5(a) shows the microstructure of the unloaded arterial tissue, and Figure 3.5(b)(c)(d) show the microstructure under the three considered loading conditions, which corresponded to the same uniaxial force of 0.8 N. For each constituent of the imaged microstructure, we provide on Figure 3.6 a polar representation of fiber orientations (local maxima of angle density with associated dispersions,

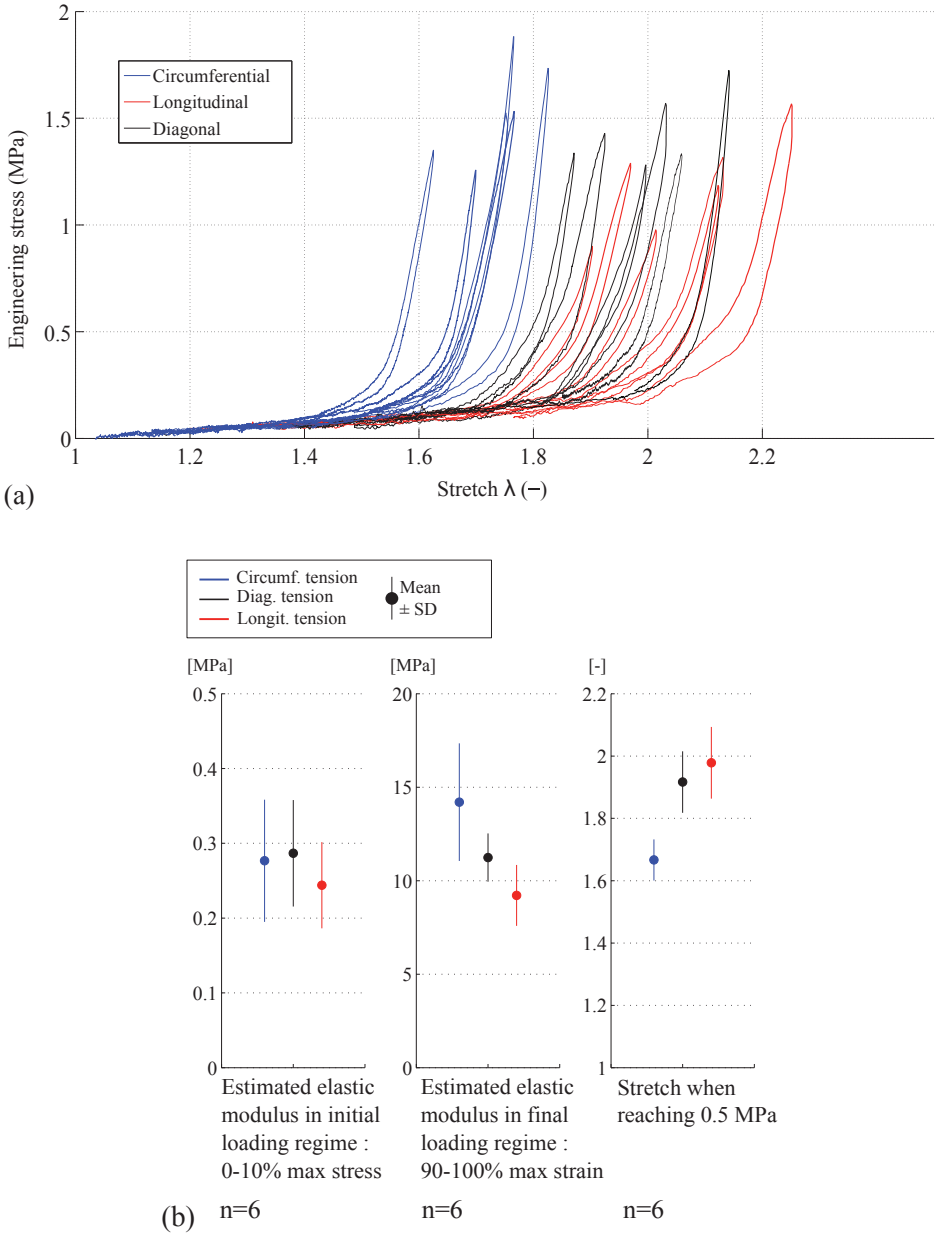

Figure 3.4 – (a) Macroscopic mechanical response: engineering stress v.s. stretch plotted for the three loading directions (blue: circumferential, black: diagonal, red: longitudinal); (b) statistical representations of the stiffness before (left) and after (middle) collagen engagement, and stretch when reaching 0.5 MPa (right); n stands for the number of investigated samples

see Appendix A.8.1 for more details) with the relative elongation λ and the fiber angle θ as polar coordinates. The angles $\pi/2$, $3\pi/4$, and π represent the circumferential, diagonal, and longitudinal directions respectively.

Adventitial collagen was organized in thick bundles showing a crimped morphology in the

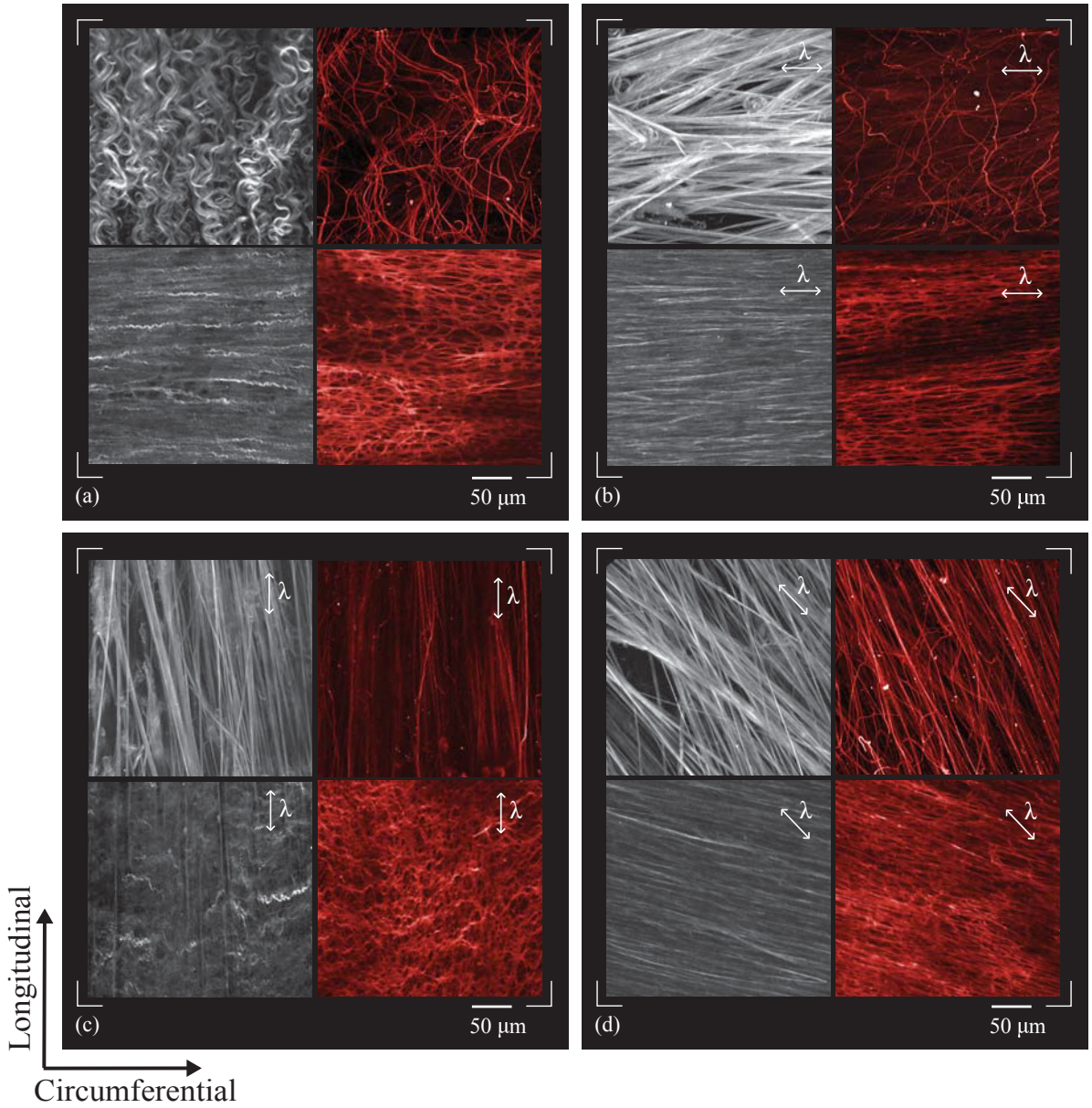

Figure 3.5 – Arterial microstructure imaged under multiphoton microscope. (a) Load-free state, (b) circumferential load (F = 0.8 N, $\lambda = 1.7$), (c) longitudinal load (F = 0.8 N, $\lambda = 2.1$), and (d) diagonal load (F = 0.8 N, $\lambda = 1.9$). The upper row of each image represents the adventitia; the lower row represents the media. Collagen network is represented in grey (left), elastin network is represented in red (right).

load-free state (Figure 3.5(a) - upper left). The analysis of in-plane fiber angles (Figure 3.6(a)) suggested a preferred direction close to the longitudinal direction, with an important dispersion ($\pm\pi/6$) due to bundle direction variability and to the influence of crimping, which limited the liability of interpretation. These collagen bundles underwent an uncrimping process and all appeared to align close to the direction of the load, whether its direction was circumferential (Figure 3.5(b) - upper left), longitudinal (Figure 3.5(c) - upper left) or diagonal (Figure 3.5(d) - upper left). In the three deformed states, in-plane fiber orientations (Figure 3.6(a)) showed

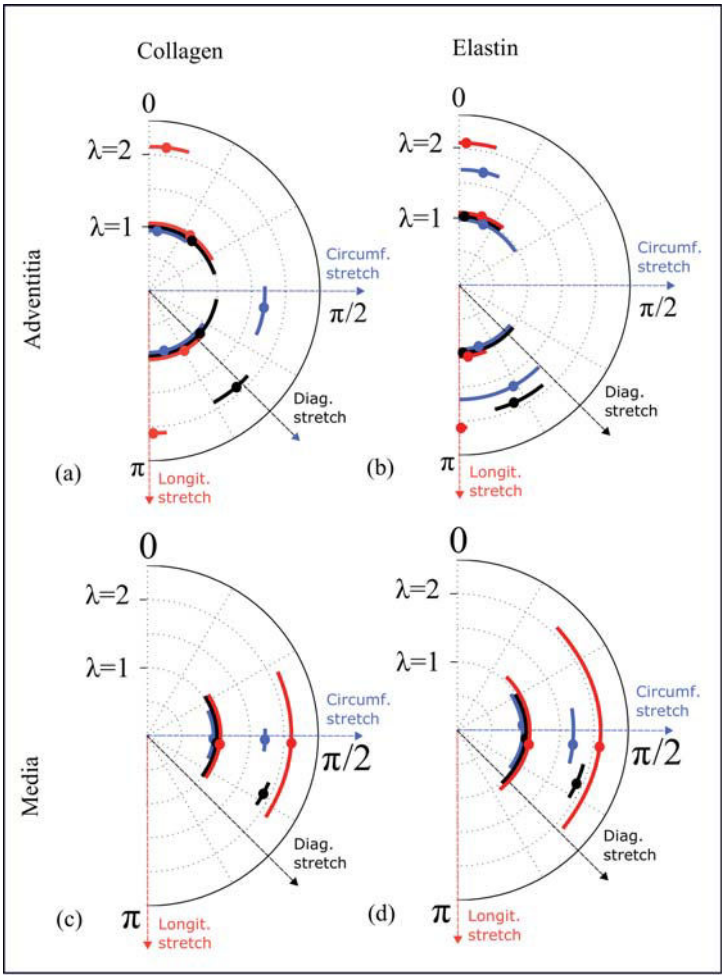

Figure 3.6 – Orientations of fiber networks represented with local angle density maxima and associated dispersions, for each constituent, layer, and load direction, under 0 and 0.8 N tensile load: (a) and (e) correspond to adventitial collagen, (b) and (f) to adventitial elastin, (c) and (g) to medial collagen, and (d) and (h) to medial elastin. The blue, black, and red colors correspond to the circumferential ($\lambda = 1.7$), diagonal ($\lambda = 1.9$), and longitudinal ($\lambda = 2.1$) directions, respectively. Represented network orientations correspond to the mechanical deformations of samples 1-3, tested respectively in the circumferential, diagonal and longitudinal directions.

identically limited dispersions ($\pm\pi/12$) around their respective local angle maximum.

Adventitial elastin took the form of a low-density meshwork, composed of thin fiber segments showing a preferred longitudinal direction with variously oriented transverse segments (Figure 3.5(a) - upper right). The analysis of in-plane fiber angles at rest (Figure 3.6(b)) confirmed the longitudinal orientation, with an important dispersion ($\pm\pi/6$) due to the variously oriented transverse fiber segments. Under load, the longitudinally oriented fiber segments underwent limited morphological changes: when the loading direction was circumferential (Figure 3.5(b) - upper right), the global orientation of the meshwork did not change significantly (a maximum of $\pi/6$ rotation - Figure 3.6(b)), although a spreading of the meshwork was noticeable (compare Figure 3.5(a) - upper right and 3.5(b) - upper right). Almost unchanged dispersions around

local density maxima (Figure 3.6(b)) confirmed this limited morphological change. When the load was applied longitudinally (Figure 3.5(c) - upper right), transverse segments aligned in the direction of the load, while the fibrous meshwork remained oriented in the longitudinal direction, which led to an unchanged angle density (Figure 3.6(b)). When the load was applied in the diagonal direction (Figure 3.5(d) - upper right), the meshwork underwent a limited reorientation towards the loading direction (a maximum rotation of $\pi/6$ and angle dispersions reduced by a factor 2 - Figure 3.6(b)), with transverse segments aligning with the principal segments orientations.

Medial collagen did not agglomerate into variously oriented bundles as in the adventitia, but took the form of thin parallel fibers distinctively oriented in the circumferential direction (Figure 3.5(a) - lower left) and showed a higher crimping frequency. Its morphology underwent limited changes under uniaxial load: when the loading direction was circumferential (Figure 3.5(b) - lower left), the fibers uncrimped and remained aligned in the circumferential direction (Figure 3.6(c)). When the loading direction was diagonal (Figure 3.5(d) - lower left), the fibers uncrimped - with a decrease of the dispersion of local angles by a factor 2 (Figure 3.6(c)) - and underwent a limited realignment in the loading direction - below $\pi/6$ rotation for the density maximum of local angles (Figure 3.6(c)). When the load was longitudinal (Figure 3.5(c) - lower left), i.e. perpendicular to the network direction, the fibers did not align in the loading direction and their crimping increased, as shown by the angular dispersion increased by a factor 2 (Figure 3.6(c)).

The medial elastin morphology was different from the one of adventitial elastin: at rest (Figure 3.5(a) - lower right), it took the form of a dense, structured meshwork preferentially oriented in the circumferential direction. Under load, it underwent limited morphology changes, namely partial alignment of transverse fiber segments in the loading direction, when the loading direction was circumferential (Figure 3.5(b) - lower right) or longitudinal (Figure 3.5(c) - lower right); the maxima of angle density remained unchanged, while the angular density dispersion decreased by a factor 2 (Figure 3.6d)); and a limited global reorientation when the loading direction was diagonal, with rotation of the angle density maximum below $\pi/6$.

3.3.3 Prediction of reorientations using an affine model

Table 3.2 presents the experimental values of local angle density maxima with the upper and lower angle bounds corresponding to the evaluated dispersions, together with the theoretical angles computed by applying the affine reorientation (Equation (3.2)) to the local angle maxima. The represented results in Table 3.2 refer to the testing of samples 1 to 3, respectively in the circumferential, diagonal and longitudinal directions. Figure 3.7 presents a statistical synthesis of fiber angles under uniaxial load, together with the theoretical angles computed by applying the affine reorientation (Equation (3.2)) to the local angle maxima. The represented results refer to the four sample groups tested in the three aforementioned directions (samples

		(a) Initial	(b) Final 1	(c) Final 2
Group 1 : samples 1-3		$\lambda_{diag} = 1.9 \pm 0.1$	$\lambda_{circ} = 1.7 \pm 0.05$	$\lambda_{long} = 2.1 \pm 0.2$
Collagen - adv.	Experimental [π]	$0.76^{+0.07}_{-0.02}$	$0.55^{+0.07}_{-0.06}$	$0.97^{+0.03}_{-0.05}$
	Affine prediction [π]	-	0.69	0.85
	Prediction error [π]	-	**25%**	**12%**
Elastin - adv.	Experimental [π]	$0.86^{+0.04}_{-0.09}$	$0.83^{+0.12}_{-0.13}$	$0.98^{+0.02}_{-0.01}$
	Affine prediction [π]	-	0.89	0.97
	Prediction error	-	**7%**	**1%**
Collagen - med.	Experimental [π]	$0.61^{+0.04}_{-0.03}$	$0.51^{+0.02}_{-0.02}$	$0.52^{+0.16}_{-0.17}$
	Affine prediction [π]	-	0.52	0.54
	Prediction error	-	**2%**	**4%**
Elastin - med.	Experimental [π]	$0.60^{+0.07}_{-0.06}$	$0.53^{+0.03}_{-0.08}$	$0.53^{+0.22}_{-0.21}$
	Affine prediction [π]	-	0.50	0.51
	Prediction error	-	**6%**	**4%**

Table 3.2 – Evaluation of the predictive accuracy of affine reorientation. Fiber angles are provided for initial and final states of two deformation scenarii (Samples 1-3) : (a) to (b) and (a) to (c)

1 to 12). Results show that the affine model predicted well the reorientation of the medial microstructure (collagen and elastin) as well as of the adventitial elastin, with prediction errors ranging from 1 to 7% (see Table 3.2 and compare black and white symbols in Figure 3.7) and a limited variability of fiber orientation between the analogous samples (Figure 3.7). Concerning adventitial collagen, for which we illustrated the ability to reorient along the different tested loading directions (Figure 3.5, Figure 3.6), the affine model largely under-predicted the fiber reorientation, as proven by the high prediction error (12 to 25%, see Table 3.2), observed independently on the analogous samples (Figure 3.7, upper left).

3.4 Discussion

Our results represent an original insight into the morphological changes that occur in the arterial tissue microstructure under variously oriented uniaxial loads. The experiments were performed on rabbit carotid arteries and focused on collagen and elastin networks of the media and of the adventitia. Our results suggest that the arterial tissue is more compliant in the longitudinal direction, as seen by a delayed stiffening phase. This result is consistent with previous studies performed by pressurizing and axially elongating dog carotids [Patel 70, Cox 75], rat and rabbit carotids [Cox 75] and by applying uniaxial tension on flat samples of human ascending aortas [Choudhury 09]. Conversely, this anisotropy has been shown contrary (stiffer tissue in the longitudinal direction) for human coronary arteries [Papageorgiou 88] and dog coronary arteries [Patel 70]. Indeed, no consensus has been gained up to now as regards the

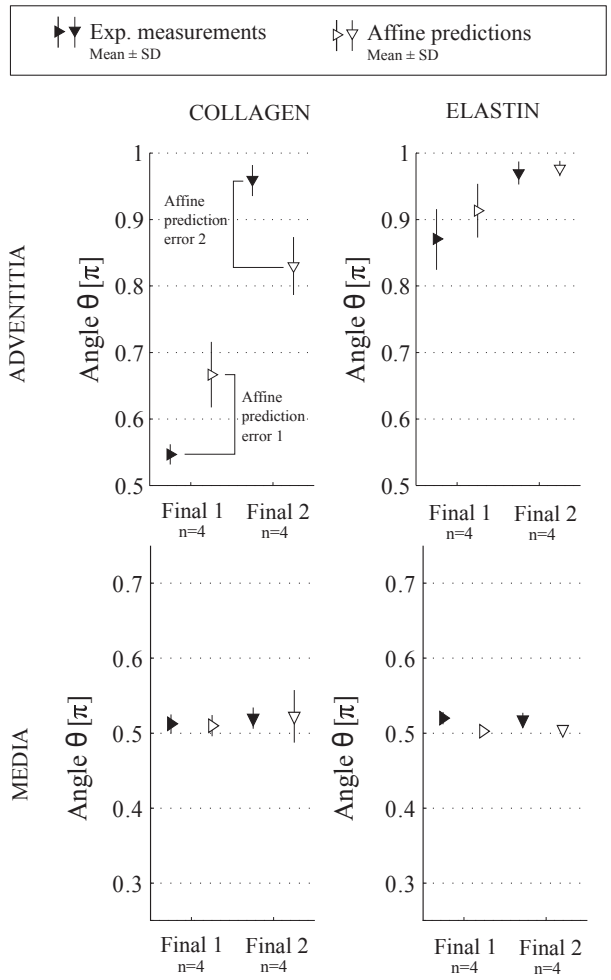

Figure 3.7 – Synthesis of the predictive accuracy analysis of affine reorientation. Final network orientations (Final state 1 and Final state 2) are averaged on n=4 samples under analogous deformation. Affine prediction errors in the case of adventitial collagen reorientation amount to 0.12π and 0.13π when reaching final states 1 and 2 respectively, corresponding to 22% and 14% error.

anisotropy of arteries, evidencing the complex interplay of load bearing contributions between the media and the adventitia. Recent results [Holzapfel 05] show clearly that the media is stiffer in the circumferential direction, while the adventitia is stiffer in the longitudinal direction. These results are in good agreement with the orientation of the fiber networks in each layer, but do not permit to draw any conclusion on the overall anisotropy of the tissue. In order to further understand the origin of this complex anisotropy, the distribution of load bearing properties between the media and adventitia should be further characterized along with the study of microstructure rearrangements.

Concerning the arterial microstructure in the load-free state, our results illustrate the layer-specific morphologies of the collagen and elastin networks which are similar to previous investigations [O'Connell 08, Rezakhaniha 12]. In the deformed configuration however, our results bring a novel comprehensive understanding of morphological changes occuring within the arte-

rial microstructure. Under uniaxial tensile loadings, affine kinematics [Billiar 97, Chandran 06] explain the reorientations of adventitial elastin, medial elastin, and medial collagen. This kinematically limited reorientation corresponds to a tight embedding of the fibers in their surrounding matrix, which could correspond to near-equivalent shear moduli of the fibers and of their surrounding matrix, or to the existence of molecular links which hinder further rotation of the inclusions within the matrix. Besides, these fibrous networks are unable to fully align in any of the presently applied uniaxial loading directions. Conversely, the adventitial collagen showed a remarkable potential to reorient in any of the applied loading directions (circumferential, longitudinal, diagonal). This reorientation is characterized by significant rotation amplitudes, that remain underestimated by affine reorientations. Although the protocols employed in the literature vary both in terms of characterization techniques (focusing on fiber decrimping [Lee 15] or on global fiber reorientation [Jayyosi 16]) and in terms of applied mechanical loadings (uniaxial, equi-biaxial [Lee 15]), our result is consistent with previous studies investigating collagen fiber kinematics in other tissues like porcine aortic leaflets [Billiar 97], bovine pericardium [Billiar 97], tissue constructs [Chandran 06] or human liver capsule [Jayyosi 15] and suggests that other mechanisms are activated in the reorientation of adventitial collagen under load.

Several limitations stem from the differences existing between our testing protocol and the real *in vivo* conditions. First of all, we should comment on the fact that we have considered temperature conditions lower than *in vivo* conditions. [Zemánek 09] studied the influence of the testing temperature on the mechanical response of the arterial wall and showed that samples are stiffer at ambient temperature than at *in vivo* temperature. There is no consensus on the impact of sample freezing on the change in the mechanical response of the sample [Zemánek 09, Canham 92, Venkatasubramanian 06, Chow 11]. However in the present study, test temperature and preservation conditions were identical for all experiments, and allowed to perform an inter sample comparison of the stiffness change during loading or among diverse load directions. Also, to our best knowledge, there is no study on the influence of the temperature on the fiber rotation. Secondly, we have applied a quasi-static elongation speed, which cannot render the dynamic conditions of the pulsatile hemodynamic load seen in large vessels. However, given the small variations in the arterial pressure and the preferred helical orientation of the adventitial collagen bundles, the orientations of the latter are believed not to vary significantly during a cardiac cycle. The choice of a quasi-static loading was made so as to ensure that the mechanical response was independent of the strain rate, as well as to limit the relaxation effects that would impair repeatability of the results. We should also comment on the choice of directions and ranges of load that go beyond the physiological load directions and ranges. While tension-inflation or equi-biaxial protocols allow the simulation of near physiological loadings, the present protocol was applied to reach our objective of comparing inter-layer and inter-constituent changes of the fiber networks within the microstructure subjected to diversified loading scenarii. Besides, the high stretches reached successively during preconditioning and imaging may have induced damage in the tissue, enhancing non-affine fiber rotation. However it is assumed that in this

case, the increase of fiber rotation would have affected all imaged fibrous networks, not only adventitial collagen. Accordingly, we did not observe any sign of damage within the imaged tissue, on any fibrous network of the arterial wall.

Furthermore, it should be mentioned that what we call "arterial microstructure" in this work is incomplete from the biological point of view, as our multiphoton microscopy provided only images of elastin and collagen fibers, with a spatial resolution of the order of 1 µm. The analysis could be complemented by the characterization of the deformations and reorientations of non-cellular components under varying levels of smooth muscle tones, as the latter mechanism is known to play an active role in arterial adaptive plasticity during the in vivo pressure cycle. At a lower scale, our analysis could also be complemented by the description of collagen fibrils rearrangements within bundles during decrimping and during post-decrimping stretching. Moreover, the observed morphology changes during uniaxial tension in carotid samples should be compared to morphology changes occurring in identically deformed carotids from other species, with different smooth muscle, collagen and elastin content. To the authors' knowledge, identical deformation protocol has not been yet applied to samples of other arteries or other species' carotids. However, and to engage the discussion, the recent study of [Keyes 11] on mouse aortas, showed that adventitial collagen could undergo high amplitude rotations under pressurization (up to $\pi/3$), while medial networks kept their orientation unchanged. On the contrary, the results of [Chen 13], performed on porcine coronary arteries, illustrated under flat biaxial tension the adventitial collagen's decrimping mechanism but a limited rotation potential. Nevertheless, our analysis was intended as a first step, focusing on the major load-bearing components of the arterial wall. Furthermore, a nano-scale imaging resolution could investigate the influence of nanoscale aldehyde cross-links on the observed morphology rearrangements. Such an analysis would give biological foundations to the observed reorientations, explaining why several fibers can encounter large rotations whilst others are restricted to small rotations.

Finally, the level of representativeness of the microscopy images with associated angle distributions of collagenous and elastic networks should be commented. In particular concerning automated angles extraction, the Fast Fourier Transform algorithm applied on adventitial collagen at rest (high density crimped bundles) provided information about local angles but did not allow the extraction of global collagen bundle orientation. In order to capture full morphological rearrangements of adventitial collagen under load, a specific method should be developed so as to analyze collagen orientation at different scales: crimping scale (10 µm) and global bundle scale (100 µm). With the objective of comparing true reorientations with affine predictions, we here overcame this image processing issue by comparing only deformed configurations, for which the orientations at crimping scale and at global bundle scale are identical.

3.5 Conclusion and outlooks

We have shown that arterial microstructure presents inter-layer differences between collagen network and elastin network morphologies. These inter-layer differences concern in particular the ability to rearrange under variously oriented uniaxial loads. We have shown that even though the fibers of the vascular microstructure undergo the same macroscopic deformation, they rearrange in their own specific way, and differently from one vascular layer to the other. This finding brings additional insight for current multiscale model formulations which take into account specific kinematics of arterial collagen and its relation to the surrounding matrix [Stylianopoulos 07, Fan 14]. It also confirms the need to consider the arterial wall as a composite structure composed of different mechanically relevant layers with different mechanical properties [Holzapfel 05]. Our results also suggest the need to further investigate the underlying mechanisms that govern adventitial collagen rearrangement, in particular uncrimping and post-uncrimping fiber rotation. Given that the affine reorientation underestimates real fiber rotation of adventitial collagen, it appears interesting to propose a micromechanical origin to collagen fiber rotation. In particular, we hypothesize that the macroscopic strain concentrated in a highly heterogeneous microstructure induces a heterogeneous field of displacement gradients, itself generating microscopic spin that can be important if the shear moduli of the fibers and of the matrix are significantly different. These spins may induce material rotation within the structure which superimposes with affine reorientation. Future multiscale models could test this hypothesis by accounting for the existence of local spin vectors, promoting fiber rotations.

Chapter 4

Kinematics of collagen fibers in carotid arteries under tension-inflation loading

Authored by: Witold Krasny, Hélène Magoariec, Claire Morin and Stéphane Avril

Published in: Journal of the Mechanical Behavior of Biomedical Materials, in press, available online 12 August 2017, DOI: 10.1016/j.jmbbm.2017.08.014.

Contribution: Witold Krasny designed the experimental setup according to the state-of-the-art and preliminary studies prepared at the Laboratory of Tribology and Dynamics of Systems (Ecole Centrale Lyon). He prepared, carried out, and postprocessed all the experiments. He also proposed and implemented the new approach of image processing. He also elaborated on his own possible relationships between the experimental observations and tensegrity models.

Contents

Résumé

La biomécanique de la matrice extracellulaire détermine le comportement mécanique de l'artère à l'échelle macroscopique (voir la revue de l'état de l'art présentée au chapitre 2). En particulier, l'organisation spatiale des réseaux de fibres de collagène joue un rôle important. De précédentes études expérimentales ont montré que dans la plupart des parois artérielles, les fibres sont disposées selon des directions préférentielles. Cependant, la question du réalignement des fibres de collagène pendant la déformation des tissus est sujette à débat : bien que certains auteurs affirment que les fibres subissent des déformations affines [Wan 12, Sacks 03a], d'autres ont montré le contraire [Billiar 97, Chandran 06, Lake 12].

Afin d'étudier cette question, le réalignement des fibres de collagène situées dans l'adventice d'artères carotides a été mesuré par microscopie multiphoton. Les images obtenues ont été analysées grâce à une nouvelle méthode de quantification basée sur la comparaison de spectres de Fourier. La cinématique des fibres a été comparée pour deux types de chargements macroscopiques appliqués sur des échantillons artériels cylindriques : traction axiale à pression interne constante (scénario 1) et gonflement à élongation axiale constante (scénario 2). Les résultats ont révélé que, bien que le tissu ait subi des élongations macroscopiques au-delà de 1,5 dans la direction circonférentielle, les directions des fibres sont demeurées inchangées lors du scénario 2 de chargement. À l'inverse, les fibres se sont réalignées significativement dans la direction axiale lors du scénario 1 de chargement. Dans les deux cas, le mouvement des fibres de collagène n'a pas satisfait le principe de la cinématique affine, avec toutefois une différence significative entre les deux cas de chargement : les prédictions affines des réorientations de fibres ont fortement sous-estimé les réorientations réelles observées lors de la traction axiale à pression constante (scénario 1), tandis qu'elles ont surestimé les réorientations réelles observées pendant le gonflement à élongation axiale constante (scénario 2). En guise d'ouverture, une interprétation de cette cinématique spécifique des fibres de collagène de l'adventice est proposée, reposant sur les interactions complexes de traction-compression qui existent entre des fibres de collagène très rigides et des protéines environnantes plus souples. Une représentation discrète, de type "tenségrité" de la matrice extracellulaire dans l'adventice est proposée, prenant en compte ces interactions. Cette représentation mécanique de la microstructure de l'adventice a permis d'interpréter la cinématique des fibres de collagène lors des deux scenarii de déformation du tissu artériel.

Originalités des méthodes appliquées :

- *Variété de scenarii de chargement : les échantillons d'artère ont subi à la fois des chargements de tension axiale à pression interne constante, et des chargements de gonflement à élongation axiale constante ;*

- *Précision de la nouvelle méthodologie d'interprétation des réarrangements de la microstruc-*

ture : la méthode incorpore une simulation numérique de la cinématique affine des fibres et permet une comparaison avec la cinématique des fibres mesurée expérimentalement.

Résultats à retenir :

- *Collagène de l'adventice : les prédictions affines ont fortement sous-estimé les réorientations des fibres lors des chargements en tension axiale à pression constante ; et elles ont surestimé les réorientations des fibres lors du chargement en gonflement à longueur constante ;*
- *Un modèle planaire de tenségrité a permis d'interpréter cette cinématique des fibres, soulignant l'influence des conditions aux limites et des interactions fibre-fibre.*

Abstract

Biomechanics of the extracellular matrix in arteries determines their macroscopic mechanical behavior. In particular, the distribution of collagen fibers and bundles plays a significant role. Experimental data showed that in most arterial walls there are preferred fiber directions. However, the realignment of collagen fibers during tissue deformation is still controversial: whilst authors claim that fibers should undergo affine deformations, others showed the contrary. In order to have an insight about this important question of affine deformations at the microscopic scale, we measured the realignment of collagen fibers in the adventitia layer of carotid arteries using multiphoton microscopy combined with an unprecedented Fourier based method. We compared the realignment for two types of macroscopic loading applied on arterial segments: axial tension under constant pressure (scenario 1) and inflation under constant axial length (scenario 2). Results showed that, although the tissue underwent macroscopic stretches beyond 1.5 in the circumferential direction, fiber directions remained unchanged during scenario 2 loading. Conversely, fibers strongly realigned along the axis direction for scenario 1 loading. In both cases, the motion of collagen fibers did not satisfy affine deformations, with a significant difference between both cases: affine predictions strongly under-estimated fiber reorientations in uniaxial tension and over-estimated fiber reorientations during inflation at constant length. Finally, we explained this specific kinematics of collagen fibers by the complex tension-compression interactions between very stiff collagen fibers and compliant surrounding proteins. A tensegrity representation of the extracellular matrix in the adventitia taking into account these interactions was proposed to model the motion of collagen fibers during tissue deformation.

Originality of the developed / applied methods:

- Variety of loading scenarii: the artery was deformed by applying both axial tension under constant internal pressure and inflation under constant axial stretch;
- Precision of the newly developed quantification methodology: the method incorporates the numerical simulation of affine fiber kinematics, and its comparison to experimentally measured fiber kinematics directly in the Fourier space.

Main results:

- Adventitial collagen: affine predictions strongly under-estimated fiber reorientations during axial tension under constant pressure and over-estimated fiber reorientations during inflation under constant length;
- A planar tensegrity model allowed interpreting this load-dependent fiber kinematics, highlighting the important role of boundary conditions and fiber-fiber interactions..

4.1 Introduction

The arterial tissue exhibits a hierarchical microstructure, made of three concentric layers, namely, starting from the arterial lumen towards the external surface of the vessel: the intima, the media, and the adventitia. The extracellular matrix of these three layers is made of arrangements of collagen and elastin fiber networks, with a specific organization depending on the layer. In particular, the non-linear mechanical behavior of the arterial tissue is often associated with the progressive rearrangements of these different fiber networks, at the 10 to 100 µm scale. In the present contribution, we chose to focus on the adventitial collagen, since it was recently shown to be the fiber network the most prone to mechanically-induced rearrangements [Schrauwen 12, Chen 13, Sugita 17, Krasny 17a]. In particular, this network, composed of thick bundles of type I collagen fibers [Dingemans 00], is the major structural component of the adventitia, due to its important load-bearing function preventing over-distensions [Humphrey 10]. Eventually, its remodeling under pathological situations such as aneurysms may degrade this load bearing function [Humphrey 00].

Various experimental loading setups coupled to live microscopy provided a better understanding of the fiber kinematics, allowing progressive improvements of structural constitutive models of the arterial wall. Namely, in the unloaded configuration, the adventitial collagen network shows randomly distributed orientations and a high degree of crimping [Dingemans 00, O'Connell 08, Rezakhaniha 12]. Upon mechanical loading, the collagen bundles progressively unfold [Canham 92, Greenwald 97]. The measurement of fiber waviness [Chen 11, Schrauwen 12, Wang 13, Sugita 17] revealed in particular that recruitment, or engagement of collagen fibers, is gradual (unsynchronized among fibers) and starts at a finite strain [Hill 12, Chow 14]. The process can differ whether the observed vascular region is close or remote from the heart (distal regions vs. proximal regions) [Zeinali-Davarani 15]. Collagen fiber bundles may also undergo a progressive realignment in response to the application of a macroscopic deformation [Arkill 10, Keyes 11, Chen 11, Chow 14, Krasny 17a]. This realignment has been observed to take place after recruitment, in order for the artery to continue deforming without damaging the engaged fibers [Wang 13], and showed discrepancies in fiber realignment amplitudes, depending on the initial fiber angle and on the type of deformation [Wan 12, Chen 13]. The fiber bundles are finally stretched upon further mechanical loading. Eventually, rupture of the collagen fibers may lead to the rupture of the adventitial layer. Consequently, a correct assessment of the mechanical fields within the adventitia relies on a correct description of the collagen network and of its evolution during loading.

The aforementioned experimental findings enhanced the first generation of structural models based on the definition of a strain energy function, which considered the arterial wall as a soft matrix material reinforced by variously distributed fibers families [Holzapfel 01, Zulliger 04, Holzapfel 05, Gasser 07], with the addition of a fiber activation stretch or of a proba-

bility distribution function, accounting for gradual recruitment at finite strain [Roy 11, Hill 12]. All these models assume an affine deformation of the collagen network, as experimentally evidenced by several contributions [Sacks 03a, Wan 12], i.e. the fibers are assigned to follow the overall material deformation: they are firmly embedded in the surrounding matrix. The resulting understanding of collagen kinematics and its integration in structural models provides today satisfactory predictions of the artery's mechanical response [Zulliger 04, Holzapfel 05]. However, questions remain about the microscopic mechanisms governing the observed rearrangements. The latter question is especially raised with regards to past studies, revealing non-affine collagen kinematics [Billiar 97, Chandran 06, Jayyosi 16, Krasny 17a], illustrating the complexity of arterial microstructure properties. Whether they are attributed to the decrimping process [Lee 15], to fiber-fiber interactions [Chow 14] or to fiber-matrix interactions [Billiar 97, Thorpe 13], non-affine collagen kinematics are currently taken into account in a novel generation of multiscale and micromechanical modeling approaches [Stylianopoulos 07, Fan 14, Zhang 13, Morin 15], but their microstructural and micromechanical origin has not yet been experimentally documented nor understood, which constitutes a limit for further refined multi-scale formulations. Specifically, few studies investigate the dependence of fiber kinematics on the loading type [Wan 12, Chen 13], and to the authors' knowledge, none have quantitatively compared fiber rotations for the same tracked fibers undergoing different loading scenarii, while comparing them to affine predicted reorientations. In the present study, we bridge this gap by answering the following questions: do particular deformation scenarii or conditions challenge affinity of fiber motion? Is the fibers' behavior different under the different loading scenarii? To this aim, we submitted carotid arteries from New Zealand White rabbits to tension-inflation tests, while quantitatively characterizing the reorientations of its adventitial collagenous microstructure with multiphoton microscopy.

4.2 Materials and methods

The materials and methods described hereafter are further detailed in the Appendix "Experimental methodology".

4.2.1 Sample preparation

Carotid arteries (n=4) were harvested at the Veterinary Campus of the Université de Lyon (VetAgro Sup, Marcy l'Étoile, FR) from healthy male New Zealand White rabbits, weighing 3 kg approximately. The cadavers, kindly provided by Centre Lago (Vonnas, FR), were previously sacrificed under compliance with the NIH Guide for Care and Use of Laboratory Animals. Immediately after excision, the samples were stored in a bath of phosphate-buffered saline (10x PBS, pH 7.1) at 5°C and tested within 36 hours after harvesting. For each sample, a 15±1 mm long cylindrical segment was extracted for mechanical testing (Figure 4.1(a), left image) as well as three 0.5 mm long rings for optical measurement of the sample thickness (Figure 4.1(a), right image). The sample tips were cannulated onto the inlet and outlet needles

using suture wire (Figure 4.1(a)). Two plastic rings previously fixed on the needles at the suture loci (Figure 4.1(f)) prevented slipping during axial tension and provided a waterproof sealing during inflation. The sealing rings provided structural support to sustain axial tension and no damage was observed on the samples at the locus of the ring after the mechanical tests.

4.2.2 Mechanical setup

We hereafter describe the mechanical setup that enabled tension-inflation of the carotid arteries. Applying an axial tension was made possible by a screw-driven high precision tensile machine (Deben® Microtest tensile/compression stage) equipped with a 150 N load cell (Figure 4.1(b) and 4.1(e)) which provided a 0.01 N precision with satisfactory stability during the tests. The two heads of the machine moved in opposite directions, allowing the operator to identify and keep track of a region of interest, while the microscope was positioned at the center of the sample. The force offset was zeroed prior to the mounting of the sample. Verifying that the axial force and sample length were unchanged after mounting allowed limiting the risk of potential pre-strain and pre-stress in the sample. A pressure loading was applied by a syringe pump (Figure 4.1(c)) (Harvard Apparatus®) equipped with a ±300 mmHg pressure transducer (FISO® optical fiber connected to the fluid network at the sample inlet) which infused phosphate-buffered saline (10x PBS, pH 7.1) at a constant ambient temperature of 20°C. Applying a target pressure was made possible by the pump and pressure transducer communicating under closed loop control (PID mode). The settings of the proportional gain and integrator constant were iteratively adjusted in order to obtain a stable pressure step, characterized by a reasonable pressurizing time and limited overshooting. During the mechanical loading, the sample was continuously immerged in PBS at a constant ambient temperature of 20°C (Figure 4.1(b)). Also, the pressure readouts at inlet and outlet were compared to ensure that the pressure was uniformly distributed and did not vary due to friction forces in the needles during infusion. An optical camera (Nikon® D7200 equipped with Nikon® AF-S VR Micro-Nikkor optical 105 mm f/2.8G IF-ED lens) was used to acquire images of the deforming arterial sample and of the three sample rings, for subsequent analysis of sample diameter and sample thickness (Figure 4.1(a)). Noticeably, the measurement of the arteries' diameter showed a limited variability along the sample length (standard deviations being as low as 2% of the measured mean diameters).

4.2.3 Multiphoton Microscopy

The multiphoton microscope (NIKON, A1R MP PLUS®) of the IVTV platform (Engineering and Ageing of Living Tissues Platform, ANR-10-EQPX-06-01, Lyon, FR) was used to image the fibrous microstructure of the tested arterial segments (Figure 4.1(d)), without prior staining or fixation. Using a 870 nm excitation wavelength [Hill 12], the collagen second harmonic generation (SHG) signal was acquired through 400-492 nm band-pass filters. The multiphoton imaging modality was well documented in previous studies [Van Zandvoort 04, O'Connell 08, Sugita 17], should additional information be needed. The imaging resolution of the microscope

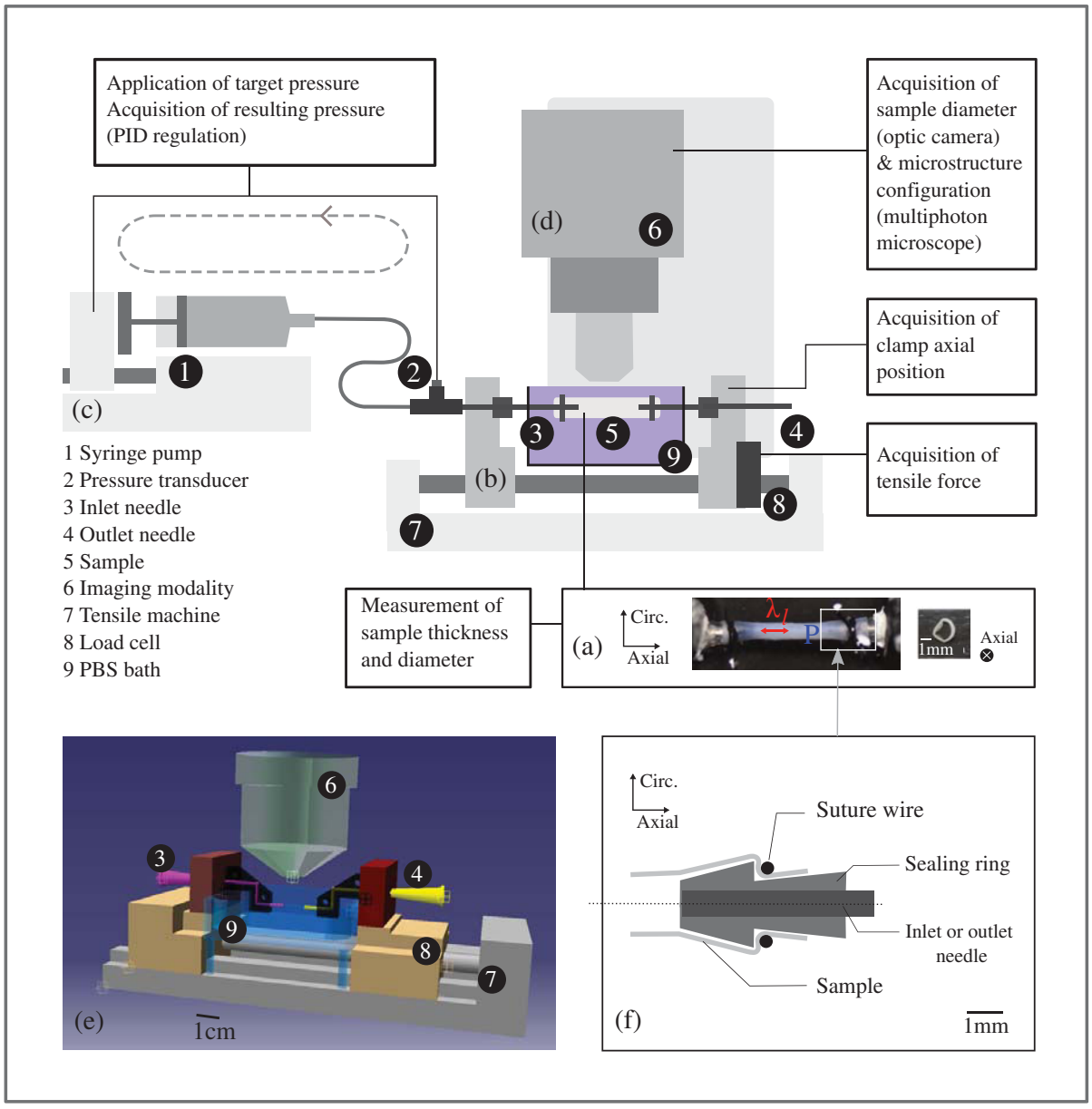

Figure 4.1 – Experimental tension-inflation setup showing (a) a sample cannulated on the needles and loaded, comprising of (b) the tensile machine, (c) the syringe pump, (d) imaging modalities (alternatively optical camera and multiphoton microscope); (e) a schematic representation of the tension-inflation setup, showing the tensile machine, the PBS bath in blue transparency, needle stiffening casings in black transparency, inlet (pink) and outlet (green) needles, the multiphoton microscope's objective in grey (center); and (f) a section sketch of the cannulated arterial sample for tension-inflation testing, presenting the sealing method.

was set to 0.5 µm in all directions [Hill 12, Schrauwen 12] with a 512 µm^2 imaging window. An optimal compromise was achieved between image quality and acquisition time by setting the scan speed to 0.5 frames per second, with two-frame averaging. These setting resulted in 60 to 90 µm thick stacks of images with acquisition times of approximately 15 minutes. A period of 5 minutes was always observed after applying an incremental load step to the artery in order to stabilize the tissue before imaging it. However, this apparent creeping occurring after each

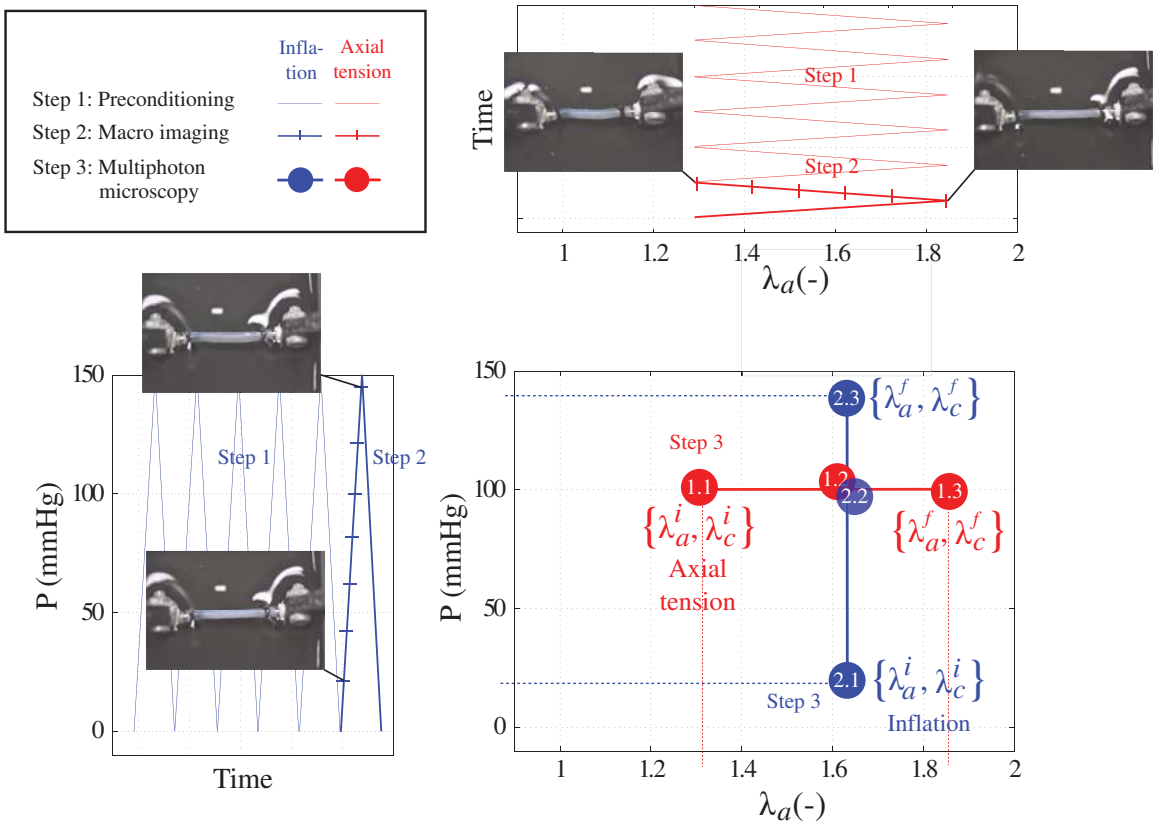

Figure 4.2 – Tension-inflation loading protocol, comprised of three loading steps for both axial tension and inflation scenario, namely (Step 1) preconditioning (thin line), (Step 2) macroscopic imaging sequence (thick line with ticks denoting macro images), and (Step 3) multiphoton microscopy sequence (thick line with circles denoting loading configurations in which the collagen morphology was acquired). The morphologies referring to load states 1.1, 1.3, 2.1 and 2.3 are used as inputs for subsequent image processing and fiber kinematics characterization (see section 4.2.5 and Figure 4.3). The tensile loading scenario is represented in red, whereas the inflation loading scenario is represented in blue.

load step applied on the arterial tissue did not change the microstructural morphology of the tissue, as observed by live imaging.

4.2.4 Loading scenario and data acquisition

In agreement with well-established tension-inflation protocols for arteries [Humphrey 10,Keyes 11], two loading scenarii were considered, namely axial tension under constant imposed pressure and inflation under constant axial stretch. Four carotids were used in the present study, carotid samples S1 and S2 were tested under both loading scenarii, while carotid samples S3 and S4 were tested under only one loading scenario, i.e. the axial tension and the inflation scenario, respectively. For each sample and each loading scenario, the loading protocol was composed of three loading steps (Figure 4.2). Step 1 consisted in five preconditioning cycles, carried out in order to cancel the tissue's deformation history, step 2 consisted in one loading cycle dedicated to the acquisition of macroscopic sample dimensions, and step 3 consisted in one final loading

cycle dedicated to the acquisition of the collagen load-dependent morphologies, by means of multiphoton microscopy.

As a result, on the one hand, three samples (S1, S2, and S3) underwent a total of seven axial tension cycles (with the two last cycles dedicated to data acquisition) between 0.1±0.02 and 0.8±0.02 N axial force, at an imposed velocity of 2 mm · min^{-1}, corresponding to an axial strain rate of 0.2 min^{-1}, with maintained pressure (P = 100 mmHg). On the other hand, three samples (S1, S2, and S4) underwent a total of seven inflation cycles (with the two last cycles dedicated to data acquisition) between 20 and 140 mmHg, by steps of 20 mmHg imposed within 30 seconds, under a maintained *in vivo* axial stretch (λ_a = 1.6±0.05). The *in vivo* stretch, defined as the stretch resulting in unchanged axial reaction force during inflation [Humphrey 10], was determined by adjusting the clamp position during the preconditioning cycles. The samples' reference cross-sectional areas A_0 were computed from the measures of the unloaded sample diameters after preconditioning (Step 1 of the protocol) and from the initial thicknesses. In the case of the axial tension load scenario, the zero axial strain position was obtained from the axial position at which the axial force returned to zero after preconditioning. The measurement of the sample length after preconditioning provided the reference length l_0 on the basis of which the macroscopic axial stretch was computed as $\lambda_a = l/l_0$. l and l_0 refer to the current and the reference inter-clamp lengths of the sample, respectively. Similarly, in the case of the inflation loading scenario, the zero circumferential strain position was obtained from the measurement of the sample diameter after preconditioning, when the inflation system was opened, forcing the pressure to return to 0 mmHg in the sample. The measurement provided the reference diameter D_0 on the basis of which the macroscopic circumferential stretch was computed as $\lambda_c = D/D_0$. D and D_0 refer to the current and the reference diameters of the sample, respectively. After preconditioning, the gauge length of the samples (between suture) measured l_0 =12±2 mm, while the unloaded sample diameter measured D_0 =2.0±0.3 mm.

Macroscopic images of the samples (Step 2 of the loading protocol) were obtained every 20 mmHg during inflation and every 0.5 mm during axial tension, corresponding to 0.2±0.05 stretching steps approximately (see thick lines with ticks on Figure 4.2, showing macroscopic imaging). Microscopy images (Step 3 of the protocol) were obtained at 1.3±0.05, 1.6±0.05, and 1.8±0.05 stretches during axial tension (referenced as loading configurations 1.1, 1.2, and 1.3, respectively (Figure4.2), and at 20 mmHg, 100 mmHg, and 140 mmHg pressures during inflation (referenced as loading configurations 2.1, 2.2, and 2.3, respectively (Figure 4.2)). The mechanical configurations 1.1 and 2.1 will be referred to in the following as "reference configurations", while the mechanical configurations 1.3 and 2.3 will be referred to as "loaded configurations".

As concerns the intermediate loading configurations 1.2 and 2.2, they were not used in the Fourier methodology enabling the characterization of fiber kinematics affinity but provided a

refined insight at the evolution of the microstructure during the loading (see Figure 4.4 in section 4.3), and a verification of the right tracking of the same imaging windows fields of view. The reference configurations included partial loading (λ_a = 1.3, P = 100 mmHg for scenario 1, λ_a = 1.6, P = 20 mmHg for scenario 2) for several reasons. First, we chose to post-process adventitial collagen images characterized by a sufficient degree of decrimping, hence avoiding imprecisions in the Fourier analysis of the global orientations of the fibers (at the bundle scale); second this choice prevented the potential buckling of the samples at high pressure and low axial stretch [Han 13], which could have impaired the analysis of macroscopic and microscopic kinematics.

4.2.5 Image analysis and characterization of fiber kinematics

The previously collected mechanical and microstructural information is now used to analyze the fiber rearrangements and the corresponding fiber kinematics for the different loading scenarii. Firstly, image stacks corresponding to the reference configurations 1.1 and 2.1 (Figure 4.2), as well as image stacks corresponding to the loaded configurations 1.3 and 2.3 (Figure 4.2), were processed using a Maximum Intensity Projection (MIP) algorithm (Figure 4.3(a1) and (a2)), revealing optimal in-plan morphology. In fact, previous studies have investigated the transmural angle (radial direction) of the fibers and showed that it is negligible in comparison to the in-plane angle [Roy 11,Rezakhaniha 12,Schrauwen 12]. As a result, although the negligible transmurality information is lost, the fibers are represented with maximal effective length, strongly improving the interpretation of their in-plane orientation. A preliminary geometrical analysis revealed that the potential evaluation error of in-plane fiber orientation caused by projecting slices of a cylinder into a 2D image, was always under 5% (maximal at the image periphery, where the tangential plane shows the highest inclination to the projection plane), and hence was considered negligible.

Secondly, the affine transformation was simulated, by numerically applying axial and circumferential deformations to the reference configurations. In more details, for the loading scenario 1 (axial tension under constant pressure), a numerical axial stretch λ_a^* together with the corresponding measured transverse contraction (resulting from diameter change) λ_c^* were gradually applied to the image of the unloaded configuration 1.1 (Figure 4.2). Similarly for loading scenario 2 (inflation under constant axial stretch), a numerical circumferential stretch λ_c^* (corresponding to outer diameter change) was gradually applied to the image of the reference configuration 2.1 (Figure 4.2). Image resolution remained unchanged by the use of subpixel interpolation.

Afterwards, the 2D Fourier spectrum moduli were extracted from the collagen morphologies for both the numerically deformed (Figure 4.3(c1)) and the experimentally loaded configurations (Figure 4.3(c2)). Use of the 2D Fourier transforms allowed removing the non-mechanical optical effects (such as contrast or brightness effects) as well as the artifacts (features occurring

at short lengthscale, such as the decrimpring process), and the inequality of imaged windows. Previous studies have proven the potential of the Fast Fourier transform (FFT 2D) for the analysis of biomedical images, and in particular the ability of the method to extract fiber angle densities or isotropy parameters [Ayres 06, D'Amore 10, Schriefl 12, Polzer 13, Chow 14, Morrill 16]. Here a special attention was paid to work with spectra being matrices of identical dimensions (Figure 4.3, red cropping square). A preliminary analysis allowed verifying that the locus of the cropping center in the image did not affect the results. Each spectrum was then multiplied by the Fourier transform of a Gaussian window whose size corresponded to the characteristic width of a collagen bundle (1/25 of the imaged window, equivalent to 20 µm), allowing the filtering of undesirable small-length features in the images and the highlighting of meaningful morphological features (namely fiber orientations at the scale of the bundles) (Figure 4.3(d)) [Zisserman 14]. The obtained 2D Fourier spectrum moduli S* and S (numerically and experimentally deformed microstructures, respectively) were finally compared using a relative norm-2 (Figure 4.3(d)).

We gradually increased the numerically applied affine deformation, eventually reaching a minimum in the relative difference between the two collagen morphologies (i.e. configurations 1.3 or 2.3 and the corresponding affine deformations of configurations 1.1 and 2.1, Figure 4.2). As a result, this minimum corresponded to the application of a fictitious stretch that should be applied to the reference microstructure in order to reach by affine deformation the most similar microstructure to the loaded experimental configuration. Eventually, this fictitious stretch was compared to the actual experimentally measured stretch. If the fictitious stretch and the actual stretch were to be equal, the kinematics at the scale of collagen fibers would actually be affine.

4.3 Results

First, we qualitatively compared the microstructure evolution between the two loading scenarii (Figure 4.4). Figure 4.4(a) shows that, under axial tension at a constant intermediate pressure, adventitial collagen fibers achieved full straightening and reoriented towards the macroscopic strain direction. On the contrary, Figure 4.4(b) shows that, under inflation at the *in vivo* stretch, collagen fibers of the adventitia achieved full straightening but the orientation of the majority of the fibers remained unchanged. Similar images, and hence similar analyses were obtained for the 2 other samples in each loading direction. Imaging always the same region of interest in the tissue at the different stages of the deformation made the characterization of fiber reorientations reliable.

As a second step, we quantitatively analyzed the kinematics of the fiber rotation for each loading scenario (Figure 4.5). For loading scenario 1 (corresponding to axial tension under constant imposed pressure), the difference δ between the numerical and the experimental morphologies started, for the three samples, at high values: this denotes different microstructure

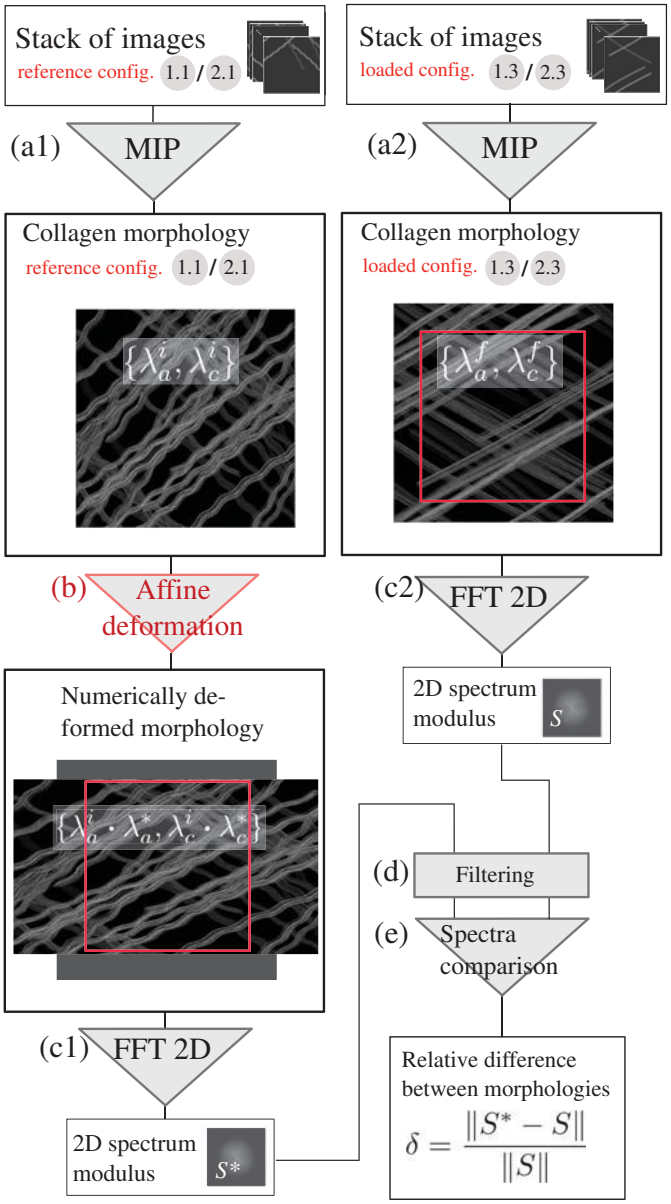

Figure 4.3 – Series of operations summarizing the image analysis and characterization methodology of fiber kinematics. The methodology consists in (i) analyzing the stacks of images in the reference (a1) and loaded (a2) configurations by means of a Maximum Intensity Projection (MIP); (ii) numerically applying a gradual affine deformation to the reference configurations (b); and (iii) comparing the microstructure configurations through their FFT spectra (c), so as to extract the affine deformation (applied numerically), which produces a microstructure with minimum relative difference between the experimental morphology and the numerically deformed one (d). For each loading scenario, the axial stretch ranges between λ_a^i (reference configuration) and λ_a^f (loaded configuration)(λ_a^i=λ_a^f in the case of the inflation loading), whereas the circumferential stretch ranges between λ_c^i (reference configuration) and λ_c^f (loaded configuration). In this figure, the used images are custom-drawn visual representations of collagen morphology, chosen for clarity and representativeness.

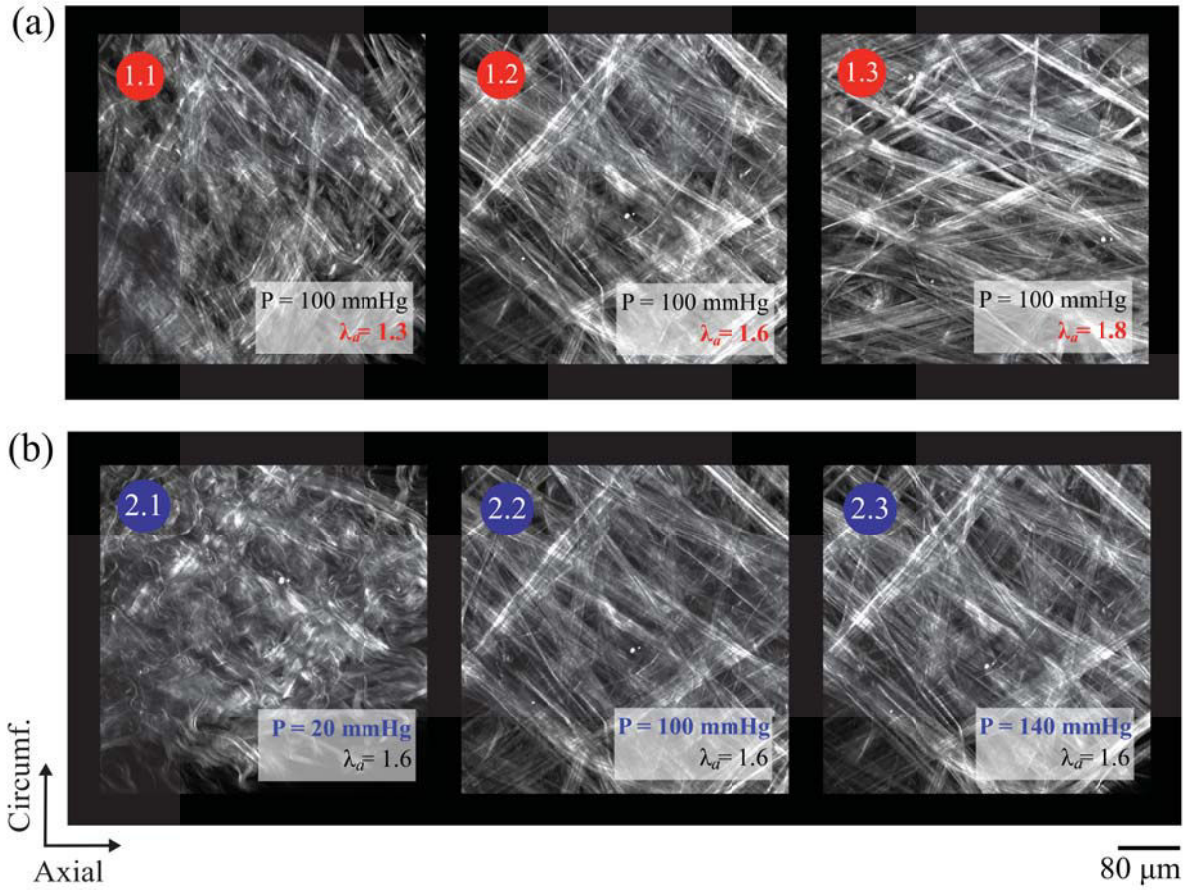

Figure 4.4 – Adventitial collagen morphology under both loading scenarii, revealed through multiphoton microscopy for sample S1: (a) tension under imposed constant pressure and (b) inflation under imposed constant axial stretch.

morphologies between the reference arterial configuration and axially loaded arterial configuration, particularly in terms of fiber orientations (Figure 4.5(a1)). As the numerically applied affine deformation increased, the fibers were gradually reoriented towards the direction of axial tension, hence coming closer to the experimental fiber orientations of the loaded configuration: the relative difference δ between the spectra decreased. When the applied affine deformation became too high, the relative difference increased again: affine deformation induced fiber rotations being larger than the ones experimentally observed (Figure 4.5(a3)). In between, the relative difference δ reached a minimum value, when the fibers of the experimentally and the numerically deformed configurations showed the closest fiber orientations (Figure 4.5(a2)). For the three tested samples S1, S2, and S3, δ reached its minimum at axial stretch values comprised between 1.85 and 2.1, i.e. to obtain similar morphologies, the numerically applied stretch needs to be 20% higher than the experimentally applied stretch (Figure 4.5, black dots). For loading scenario 2, δ starts, for the three samples, at very low values: this denotes similar microstructure morphologies between the reference and the loaded arterial configurations, particularly in terms of fiber orientations (Figure 4.5(b1)). As the numerically applied circumferential stretch increased, the fibers reoriented towards the circumferential load direction, hence driving away

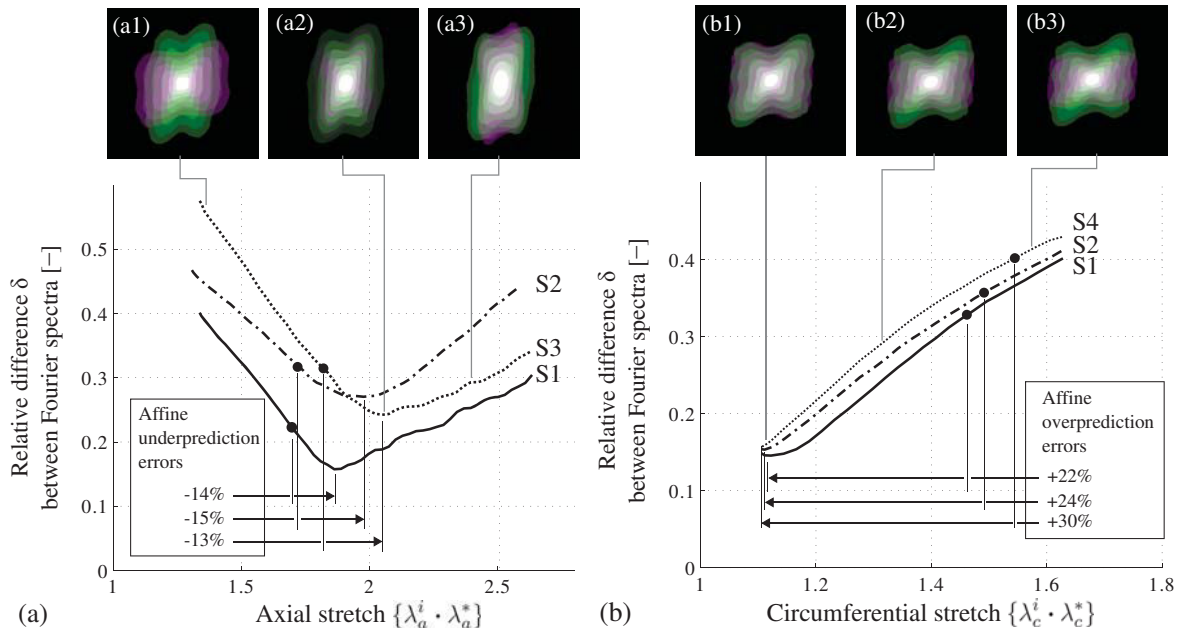

Figure 4.5 – Evolution of the relative difference δ between spectra corresponding to the numerically deformed morphology and the experimentally deformed morphology. (a) Loading scenario 1 (axial tension under constant imposed pressure): evolution of δ with the stretch numerically applied in the longitudinal direction λ_a^*; (b) loading scenario 2 (inflation under constant axial stretch): evolution of δ with the stretch numerically applied in the circumferential direction λ_c^*. On each plot, the three curves refer to the three tested samples (either S1, S2, and S3 or S1, S2, and S4) and black dots • indicate the experimentally applied stretches λ_a^f and λ_c^f. For each loading scenario, examples of superimposed spectra are provided for one carotid samples in (a1)-(a3) and (b1)-(b3) for different stretches numerically applied to the reference configuration. The purple (resp. green) spectrum corresponds to the numerically applied affine deformation (resp. to the experimentally applied loading). The difference between the experimental and the numerical stretches minimizing the difference between morphology spectra is represented by horizontal arrows in each figure. Accordingly, prediction errors of affine kinematics are quantified under both loading scenarii. Prediction errors are negative when affine kinematics underpredicts the experimental stretch, and positive when affine kinematics overpredicts the experimental stretch.

from the fiber orientations of the experimentally loaded configuration: this led to a continuously increasing relative difference δ between the spectra ((Figure 4.5(b2) and (b3)). For the three tested samples S1, S2, and S4, the minimum of δ was reached at circumferential stretch values comprised between 1.1 and 1.13, i.e. to have comparable morphologies, the numerically applied stretch needs to be 30% lower than the experimentally applied stretch.

4.4 Discussion

The mechanically-induced reorientation of collagen fibers was the focus of several contributions, studying different collageneous tissues, such as tendon [Lake 12], collagenous constructs [Chandran 06], skin [Bancelin 15,Lynch 17], bovine pericardium [Billiar 97], liver capsule [Jayyosi 16],

and carotid artery [Krasny 17a]. The debated question concerns the affine character of the reorientation process: do the fibers follow the strain imposed by their surrounding matrix, or are other mechanisms active in the reorientation process? The previously cited studies showed that collagen fibers present complex and potentially non-affine kinematics under load. However, while the reorientation of collagen fibers has been widely characterized, none of the contributions had investigated the effect of loading types on fiber kinematics while characterizing the affine character of the fiber reorientations. However, the results collected in the present paper suggest that the loading scenario, and more precisely the local strain tensor, plays an important role on bundle kinematics. We therefore propose to compare our results to the other available studies, paying a special attention to the loading scenario which was imposed to the arterial tissue.

In the present contribution, we investigated the kinematics of adventitial collagen bundles, when subjecting the arterial tissue to two different loading scenarii, namely axial tension under constant pressure and inflation under constant axial stretch, while the microscopic configuration of adventitial collagen was acquired by means of multiphoton microscopy. Regarding the first loading scenario, maintaining a constant pressure (P = 100 mmHg) while applying axial stretches produced a pronounced reorientation of adventitial collagen fibers. To our best knowledge, the contribution the closest to ours is the one of [Chen 13], who studied the behavior of collagen fibers of coronary arteries under axial tensile loading while maintaining a constant circumferential stretch. In these tests, fiber reorientations showed limited reorientations (their rotation being 13% lower than predicted by the affine kinematics). The discrepancy with our results may originate in that, under such a deformation, no transverse strain of the sample is possible (through the use of a balloon catheter). In the present study however, the transverse strain observed while applying an axial tension to the samples S1; S2 and S3 was measured 15%, 18% and 18%, respectively. As a result, the deformations applied by [Chen 13] induced a different strain state within the tissue as compared to our protocol. This may explain the different fiber kinematics.

We also investigated the fiber kinematics under inflation tests at a constant imposed axial strain. The applied methodology for the characterization of fiber kinematics suggests that inflating the artery at the constant in vivo length does not produce noticeable rotations of collagen fibers in the adventitia. Collagen fibers first straighten (engagement) and then keep their orientation unchanged. The same result was also obtained by [Schrauwen 12], who submitted carotid arteries to inflation after applying an initial stretch of $\lambda = 1.5$. They measured fiber waviness and orientation across a given region of interest. Results showed that after unfolding (waviness parameter > 0.8, corresponding to an applied pressure of 60 mmHg), the peak orientation density did not vary further during the deformation (maximum pressure 120 mmHg), indicating that fibers did not reorient during deformation. Microscopy images also suggested, that the global orientations of the crimped fibers did not vary noticeably during the decrimping

process occurring early in the inflation procedure (0 to 60 mmHg). Also, in the contribution of [Chen 13] and despite the different type of artery, adventitial collagen was shown to behave similarly to our results. Referring to the presented results [Chen 13] and interpreting fiber reorientations under increasing circumferential stretches ($\lambda = 1$ to $\lambda = 1.7$) at a given axial stretch ($\lambda = 1.5$), which is a loading scenario kinematically equivalent to inflation at constant axial stretch, we note that fibers showed limited reorientations (their rotation being 30% lower than predicted by the affine kinematics). To our best knowledge, only [Keyes 11] obtained results with different trends although applying an analogous mechanical protocol. They found that adventitial collagen fibers reorient significantly from axial to circumferential directions under high pressure. These differences may be attributed to a different tissue type and a different methodology, given that a fixed region of interest was not tracked during the overall microscopy procedure of these authors.

The kinematics of collagen bundles are also modified when the applied loading scenario induces yet other macroscopic strains. Indeed, [Wan 12] compared three inflation configurations (increasing internal pressure) while simultaneously reducing axial stretch. They found that collagen in mouse adventitia shows affine kinematics in the physiological range of deformations. Furthermore, [Sacks 03a] documented collagen kinematics under planar biaxial deformation with conclusions supporting the affine assumption for fiber kinematics, i.e. fibers following the macroscopic strain. In a previous study [Krasny 17a], we focused on uniaxial tensile tests of strips of carotid arteries, showing that collagen bundles reorient faster than predicted by affine kinematics. The discrepancies between the presented results and those of the latter studies most certainly lie in different mechanical protocols, inducing different strain paths.

The complex rearrangements of collagen fibers under macroscopic loading raise the question of the underlying mechanisms governing their complex kinematics. While fiber uncrimping is intrinsically a non-affine mechanism [Fan 14, Lee 15], we show in the present study that the non-affine character of collagen motion concerns also rigid motions of collagen fibers at the fiber lengthscale, regardless of its crimped or straight state. In order to explain the motion of collagen fibers, fiber-matrix interactions have to be taken into account. Previous studies have investigated the role of the non-collagenous matrix in the micromechanics of soft biological tissues, hence influencing collagen kinematics [Billiar 97, Thorpe 13]. In particular, recent modeling results have suggested that the non-linear mechanical response of the tissue is due to structural effects (spin effects) of the fibers network in interaction with the surrounding matrix [Morin 15]. Presumably, a redistribution of microscopic stress through proteoglycans distributed in the matrix [Thorpe 13] influences fiber motion, with potential inner sliding inside each collagen fiber being responsible for the tissue's plastic response [Lynch 17]. Besides, fiber-fiber interactions have been considered both in experimental investigations [Chow 14] as in modeling formulations [Lanir 79, Stylianopoulos 07, Cardamone 09, Morin 15]. While [Lanir 79] proposed a schematic representation of the collagen and elastin network structure in general-

ized collagenous tissues, with collagen undulation induced by the elastin exerting tension on them, [Chow 14] illustrated structural and mechanobiological interactions between fibers, eventually showing that, in porcine thoracic aortas, the elastic fibers are under tension and induce an intrinsic compressive stress on the collagen. From the modeling point of view, [Stylianopoulos 07] showed that a network composed of straight fibers interacting with each other via freely rotating crosslinks, incorporated as structural description of a Representative Volume Element in a multiscale model, provides good predictions of arterial biomechanics. Concerning the contribution of [Morin 15], the developed micromechanical model predicts the load-induced decrimping and rotations of the fibers and the subsequent stiffening of the mechanical behavior of a Representative Volume Element, accounting for both fiber-fiber interactions and fiber-matrix interactions, while introducing linear elastic constitutive behavior for fibers and matrix phases.

These observations, coupled to (i) the evidenced coexistence of collagen and elastin in the adventitial layer of arteries such as the rabbit carotid [Krasny 17a] or the pig coronary artery [Chen 13], and to (ii) findings about the load-bearing properties of collagen fibers (the elastic modulus of collagen fibers being greater than the elastic modulus of elastic fibers by a factor 10^3 [Wenger 07, Burton 54, Faury 01]) and to (iii) the current understanding of both collagen-elastin fiber interactions and rearrangements [Lanir 79, Chow 14, Ferruzzi 11, Wang 13], suggest possible links with the cellular tensegrity theory [Ingber 93, Stamenović 96, Stamenovic 00]. The cellular tensegrity theory, developed for subcellular descriptions, proposes a representation of the cellular cytostructure through a network of high-strength microtubules, maintained in compression by a network of low-strength actin fibers under tension, the whole system being in static equilibrium in the absence of an external load. Such theory can be extended to collagenous networks as shown in Figure 4.6, where a simplified tensegrity model inspired from [Luo 08] is introduced to represent arterial adventitia with rigid collagen fibers and compliant links between the collagen fibers [Chow 14]. Such a model may explain the results observed in the present study: under inflation loading at a constant axial stretch, fiber rotation is impossible, as it would imply a transverse strain, the fibers being rigid. Conversely, under axial tensile loading at a fixed inner pressure, fiber rotation is the only way to allow the extension. Noticeably, this model may also explain the results of [Chen 13]; namely when applying an axial tension while maintaining the circumferential stretch constant (hence disabling transverse strain), fiber rotations were limited and overpredicted by affine predictions. All in all, this representation of the adventitial microstructure, based on a previously applied tensegrity model [Luo 08], could explain the complex kinematics of collagen fibers and their dependence on the type of loading scenario that we observed in the present study.

Still, several limitations to this study should be mentioned. In fact, the deformations undergone by the arterial samples match only partially the *in vivo* mechanical loading. This is obviously the case of axial tension under constant pressure, but also to a certain extent of inflation at a fixed *in vivo* stretch. Also, the test temperature was maintained at 20°C, while it is 38-40°C *in vivo*, and the deformation was applied under quasi static conditions, which cannot render the

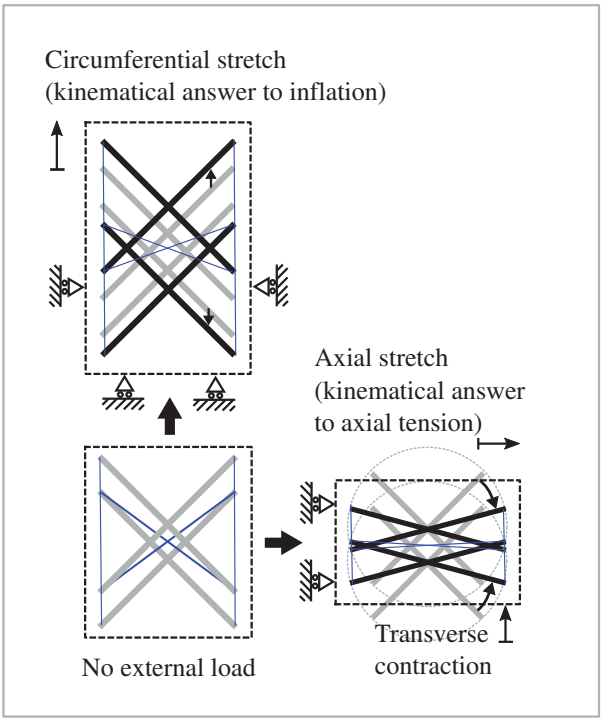

Figure 4.6 – Schematic representation of adventitial microstructure inspired from the tensegrity structure of Luo et al 2008 [Luo 08]. Black segments represent here low-compliant collagen bundles, while blue segments represent high-compliant binding fibers which exert compressive forces on the collagen bundles under zero load. The two considered loading scenarii are represented, characterized by free transverse strain boundary condition in the case of scenario 1 (axial tension), and by fixed axial length boundary condition in the case of scenario 2 (inflation). The grey segments represent the initial positions of collagen bundles, before deformation, to be compared with final positions in black, after deformation.

dynamic nature of the pulsatile loading *in vivo* (of the order of 1 Hz). Moreover, the applied range of pressure did not match the *in vivo* amplitude between systole and diastole, which ranges between 105±15 and 125±15 mmHg [Govyrin 57] in the rabbit artery. Besides, excision of the arterial tissue from its native environment initiated, prior to testing, the destructive action of degradative enzymes affecting collagen content. In the meantime, as the tissue was stored in PBS, it was prone to a modification of residual stress, as a result of the evolving fixed-charge density accumulated by proteoglycans [Azeloglu 08], eventually causing a swelling of the tissue. As a result, it cannot be neglected that this residual stress, resulting from sample storing in PBS, influences both the mechanical response and collagen fiber kinematics. However, the objective of our contribution was to investigate a possible dependence of fiber kinematics to different loading scenarii, rather than to characterize the fiber kinematics under *in vivo* conditions. As a result, the choice of test temperature and of pressure range did not impair our observations and conclusions. Concerning loading dynamics, the quasi-static deformation protocol with tissue preconditioning allowed live imaging under multiphoton microscopy with repeatable results, which would not be possible if a dynamic pulsatile loading would have been applied as it is the case *in vivo*. Another limitation concerns the application of a Maximum

Intensity Projection (MIP) algorithm (see section 4.2.5) to the 3D images stack and the resulting 2D morphology that we analyzed. Indeed, fibers localized on the outermost circumferential layers of the artery appeared the brightest and uninterrupted in the resulting 2D morphology. As for deeper fibers, they appeared eventually overlapped by the outer fibers, with a decreased contrast on the image. As a result, although they are identical from the biological point of view, the different fibers did not contribute to the overall image spectrum with the same weight. This limitation highlights the importance of following the same region of interest during the microscopy procedure, given that the discrepancy of contributions relative to the different fibers with regards to the resulting 2D spectrum is identical in the different compared projected (MIP) morphologies. Finally, a limitation originates in the spectral comparison between, on the one hand, a morphology characterized by a slight crimping of fiber, and on the other hand, a morphology characterized by fully engaged, straight fibers. In fact, when choosing the reference morphology for spectrum analysis, a part of the computed spectrum difference δ originates in the undulated character of the fibers, and another part originates in the different fiber orientations at the fiber bundle scale. A preliminary analysis of spectrum sensitivity, using fictitious collagen images, showed that the "undulation" contribution to the computed spectrum difference was negligible with regards to the orientation contribution, provided that the small lengthscales corresponding to fiber crimping were excluded from our analysis. However, this is not anymore true when fiber crimping is important, hindering an analysis of global bundle orientation (as it is the case in the unloaded configurations in [Krasny 17a]). This is the major reason, why the reference configurations of the loading scenarii were chosen to induce a partial loading ($\lambda_a = 1.3$, P = 100 mmHg for scenario 1, $\lambda_a = 1.6$, P = 20 mmHg for scenario 2): in fact the fibers appeared close to engagement or partially engaged. Another reason for this choice of loading originated in the need to prevent the potential buckling of the samples at high pressure and low axial stretch [Han 13], which would have disabled the analysis of macroscopic and microscopic kinematics. As concerns the interpretation of the adventitial microstructure using a tensegrity model, it must be mentioned that, at this stage of knowledge about the arterial microstructure, its physical validity is conditioned by the verification of several assumptions. In particular, collagen bundles are not capable of supporting the compressive forces exerted by elastin (which results in their crimped state under zero external load). However, this role in the overall force equilibrium may be played by proteoglycans: due to their ability to trap water molecules along with the sodium ions that equilibrate their electric charge [Azeloglu 08, Buschmann 95], the hydrated proteoglycans provide a mechanical resistance to compression. Another assumption concerns the nature of the bindings between collagen and elastin, which should be characterized experimentally in the future.

4.5 Conclusion

Despite the aforementioned limitations, the original outcomes of the present study significantly contribute to a better understanding of arterial kinematics at the microscopic scale. From the

experimental side, future work should characterize the interactions between collagen and other binding proteins such as elastin. From the modeling side, tensegrity models could represent arterial microstructure and its associated mechanics, and future work should further test their applicability at the tissue level with collagen, elastin and proteoglycans as principal components (Figure 4.6).

Chapter 5

Modeling arteries on the basis of fiber-scale micromechanics

Contribution: This chapter is an extension of: "The concept of frozen elastic energy as a consequence of changes in microstructure morphology" authored by Witold Krasny, Claire Morin, Stéphane Avril, Hélène Magoariec and Christian Hellmich, published in Computer Methods in Biomechanics and Biomedical Engineering (Volume 18, 2015 - Issue sup1, Pages 1966-1967, DOI: 10.1080/10255842.2015.1069581). Witold Krasny adapted the codes of the model preliminarily implemented at Sainbiose Laboratory (IMT Mines Saint Etienne). Results of Section 5.4 were obtained during the 1.5 month long stay of Witold Krasny at the Institute for Mechanics of Materials and Structures, led by Prof. Christian Hellmich at the Vienna University of Technology, in Winter 2015.

Contents

Résumé

Le présent chapitre développe les aspects de modélisation multi-échelle de la paroi artérielle. Plus précisément, nous procédons en deux temps : nous proposons tout d'abord un modèle simplifié de l'adventice, puis nous étudions la trajectoire-dépendance de la rotation des fibres et donc de la réponse mécanique.

Le chapitre commence par une présentation des fondements théoriques en micromécanique des milieux continus soumis à de grandes transformations. La théorie est alors appliquée à un volume élémentaire représentatif (VER), choisi comme une modélisation simple de l'adventice. Nous appliquons à ce VER un scénario de chargement visant à reproduire la déformation expérimentale des échantillons artériels plats chargés en traction uniaxiale (voir chapitre 3). Lors de ce chargement, une élongation est appliquée dans une direction et simultanément une contraction d'intensité proportionnelle, imitant la contraction de Poisson du tissu est appliquée dans une direction orthogonale. Des paramètres physiologiques issus de la littérature [Wenger 07, Keyes 11, O'Connell 08] ont été choisis pour représenter l'adventice, tant en termes de morphologie spatiale (orientation initiale des faisceaux de collagène, fraction volumique du collagène) qu'en termes de propriétés mécaniques microscopiques (modules de Young et coefficients de Poisson des fibres et de la matrice). Nous présentons ensuite une analyse de sensibilité étudiant l'influence de la fraction volumique des fibres, ainsi que de la rigidité de la matrice, sur (i) la réorientation des fibres et (ii) l'état de contrainte macroscopique. Le modèle micromécanique prédit avec succès la réponse mécanique non linéaire de l'adventice de l'artère résultant de la réorientation des fibres. Il est intéressant de noter que les réorientations des fibres prédites par le modèle sont plus importantes que les réorientations prédites par la règle de cinématique affine, en cohérence donc avec les résultats expérimentaux présentés au Chapitre 3. En outre, l'augmentation de la fraction volumique de fibres augmente l'amplitude de rotation totale des fibres, amplifiant d'autant plus leur comportement non affine ainsi que la non linéarité de la réponse mécanique. Au contraire, lorsque les fractions volumiques de fibres tendent vers zéro ou que la rigidité de la matrice augmente, la cinématique des fibres se rapproche progressivement de la cinématique affine. Etant donné que la rotation des fibres est calculée via le schéma de Mori-Tanaka [Mori 73, Benveniste 87], qui prend en compte l'effet rigidifiant des fibres environnantes dans l'estimation de la rigidité de la matrice, ce résultat suggère une influence importante des interactions fibre-fibre, qui accélèrent les réorientations des fibres dès que leur fraction volumique est élevée.

Dans la deuxième partie du chapitre, une série de scénarii de chargement-déchargement biaxiaux est considérée et appliquée au VER d'un matériau fibreux. Divers chargements-déchargements séquencés sont testés. La réponse mécanique du VER fibreux est étudiée en termes d'orientations des fibres, de contraintes macroscopiques de Cauchy et de densité d'énergie élastique accumulée et restituée. En comparant des scenarii de chargement atteignant des états de déformation bi-

axiaux identiques en suivant différentes trajectoires, les résultats révèlent que les réorientations des fibres ainsi que l'état de contrainte de Cauchy dans le VER dépendent de la trajectoire suivie pour appliquer le chargement. Par ailleurs, lorsque le VER est soumis à des cycles de chargement-déchargement pour lesquels le déchargement suit la trajectoire inverse de la trajectoire de charge, les fibres retournent en position initiale et le VER restitue l'intégralité de son énergie élastique. Par contre lorsque le déchargement suit une autre trajectoire que celle du chargement, les fibres ne reviennent pas à leur configuration initiale, et par conséquent, une fraction de l'énergie élastique reste stockée dans le VER au terme du déchargement.

Originalité des méthodes appliquées :

- *L'approche micromécanique en modélisation multiéchelle : bien que déjà appliquée en mécanique de l'os, cette approche est appliquée pour la première fois dans le contexte des tissus biologiques mous [Morin 15] ;*
- *Multitude de configurations testées : le modèle est appliqué à l'adventice artérielle (cas d'application physiologique) et à un matériau fibreux (cas d'application général). Dans ce dernier cas, les tests sont effectués selon différents scenarii de chargement.*

Résultats à retenir :

- *Le modèle micromécanique a prédit avec succès le comportement mécanique non linéaire de l'adventice artérielle, incluant une rigidification caractéristique du tissu qui est la conséquence de la réorientation des fibres ;*
- *Les réorientations des fibres, prédites par le modèle, se sont révélées supérieures en amplitude au réorientations affines, un résultat cohérent avec les observations expérimentales discutées au chapitre 3 ;*
- *Le caractère non-affine de la cinématique des fibres a été amplifié en augmentant la fraction volumique des fibres ou en diminuant la rigidité de la matrice, ce qui suggère l'importante influence des interactions fibre-fibre sur le comportement mécanique de l'artère [Mori 73] ;*
- *Le modèle a prédit la "trajectoire-dépendance" d'un matériau fibreux subissant des déformations biaxiales, avec potentiellement une énergie élastique stockée, conséquence du changement de morphologie de la microstructure lors d'un cycle de chargement.*

Abstract

In the present Chapter, a continuum micromechanics model is first applied to the arterial adventitia. After explaining the model's formulation comprising (i) basics of continuum micromechanics, (ii) the construction of a Representative Volume Element (RVE), and (iii) the upscaling methodology of microscopic elastic properties, a loading scenario is proposed, aiming at reproducing the experimental strain states achieved under uniaxial tension (Chapter 3). Accordingly, a tensile displacement was prescribed under a given direction to the RVE, while simultaneously prescribing a compressive displacement to the RVE in the orthogonal direction, hence mimicking the tissue's Poisson contraction. Physiological parameters were chosen to describe the RVE representing the arterial adventitia, both in terms of spatial morphology as in terms of microscopic mechanical properties. After discussing the latter loading case, a sensitivity analysis is proposed investigating the influence of the fibers' volume fraction and of the stiffness of the matrix on (i) the reorientation of the fibers and on (ii) the homogenized macroscopic Cauchy stress. The micromechanical model successfully predicted the material's characteristic stiffening as a consequence of fiber reorientations. Interestingly, fiber reorientations exceeded affine reorientations, consistently with experimental results (Chapter 3). Moreover, increasing the fiber volume fraction increased the total fiber rotation, enhancing non-affine behavior and the material stiffening effect. This result highlights the important influence of fiber-fiber interactions, which accelerate fiber reorientations as soon as their volume fraction is sufficiently high. The second sensitivity study showed that when the stiffness of the matrix increased, fiber motion approached the affine behavior, illustrating one of the mechanical roles of the matrix, which through its compliance promotes fiber-fiber interactions and therefore accelerates their realignment. In the second part of the chapter, a variety of biaxial loading-unloading scenarii is considered and applied to a random fibrous RVE. Comparing loading scenarii reaching identical macroscopic strain states following different deformation paths, results reveal that the fibers' load-induced reorientations as well as the Cauchy stress within the RVE are trajectory dependent. Moreover, when the unloading occurred in the exact same reverse path as the loading, the fibers returned to their initial positions and the RVE was able to release all its elastic energy. On the contrary, when the unloading did not follow the exact reverse loading path, the fibers did not retrieve their initial position, while the elastic energy wasn't totally released, resulting in frozen elastic energy as consequence of a change in microstructure morphology.

Originality of the applied method

- The continuum micromechanics approach was widely applied to model bone mechanics but is presently applied for the first time to soft biological tissues [Morin 15];
- Introduction of a load-induced rotation of the fibers, being eventually larger than affine kinematics.

Main results

– The multiscale model based on continuum micromechanics successfully predicted the nonlinear mechanical behavior of the arterial adventitia, with a characteristic stiffening which originated in the load-induced reorientation of the fibers;

– Fiber reorientations exceeded affine reorientations, consistently with experimental observations;

– Non affinity of fiber motion was amplified by an increase of the fibers' volume fraction or by the decrease of the matrix stiffness, hence correlating with fiber-fiber interactions through the Mori-Tanaka homogenization scheme;

– The model was able to capture loading trajectory dependence of a fibrous material undergoing biaxial deformations, with a potential frozen elastic energy as a consequence of morphology change after complete unloading.

5.1 Introduction

Constitutive modeling of soft biological tissues has been the topic of abundant literature. As described in Chapter 2, these biological tissues, made of variously oriented and crimped fibers embedded in a soft matrix, exhibit a highly nonlinear anisotropic behavior with the ability to sustain large reversible strains. In parallel, experimental mechanical tests performed on soft tissues and coupled to multiphoton microscopy [Schrauwen 12, Chen 13] revealed that this nonlinear behavior originates in geometrical changes in the microstructure. In Chapter 3, we illustrated that the most relevant load-induced morphological rearrangements occurring in the artery concern adventitial collagen. Indeed the latter load-bearing fibers undergo a progressive decrimping [Hill 12, Zeinali-Davarani 15] and realignement along the load direction [Schrauwen 12, Chen 13, Keyes 13]. They exhibit, as shown in Chapters 3 and 4, non-affine kinematics and load-dependance. While Existing constitutive models are mainly phenomenological hyperelastic models developed at the macroscopic scale [Holzapfel 01, Holzapfel 05, Gasser 07, Zulliger 04, Holzapfel 15a], the aforementioned experimental results confirm the growing need to understand the relationship between phenomena taking place in the microstructure and the macroscopic mechanical response of the artery (Figure 5.1); subsequently driving forward multiscale approaches [Freed 05, Grytz 09, Stylianopoulos 07, Maceri 10, Nierenberger 13, Marino 13, Raina 13] which share a common objective: explain the arterial behavior from internal composition and structure.

We here propose to model the reorientation of the fibers within the artery by adopting a continuum micromechanics approach [Hill 65, Zaoui 02], through an extension of Eshelby's inclusion problems [Eshelby 57] applied to statistically distributed inclusions interacting with their surrounding matrix [Mori 73, Benveniste 87, Hellmich 02, Hellmich 04, Hellmich 08]. This methodology, unprecedently applied to the arterial tissue, is characterized by (i) load-induced fiber reorientation, (ii) a semi analytical scheme providing fast computational performance, (iii) a limited number of material parameters as we do not describe the exact geometry of the fibers and neglect friction between components of the microstructure. In the following, we investigate the ability of the proposed model [Morin 15] to capture, through microstructure morphology changes, the mechanical response of soft tissues, and discuss underlying mechanisms governing fiber motion. In particular, we address the following questions:

- To which extent does the loading-induced rotation of the fibers predict the behavior of the arterial tissue on both macroscopic and microscopic scales?

- What is the effect of the mechanical interactions between constituents of the microstructure on the amplitude of fiber rotation?

- May the model capture other mechanical properties of fibrous materials that originate in the behavior of their microstructure?

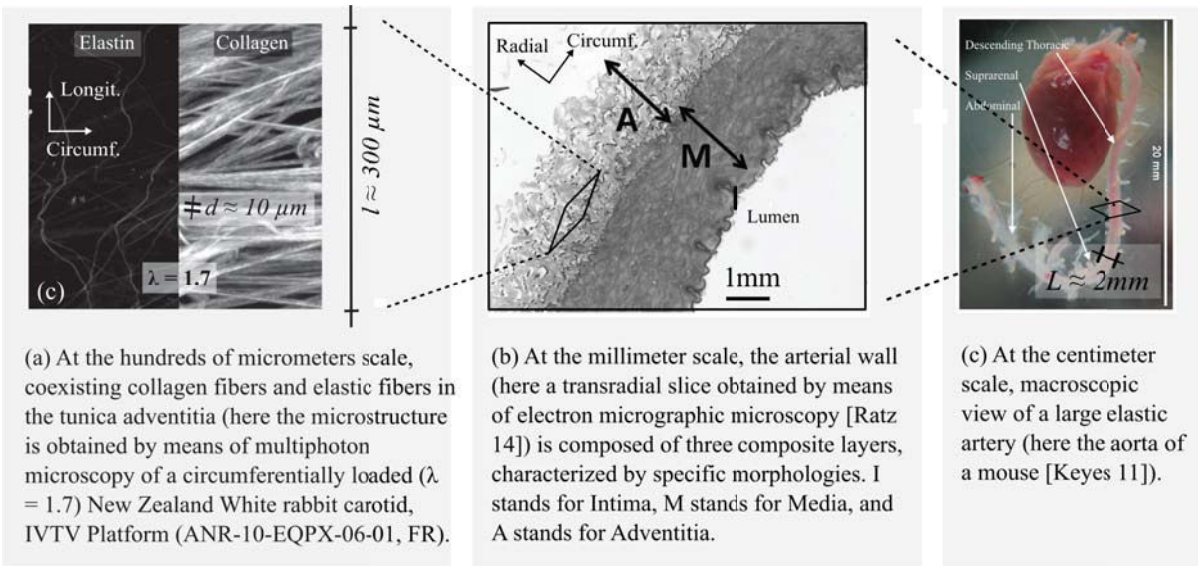

(a) At the hundreds of micrometers scale, coexisting collagen fibers and elastic fibers in the tunica adventitia (here the microstructure is obtained by means of multiphoton microscopy of a circumferentially loaded (λ = 1.7) New Zealand White rabbit carotid, IVTV Platform (ANR-10-EQPX-06-01, FR).

(b) At the millimeter scale, the arterial wall (here a transradial slice obtained by means of electron micrographic microscopy [Ratz 14]) is composed of three composite layers, characterized by specific morphologies. I stands for Intima, M stands for Media, and A stands for Adventitia.

(c) At the centimeter scale, macroscopic view of a large elastic artery (here the aorta of a mouse [Keyes 11]).

Figure 5.1 – Multiscale view of the arterial structure, providing characteristic lengthscales.

In the present Chapter, the model formulation is provided, comprising a presentation of the theoretical framework of continuum micromechanics and of the homogenization scheme. Secondly, the multiscale model is applied to the arterial adventitia and the results of loading scenario equivalent to the experimentally applied uniaxial tension (section 3.2.2) are discussed. Finally, the model is applied to a random fibrous material and the results obtained from the application of various biaxial loading-unloading scenarii are discussed.

5.2 Model formulation

5.2.1 Fundamentals of continuum micromechanics

The first step in the implementation of the multiscale approach consists in choosing a simplified description of the tissue's microstructure obeying the rules of continuum micromechanics. Continuum micromechanics is aimed at determining the effective behavior of a material which is macroscopically homogeneous but microscopically heterogeneous. This material fills a Representative Volume Element fulfilling the separation of lengthscale requirement [Zaoui 02]. The corresponding relationship, with L standing for the minimum characteristic length between that of the material and that of the loading applied on it, l standing for the size of the RVE, and d standing for the characteristic size of a heterogeneity in its microstructure, reads as:

$$L \gg l \gg d. \tag{5.1}$$

Due to the complexity of the arterial microstructure, the RVE cannot be described in complete detail. We therefore choose a limited number of homogeneous subdomains making up a simplified description of the RVE. These homogeneous subdomains are called material phases. Each phase is thus characterized by its shape, volume fraction, and elastic properties. The

relation between homogeneous deformations acting on the boundary of the RVE and resulting average stresses (i.e. the "homogenized" mechanical behavior of the overall material), can then be estimated from the mechanical behavior of the aforementioned homogeneous phases and from their morphology, their volume fractions, as well as mutual interactions.

We consider an RVE composed of n phases exhibiting a hypoelastic material behavior:

$$\overset{\triangle}{\boldsymbol{\sigma}}_i = \mathbb{C}_i : \boldsymbol{d_i} \quad (i \in \{1, ..., n\}), \tag{5.2}$$

where $\boldsymbol{d}_i$ is the microscopic second-order strain rate tensor, $\boldsymbol{\sigma}_i$ is the microscopic second-order Cauchy stress tensor, $\mathbb{C}_i$ is the fourth-order stiffness tensor relative to the considered phase. For sake of simplicity, we assume that all phases exhibit an isotropic mechanical behavior, thus:

$$\mathbb{C}_i = 3k_i\mathbb{J} + 2\mu_i\mathbb{K}, \tag{5.3}$$

where k_i and μ_i are respectively the compressibility and shear moduli of the i-th phase, $\mathbb{J}$ is the fourth-order spherical projector with components $J_{ijkl} = \frac{1}{3}\delta_{ij}\delta_{kl}$ and $\mathbb{K}$ is the fourth-order deviatoric projector:

$$\mathbb{K} = \mathbb{I} - \mathbb{J} \tag{5.4}$$

and where $\mathbb{I}$ is the fourth-order identity tensor, with components $I_{ijkl} = \frac{1}{2}(\delta_{ik}\delta_{jl} + \delta_{il}\delta_{jk})$.
$\overset{\triangle}{\boldsymbol{\sigma}}_i$ denotes an objective derivative of the stress tensor, defined as:

$$\overset{\triangle}{\boldsymbol{\sigma}} = \dot{\boldsymbol{\sigma}} + \boldsymbol{\sigma} \cdot \tilde{\boldsymbol{\omega}} - \tilde{\boldsymbol{\omega}} \cdot \boldsymbol{\sigma}, \tag{5.5}$$

where the dot denotes the time derivative and $\tilde{\boldsymbol{\omega}}$ is a second-order skew-symmetric tensor defining the rotation of the material point. Different choices exist for this tensor; we chose the Jaumann objective rate, taking $\boldsymbol{\omega}$ as the microscopic spin tensor defined as the skew-symmetric part of the Eulerian velocity gradient.

5.2.2 Upscaling of elastic properties

The RVE is subjected to Hashin boundary conditions: a homogeneous strain rate $\boldsymbol{D}$ is applied at its boundary in terms of a prescribed velocity field $\dot{\boldsymbol{\xi}}$, reading as:

$$\dot{\boldsymbol{\xi}} = \boldsymbol{D} \cdot \boldsymbol{X} \tag{5.6}$$

with $\boldsymbol{X}$ labelling the location vector on the boundary surface of the RVE. These Hashin boundary conditions ensure that the kinematically compatible microscopic strain rates inside the RVE fulfill the average condition:

$$\boldsymbol{D}(\boldsymbol{X}, t) = \sum_{i=1}^{n} \alpha_i \cdot \boldsymbol{d}_i \tag{5.7}$$

where α_i are the volume fractions of phase i, and $\boldsymbol{d}_i$ stands for the averaged strain rate over the volume of phase i.
Similarly, the equilibrated phase stresses $\boldsymbol{\sigma}_i$ fullfil the average condition:

$$\boldsymbol{\Sigma}(\boldsymbol{X}, t) = \sum_{i=1}^{n} \alpha_i \cdot \boldsymbol{\sigma}_i \tag{5.8}$$

where $\boldsymbol{\sigma}_i$ refer to microscropic stress tensors averaged over the volume of each phase and $\boldsymbol{\Sigma}$ refers to the overall averaged homogeneous stress.
The relations between the macroscopically applied strain rate and the microscopic averages of the strain rate and of the spin over each phase follow from the combination of the Eshelby solution for a matrix inclusion problem together with the superposition principle. Eshelby indeed analyzed the special case of a single ellipsoidal inclusion embedded in an infinite matrix [Eshelby 57, Hill 65] and evidenced that, when a macroscopic deformation is applied at the boundaries of the infinite domain, the strain and the spin in the inclusion are uniform and are linearly dependent on the strain tensor remotely imposed in the matrix. This result can be extended to more complex microstructural configurations showing numerous ellipsoidal inclusions. The strains are then not anymore uniform, and a mean field approach is chosen. The superposition principle allows to relate the microscopic strain rate and spin linearly to the macroscopic strain rate through:

$$\boldsymbol{d}_i = \mathcal{A}_i : \boldsymbol{D} \quad (i \in \{1, ..., n\}) \tag{5.9}$$

$$\boldsymbol{\omega}_i = \mathcal{R}_i : \boldsymbol{D} \quad (i \in \{1, ..., n\}) \tag{5.10}$$

where $\mathcal{A}_i$ is the strain concentration operator, $\mathcal{R}_i$ is the spin concentration operator, $\boldsymbol{d}_i$ is the microscopic strain rate tensor previously defined, and $\boldsymbol{\omega}_i$ is the microscopic spin, corresponding to phase i. When the interaction between inclusions cannot be neglected, the strain and spin concentration tensors account for the presence of neighboring inclusions, resulting in different approximations for the effective behavior. In this work, we chose a matrix-inclusions representation for our RVE and therefore used the Mori-Tanaka scheme [Mori 73, Benveniste 87]. While the microscopic averaged strain rates enter the constitutive relations and allow determining the macroscopic stress response of the material, the microscopic spin tensor allows to determine the load-induced rotation of each phase, according to:

$$\dot{\boldsymbol{x}}_j = \tilde{\boldsymbol{\omega}}_{\boldsymbol{f}} \cdot \boldsymbol{x}_j \quad (j = \{r, \theta, \phi\}) \tag{5.11}$$

where $\boldsymbol{x}_j, (j = \{r, \theta, \phi\})$ are the vectors of the orthogonal basis associated with a given inclusion phase. The spin tensor also enters the constitutive relation through the objective stress rate.

In order to follow, during the RVE's deformation, the absorbtion and release of elastic energy, we compute the elastic instantaneous energy density as follows:

$$\Phi = \boldsymbol{\Sigma}(\boldsymbol{X}, t) : \boldsymbol{D}. \tag{5.12}$$

5.2.3 Algorithm

The loading was applied incrementally to the RVE following an explicit scheme. The mechanical response of the RVE to the loading increment was determined in 4 steps, which are:

1. Concentration of the loading in the RVE using the concentration relationships (Eq. 5.9 and 5.10);

2. Determination of the local response of each phase using the constitutive hypoelastic law (Eq. 5.2);

3. Determination of the instantaneous rotation of each phase by means of the spin (Eq. 5.11), which led to an update of the morphology;

4. Determination of the macroscopic response by means of the homogenization rule (Eq. 5.8).

5.3 Application to the arterial adventitia

5.3.1 Building a RVE of the arterial adventitia

Previous experimental investigations have illustrated the complexity of arterial microstructure (sections 2.3). Its composite architecture does not allow to consider a single RVE that would stand reliably for the description of all material points across the entire arterial wall. As a result, relevant RVEs should be defined, in order to model separately the tunica intima, the tunica media, and the tunica adventitia (see section 2.3.2).
In this work, we chose to first focus on the modeling of the tunica adventitia, since its collagen bundles exhibit a complex kinematics. To this aim, we model a representative volume element of the adventitial tissue, with a characteristic dimension of 300 µm. It is made of a matrix phase (comprising the aqueous solution as well as the few elastin fibers), in which the diverse collagen bundles, modeled as infinitely long cylinders with different orientations, are embedded (Figure 5.2). The orientation of each fiber family is characterized by two Euler angles (θ, ϕ). The θ angle corresponds to the angle between the fiber's long axis and the radial direction of the adventitial tissue. In the present work and according to experimental measurements, we consider two fiber families, with respective fiber angles of $\pi/6$ and $5\pi/6$. The angle ϕ corresponds to the angle between the projected direction of the fiber onto the circumferential-radial plan and the radial direction. Due to the low transmural angle, we chose that all fiber families lie in the circumferential-axial plan, therefore ϕ is equal to $\pi/2$ for all fiber families. This representation of an adventitial representative volume element fulfills the separation of scale principle, the mean value of collagen bundles diameter being 5 µm and the carotid artey diameter being about 4 mm. Finally, the matrix-inclusion nature of the modelled tissue speaks for the choice of a Mori-Tanaka scheme to define the concentration tensors.

The simulation was run using physiological parameters (Table 5.1). Concerning the matrix parameters we used the two following assumptions: (i) the matrix is assumed quasi incompressible ($\nu = 0.49$) as it is rich in water molecules; (ii) its bulk stiffness property is mainly conferred by variously oriented elastic fibers for which the stiffness properties are known [Burton 54, Faury 01].

			Experimental sources
Number of fiber families	N	2	-
Initial in-plane orientations of fiber families	θ_i	$[\pi/6; 5\pi/6]$	[Krasny 17a, Schrauwen 12]
Initial transmural orientations of fiber families	ϕ_i	$[\pi/2; \pi/2]$	[Rezakhaniha 12, Schrauwen 12]
Young's modulus of the matrix	E_m	1 MPa	[Burton 54, Faury 01]
Poisson ratio of matrix	ν_m	0.49	-
Young's modulus of collagen fibers	E_i	500 MPa	[Wenger 07]
Poisson ratio of collagen fibers	ν_i	0.3	[Wenger 07]
Fibers volume fraction	f_i	0.7	[O'Connell 08, Keyes 11]
Strain rate (along x_2)	D	0.01	-
Maximum stretch	λ	1.5	[Schrauwen 12, Chen 13]

Table 5.1 – Material parameters defining the adventitial RVE.

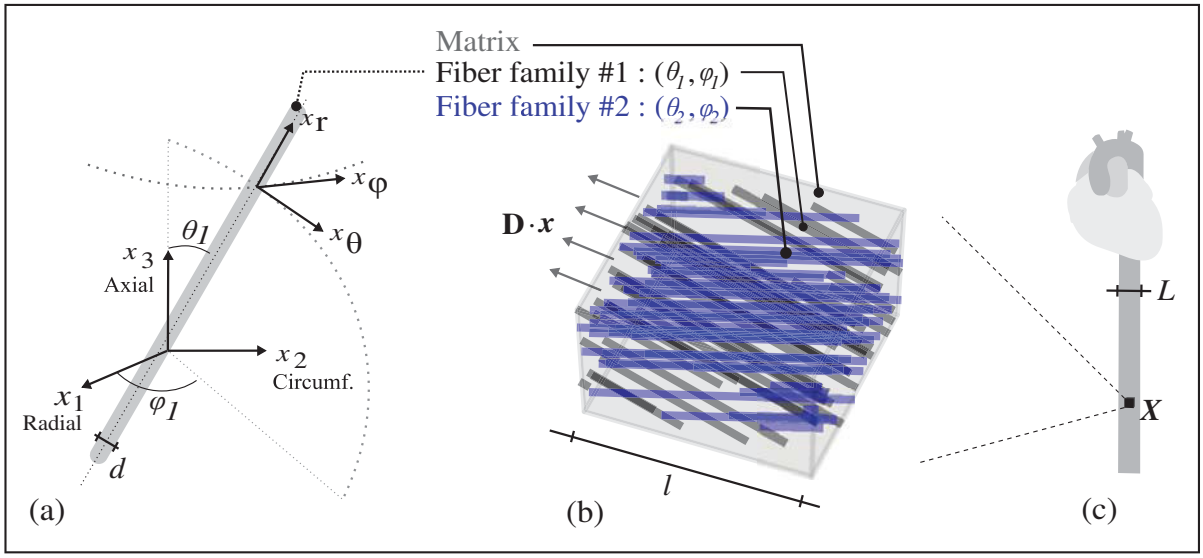

Figure 5.2 – (a) Schematic representation of a material point $\boldsymbol{X}$ of the collagenous adventitia of the aorta modeled by (b) a Representative Volume Element made of two variously oriented fiber families, with a homogeneous strain rate $\boldsymbol{D}$ applied at its boundary; (c) three dimensional spatial parameterization of fiber family 1 orientation (θ_1, ϕ_1). The [x_1 (radial), x_2 (circumferential), x_3 (axial)] frame is attached to the RVE, while the [x_r, x_θ, x_ϕ] frame follows each fiber family.

5.3.2 Loading path

The RVE was loaded by applying a prescribed strain rate in two directions in order to mimic tension tests applied on flat arterial samples (section 3.2.2), as follows. A tensile strain rate in the direction of the x_2-axis (circumferential) was applied until a maximum stretch of 1.5 was achieved, while simultaneously applying a compressive strain rate in the transverse direction of the x_3-axis (axial) in order to simulate the Poisson effect of the sample. The ratio of the

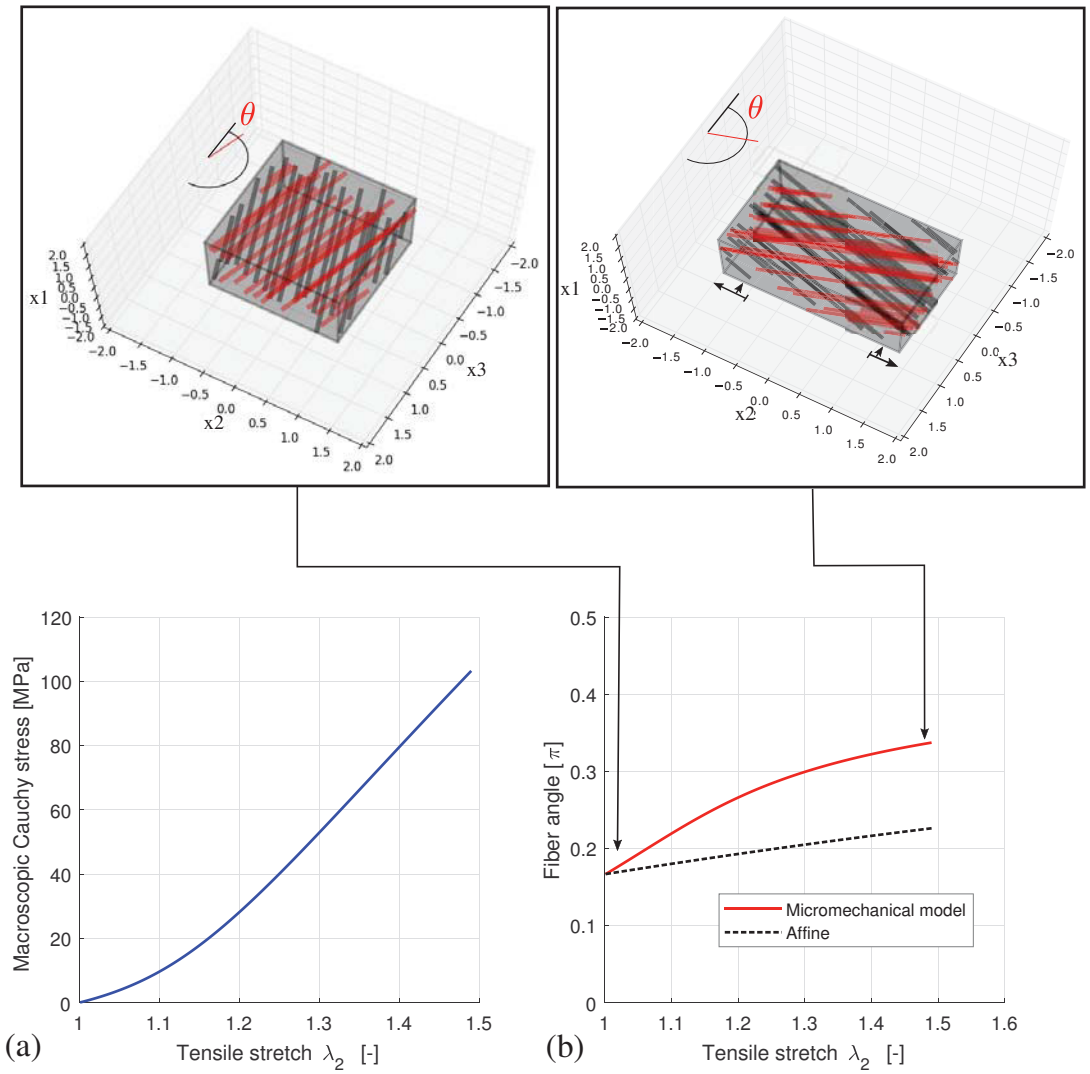

Figure 5.3 – (a) Macroscopic Cauchy stress σ_{22} as function of the tensile stretch λ_2; (b) Orientation angle of the $\pi/6$ fiber family as function of the tensile stretch λ_2. The deforming RVE is sketched graphically above the plots (before deformation: left and after deformation: right), for the sake of visualization, the $\pi/6$ fiber family whose orientation is plotted in the lower figure is represented in red.

transverse strain rate to the principal tensile strain rate was 15%, according to experimental observations.

5.3.3 Results: modeling the arterial adventitia

Figure 5.3 presents (a) the mechanical response of the RVE to the applied tensile loading including Poisson contraction and (b) the fiber rotation of one of the two symmetrical fiber families: the $\pi/6$ family (red) as function of the tensile stretch. As the prescribed strain rates on the RVE can be converted to an circumferentially applied tensile stretch, together with a axially applied compressive stretch (Poisson effect), it was possible to compute the affine fiber

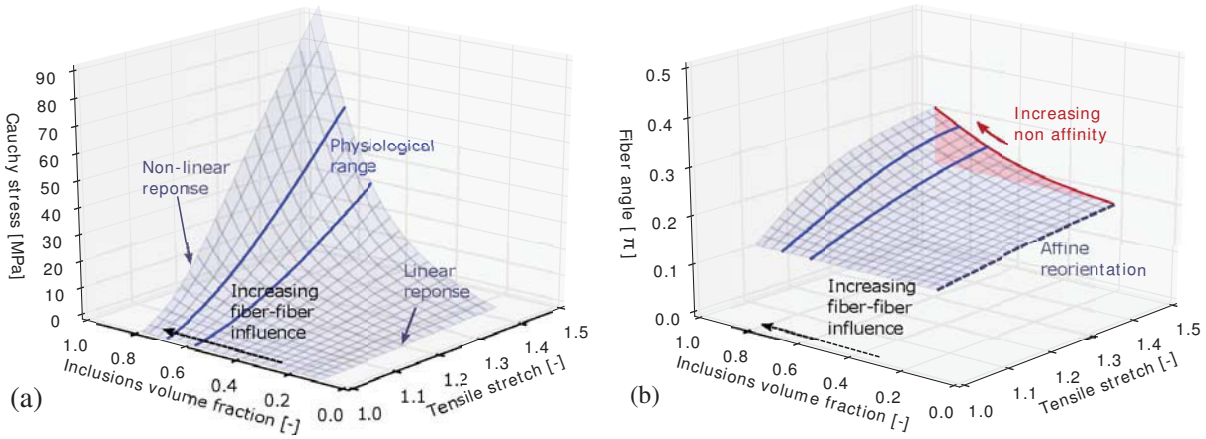

Figure 5.4 – (a) Macroscopic Cauchy stress in the RVE and (b) fiber angle of the $\pi/6$ fiber family as functions of the applied tensile stretch and of the inclusions (fibers) volume fraction. The blue lines represent the boundaries of the collagen volume fractions range, in the arterial adventitia.

reorientation analytically (black dotted line on Figure 5.3(b), see also Appendix A.8.1, Equation 11) and compare it to the reorientations computed by the model. We notice an early phase stiffening (stretch ranging from 1 to 1.2) of the material along with a progressive realignment of the fibers. Noticeably, the realignment amplitude predicted by the model was significantly higher than the affine realignment.

Figure 5.4 presents the sensitivity of both the mechanical response (stress-strain relationship, see Figure 5.3(a)) and the fiber reorientation (see Figure 5.3(b)), to the volume fraction of cylindrical inclusions, representing collagen bundles. The physiological range of collagen volume fraction in the adventitia layer of the artery [O'Connell 08,Keyes 13] is represented between the blue thick lines. Results show that, when the fiber volume fraction was low (0.1-0.2), the mechanical response of the RVE was linear and reached low stress levels (of the order of 10 MPa) which is consistent with the low quantity of stiff fibers contributing to the effective stiffness and with their limited reorientation. The limited fiber reorientation tended, under the correspondingly low fiber volume fractions, to affine reorientation, as sketched in Figure 5.4(b). When the fiber volume fraction increased, eventually reaching physiological values, the mechanical response became nonlinear, as already illustrated in Figure 5.3, while the rotation of fibers was further accentuated (i.e. the non-affine contribution to the overall fiber rotation increased, see red curve on Figure 5.4(b)). The high values reached by the macroscopic Cauchy stress when the inclusion volume fraction was high (of the order of 80 MPa) were, in turn, consistent with the high quantity of stiff fibers contributing the effective stiffness, as well as to the increased reorientation of the fibers, which became more parallel to the load direction as compared to the previous case.

Figure 5.5 presents this time the sensitivity of both the mechanical response and the fiber

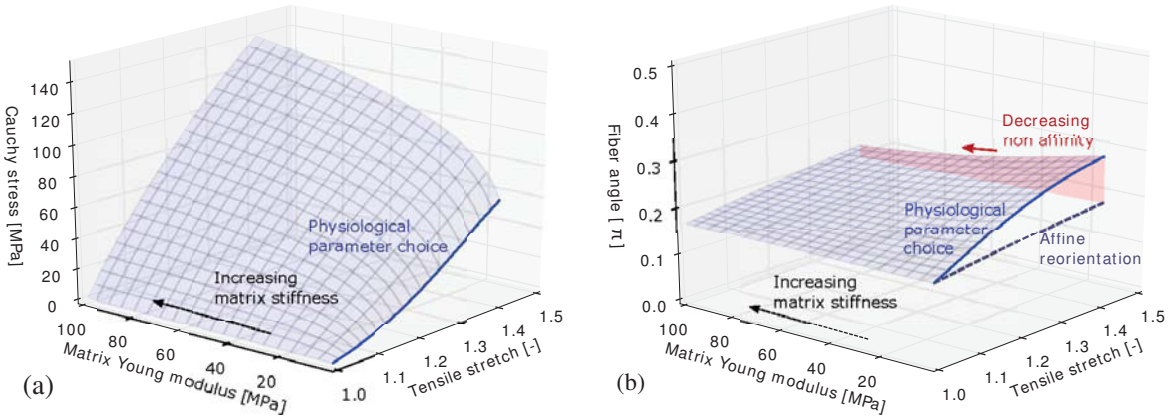

Figure 5.5 – (a) Macroscopic Cauchy stress in the RVE and (b) fiber angle of the $\pi/6$ fiber family as functions of the applied tensile stretch and of the stiffness modulus of the matrix phase. The blue lines represent the physiological choice for the matrix stiffness, in the arterial adventitia.

reorientation, to the Young's modulus of the matrix phase. The choice of physiological value for the Young's modulus of the matrix phase in the adventitia [Burton 54, Faury 01] is represented by the blue thick line on both plots. Results show that, when the Young's modulus of the matrix increased, the mechanical response lost its characteristic stiffening behavior 5.5(a). Concerning the fiber reorientations 5.5(b), the magnitude of rotation decreased when the Young's modulus of the matrix increased, eventually tending to the magnitude of affine predicted reorientation.

5.3.4 Discussion

Although already successfully applied in the context of bone multiscale biomechanics under the infinitely small strains framework [Hellmich 02, Hellmich 04, Hellmich 08, Fritsch 09, Morin 14, Scheiner 13], the present modeling methodology is an unprecedented method for the study of the multiscale mechanical behavior of soft biological tissues, introducing a limited number of physical parameters. In the present contribution, and as the model is in early stage of development, a simple loading case was simulated using physiological material parameters provided by the existing literature, under a loading scenario corresponding to uniaxial tension on flat sample (section 3.2.2). Firstly, Figure 5.3 shows that the multiscale model allowed to qualitatively reproduce the nonlinear macroscopic response of soft biological tissues submitted to an external load. As each material phase (matrix and fibers) was governed by a linear hypoelastic constitutive behavior, the stiffening of the response appeared to be driven by the progressive reorientation of the fiber-like inclusions within the RVE. This reorientation was non-affine, with rotation amplitudes that exceeded affine predictions, consistently with experimental results illustrating adventitial collagen reorientation submitted to uniaxial loadings (section 3.3.3). The applied stretch at which the stiffening occured (1.05 ± 0.05) was lower than those obtained from the previously documented experimental mechanical responses of the artery (1.4 ± 0.1) (refering to [Hill 12] and section 3.3.1). This discrepancy may be due to the fact that the collagen unfold-

ing mechanisms, which occur in the early phase of the material's deformation, are not included in the present version of the developed model. This may also explain why the stiffening occured also earlier than in the experimental mechanical response of the adventitia alone [Holzapfel 05].

Furthermore, the order of magnitude of the macroscopic stress reached at 1.5 stretch (≈100 MPa) also differed significantly from previously documented experimental mechanical responses of the artery refering to [Hill 12] (≈1 MPa) and section 3.3.1 (≈1 MPa) or of the adventitia alone [Holzapfel 05] (≈ 100 kPa). These differences probably originate in the choice of Young's modulus of the fiber phase in the model, provided by the previously documented Young's modulus of single collagen fibers [Wenger 07]. In the adventitia however, collagen fibers are bundled together. Consequently, an effective modulus of lower magnitude should be applied to the collagen fibers phase, accounting for the heterogeneous nature of collagen bundles.

Results also illustrate that the non-affinity of fiber motion is correlated with a higher volume fraction of the fibers. As, during the computation, the incremental spin of the fibers was governed by the Mori-Tanaka's scheme for heterogeneous materials [Mori 73], a low fiber volume fraction translates into a lower mechanical influence from one fiber to the other, while a high volume fraction of fibers, in turn, means the fibers feel mechanically the presence of their neighboring fibers. As we noticed, an increase of fiber volume fraction induced an increase of non-affine fiber motion which corresponds to experimentally observed fiber kinematics. This result confirms the important role of fiber-fiber interactions in the non-affine motion of collagen fibers in the adventitia, hence more generally in the micromechanical mechanisms occurring in the arterial microstructure during deformation. Also, a further sensitivity analysis suggest, that the affinity of fiber kinematics is directly linked to the modulus of the matrix i.e. when the modulus of the matrix increased, the fibers network in the RVE rotated more affinely. This results is consistent with the observations of [Zhang 13], who modeled the arterial wall using a different description of soft biological tissue (crosslinked fibers which store energy during the deformation). In such a material configuration, from the point of view of the present multiscale Eshelby-derived model, the fraction of the total deformation underwent by the matrix is lower, and more comparable to the one underwent by the fibers. Also, the spin felt by the fibers is lower.

However it should be reminded that the model, being in its early stage of development, shows several limitations. First of all, elastin was integrated isotropically in the matrix whereas experiments illustrated that it shows preferred orientations in the adventitia [Chen 13] (see also section 3.3.2), although in very limited quantity. Moreover the presently applied version of the model did not include a mesoscale additional RVE accounting for fiber unfolding or fibrils reorganization within a collagen bundle. An updated version of the model including the latter feature exits but its testing did not enter in the scope of the present doctoral work. Among other improvements, this extended version of the model will allow the representation of an

evolving effective modulus of the collagen bundles during the deformation, stressing the stiffening phenomenon of the macroscopic mechanical response. Finally, it should be mentioned that imposing a compressive transverse strain rate to simulate the Poisson contraction might not exactly reproduce the zero normal stress condition which characterized uniaxial tension on flat samples, although it was chosen as the best way to mimic the loading experimentally applied (see section 3.2.2 and Appendix A.6.1). This limitation highlights the interest of a stress-driven deformation algorithm allowing the imposing of mechanically sound boundary conditions. The testing of the latter version of the model constitutes ongoing work which did not enter in the scope of this thesis. Other developments concern the application of the methodology to a RVE representing a simplified microstructure of the arterial media, made up of concentric elastic lamellae and circumferentially oriented collagen bundles. These advances are targeted to simulate, in the near future, the response of the total composite artery and to compare the observed results to experimental data.

5.4 Application to a random fibrous material

5.4.1 Building a RVE of a fibrous material

We investigate the ability of the proposed model [Morin 15] to capture, through microstructure morphology changes, the possible path dependence of their response to multiaxial loading, and a remaining frozen elastic energy after complete unloading of the tissue.
In the following, we focus on the modeling of a random fibrous material. To this aim, we model a representative volume element characterized a matrix phase, in which the diverse reinforcing fibers, modeled as infinitely long cylinders with different orientations, are embedded (the shape of the microscopic phases in analogous to the modeled RVE of the adventitia). The orientation of each fiber family is characterized by the two same Euler angles (θ, ϕ) described in section 5.3.1. We consider six fiber families, with the angle θ distributed in the angles interval: $[\pi/4, 5\pi/6]$. Concerning the angles ϕ, we chose that all fiber families lie in the circumferential-axial plan, therefore ϕ is equal to $\pi/2$ for all fiber families. We assume that the RVE fulfills the separation of scale principle. Again, we chose a Mori-Tanaka scheme to define the concentration tensors. The (randomly chosen) material parameters of the fibrous material are provided in Table 5.2.

5.4.2 Loading paths

In order to analyze trajectory dependence and understand how the material absorbs and releases elastic energy in its microstructure, the RVE was loaded under prescribed stretching by means of:

- **Three different loading paths**
  A biaxial macroscopic strain state was reached under three simultaneous or sequenced

Number of fiber families	N	6
Initial in-plane orientations of fiber families	θ_i	$\pi/4$ to $3\pi/4$, steps of $\pi/10$
Initial transmural orientations of fiber families	ϕ_i	$\pi/2$ for all 6 fiber families
Bulk moduli contrast between both phases	k_i/k_m	10^5
Bulk moduli contrast between both phases	μ_i/μ_m	10^5
Fibers volume fraction	f_i	0.7
Maximum stretch	λ_2, λ_3	1.5

Table 5.2 – Material parameters defining the random fibrous RVE.

	Load stepping	**Load direction**	**Unload direction**
1	Simultaneous	$\mathbf{x}_2$ and $\mathbf{x}_3$	N/A
2	Sequenced	$\mathbf{x}_2$ then $\mathbf{x}_3$	N/A
3	Sequenced	$\mathbf{x}_3$ then $\mathbf{x}_2$	N/A
4	Sequenced	$\mathbf{x}_2$ then $\mathbf{x}_3$	$\mathbf{x}_3$ then $\mathbf{x}_2$
5	Sequenced	$\mathbf{x}_2$ then $\mathbf{x}_3$	$\mathbf{x}_2$ then $\mathbf{x}_3$

Table 5.3 – Loading paths for the testing of the mechanical behavior of the fibrous material.

loading paths (Table 5.3 - Paths 1 to 3). When the loading was sequenced, the boundary conditions imposed on the faces whose normal vector is perpendicular to the loading consisted in imposing an unchanged stretch.

– **Two different loading-unloading paths**
Closed elastic deformation cycles (Table 5.3 - Paths 4 and 5) are performed so as to impose on the system to return to its macroscopic undeformed initial state at the end of the cycle.

Accordingly, under the loading 5 for example, the RVE underwent a stretching λ_2 in the x_2 direction until the value 1.5 (Table 5.2) was reached, while maintaining unchanged the $\lambda_3 = 1$ stretch in the x_2 direction. Then the RVE underwent a second loading sequence with a stretching λ_3 in the x_3 direction until the value 1.5 was reached, while maintaining unchanged the $\lambda_2 = 1.5$ stretch in the x_2 direction. Afterwards, the RVE underwent a first unloading sequence with an "unstretching" λ_2 in the x_2 direction until the value 1 was reached, while maintaining unchanged the $\lambda_3 = 1.5$ stretch in the x_3 direction. Finally, the RVE underwent a second unloading sequence with an "unstretching" λ_3 in the x_3 direction until the value 1 was reached, while maintaining unchanged the $\lambda_2 = 1$ stretch in the x_2 direction.

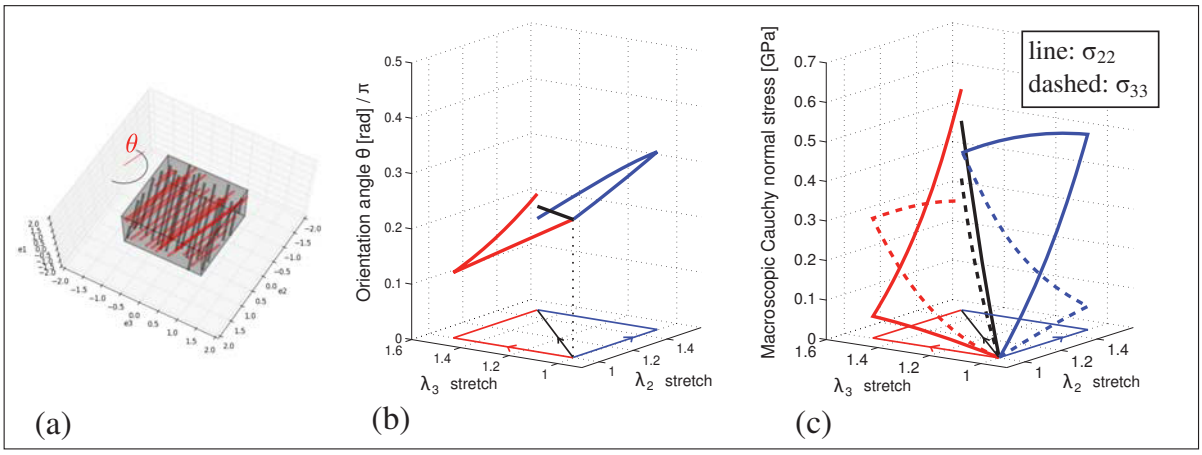

Figure 5.6 – (a) Sketch of a fibrous RVE showing the θ angle of a given fiber family; (b) evolution of the orientation angle of the $\pi/4$ fiber family along the loading path; (c) macroscopic Cauchy stress components σ_{22} (plane line) and σ_{33} (dashed line) plotted against the λ_2 and λ_3 components of the macroscopic stretch for the loading paths 1 to 3 (Table 5.3).

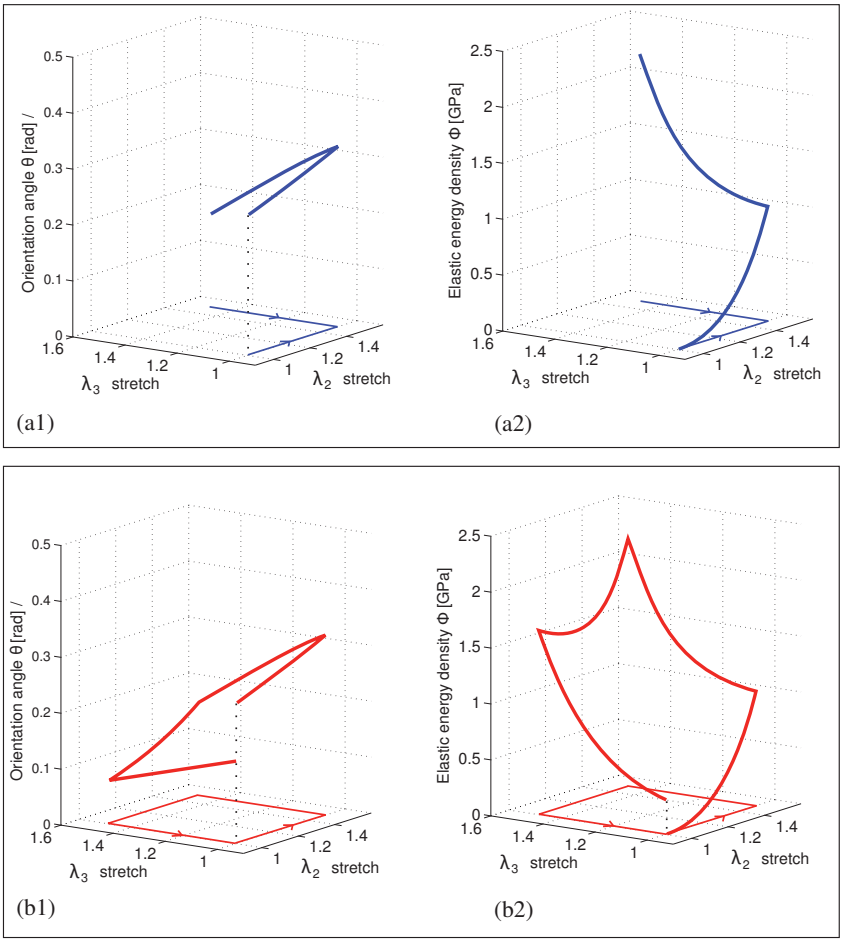

Figure 5.7 – (a1) Orientation angle of the $\pi/4$ fiber family and (a2) macroscopic elastic energy density plotted against the λ_2 and λ_3 components of the macroscopic stretch for the loading path 4 (Table 5.3). Analogous variables are plotted in (b1) and (b2) for the loading path 5

.

5.4.3 Results: modeling a random fibrous material

Figure 5.6 represents (a) the sketch of a random fibrous material, (b) the rotation of one representative fiber family (evolution of the orientation angle θ of the $\pi/4$ fiber family) along the loading paths 1 to 3, (c) the σ_{22} (plane line) and σ_{33} (dashed line) Cauchy stresses. All quantities are represented in the x_2-x_3 plane. We here consider the loading paths 1 to 3 (Table 5.3). For the sake of visualization, the deformation paths are shown in the x_2-x_3 plane in thin lines, with the arrows depicting the direction of the loading (notice the loading sequences on path lines in Figure 5.6(b) and (c). These results confirm a feature already discussed in the context of the modeling of the arterial adventitia: the macroscopic stiffening of the material originated in the reorientation of the fibers in the direction of the load (see plane lines in Figure 5.6(c) during λ_2 stretching, and see dashed lines during λ_3 stretching, with related fiber reorientations in Figure 5.6(b)). Although the final macroscopic strain tensor is identical for the three considered loading paths, the fibers do not reach the same final orientations (Figure 5.6(b)). This path dependent fiber rotation induces a noticeable path dependence of the final macroscopic stress state (Figure 5.6(c)).
As sketched on the x_2-x_3 planes, Fig 5.7 represents biaxial loading-unloading paths 4 and 5 (Table 5.3). When unloading occured following the exact reverse path as the loading (as it is the case on the path 4), the fibers returned to their initial position (Figure 5.7(a1)). In parallel, the elastic energy increased then diminished eventually leading to its complete release (Figure 5.7(a2)). However when the unloading followed another path than the reverse loading path (path 5), the fibers did not return to their initial position (Figure 5.7(b1)), eventually trapping residual elastic energy in the RVE at the end of the unloading (Figure 5.7(b2)).

5.4.4 Discussion

The response of the model to multiaxial loading cases suggests further micromechanical properties of fibrous tissues such as the artery. Namely, contrary to usual hyperelastic phenomenological models initially inspired from rubber mechanics [Mooney 40, Rivlin 48], the present micromechanical model allows reaching multiple stress states for the same deformation state, depending on the choice of the deformation trajectory (Figure 5.6). More precisely, the path dependence originates in the progressive micro-configurational changes occurring within the RVE and resulting in a history-dependent microscopic configuration of the fibers orientations. As a result, the reversibility of the mechanical response is preserved only if the unloading path follows the exact reverse path (Figures 5.7); in this case, fibers return to their exact initial configuration and the macroscopic mechanical state is free of residual stresses. All the elastic energy stored in the system during loading is released during unloading. On the contrary when unloading follows a path different to the loading one, fibers do not reach their initial configuration although the final macroscopic deformation state is forced identical to the initial macroscopic configuration. As a consequence, the macroscopic Cauchy stress does not return to zero, there is an insufficient release of absorbed elastic energy (observed hysteresis), resulting

in final "frozen" elastic energy in the material as a consequence of the change in microstructure morphology.

5.5 Conclusion and outlooks

All in all, the presented micromechanical model [Morin 15] is satisfactorily able to capture the nonlinear mechanical response of the arterial tissue on the basis of its collagen content and load-induced morphology changes. It provides a new insight, of a micromechanical nature, on the mechanisms that may occur in the arterial microstructure, leading to non-affine fiber motion, namely the importance of fiber-matrix interactions. Moreover, it is able to capture another possible mechanical property of fibrous materials, namely path dependence of the response and frozen elastic energy remaining in the system after complete unloading. This behavior originates in the micro-configurational changes occurring in the microstructure due to the application of loads and resulting in history dependent configurations of fiber orientations.

Chapter 6

Global discussion and outlooks

Contents

Résumé

Ce chapitre propose une discussion générale sur la base des résultats obtenus à la fois via le travail expérimental et le travail de modélisation, effectués lors de la thèse. Les expériences ont confirmé la complexité de la morphologie de la microstructure vasculaire, qui est largement caractérisée dans la littérature [Dingemans 00, O'Connell 08]. En particulier, elles ont illustré pour la première fois la cinématique potentiellement non-affine des fibres de collagène dans la couche externe de l'artère (adventice), lors de la déformation de l'artère. Ce genre de cinématique a été observé par le passé sur le péricarde [Chandran 06], sur la capsule du foi [Jayyosi 17], sur la peau [Jayyosi 17] ou sur le tendon [Lake 12]. Ce résultat suggère l'existence de mécanismes microscopiques inconnus régissant le mouvement des fibres et par conséquent l'élasticité artérielle. Ce phénomène n'a pas été identifié sur les autres réseaux fibreux vasculaires, dont la morphologie a semblé plus structurée, réticulée et dont la cinématique s'est révélée affine, c'est-à-dire facilement prévisible.

La principale limitation associée aux études expérimentales effectuées concerne le biais qui existe entre l'environnement biologique et mécanique in vivo et l'environnement ex vivo propre aux conditions de laboratoire, ce qui modifie les propriétés mécaniques des artères testées à l'échelle microscopique, avec des conséquences à l'échelle macroscopique. Sur ce point nous précisons dans ce chapitre que l'objectif des expériences n'était pas une imitation la plus fidèle possible du comportement mécanique de l'artère en condition in vivo mais plutôt une comparaison inter-couches et selon divers scenarii de chargement du comportement mécanique d'échantillons artériels préparés de manière identique. D'autres limitations, concernant la précision des méthodes de post-traitement des images de microscopie, sont également mentionnées. En particulier, la difficulté réside dans le développement de méthodes permettant d'analyser les rotations globales des fibres de collagène, indépendamment de leur tortuosité (c'est-à-dire sans prendre en compte les réorientations par segments à l'échelle des ondulations) et permettant également une comparaison de la réorientation réelle des fibres avec la rotation prédite par la cinématique affine. Les résultats de ce travail expérimental mettent en évidence le besoin de caractériser les liaisons entre le collagène et les autres protéines présentes dans la microstructure artérielle comme l'élastine et les protéoglycanes dont les influences sur l'intégrité mécanique de l'artère ne sont pas encore documentées.

Le modèle multiéchelle, développé dans le cadre de la micromécanique des milieux continus, et appliqué pour la première fois à l'artère, prédit la non linéarité de la réponse mécanique du tissu ainsi que les réorientations des fibres associées à la déformation. Ces résultats sont conformes aux observations expérimentales publiées précédemment dans la littérature [Chen 13, Sugita 17] et à celles décrites au chapitre 4. Le modèle a aussi révélé sa capacité à prévoir une possible trajectoire dépendance de la rotations des fibres, résultant en la non restitution d'une fraction de l'énergie élastique stockée dans la microstructure. A la connaissance de l'auteur, ce genre

de comportement mécanique n'a jamais été caractérisé de manière multi-échelle dans la littérature. Les développements en cours et futurs du modèle sont enfin présentés et concernent la modélisation de l'hétérogénéité des faisceaux de collagène, la modélisation du comportement de la média, ainsi que l'implémentation de la réponse du VER à des états de contrainte imposés.

En fin de chapitre, la possibilité de l'implémentation d'un modèle alternatif du comportement mécanique de la microstructure de l'artère. L'approche présentée, appliquée par le passé notamment au cytosquelette cellulaire [Ingber 93, Ingber 06] est basé sur la théorie de la tenségrité. Cette proposition de modélisation future est motivée par la capacité du modèle planaire de tenségrité de [De Jager 04, Luo 08] de prédire la cinématique des fibres de collagène de l'advantice, lors des différents scenarii de traction-gonflement (voir section 4.3 pour plus de détails). Après une présentation des principes de bases régissant les structures de tenségrité [Fuller 61, Skelton 01], on étudie leur applicabilité à la microstructure de la couche adventice de l'artère. Pour finir, en en guise de perspective, les verrous à lever pour implémenter de ce genre de modèle sont présentés et constituent ainsi une proposition de plan de travail futur dédié à la modélisation de l'artère.

Abstract

In the present Chapter, a general discussion is proposed, overviewing the results obtained through both the experimental and modeling work carried out during the thesis. Experiments have confirmed the high complexity of the vascular microstructure's morphology. In particular they have illustrated for the first time non-affine, load-dependent collagen fiber kinematics in the outer layer of the artery (adventitia), suggesting unknown microscopic mechanisms governing fiber motion, hence arterial elasticity. This microstructural load-induced behavior differed significantly with this of other vascular fibrous networks, whose morphology appeared to be more structured, crosslinked and whose kinematics remained affine, i.e. easily predictable. The principal limitation associated with the applied experimental procedures concerns the discrepancy between the *in vivo* biological and mechanical environment, and the *ex vivo* environment, which may alter the mechanical properties of the tested arteries at the microscopic scale, with consequences at the macroscopic scale. We hereafter discuss that mimicking the exact native behavior of the artery was not the objective of the experiments. The aim was rather an inter-layer and inter-load-scenario comparison of the mechanical behavior of identically prepared arterial samples. Other limitations concerned the precision of image post treatment methods which are also mentioned. The novel results highlight the pressing need to characterize the bindings between collagen and other load bearing proteins in the arterial microstructure, such as elastin and proteoglycans, whose influence on the mechanical integrity of the artery is unsettled. The multiscale model, characterized by an unprecedented continuum micromechanics approach to arterial biomechanics and applied to the adventitia, was able to predict the nonlinearity of the mechanical response of the tissue along with the associated load-induced reorientation of its constitutive fibers. It also predicted a possible path dependence of the microstructure rearrangements, inducing possible frozen elastic energy within its structure. Ongoing and future model developments concern (i) the implementation of an additional mesoscale upscaling step accounting for the heterogeneity of collagen bundles, (ii) an algorithmic scheme allowing stress-driven loading, and (iii) the duplicating of the approach to a Representative Volume Element of the media layer of the artery. As a final outlook, the possibility of implementing an alternative multiscale model of the mechanical behavior of the artery, based on tensegrity theory, is discussed. This proposition is motivated by the successful prediction of the experimentally observed load dependent fiber kinematics by a simple planar tensegrity model provided by the literature.

6.1 Introduction

The outcomes of the experimental procedures (Chapters 3 and 4) as well as of the micromechanical modeling (Chapter 5), acquired and discussed in the framework of the present doctoral research contribution, provide insights into the multiscale mechanical behavior of arteries. In the preceding Chapters we discussed the obtained results, by proposing a detailed comparison with the results documented in the existing literature, commenting consistencies and discrepancies, and mentioning limitations. However, future scientific work was only briefly mentioned up to this point. In the present chapter, we propose a discussion about the obtained results as a whole, both from experimental and modeling points of view, and suggest follow-up scientific investigations by detailing a selection of short-term future steps. More precisely, the chapter is organized as follows: first the global experimental outcomes are discussed. Afterwards, modeling results are discussed along with associated outlooks that consists in current and future developments of the model. Finally, an alternative multiscale modeling strategy, based on tensegrity, is introduced on the basis of the previously discussed results. The final section is presented as a preliminary framework for the possible future implementation of such model. Throughout this general discussion chapter, regular references will be made to Figure 6.2, which sketches schematically the overall results and outlooks associated with the present doctoral thesis.

6.2 Outcomes of the experimental procedures

6.2.1 Confirmed results

Experimentally, our results have confirmed the anisotropy of the stress-strain relationship [Choudhury 09, Holzapfel 05] (section 3.3.1) (Figure 6.2-A1). They have also confirmed the complexity of the arterial extracellular matrix within the microstructure (section 3.3.2), with a stratified morphology showing important discrepancies in composition and spatial organization between the tunica media and tunica adventitia, consistently with [Dingemans 00, O'Connell 08, Arkill 10, Chen 11, Chen 13, Keyes 11, Keyes 13] (Figure 6.2-A2). In particular, biological fibrous components such as elastin and collagen took various forms within the microstructure. For example in the adventitia, a low density network of elastin coexisted among the thick collagen bundles and took the form of thin crosslinked fiber segments showing a preferred longitudinal direction, whereas in the media, elastin took the form of dense fenestrated lamellae tightly embedding the smooth muscle cells. These observations were similar to those of [Ushiki 02, Raspanti 06, O'Connell 08, Koch 14] (Figure 6.2-A2). Importantly, the correlation between fiber recruitment, and the stiffening of the mechanical response, which was the topic of numerous past studies [Hill 12, Schrauwen 12, Wang 13, Sugita 17] (Figure 6.2-A1 and A2) was also confirmed (section 3.3).

6.2.2 Novel results

The major advances relative to the present thesis concern the evidenced layer-specific fiber kinematics (Figure 6.2-A2)), which turned out to be well predicted by the affine rule as far as medial elastin, medial collagen, and adventitial elastin networks were concerned. Conversely the affine rule was a poor predictor of the motion of adventitial collagen fibers (section 3.3.3). This result extended the list of collageneous tissues which previously showed a potentially non-affine behavior of their collagen fibers. In fact the mechanically-induced reorientation of collagen fibers was the focus of several contributions dedicated to tendon [Lake 12], collagenous constructs [Chandran 06], skin [Lynch 17], bovine pericardium [Billiar 97], and the liver capsule [Jayyosi 16, Jayyosi 17]. Such results obtained for the carotid artery were, to the author's knowledge, not documented before.

Pushing forward the analysis of non-affine adventitial collagen kinematics, another important experimental result derived from the present work concerns the load-dependence of fiber kinematics (section 4.3). In fact affine predictions were found to (i) underestimate fiber realignment when the transverse contraction of the tissue was enabled (which was the case when applying an uniaxial tension loading on flat arterial samples, and when applying an axial tension loading under constant pressure on cylindrical samples); and (ii) overestimate fiber realignment when the transverse strain was disabled (which is the case when applying an inflation loading under constant axial stretch). These findings, consistent with the load-dependence of fiber kinematics suggested by [Chen 13], highlight the important role of boundary conditions in the fiber motion. Moreover, they suggest that adventitial collagen fibers are characterized by a relative freedom of movement, challenging the hypothesis of a tight embedding in a stiff surrounding matrix which would be implied by affine kinematics (an hypothesis which characterizes hyperelastic models [Holzapfel 01, Gasser 07]).

6.2.3 Principle drawbacks and limitations

6.2.3.1 *Ex vivo* mechanobiological environment

The principal limitation arising from the applied experimental protocols is the gap between the *ex vivo* mechanobiological environment and the native, *in vivo*, environment. In fact, due to tissue storing in PBS after excision and the (minimized) delay between excision and testing (sections 3.2.1, 4.2.1, see also Appendix A.5.1 and A.5.2), the action of degradative enzymes may have modified both the microstructural composition as well as the residual stress in the artery, hence potentially modifying the artery's mechanical response. Moreover, concerning rabbit carotids (which were tested in the applied protocols), the arteries undergo, in their native environment under normal ventricular activity, pressure steps of approximately 20 mmHg between diastole and systole [Govyrin 57] with a diastolic pressure of about 105±15 mmHg suggesting that collagen fibers operate around their recruitment threshold stretch (section 4.3). This operating mode is suited to fulfilling the adventitia layer's mechanical role: preventing

eventually overdistentions of the artery [Humphrey 10]. Hence obviously, investigating collagen rearrangements ranging from total crimping under load-free state, up to full engagement and realignment at high stretch (70-100%), or under pressures ranging from 20 mmHg to 140 mmHg, is far from those aforementioned physiological mechanical conditions. However, the objective of the present work was to study a variety of mechanical loadings, maximizing fiber motion, in order to visualize experimentally enhanced microscopic mechanisms for a favored characterization. In other words, even if fiber kinematics is altered *ex vivo*, new findings about the organization of the microstructure and underlying mechanisms are possible. Accordingly, the aim of the experimental strategy was to compare the tissue's response to different loading scenarii (1D and 2D) on identically stored and prepared samples. Hence, we considered that this limitation did not impair our results.

6.2.3.2 Automated image quantification methods

Another general difficulty and limitation concerned the liability of the automated image quantification methods (sections 3.2.4 and 4.2.5, see also Appendix A.8.1 and A.8.2). Due to (i) intrinsic imperfections of an imaging facility such as multiphoton microscopy and (ii) the complexity of morphological features of the biological tissues such as crimped variously oriented collagen bundles, it appears that automated methods should be applied with caution. In particular, we have commented in Chapters 3 and 4 the difficulty to quantify the orientations of collagen bundles, above a certain crimping threshold. Accordingly, we have addressed this issue by applying two specific image post-processing methodologies. On the one hand in section 3.2.4 (see also Appendix A.8.1), when quantifying layer-specific fiber orientations, we considered a fictitious loading scenario, which involved only loaded configurations. Hence the load-free configuration of adventitial collagen bundles did not need to be considered during the analysis of affinity of fiber kinematics. On the other hand in section 4.2.5 (see also Appendix A.8.2), we chose, in order to analyze the kinematics of adventitial collagen, to compare two microstructure configurations in the Fourier domain. Both configurations were loaded such that collagen bundles appeared engaged or close to engagement, providing sufficiently clear global orientations. The methodology also involved filtering the Fourier spectra allowing minimization of the influence of low-scale orientations on the microscopy images, such as those corresponding to the crimped state. It should also be mentioned that, depite the in-depth imaging potential of the multiphoton microscope ($\approx$50 µm), and despite the applied imaging method (namely microscopy with both intima facing the objective and adventitia facing the objective, section 3.2.3), the innermost fibers of the microstructure could not be imaged or were imaged with poor quality, impairing the extraction of fiber angle densities in these innermost regions of the artery.

6.2.3.3 Partial analysis of the extracellular matrix

It should also be mentioned that although the experimental analysis and results focused on collagen and elastin, other biological components are known to play a mechanical role in the

arterial microstructure (section 2.3.2.2). In particular smooth muscle cells provide adaptive plasticity to the artery's mechanical response [Ratz 15]; proteoglycan configurations and hydration levels in turn influence the residual stress within the artery, but also its elasticity, strength, and provide compressive resistance [Buschmann 95, Cardamone 09]. Fibroblasts in turn are cells that regulate, through mechanotransduction mechanisms [Sartore 01, Humphrey 08b] the collagen turnover, hence playing a role in tissue remodeling. These three components of the arterial microstructure should be studied experimentally in future studies, focusing in particular on their load-induced reconfigurations and kinematics (Figure 6.2-C2).

6.2.4 Importance of micromechanical phenomena

All in all, our multiscale characterization of the mechanical behavior of the artery contributes to a better understanding of underlying micromechanical phenomena taking place during arterial deformation. As it is known today that the outcomes of vascular pathologies are strongly dependent on local phenomena such as extracellular matrix damage (in the case of aneurysms [Taylor 09, Romo 14]), or cascades of tissue degradation (in the case of atherosclerosis, [Libby 92, Weber 08]), progress in this field appears to be very important. The results commented in this thesis, both from the experimental and modeling points of view, highlight in particular the important role of fiber-fiber interactions, which play an important role in the tissue's mechanical response (section 5.3.3) and on fiber kinematics (sections 5.3.3 and 4.3).

In this context, although they have proven remarkably computational accuracy, hyperelastic models based of the phenomenological definition of strain energy functions [Holzapfel 01, Holzapfel 05, Gasser 07, Zulliger 04] were not designed for providing neither microscopic deformations and stress fields, inter-constituent interactions, nor biological processes that continuously modify the microstructure. In the objective of simulating and predicting the evolution of vascular pathologies, our work thus confirms the growing relevance of multiscale approaches to arterial modeling as already developed by [Freed 05, Grytz 09, Raina 13, Marino 13], given their ability to include a wide range of phenomena at the fiber scale, including complex, non-affine fiber kinematics [Stylianopoulos 07]. In the next section, we discuss the preliminary outcomes and benefits of a multiscale model based on continuum micromechanics (Chapter 5).

6.3 Outcomes of the micromechanical model

6.3.1 Modeling results and related experimental outlooks

The multiscale model described in Chapter 5 is an unprecedented methodology in the context of soft tissues, currently under development [Morin 15]. It was adapted and tested, as a preliminary step, on a simple loading configuration, designed to correspond kinematically to the experimental uniaxial tests discussed in section 3.2.2 and performed on flat arterial samples. Given the relative simplicity of morphology and remarkable realignment properties of adventitial collagen, it was chosen to test the model on a Representative Volume Element of the tunica

adventitia, representing collagen bundles by infinitely long cylindrical inclusions, surrounded by a continuous matrix comprising elastin, proteoglycans, hydrated fibroblasts, and other biological components of the adventitia [Wight 89, Shi 96, Arkill 10]. This version successfully predicted material stiffening during loading (section 5.3.3). The stiffening resulted from the rotation of the collagen fibers (Figure 6.2-B1 and B2). In particular, the results evidenced the non-affine character of fiber reorientation, with non-affinity correlated to fiber volume fraction, a physical parameter which directly affects the intensity of fiber-matrix and fiber-fiber interactions through the Mori-Tanaka homogenization scheme [Mori 73,Benveniste 87] (Figure 6.2-B2). This particular finding raises the question of the nature of these interactions and suggests further experimental characterization. For example, the study of the inter-constituent crosslinking and binding mechanisms existing in the arterial microstructure, which might play a role in the interactions between collagen, elastin, and proteoglycans [Eyre 84], could be performed. The developped mechanical setups coupled to microscopy (sections 3.2 and 4.2) could provide interesting insights about specific binding proteins such as Fibulin-5 or Fibrilin [Yanagisawa 02] and their possible load-induced rearrangements (Figure 6.2-C2).

6.3.2 Current and future developments of the model

6.3.2.1 Importance of boundary conditions

As previously mentioned, the micromechanical model has been tested on a simple loading configuration, kinematically similar to uniaxial tests on flat arterial samples, with displacement-driven deformation (section 5.3.2). We saw, when applying uniaxial tension on flat samples, that the transverse contraction needed to be imposed in the model by applying an experimentally observed compressive strain. It is however possible to improve this modeled loading scenario by implementing stress-driven load cases. By doing so, the RVE can be loaded with a greater analogy to the one experimentally applied, i.e. a prescribed incremental tensile stress (σ_{22}, Figure 6.1(a)), is applied along with zero force imposed on the lateral boundaries. The model may then test the observations commented in section 4.3, concerning the load-dependence of fiber kinematics, hence their dependence to different boundary condtions: experiments showed a limited reorientation of the fibers when the transerse contraction of the tissue wasdisabled, and an important reorientation of the fibers when the transverse contraction was enabled.

6.3.2.2 Three-scales homogenization scheme

The used version of the micromechanical model considers two distinct scales: (i) the macroscopic scale, which governs homogenized mechanical tensors representing the deformation and stress states at a given material point and (ii) a microscopic scale at which the material point is modeled by a Representative Volume Element composed of two phases: the fibers and their surrounding medium. Both phases are approximated in the model as homogeneous and isotropic. As discussed in section 5.3.3, this model was able to predict material stiffening induced by fiber rotation in the direction of the strain. We know however from existing litterature [Raspanti 06,

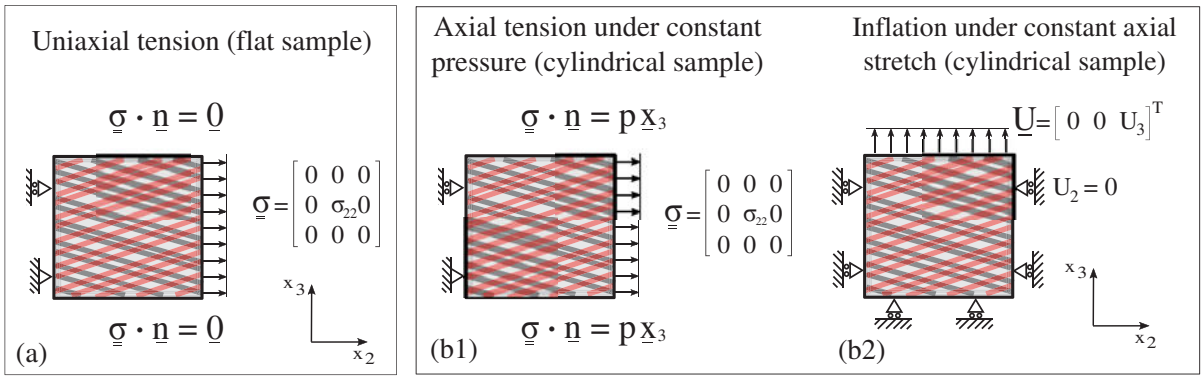

Figure 6.1 – Boundary conditions allowing the simulation of the experimentally applied loadings: (a) uniaxial tension on flat samples; (b1) axial tension under constant pressure on cylindrical samples; (b2) inflation under constant axial stretch on cylindrical samples.

Ushiki 02, Berillis 13] that a collagen bundle exhibits a heterogeneous microstructure itself (parallel fibrils coated by transverse proteoglycans, see section 2.3.2.3), with reorganizations that may occur at the scale of the fibrils. Hence its mechanical behavior can be estimated by the introduction of an RVE within this phase [Fritsch 09], with dimension $l_2 < d$ comprising again smaller phases with characteristic length $d_2 \ll l_2$ (see section 5.2.1 for the detailed presentation of the separation of scales principle), leading to a three-scales homogenization scheme (Figure 6.2-D2). This version of the micromechanical model is now implemented, although its development and testing did not enter in the scope of this PhD thesis. Noticeably, its formulation may also be used to model the decrimping process of the bundles, considering that during the decrimping of the collagen bundles, fiber segments reorient at a subscale of the global bundle reorientation.

6.3.2.3 Modeling the media tunica

Other ongoing developments of the micromechanical model concern the application of the described methodology in section 5.2 to a RVE representing a simplified microstructure of the arterial media. As documented in the existing literature (section 2.3.2.2) the media is made of concentric elastic lamellae and circumferentially oriented collagen bundles. The adaptation of the model thus implies downscaling the input macroscopic deformation into another shape of inclusions (oblate spheroids obtained as a special case of ellipsoidal inclusions studied by [Eshelby 57] (Figure 6.2-D2). Combining the modeled RVEs of both the media and the adventitia in a structural model will allow the simulation, in the future, of the response of the total composite artery and the comparison of the simulation results with experimental results. Besides, the experimentally observed anisotropy of the arteries (section 3.3.1) may also be tested numerically (Figure 6.2-D2).

6.3.2.4 Determining material constants of the matrix phase

As described in section 5.2, the current version of the micromechanical model applied to the arterial adventitia consists in upscaling the microscopic elastic properties of a biphasic RVE. In

this RVE, we chose to represent (i) collagen bundles using homogeneous cylindrical inclusions, and (ii) their surrounding medium, composed of water and various biological components, as a homogeneous matrix. Concerning in particular this matrix phase, its mechanical properties are governed by an isotropic stiffness corresponding to the stiffness of elastin fibers, which we considered diluted in the matrix. This choice raises the question of the biological components that contribute to the mechanical behavior of the matrix, hence the material parameters that should be chosen for the matrix. More generally, these considerations question the physical nature of the matrix surrounding the fibers. Today's knowledge about the arterial microstructure in the adventitia states that what is considered in the micromechanical model as the surrounding matrix is composed of variously oriented elastic fibers [O'Connell 08, Arkill 10, Chen 13] but also fibroblasts [Shi 96, Sartore 01] and proteoglycans [Wight 89]. An important challenge consists therefore in finding relevant material parameters for, or to introduce a refined description of the matrix. Besides, the dual nature of the aforementioned matrix: a solid, as it is the case in the presently applied micromechanical model, or a fluid (given the possible diffusion of water) is also a complex question. In particular future studies should investigate whether the fluid in the matrix is drained during the deformation, potentially governig the tissue's incompressibility.

6.3.2.5 Other modeling outlooks

A final outlook for further development of the micromechanical model concerns trajectory dependence and possible frozen elastic energy results, observed on a random modelled fibrous material. This interesting result, which originates in the hypoelastic constitutive law governing the mechanical behavior of both phases of the RVE should, together with the progressive, load-induced fiber rotation, be compared with mechanical experiences run on a selection of fibrous materials.

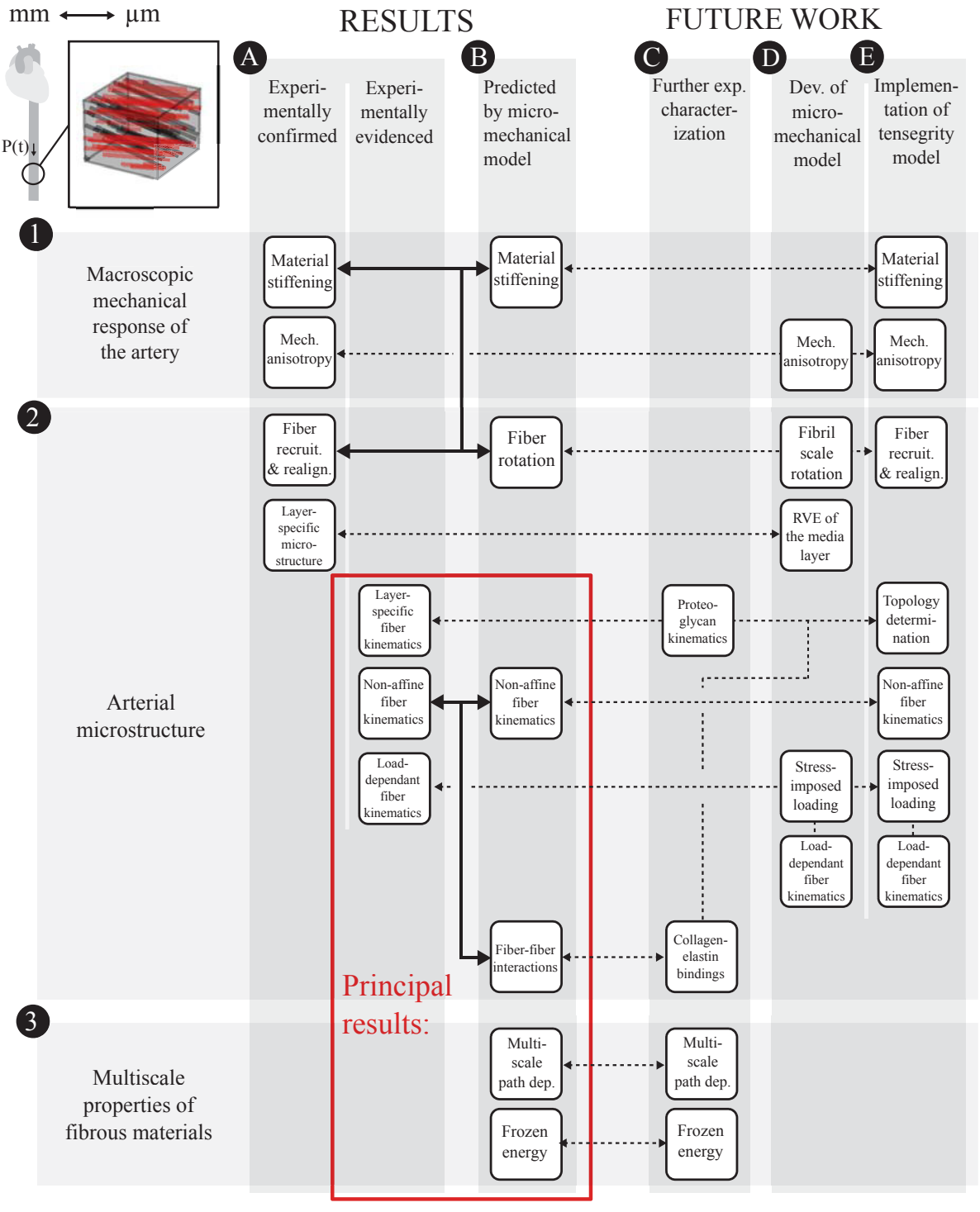

Figure 6.2 – Global overview of the doctoral work's outcomes and future work.

6.4 Alternative multiscale modeling of the arterial wall based on tensegrity

As already introduced in section 4.4, another outlook that arises from the aforementioned results consists in implementing a tensegrity-based model for the artery, and more specifically as a first step for the arterial adventitia. In the following section, a dedicated state-of-the-art is presented; the concept of tensegrity, then the applicability of tensegrity structures to the adventitia are discussed, and the scientific challenges (involving both future experimental and modeling work) that would need to be addressed in order to implement such a model, are listed.

6.4.1 Tensegrity structures: state-of-the-art

6.4.1.1 Physical principle

The concept of "tensegrity" was invented by Buckminster Fuller while studying how forces are distributed through geodesic domes [Fuller 61]. Fuller imagined a web-like mechanical structure that consisted of two types of interacting members: tensile ones (cables) and compressive ones (bars) (Figure 6.3(a)). In a tensegrity structure being in the reference "initial" state, compression forces in the bars balance tension forces in the cables. A detailed review of assumptions underlying the previously studied tensegrity structures has been provided by [De Jager 04].

6.4.1.2 Applications

While Fuller [Fuller 61] initially applied his newly invented tensegrity concept to a new generation of deployable, adaptive, high performance structures in the context of aerospace engineering, tensegrity were applied since the early 90s in the domain of cellular biology, with the objective of explaining how cells and tissues are constructed [Ingber 93]. The latter provided a milestone in understanding the complex pattern and structure that is observed within the cytoskeleton (CSK) of living cells. Cellular tensegrity theory constitutes today an alternative approach to cell biomechanics that emphasizes the discrete nature of stress bearing elements in the cell while being based on the known structural properties of the cytoskeleton [Stamenović 96]. In the design of tensegrity structures, it is possible calibrate and tune the structure with respect to target stiffness properties, by appropriately selecting continuous topology parameters [Skelton 01, De Jager 04] that govern a given modeled morphology. In fact, equilibrium in such a structure is possible for numerous configurations or shapes [De Jager 04]. Noticeably in living tissue, this structural tuning is a continuous biochemical process, leading [Ingber 93] to propose that tensegrity may represent one of the most basic principles of biological design. More recently, [Luo 08] downscaled the application of the tensegrity theory, by describing the ultrastructure of stress fibers using a previously studied planar tensegrity structure [De Jager 04, De Jager 06] (Figure 6.3(c) and (d)). Stress fibers are contractile bundles in the cytoskeleton that stabilize cell structure by exerting traction forces on the extracellular matrix. [Luo 08] showed that the chosen tensegrity network can predict several key behaviors of stress fibers measured in living cells, including viscoelastic retraction, fiber splaying after

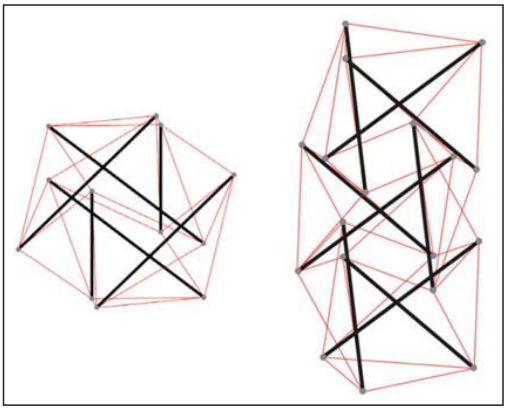

(a) Example of tensegrity topologies designed in [Xu 10]: compressional bars are represented in black whereas tensional cables are represented in red.

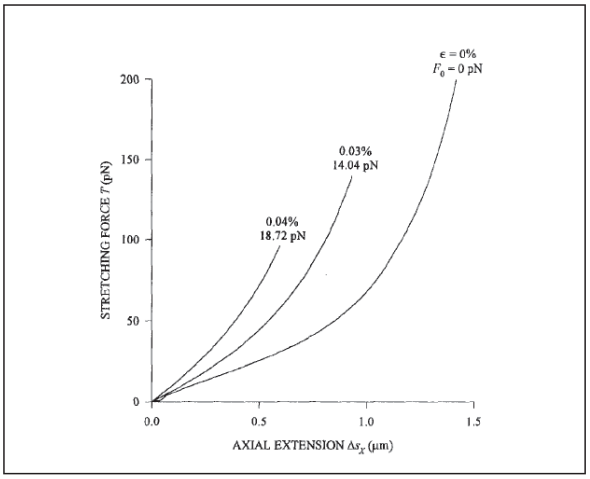

(b) Stretching force vs. extension of a six struts tensegrity structure studied by [Coughlin 97]

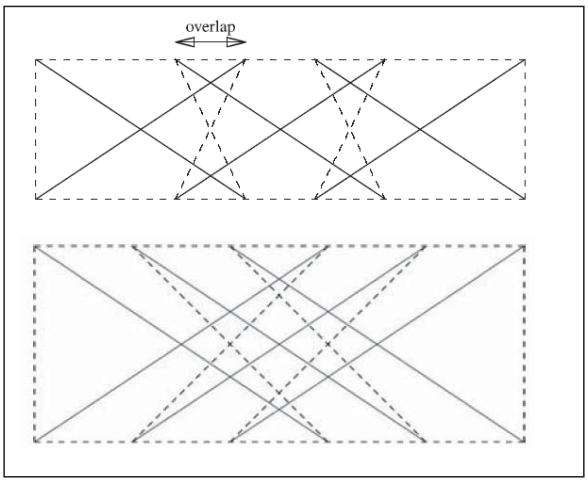

(c) Planar tensegrities studied by [Dejager 04, Dejager 06] characterized by overlapping compressive bars

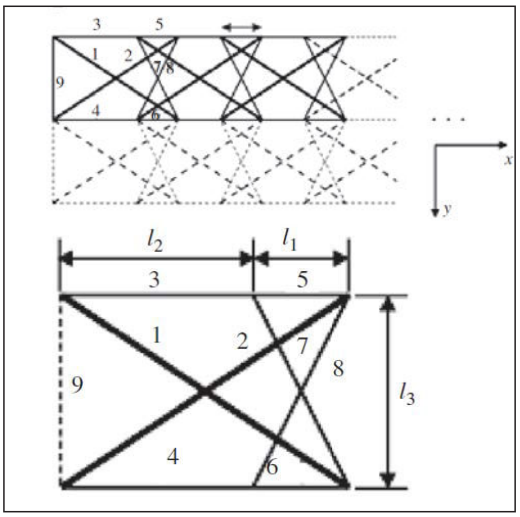

(b) Planar tensegrity applied to stress fibers by [Luo 08]

Figure 6.3 – Selection and illustration of previously studied, planar or three-dimensional, tensegrity structures.

severing, non-uniform contraction, and elliptical strain of a puncture wound within the fiber.

These successful results illustrate the wide applicability of tensegrity structures, noticeably at multiple size scales in the hierarchy of mechanobiological systems [Ingber 03, Ingber 06].

6.4.2 Applicability to adventitial microstructure

6.4.2.1 Motivations

As previously pointed out, tensegrity networks appear as an interesting candidate to model biomechanical systems characterized by complex fibrous or filamentous patterns and organizations, as well as inner prestressing states. Moreover, it has been commented that tensegrities can be relevant across a wide range of scales within the living systems [Ingber 06]. Pushing forward these general considerations, we review several characteristics of the arterial microstructure in the light of tensegrities.

1. **Fiber-fiber interactions**
   As previously documented by [Dingemans 00, O'Connell 08, Chen 13] and as discussed in section 3.3.2, the arterial microstructure is made of a complex coexisting, intertwined networks of collagen and elastin. In particular, [Lanir 79, Chow 14] have documented that elastin and collagen interact with one another, with elastin fibers exerting a compressive loading on the collagen bundles, forcing the latter fibers to crimp when the network is free of external load. An internally stressed mechanical equilibrium is thus established among the different constituents of the arterial microstructure. Morever, although the exact nature of the bonds between collagen and elastin is not known, the work of [Stylianopoulos 07] suggests that a system of freely rotating crosslinks between fibers is a good candidate to model fiber-fiber interactions, hence fiber kinematics in arteries. Importantly, the commented fiber-fiber interactions are responsible for non-affine fiber kinematics, as they offer the possibility for the fibers to minimize their inner stretch during deformation [Stylianopoulos 07]. In summary, existing modeling approaches assume the existence of fiber-fiber interactions.

2. **Stiffness contributions of elastin and collagen**
   Previous findings about the load-bearing properties of both collagen and elastic fibers reveal that the elastic modulus of collagen fibers is greater than the elastic modulus of elastic fibers by a factor 10^3 [Wenger 07, Burton 54, Faury 01]. This stiffness contrast between the two interacting load-bearing components is consistent with that which governs the interactions between cables (high compliance) and bars (low compliance) in tensegrities.

3. **Morphological relevance and load-dependent fiber kinematics**
   As described previously, tensegrity topologies are various and a great deal of configurations can lead to a stable mechanical equilibrium under zero external load [De Jager 04]. As a results, the specific but well documented arterial morphology [Dingemans 00, O'Connell 08, Arkill 10] should not, at this stage, be a drawback to the applicability of tensegrity models to the artery. In section 4.4 we commented that a planar tensegrity model inspired from [Luo 08], introduced to represent the arterial adventitia, was able to explain the load-specific non-affine kinematics of collagen fibers characterized in section 4.3, as well as those documented by [Chen 13]. In more details we remind the observations that were

drawn in section 4.4: under inflation loading at a constant axial stretch, fiber rotation is impossible, as it would imply a transverse strain, the fibers being rigid. Conversely, under axial tensile loading at a fixed inner pressure, fiber rotation is the only way to allow the extension (Figure 4.6).

4. **Mechanical response**
   A tensegrity description of the cells cytoskeleton has already revealed a gradual during an externally applied deformation [Coughlin 97, Stamenović 96], consistently with the fundamental mechanical property of living cells [Wang 93]. This material stiffening under load also characterizes the mechanical response of the arterial tissue, providing an additional analogy suggesting the applicability of tensegrity to modeling the arterial microstructure. [Coughlin 97] also commented that when the pre-stress of the structure decreases, the stiffening effect decreases (Figure 6.3(c)).

6.4.2.2 Determining a relevant tensegrity topology

In section 3.3.2, we analyzed the realignment magnitudes of the various fiber networks that compose the arterial microstructure, in the two composite arterial layers: the tunica media and the tunica adventitia. We showed that, although the stratified medial microstructure is complex from the morphological point of view, with collagen and elastin fibers taking various forms, its behavior satisfies the affine assumption. In the adventitia however, helically oriented collagen bundles show a more complex behavior, characterized by load-specific, non-affine fiber kinematics, as detailed in sections 3.2.5 and 4.3. Besides, fiber-fiber interactions, which are proper to tensegrity structures, are likely to correlate with non-affine fiber kinematics, as documented by [Stylianopoulos 07]. It appears therefore more interesting to apply tensegrity to a Representative Volume Element of the tunica adventitia, where elastin and collagen fibers coexist. Due to the limited transmurality of fiber orientations, and the dominance of two symetrical families of collagen fibers, the planar tensegrity studied by [De Jager 04, De Jager 06] and [Luo 08] can be chosen as a starting point, providing a relevant fiber topology. Accordingly, two design parameters are introduced that determine the morphology of the structure, namely the overlap factor and the slenderness ratio (Figure 6.3(c) and (d)), which together determine the fiber angles.

6.4.2.3 Establishing the force equilibrium and computing the mechanical response

For a simple topology, applying equilibrium conditions by means of a classical Newtonian formulation provides a set of equations that include the forces internal to the structure [De Jager 04], with constitutive behaviors of bars and cables derived from continuum mechanics. In order to determine the mechanical response of the tensegrity structure to an externally applied load, the set of equations can be solved either analytically or numerically depending on the loading assumptions made and on the loading configurations. Thus, under the assumption of infinitesimal strains and infinitely rigid bars, the set of equations is linear and can be solved analytically, pro-

viding instantaneous stiffnesses of the system, as function of (i) topological parameters (namely position and sizes of tendons, struts) and of (ii) the pre-stressing state [De Jager 04].

It is also possible to formulate the fully nonlinear equilibrium conditions, taking care of geometrical and material nonlinearities, and of pre-stress. This approach, suited under finite strain framework, provides a set of nonlinear equations for which no solution can be obtained analytically [De Jager 06], and which becomes a numerical problem. For example, [Stamenović 96] determined numerically, under finite strain framework, the mechanical response of a tensegrity structure representing the cytoskeleton, by evaluating the axial extension resulting from an increasing stretching force. The results were obtained by computing the virtual work of a stretching force during an incremental axial extension of the structure. [Luo 08] in turn performed dynamic simulations on the previously sketched planar tensegrity network modeling a stress fiber (Figure 6.3(d)) and determined transient mechanical states using a commercial structural analysis software (ANSYS®).

The latter method seems particularly suited for the calculation of the mechanical response of a tensegrity structure representing the arterial adventitia, as it would enable the application of various loadings while easily modifying the structure's topology and analyzing the consequences on the stress-strain relationship.

6.4.2.4 Open questions and challenges

As previously described, numerous analogies between the tensegrity structures and arterial microstructure (in particular the microstructure of the adventitia) suggest that they are good candidates for a future multiscale model applied to the artery. However, several questions arise, which will need to be addressed in order to fully justify the morphological and micromechanical relevance of such approach. Most importantly, these open questions concern (i) the mechanical contributions of proteoglycans, (ii) the nature of biological bonds between collagen, elastin and other binding proteins, (iii) the coherence between the experimentally observed kinematics of elastin fibers and the one predicted by the tensegrity topology, and (iv) the mechanical conditions under which a force shift occurs in the compressive bars, which should represent collagen recruitment. In table 6.1, a summarized framework for the implementation of a tensegrity-based mechanical model of the arterial adventitia is proposed.

	Scientific framework	References
Implementation	To run topology finding methods	[Juan 08]
	To verify consistence of the topology with the morphology of the adventitia	[O'Connell 08, Chen 13, Krasny 17]
	To determine under which conditions may occur a load shift in the stiff bars	[Fuller 61, Dejager 06]
	To apply material parameters for bars and cables	[Burton 54; Faury 01, Wenger 07]
	To implement displacement driven and/or stress driven loading under large strain formalism	[Mooney 40, Stamenovic 96, Luo 08]
Analysis	To run loading scenarii	[Luo 08]
Characterization	To characterize fiber engagement / recruitment	[Schrauwen 12]
	To verify material stiffening	[Holzapfel 05]
	To quantify fiber kinematics	[Chen 13, Krasny 17]
	To measure affinity of fiber rotation	[Krasny 17]
	To characterize laod dependance of fiber kinematics	[Chen 13, Krasny 17]
	To characterize the structure's anisotropy	[Holzapfel 05, Choudhury 11]

Table 6.1 – Summarized framework for the implementation of a multiscale mechanical model of the arterial adventitia, based on tensegrity.

Conclusion générale - *General conclusion*

Le présent travail doctoral a soulevé initialement plusieurs questions (section 2.6), découlant de la revue de l'état de l'art. Ces questions concernaient le besoin d'une meilleure compréhension du couplage qui existe entre, d'une part la composition et les réarrangements de la microstructure, et d'autre part la réponse mécanique du tissu artériel. Afin de répondre à ces questions, un ensemble de méthodes expérimentales et de modélisation a été développé.

En particulier, des dispositifs de traction uniaxiale et de traction-gonflement ont été mis en place (sections 3.2.2 et 4.2.2), permettant de tester des échantillons artériels en acquérant *in situ* des images de la microstructure de ces échantillons par microscopie multiphoton. Ces dispositifs, appliqués lors de ce doctorat aux tests d'échantillons de carotides de lapins (sections 3.2.1 et 4.2.1), pourront être adaptés à d'autres types d'échantillons biologiques, plans ou cylindriques, et de tailles variées. De manière complémentaire, des méthodes de post-traitement des données expérimentales ont été implémentées, comprenant (i) une routine d'extraction des densités d'angles des fibres de la microstructure, sur image totale ou partitionnée (section 3.2.4); (ii) une routine de filtrage et comparaison de spectres de Fourier extraits des images de microscopie, permettant l'identification de morphologies similaires (section 4.2.5); (iii) une routine de mesure des dimensions de l'artère par seuillage d'image macro (section 4.2.4). Ces routines, implémentées sur Matlab, pourront également être appliquées à d'autres images provenant des tests d'autres tissus biologiques. Parallèlement aux travaux expérimentaux, des méthodes de modélisation ont été implémentées. En particulier, un modèle micromécanique, appliqué pour la première fois dans le contexte de la biomécanique artérielle, a été adapté afin de modéliser la couche externe (adventice) de l'artère (section 5.3). Des routines de post-traitement ont été également développées.

Les résultats expérimentaux, portant sur (i) l'élasticité non-linéaire de tissu artériel (section 3.3.1), (ii) les cinématiques des différents réseaux fibreux de l'artère soumis à des déformations uniaxiales (section 3.3.3) et (iii) le caractère non-affine des cinématiques de fibres de collagène de la couche externe de l'artère soumise à divers scenarii de traction-gonflement (section 4.3),

ont permis d'avancer dans la validation du modèle micromécanique. En effet celui-ci a réussi à prédire un comportement mécanique analogue, tant au niveau de la réponse mécanique macroscopique du tissu, qu'au niveau de la cinématique des fibres qui composent sa microstructure (section 5.3.3). Ainsi l'ensemble des résultats expérimentaux et des résultats de modélisation a permis de répondre aux questions posées. Ces résultats permettent de progresser dans la compréhension des mécanismes qui régissent le couplage entre la microstructure de l'artère et ses propriétés mécaniques. Ils soulignent particulièrement le rôle important que jouent les interactions fibre-fibre, susceptibles d'influencer significativement les réarrangements de la microstructure de l'artère pendant la déformation, et donc ses propriétés mécaniques macroscopiques.

Les perspectives de ce travail concernent notamment (i) la caractérisation expérimentale de ces interactions via l'analyse des mécanismes de liaison et d'ancrage des réseaux fibreux d'élastine et de collagène (section 6.3.1), et (ii) la poursuite du développement du modèle micromécanique (section 6.3.2) et l'implémentation d'un modèle de tenségrité (section 6.4.2), deux modèles qui permettent de rendre compte de ces interactions mécaniques à l'échelle microscopique, tout en permettant de remonter au comportement mécanique macroscopique de l'artère modélisée.

Bibliography

[Acosta 17] Victor Acosta, Jerôme Molimard & Stéphane Avril. *3D full-field strain measurements across a whole porcine aorta subjected to tensile loading using OCT-DVC.* Submitted to Frontiers, 2017.

[Arkill 10] Kenton P Arkill, Julian Moger & C Peter Winlove. *The structure and mechanical properties of collecting lymphatic vessels: an investigation using multimodal nonlinear microscopy.* Journal of Anatomy, vol. 216, no. 5, pages 547–555, 2010.

[Ayres 06] Chantal Ayres, Gary L Bowlin, Scott C Henderson, Leander Taylor, Jackie Shultz, John Alexander, Todd A Telemeco & David G Simpson. *Modulation of anisotropy in electrospun tissue-engineering scaffolds: Analysis of fiber alignment by the fast Fourier transform.* Biomaterials, vol. 27, no. 32, pages 5524–5534, 2006.

[Ayres 08] Chantal Ayres, B Shekhar Jha, Hannah Meredith, James R Bowman, Gary L Bowlin, Scott C Henderson & David G Simpson. *Measuring fiber alignment in electrospun scaffolds: a user's guide to the 2D Fast Fourier Transform approach.* Journal of Biomaterials Science, Polymer Edition, vol. 19, no. 5, pages 603–621, 2008.

[Azeloglu 08] Evren U Azeloglu, Michael B Albro, Vikrum A Thimmappa, Gerard A Ateshian & Kevin D Costa. *Heterogeneous transmural proteoglycan distribution provides a mechanism for regulating residual stresses in the aorta.* American Journal of Physiology-Heart and Circulatory Physiology, vol. 294, no. 3, pages H1197–H1205, 2008.

[Bancelin 15] Stéphane Bancelin, Barbara Lynch, Christelle Bonod-Bidaud, Guillaume Ducourthial, Sotiris Psilodimitrakopoulos, Petr Dokládal, Jean-Marc Allain, Marie-Claire Schanne-Klein & Florence Ruggiero. *Ex vivo multiscale quantitation of skin biomechanics in wild-type and*

genetically-modified mice using multiphoton microscopy. Scientific reports, vol. 5, page 17635, 2015.

[Bednarek 11] Melissa L Bednarek, John E Speich, Amy S Miner & Paul H Ratz. *Active tension adaptation at a shortened arterial muscle length: inhibition by cytochalasin-D.* American Journal of Physiology-Heart and Circulatory Physiology, vol. 300, no. 4, pages H1166–H1173, 2011.

[Bendeck 91] Michelle P Bendeck & B Lowell Langille. *Rapid accumulation of elastin and collagen in the aortas of sheep in the immediate perinatal period.* Circulation research, vol. 69, no. 4, pages 1165–1169, 1991.

[Benveniste 87] Y1 Benveniste. *A new approach to the application of Mori-Tanaka's theory in composite materials.* Mechanics of materials, vol. 6, no. 2, pages 147–157, 1987.

[Bergel 61] DH Bergel. *The static elastic properties of the arterial wall.* The Journal of physiology, vol. 156, no. 3, pages 445–457, 1961.

[Berillis 13] Panagiotis Berillis. *The role of collagen in the aorta's structure.* The open circulation and vascular journal, vol. 6, no. 1, 2013.

[Bigun 04] Josef Bigun, Tomas Bigun & Kenneth Nilsson. *Recognition by symmetry derivatives and the generalized structure tensor.* IEEE Transactions on Pattern Analysis and Machine Intelligence, vol. 26, no. 12, pages 1590–1605, 2004.

[Billiar 97] KL Billiar & MS Sacks. *A method to quantify the fiber kinematics of planar tissues under biaxial stretch.* Journal of Biomechanics, vol. 30, no. 7, pages 753–756, 1997.

[Blanchoin 14] Laurent Blanchoin, Rajaa Boujemaa-Paterski, Cécile Sykes & Julie Plastino. *Actin dynamics, architecture, and mechanics in cell motility.* Physiological reviews, vol. 94, no. 1, pages 235–263, 2014.

[Bursac 07] Predrag Bursac, Ben Fabry, Xavier Trepat, Guillaume Lenormand, James P Butler, Ning Wang, Jeffrey J Fredberg & Steven S An. *Cytoskeleton dynamics: fluctuations within the network.* Biochemical and biophysical research communications, vol. 355, no. 2, pages 324–330, 2007.

[Burton 54] Alan C. Burton. *Relation of Structure to Function of the Tissues of the Wall of Blood Vessels.* Physiological Reviews, vol. 34, no. 4, pages 619–642, 1954.

[Buschmann 95] MD Buschmann, AJ Grodzinsky*et al.* *A molecular model of proteoglycan-associated electrostatic forces in cartilage mechanics.* J Biomech Eng, vol. 117, no. 2, pages 179–92, 1995.

[Canham 89] Peter B Canham, HelenM Finlay, Jan G Dixon, Derek R Boughner & Aendrew CHen. *Measurements from light and polarised light microscopy of human coronary arteries fixed at distending pressure.* Cardiovascular research, vol. 23, no. 11, pages 973–982, 1989.

[Canham 92] Peter B Canham, Peter Whittaker, Sharon E Barwick & Monika E Schwab. *Effect of pressure on circumferential order of adventitial collagen in human brain arteries.* Canadian journal of physiology and pharmacology, vol. 70, no. 2, pages 296–305, 1992.

[Cardamone 09] L Cardamone, A Valentin, JF Eberth & JD Humphrey. *Origin of axial prestretch and residual stress in arteries.* Biomechanics and modeling in mechanobiology, vol. 8, no. 6, pages 431–446, 2009.

[Carew 68] Thomas E Carew, Ramesh N Vaishnav & Dali J Patel. *Compressibility of the arterial wall.* Circulation research, vol. 23, no. 1, pages 61–68, 1968.

[Cavinato 17] Cristina Cavinato, Clementine Helfenstein-Didier, Thomas Olivier, Sabine Rolland Du Roscoat, Norbert Laroche & Pierre Badel. *Biaxial loading of arterial tissues with 3D in situ observations of adventitia fibrous microstructure: a method coupling multi-photon confocal microscopy and bulge inflation test.* Journal of the Mechanical Behavior of Biomedical Materials, 2017.

[Chandran 06] Preethi L Chandran & Victor H Barocas. *Affine versus non-affine fibril kinematics in collagen networks: theoretical studies of network behavior.* Journal of Biomechanical Engineering, vol. 128, no. 2, pages 259–70, apr 2006.

[Chen 11] Huan Chen, Yi Liu, Mikhail N. Slipchenko, Xuefeng Zhao, Ji Xin Cheng & Ghassan S. Kassab. *The layered structure of coronary adventitia under mechanical load.* Biophysical Journal, vol. 101, no. 11, pages 2555–2562, 2011.

[Chen 13] Huan Chen, Mikhail N Slipchenko, Yi Liu, Xuefeng Zhao, Ji-Xin Cheng, Yoram Lanir & Ghassan S Kassab. *Biaxial deformation of collagen and elastin fibers in coronary adventitia.* Journal of Applied Physiology, vol. 115, no. 11, pages 1683–1693, 2013.

[Choudhury 09] Nusrat Choudhury, Olivier Bouchot, Leonie Rouleau, Dominique Tremblay, Raymond Cartier, Jagdish Butany, Rosaire Mongrain & Richard L Leask. *Local mechanical and structural properties of healthy and diseased human ascending aorta tissue.* Cardiovascular Pathology, vol. 18, no. 2, pages 83–91, 2009.

[Chow 11] Ming-Jay Chow & Yanhang Zhang. *Changes in the mechanical and biochemical properties of aortic tissue due to cold storage.* Journal of Surgical Research, vol. 171, no. 2, pages 434–442, 2011.

[Chow 14] Ming-Jay Chow, Raphaël Turcotte, Charles P Lin & Yanhang Zhang. *Arterial extracellular matrix: a mechanobiological study of the contributions and interactions of elastin and collagen.* Biophysical Journal, vol. 106, no. 12, pages 2684–2692, 2014.

[Cicchi 14] Riccardo Cicchi, Christian Matthäus, Tobias Meyer, Annika Lattermann, Benjamin Dietzek, Bernhard R Brehm, Jürgen Popp & Francesco Saverio Pavone. *Characterization of collagen and cholesterol deposition in atherosclerotic arterial tissue using non-linear microscopy.* Journal of biophotonics, vol. 7, no. 1-2, pages 135–143, 2014.

[Clark 85] J. M. Clark & S. Glagov. *Transmural organization of the arterial media. The lamellar unit revisited.* Arteriosclerosis, Thrombosis, and Vascular Biology, vol. 5, no. 1, pages 19–34, jan 1985.

[Coughlin 97] MF Coughlin & D Stamenovic. *A tensegrity structure with buckling compression elements: application to cell mechanics.* Transactions - American Society of Mechanical Engineers - Journal of Applied Mechanics, vol. 64, pages 480–486, 1997.

[Cox 75] RH Cox. *Anisotropic properties of the canine carotid artery in vitro.* Journal of biomechanics, vol. 8, no. 5, pages 293–300, 1975.

[D'Amore 10] Antonio D'Amore, John A Stella, William R Wagner & Michael S Sacks. *Characterization of the complete fiber network topology of planar fibrous tissues and scaffolds.* Biomaterials, vol. 31, no. 20, pages 5345–5354, 2010.

[Davies 02] Ryan R Davies, Lee J Goldstein, Michael A Coady, Shawn L Tittle, John A Rizzo, Gary S Kopf & John A Elefteriades. *Yearly rupture or dissection rates for thoracic aortic aneurysms: simple prediction based on size.* The Annals of thoracic surgery, vol. 73, no. 1, pages 17–28, 2002.

[De Jager 04] Bram De Jager & Robert E Skelton. *Symbolic stiffness optimization of planar tensegrity structures.* Journal of intelligent material systems and structures, vol. 15, no. 3, pages 181–193, 2004.

[De Jager 06] Bram De Jager & Robert E Skelton. *Stiffness of planar tensegrity truss topologies.* International Journal of solids and structures, vol. 43, no. 5, pages 1308–1330, 2006.

[Denk 04] Winfried Denk & Heinz Horstmann. *Serial block-face scanning electron microscopy to reconstruct three-dimensional tissue nanostructure.* PLoS Biology, vol. 2, no. 11, 2004.

[Dingemans 00] K P Dingemans, P Teeling, J H Lagendijk & A E Becker. *Extracellular matrix of the human aortic media: an ultrastructural histochemical and immunohistochemical study of the adult aortic media.* The Anatomical Record, vol. 258, no. 1, pages 1–14, jan 2000.

[Dobrin 86] Philip B Dobrin. *Biaxial anisotropy of dog carotid artery: estimation of circumferential elastic modulus.* Journal of biomechanics, vol. 19, no. 5, pages 351–358, 1986.

[Duprey 10] A. Duprey, K. Khanafer, M. Schlicht, S. Avril, D. Williams & R. Berguer. *In Vitro Characterisation of Physiological and Maximum Elastic Modulus of Ascending Thoracic Aortic Aneurysms Using Uniaxial Tensile Testing.* European Journal of Vascular and Endovascular Surgery, vol. 39, no. 6, pages 700 – 707, 2010.

[Eisenstein 75] Reuben Eisenstein, Sven-Erik Larsson, Klaus E Kuettner, Nino Sorgente & Vincent C Hascall. *The ground substance of the arterial wall Part 1. Extractability of glycosammoglycans and the isolation of a proteoglycan from bovine aorta.* Atherosclerosis, vol. 22, no. 1, pages 1–17, 1975.

[Eshelby 57] John D Eshelby. *The determination of the elastic field of an ellipsoidal inclusion, and related problems.* In Proceedings of the Royal Society of London A: Mathematical, Physical and Engineering Sciences, volume 241, pages 376–396. The Royal Society, 1957.

[Esterly 68] James A Esterly, Seymour Glagov & DJ Ferguson. *Morphogenesis of intimal obliterative hyperplasia of small arteries in experimental pulmonary hypertension. An ultrastructural study of the role of smooth-muscle cells.* The American journal of pathology, vol. 52, no. 2, page 325, 1968.

[Eyre 84] David R Eyre, Mercedes A Paz & Paul M Gallop. *Cross-linking in collagen and elastin.* Annual review of biochemistry, vol. 53, no. 1, pages 717–748, 1984.

[Fan 14] Rong Fan & Michael S Sacks. *Simulation of planar soft tissues using a structural constitutive model: finite element implementation and validation.* Journal of Biomechanics, vol. 47, no. 9, pages 2043–2054, 2014.

[Farand 07] Paul Farand, André Garon & Gerard E. Plante. *Structure of large arteries: Orientation of elastin in rabbit aortic internal elastic lamina and in the elastic lamellae of aortic media.* Microvascular Research, vol. 73, no. 2, pages 95–99, 2007.

[Faury 01] Gilles Faury. *Function–structure relationship of elastic arteries in evolution: from microfibrils to elastin and elastic fibres.* Pathologie Biologie, vol. 49, no. 4, pages 310–325, 2001.

[Ferruzzi 11] J Ferruzzi, D Vorp & J D Humphrey. *On constitutive descriptors of the biaxial mechanical behaviour of human abdominal aorta and aneurysms.* Journal of the Royal Society, Interface, vol. 8, no. 56, pages 435–450, 2011.

[Fillinger 07] Mark Fillinger. *Who should we operate on and how do we decide: predicting rupture and survival in patients with aortic aneurysm.* In Seminars in vascular surgery, volume 20, pages 121–127. Elsevier, 2007.

[Freed 05] Alan D Freed & Todd C Doehring. *Elastic model for crimped collagen fibrils.* Journal of biomechanical engineering, vol. 127, no. 4, pages 587–593, 2005.

[Fridez 01] P. Fridez, A. Makino, H. Miyazaki, J.-J. Meister, K. Hayashi & N. Stergiopulos. *Short-Term Biomechanical Adaptation of the Rat Carotid to Acute Hypertension: Contribution of Smooth Muscle.* Annals of Biomedical Engineering, vol. 29, no. 1, pages 26–34, 2001.

[Fritsch 09] Andreas Fritsch, Christian Hellmich & Luc Dormieux. *Ductile sliding between mineral crystals followed by rupture of collagen crosslinks: experimentally supported micromechanical explanation of bone strength.* Journal of theoretical biology, vol. 260, no. 2, pages 230–252, 2009.

[Fujimoto 99] JG Fujimoto, Stephen A Boppart, GJ Tearney, BE Bouma, C Pitris & ME Brezinski. *High resolution in vivo intra-arterial imaging with*

optical coherence tomography. Heart, vol. 82, no. 2, pages 128–133, 1999.

[Fuller 61] R Buckminster Fuller. *Tensegrity.* Portfolio and Art News Annual, vol. 4, 1961.

[Fung 93] Yuan-Cheng Fung. *Mechanical properties and active remodeling of blood vessels.* In Biomechanics, pages 321–391. Springer, 1993.

[Gasser 07] T Christian Gasser & Gerhard A Holzapfel. *Finite element modeling of balloon angioplasty by considering overstretch of remnant non-diseased tissues in lesions.* Computational Mechanics, vol. 40, no. 1, pages 47–60, 2007.

[Gasser 10] T Christian Gasser, Martin Auer, F Labruto, J Swedenborg & J Roy. *Biomechanical rupture risk assessment of abdominal aortic aneurysms: model complexity versus predictability of finite element simulations.* European Journal of Vascular and Endovascular Surgery, vol. 40, no. 2, pages 176–185, 2010.

[Gasser 12] T. Christian Gasser, Sara Gallinetti, Xiao Xing, Caroline Forsell, Jesper Swedenborg & Joy Roy. *Spatial orientation of collagen fibers in the abdominal aortic aneurysm's wall and its relation to wall mechanics.* Acta Biomaterialia, vol. 8, no. 8, pages 3091–3103, 2012.

[Geest 06] Jonathan P Vande Geest, Michael S Sacks & David A Vorp. *A planar biaxial constitutive relation for the luminal layer of intra-luminal thrombus in abdominal aortic aneurysms.* Journal of biomechanics, vol. 39, no. 13, pages 2347–2354, 2006.

[Genovese 13] K Genovese, Y-U Lee, a Y Lee & J D Humphrey. *An improved panoramic digital image correlation method for vascular strain analysis and material characterization.* Journal of the Mechanical Behavior of Biomedical Materials, vol. 27, pages 132–42, 2013.

[Ghazanfari 12] S Ghazanfari, A Driessen-Mol, GJ Strijkers, FMW Kanters, FPT Baaijens & CVC Bouten. *A comparative analysis of the collagen architecture in the carotid artery: second harmonic generation versus diffusion tensor imaging.* Biochemical and biophysical research communications, vol. 426, no. 1, pages 54–58, 2012.

[Gleason 04a] R L Gleason, S P Gray, E Wilson & J D Humphrey. *A multiaxial computer-controlled organ culture and biomechanical device for mouse carotid arteries.* Journal of Biomechanical Engineering, vol. 126, no. 6, pages 787–795, 2004.

[Gleason 04b] RL Gleason, LA Taber & JD Humphrey. *A 2-D model of flow-induced alterations in the geometry, structure, and properties of carotid arteries.* Journal of biomechanical engineering, vol. 126, no. 3, pages 371–381, 2004.

[Gonzalez 02] Rafael C Gonzalez & Richard E Woods. *Processing*, 2002.

[Govyrin 57] VA Govyrin. *Measurement of arterial pressures in intact rabbits.* Bulletin of Experimental Biology and Medicine, vol. 44, no. 1, pages 896–897, 1957.

[Greenwald 97] SE Greenwald, JE Moore, A Rachev, TPC Kane & J-J Meister. *Experimental investigation of the distribution of residual strains in the artery wall.* Journal of Biomechanical Engineering, vol. 119, no. 4, pages 438–444, 1997.

[Gross 49] Jerome Gross. *The structure of elastic tissue as studied with the electron microscope.* The Journal of Experimental Medicine, vol. 89, no. 6, pages 699–708, 1949.

[Grytz 09] Rafael Grytz & Günther Meschke. *Constitutive modeling of crimped collagen fibrils in soft tissues.* Journal of the Mechanical Behavior of Biomedical Materials, vol. 2, no. 5, pages 522–533, 2009.

[Han 13] Hai-Chao Han, Jennifer KW Chesnutt, Justin R Garcia, Qin Liu & Qi Wen. *Artery buckling: new phenotypes, models, and applications.* Annals of Biomedical Engineering, vol. 41, no. 7, pages 1399–1410, 2013.

[Hayashi 74] K Hayashi, M Sato, HK Handa & K Moritake. *Biomechanical study of the constitutive laws of vascular walls.* Experimental Mechanics, vol. 14, no. 11, pages 440–444, 1974.

[Hellmich 02] Christian Hellmich & Franz-Josef Ulm. *Micromechanical model for ultrastructural stiffness of mineralized tissues.* Journal of engineering mechanics, vol. 128, no. 8, pages 898–908, 2002.

[Hellmich 04] Christian Hellmich, Jean-Francois Barthélémy & Luc Dormieux. *Mineral–collagen interactions in elasticity of bone ultrastructure–a continuum micromechanics approach.* European Journal of Mechanics-A/Solids, vol. 23, no. 5, pages 783–810, 2004.

[Hellmich 08] Christian Hellmich, Cornelia Kober & Bodo Erdmann. *Micromechanics-based conversion of CT data into anisotropic elasticity tensors, applied to FE simulations of a mandible.* Annals of biomedical engineering, vol. 36, no. 1, page 108, 2008.

[Hill 65] RODNEY Hill. *Continuum micro-mechanics of elastoplastic polycrystals.* Journal of the Mechanics and Physics of Solids, vol. 13, no. 2, pages 89–101, 1965.

[Hill 12] Michael R. Hill, Xinjie Duan, Gregory A. Gibson, Simon Watkins & Anne M. Robertson. *A theoretical and non-destructive experimental approach for direct inclusion of measured collagen orientation and recruitment into mechanical models of the artery wall.* Journal of Biomechanics, vol. 45, no. 5, pages 762–771, 2012.

[Holzapfel 01] Gerhard A Holzapfel & Thomas C Gasser. *A viscoelastic model for fiber-reinforced composites at finite strains: Continuum basis, computational aspects and applications.* Computer Methods in Applied Mechanics and Engineering, vol. 190, no. 34, pages 4379–4403, 2001.

[Holzapfel 05] Gerhard A Holzapfel, Gerhard Sommer, Christian T Gasser & Peter Regitnig. *Determination of layer-specific mechanical properties of human coronary arteries with nonatherosclerotic intimal thickening and related constitutive modeling.* American Journal of Physiology-Heart and Circulatory Physiology, vol. 289, no. 5, pages H2048–H2058, 2005.

[Holzapfel 07] Gerhard A Holzapfel & Thomas C Gasser. *Computational stress-deformation analysis of arterial walls including high-pressure response.* International journal of cardiology, vol. 116, no. 1, pages 78–85, 2007.

[Holzapfel 15a] Gerhard A Holzapfel, Justyna A Niestrawska, Ray W Ogden, Andreas J Reinisch & Andreas J Schriefl. *Modelling non-symmetric collagen fibre dispersion in arterial walls.* Journal of the Royal Society Interface, vol. 12, no. 106, page 20150188, 2015.

[Holzapfel 15b] Gerhard A Holzapfel & Ray W Ogden. *On the tension–compression switch in soft fibrous solids.* European Journal of Mechanics-A/Solids, vol. 49, pages 561–569, 2015.

[Hooke 31] Robert Hooke. *Lectures de potentia restitutiva.* Or of Spring Explaining the Power of Springing Bodies, London: John Martyn, vol. 1678, 1931.

[Humphrey 00] JD Humphrey & PB Canham. *Structure, mechanical properties, and mechanics of intracranial saccular aneurysms.* Journal of Elasticity and the Physical Science of Solids, vol. 61, no. 1-3, pages 49–81, 2000.

[Humphrey 02] JD Humphrey & KR Rajagopal. *A constrained mixture model for growth and remodeling of soft tissues.* Mathematical models and methods in applied sciences, vol. 12, no. 03, pages 407–430, 2002.

[Humphrey 08a] J. D. Humphrey, P. B. Wells, S. Baek, J. J. Hu, K. McLeroy & A. T. Yeh. *A theoretically-motivated biaxial tissue culture system with intravital microscopy.* Biomechanics and Modeling in Mechanobiology, vol. 7, no. 4, pages 323–334, 2008.

[Humphrey 08b] Jay D Humphrey. *Mechanisms of arterial remodeling in hypertension.* Hypertension, vol. 52, no. 2, pages 195–200, 2008.

[Humphrey 09] JD Humphrey, JF Eberth, WW Dye & RL Gleason. *Fundamental role of axial stress in compensatory adaptations by arteries.* Journal of biomechanics, vol. 42, no. 1, pages 1–8, 2009.

[Humphrey 10] J.D. Humphrey. Cardiovascular solid mechanics: Cells, tissues, and organs. Springer, 2010.

[Ingber 93] Donald E Ingber*et al.* *Cellular tensegrity: defining new rules of biological design that govern the cytoskeleton.* Journal of Cell Science, vol. 104, pages 613–613, 1993.

[Ingber 03] Donald E Ingber. *Tensegrity I. Cell structure and hierarchical systems biology.* Journal of cell science, vol. 116, no. 7, pages 1157–1173, 2003.

[Ingber 06] Donald E Ingber. *Cellular mechanotransduction: putting all the pieces together again.* The FASEB journal, vol. 20, no. 7, pages 811–827, 2006.

[Ives 86] CL Ives, SG Eskin & LV McIntire. *Mechanical effects on endothelial cell morphology: in vitro assessment.* In vitro cellular & developmental biology, vol. 22, no. 9, pages 500–507, 1986.

[Jähne 93] Bernd Jähne. Spatio-temporal image processing: theory and scientific applications, volume 751. Springer Science & Business Media, 1993.

[Jayyosi 15] Charles Jayyosi. *Caractérisation mécanique et microstructurale du comportement à rupture de la capsule de Glisson pour la prédiction du risque de lésions des tissus hépatiques humains.* PhD thesis, Université de Lyon 1, 2015.

[Jayyosi 16] Charles Jayyosi, Michel Coret & Karine Bruyere-Garnier. *Characterizing liver capsule microstructure via in situ bulge test coupled*

with multiphoton imaging. Journal of the Mechanical Behavior of Biomedical Materials, vol. 54, pages 229–243, 2016.

[Jayyosi 17] Charles Jayyosi, J-S Affagard, Guillaume Ducourthial, Christelle Bonod-Bidaud, Barbara Lynch, Stéphane Bancelin, Florence Ruggiero, M-C Schanne-Klein, J-M Allain, Karine Bruyère-Garnier*et al.* *Affine kinematics in planar fibrous connective tissues: an experimental investigation.* Biomechanics and Modeling in Mechanobiology, pages 1–15, 2017.

[Kabir 13] Mohammad M Kabir, VVG Krishna Inavalli, Tung-Yuen Lau & Kimani C Toussaint. *Application of quantitative second-harmonic generation microscopy to dynamic conditions.* Biomedical optics express, vol. 4, no. 11, pages 2546–2554, 2013.

[Kao 11] Philip H Kao, Steve Lammers, Lian Tian, Kendall Hunter, Kurt R Stenmark & H Jerry Qi. *A Microstructurally-Driven Model for Pulmonary Artery Tissue.* Journal of Biomechanical Engineering, vol. 133, no. 5, pages 1–37, 2011.

[Keyes 11] Joseph T Keyes, Stacy M Borowicz, Jacob H Rader, Urs Utzinger, Mohamad Azhar & Jonathan P Vande Geest. *Design and demonstration of a microbiaxial optomechanical device for multiscale characterization of soft biological tissues with two-photon microscopy.* Microscopy and Microanalysis, vol. 17, no. 02, pages 167–175, 2011.

[Keyes 13] Joseph T Keyes, Danielle R Lockwood, Urs Utzinger, Leonardo G Montilla, Russell S Witte & Jonathan P Vande Geest. *Comparisons of planar and tubular biaxial tensile testing protocols of the same porcine coronary arteries.* Annals of Biomedical Engineering, vol. 41, no. 7, pages 1579–1591, 2013.

[Koch 14] Ryan G. Koch, Alkiviadis Tsamis, Antonio D'Amore, William R. Wagner, Simon C. Watkins, Thomas G. Gleason & David A. Vorp. *A custom image-based analysis tool for quantifying elastin and collagen micro-architecture in the wall of the human aorta from multi-photon microscopy.* Journal of Biomechanics, vol. 47, no. 5, pages 935–943, 2014.

[Krasny 17a] W Krasny, C Morin, H Magoariec & S Avril. *A comprehensive study of layer-specific morphological changes in the microstructure of carotid arteries under uniaxial load.* Acta Biomaterialia - manuscript accepted, vol. 0, no. 00, pages 00–00, 2017.

[Krasny 17b] Witold Krasny, Hélène Magoariec, Claire Morin & Stéphane Avril. *Kinematics of collagen fibers in carotid arteries under tension-inflation loading.* Journal of the Mechanical Behavior of Biomedical Materials, 2017.

[Lake 12] Spencer P Lake, Mohammad F Hadi, Victor K Lai & Victor H Barocas. *Mechanics of a fiber network within a non-fibrillar matrix: model and comparison with collagen-agarose co-gels.* Annals of Biomedical Engineering, vol. 40, no. 10, pages 2111–2121, 2012.

[Lally 04] C Lally, AJ Reid & PJ Prendergast. *Elastic behavior of porcine coronary artery tissue under uniaxial and equibiaxial tension.* Annals of biomedical engineering, vol. 32, no. 10, pages 1355–1364, 2004.

[Lanir 79] Y Lanir. *A structural theory for the homogeneous biaxial stress-strain relationships in flat collagenous tissues.* Journal of biomechanics, vol. 12, no. 6, pages 423–436, 1979.

[Lee 15] Chung-Hao Lee, Will Zhang, Jun Liao, Christopher A Carruthers, Jacob I Sacks & Michael S Sacks. *On the presence of affine fibril and fiber kinematics in the mitral valve anterior leaflet.* Biophysical journal, vol. 108, no. 8, pages 2074–2087, 2015.

[Li 16] Kewei Li, Ray W Ogden & Gerhard A Holzapfel. *Computational method for excluding fibers under compression in modeling soft fibrous solids.* European Journal of Mechanics-A/Solids, vol. 57, pages 178–193, 2016.

[Libby 92] Peter Libby, David Schwartz, Edi Brogi, Hiroyuki Tanaka & Steven K Clinton. *A cascade model for restenosis. A special case of atherosclerosis progression.* Circulation, vol. 86, no. 6 Suppl, pages III47–52, 1992.

[Luo 08] Yaozhi Luo, Xian Xu, Tanmay Lele, Sanjay Kumar & Donald E Ingber. *A multi-modular tensegrity model of an actin stress fiber.* Journal of Biomechanics, vol. 41, no. 11, pages 2379–2387, 2008.

[Lynch 17] Barbara Lynch, Stéphane Bancelin, Christelle Bonod-Bidaud, Jean-Baptiste Gueusquin, Florence Ruggiero, Marie-Claire Schanne-Klein & Jean-Marc Allain. *A novel microstructural interpretation for the biomechanics of mouse skin derived from multiscale characterization.* Acta Biomaterialia, vol. 50, pages 302–311, 2017.

[Maceri 10] Franco Maceri, Michele Marino & Giuseppe Vairo. *A unified multi-scale mechanical model for soft collagenous tissues with regular fiber*

arrangement. Journal of biomechanics, vol. 43, no. 2, pages 355–363, 2010.

[Marino 13] Michele Marino & Giuseppe Vairo. *Multiscale elastic models of collagen bio-structures: from cross-linked molecules to soft tissues*. In Multiscale Computer Modeling in Biomechanics and Biomedical Engineering, pages 73–102. Springer, 2013.

[Mohan 82] Dinesh Mohan & John W Melvin. *Failure properties of passive human aortic tissue. IâĂŤuniaxial tension tests*. Journal of biomechanics, vol. 15, no. 11, pages 887895–893902, 1982.

[Moll 11] FLea Moll, JT Powell, G Fraedrich, F Verzini, S Haulon, M Waltham, JA Van Herwaarden, PJE Holt, JW Van Keulen, B Rantner*et al. Management of abdominal aortic aneurysms clinical practice guidelines of the European society for vascular surgery*. European Journal of Vascular and Endovascular Surgery, vol. 41, pages S1–S58, 2011.

[Mooney 40] M. Mooney. *A theory of large elastic deformation*. Journal of Applied Physics, vol. 11, no. 9, pages 582–592, 1940.

[Mori 73] T. Mori & K. Tanaka. *Average stress in matrix and average elastic energy of materials with misfitting inclusions*. Acta Metallurgica, vol. 21, no. 5, pages 571–574, 1973.

[Morin 14] Claire Morin & Christian Hellmich. *A multiscale poromicromechanical approach to wave propagation and attenuation in bone*. Ultrasonics, vol. 54, no. 5, pages 1251–1269, 2014.

[Morin 15] Claire Morin, Stéphane Avril & Christian Hellmich. *The fiber reorientation problem revisited in the context of Eshelbian micromechanics: theory and computations*. Pamm, vol. 15, no. 1, pages 39–42, 2015.

[Morin 17] Claire Morin, Witold Krasny & Stéphane Avril. *Multiscale mechanical behavior of large arteries*. Elsevier Encyclopedia of Biomedical Engeineering, 2017.

[Morrill 16] Erica E Morrill, Azamat N Tulepbergenov, Christina J Stender, Roshani Lamichhane, Raquel J Brown & Trevor J Lujan. *A validated software application to measure fiber organization in soft tissue*. Biomechanics and Modeling in Mechanobiology, vol. 15, no. 6, pages 1467–1478, 2016.

[Nagayama 04] Kazuaki Nagayama & Takeo Matsumoto. *Mechanical anisotropy of rat aortic smooth muscle cells decreases with their contraction.* JSME International Journal Series C Mechanical Systems, Machine Elements and Manufacturing, vol. 47, no. 4, pages 985–991, 2004.

[Nierenberger 13] Mathieu Nierenberger, Yves Rémond & Saïd Ahzi. *A new multi-scale model for the mechanical behavior of vein walls.* Journal of the mechanical behavior of biomedical materials, vol. 23, pages 32–43, 2013.

[O'Connell 08] Mary K. O'Connell, Sushila Murthy, Samson Phan, Chengpei Xu, JoAnn Buchanan, Ryan Spilker, Ronald L. Dalman, Christopher K. Zarins, Winfried Denk & Charles A. Taylor. *The three-dimensional micro- and nanostructure of the aortic medial lamellar unit measured using 3D confocal and electron microscopy imaging.* Matrix Biology, vol. 27, no. 3, pages 171–181, 2008.

[Ohashi 05] Toshiro Ohashi & Masaaki Sato. *Remodeling of vascular endothelial cells exposed to fluid shear stress: experimental and numerical approach.* Fluid dynamics research, vol. 37, no. 1, pages 40–59, 2005.

[Okamoto 02] Ruth J Okamoto, Jessica E Wagenseil, William R DeLong, Sara J Peterson, Nicholas T Kouchoukos & Thoralf M Sundt III. *Mechanical properties of dilated human ascending aorta.* Annals of Biomedical Engineering, vol. 30, no. 5, pages 624–635, 2002.

[Ookawa 92] Keiko Ookawa, Masaaki Sato & Norio Ohshima. *Changes in the microstructure of cultured porcine aortic endothelial cells in the early stage after applying a fluid-imposed shear stress.* Journal of biomechanics, vol. 25, no. 11, pages 1321–1328, 1992.

[O'Rourke 07] Michael F O'Rourke & Junichiro Hashimoto. *Mechanical factors in arterial aging: a clinical perspective.* Journal of the American College of Cardiology, vol. 50, no. 1, pages 1–13, 2007.

[Papageorgiou 88] GL Papageorgiou & NB Jones. *Circumferential and longitudinal viscoelasticity of human iliac arterial segments in vitro.* Journal of biomedical engineering, vol. 10, no. 1, pages 82–90, 1988.

[Patel 70] Dali J Patel & Joseph S Janicki. *Static elastic properties of the left coronary circumflex artery and the common carotid artery in dogs.* Circulation Research, vol. 27, no. 2, pages 149–158, 1970.

[Phillippi 14] Julie A Phillippi, Benjamin R Green, Michael A Eskay, Mary P Kotlarczyk, Michael R Hill, Anne M Robertson, Simon C Watkins,

David A Vorp & Thomas G Gleason. *Mechanism of aortic medial matrix remodeling is distinct in patients with bicuspid aortic valve.* The Journal of thoracic and cardiovascular surgery, vol. 147, no. 3, pages 1056–1064, 2014.

[Polzer 13] Stanislav Polzer, T Christian Gasser, Caroline Forsell, Hana Druckmüllerova, Michal Tichy, Robert Staffa, Robert Vlachovsky & Jiri Bursa. *Automatic identification and validation of planar collagen organization in the aorta wall with application to abdominal aortic aneurysm.* Microscopy and Microanalysis, vol. 19, no. 06, pages 1395–1404, 2013.

[Raina 13] Arun Raina & Christian Linder. *Modeling reorientation phenomena in nonwoven materials with random fiber network microstructure.* PAMM, vol. 13, no. 1, pages 249–250, 2013.

[Raspanti 06] Mario Raspanti, Marina Protasoni, Alessandro Manelli, Stefano Guizzardi, Vittorio Mantovani & Andrea Sala. *The extracellular matrix of the human aortic wall: ultrastructural observations by FEG-SEM and by tapping-mode AFM.* Micron, vol. 37, no. 1, pages 81–86, 2006.

[Ratz 15] Paul H Ratz. *Mechanics of vascular smooth muscle.* Comprehensive physiology, 2015.

[Ratz 16] Paul H Ratz. *Vascular Structure and Function.* Vascular Smooth Muscle: Structure and Function in Health and Disease, page 47, 2016.

[Reymond 12] Philippe Reymond, Nico Westerhof & Nikos Stergiopulos. *Systolic hypertension mechanisms: effect of global and local proximal aorta stiffening on pulse pressure.* Annals of biomedical engineering, vol. 40, no. 3, pages 742–749, 2012.

[Rezakhaniha 12] R. Rezakhaniha, A. Agianniotis, J. T C Schrauwen, A. Griffa, D. Sage, C. V C Bouten, F. N. Van De Vosse, M. Unser & N. Stergiopulos. *Experimental investigation of collagen waviness and orientation in the arterial adventitia using confocal laser scanning microscopy.* Biomechanics and Modeling in Mechanobiology, vol. 11, no. 3-4, pages 461–473, 2012.

[Richardson 89] Peter D Richardson & SM Keeny. *Anisotropy of human coronary artery intima.* In Bioengineering Conference, 1989., Proceedings of the 1989 Fifteenth Annual Northeast, pages 205–206. IEEE, 1989.

[Ritty 03] Timothy M Ritty, Robyn Roth & John E Heuser. *Tendon cell array isolation reveals a previously unknown fibrillin-2-containing macromolecular assembly.* Structure, vol. 11, no. 9, pages 1179–1188, 2003.

[Rivlin 48] R. S. Rivlin. *Large Elastic Deformations of Isotropic Materials. I. Fundamental Concepts.* Philosophical Transactions of the Royal Society A: Mathematical, Physical and Engineering Sciences, vol. 240, no. 822, pages 459–490, 1948.

[Romo 14] Aaron Romo, Pierre Badel, Ambroise Duprey, Jean-Pierre Favre & Stéphane Avril. *In vitro analysis of localized aneurysm rupture.* Journal of biomechanics, vol. 47, no. 3, pages 607–616, 2014.

[Roy 81] Charles S Roy. *The elastic properties of the arterial wall.* The Journal of physiology, vol. 3, no. 2, pages 125–159, 1881.

[Roy 11] Sylvain Roy, Christophe Boss, Rana Rezakhaniha & Nikos Stergiopulos. *Experimental characterization of the distribution of collagen fiber recruitment.* Journal of Biorheology, vol. 24, no. 2, pages 84–93, mar 2011.

[Sacks 03a] Michael S Sacks. *Incorporation of experimentally-derived fiber orientation into a structural constitutive model for planar collagenous tissues.* Journal of Biomechanical Engineering, vol. 125, no. 2, pages 280–287, 2003.

[Sacks 03b] Michael S Sacks. *Incorporation of experimentally-derived fiber orientation into a structural constitutive model for planar collagenous tissues.* Journal of Biomechanical Engineering, vol. 125, no. 2, pages 280–287, 2003.

[Sáez 14] P Sáez, Estefanía Peña & Miguel Angel Martínez. *A structural approach including the behavior of collagen cross-links to model patient-specific human carotid arteries.* Annals of biomedical engineering, vol. 42, no. 6, pages 1158–1169, 2014.

[Sáez 16] P Sáez, A García, E Peña, TC Gasser & MA Martínez. *Microstructural quantification of collagen fiber orientations and its integration in constitutive modeling of the porcine carotid artery.* Acta Biomaterialia, vol. 33, pages 183–193, 2016.

[Saitta-Rezakhaniha 10] Rana Saitta-Rezakhaniha. *Biomechanics of Vascular Wall: the Role of Structural Organization of Elastin and Collagen.* Ecole Polytechnique Fédérale de Lausanne, 2010.

[Sander 09] Edward A Sander & Victor H Barocas. *Comparison of 2D fiber network orientation measurement methods.* Journal of biomedical materials research Part A, vol. 88, no. 2, pages 322–331, 2009.

[Sartore 01] Saverio Sartore, Angela Chiavegato, Elisabetta Faggin, Rafaella Franch, Massimo Puato, Simonetta Ausoni & Paolo Pauletto. *Contribution of adventitial fibroblasts to neointima formation and vascular remodeling.* Circulation research, vol. 89, no. 12, pages 1111–1121, 2001.

[Sato 79] M Sato, H Niimi, A Okumura, H Handa, K Hayashi & K Moritake. *Axial mechanical properties of arterial walls and their anisotropy.* Medical and Biological Engineering and Computing, vol. 17, no. 2, pages 170–176, 1979.

[Scheiner 13] Stefan Scheiner, Peter Pivonka & Christian Hellmich. *Coupling systems biology with multiscale mechanics, for computer simulations of bone remodeling.* Computer Methods in Applied Mechanics and Engineering, vol. 254, pages 181–196, 2013.

[Schlatmann 77] Thomas JM Schlatmann & Anton E Becker. *Histologic changes in the normal aging aorta: implications for dissecting aortic aneurysm.* The American journal of cardiology, vol. 39, no. 1, pages 13–20, 1977.

[Schmid 05] F Schmid, G Sommer, M Rappolt, CAJ Schulze-Bauer, P Regitnig, Gerhard A Holzapfel, P Laggner & H Amenitsch. *In situ tensile testing of human aortas by time-resolved small-angle X-ray scattering.* Journal of synchrotron radiation, vol. 12, no. 6, pages 727–733, 2005.

[Schneider 12] Caroline A Schneider, Wayne S Rasband & Kevin W Eliceiri. *NIH Image to ImageJ: 25 years of image analysis.* Nature methods, vol. 9, no. 7, pages 671–675, 2012.

[Schrauwen 12] J. T C Schrauwen, A. Vilanova, R. Rezakhaniha, N. Stergiopulos, F. N. van de Vosse & P. H M Bovendeerd. *A method for the quantification of the pressure dependent 3D collagen configuration in the arterial adventitia.* Journal of Structural Biology, vol. 180, no. 2, pages 335–342, 2012.

[Schriefl 12] J. Schriefl, J. Reinisch, S. Sankaran, David M. Pierce & Gerhard A. Holzapfel. *Quantitative assessment of collagen fibre orientations from two-dimensional images of soft biological tissues.* Journal of The Royal Society Interface, vol. 9, pages 3081–3093, 2012.

[Schriefl 13] Andreas J Schriefl, Heimo Wolinski, Peter Regitnig, Sepp D Kohlwein & Gerhard A Holzapfel. *An automated approach for three-dimensional quantification of fibrillar structures in optically cleared soft biological tissues.* Journal of The Royal Society Interface, vol. 10, no. 80, page 20120760, 2013.

[Serruys 94] Patrick W Serruys, Peter De Jaegere, Ferdinand Kiemeneij, Carlos Macaya, Wolfgang Rutsch, Guy Heyndrickx, Hakan Emanuelsson, Jean Marco, Victor Legrand, Pierre Materne*et al. A comparison of balloon-expandable-stent implantation with balloon angioplasty in patients with coronary artery disease.* New England Journal of Medicine, vol. 331, no. 8, pages 489–495, 1994.

[Shi 96] Yi Shi, James E O'Brien, Ali Fard, John D Mannion, Dian Wang & Andrew Zalewski. *Adventitial myofibroblasts contribute to neointimal formation in injured porcine coronary arteries.* Circulation, vol. 94, no. 7, pages 1655–1664, 1996.

[Skelton 01] Robert E Skelton, Rajesh Adhikari, J-P Pinaud, Waileung Chan & J William Helton. *An introduction to the mechanics of tensegrity structures.* In Decision and Control, 2001. Proceedings of the 40th IEEE Conference on, volume 5, pages 4254–4259. IEEE, 2001.

[Smolensky 05] Alexander V Smolensky, Joseph Ragozzino, Susan H Gilbert, Chun Y Seow & Lincoln E Ford. *Length-dependent filament formation assessed from birefringence increases during activation of porcine tracheal muscle.* The Journal of physiology, vol. 563, no. 2, pages 517–527, 2005.

[Sokolis 02] Dimitrios P Sokolis, Harisios Boudoulas & Panayotis E Karayannacos. *Assessment of the aortic stress–strain relation in uniaxial tension.* Journal of biomechanics, vol. 35, no. 9, pages 1213–1223, 2002.

[Sokolis 06] Dimitrios P Sokolis, Emmanuel M Kefaloyannis, Mirsini Kouloukoussa, Evangelos Marinos, Harisios Boudoulas & Panayotis E Karayannacos. *A structural basis for the aortic stress–strain relation in uniaxial tension.* Journal of biomechanics, vol. 39, no. 9, pages 1651–1662, 2006.

[Sommer 10] Gerhard Sommer, Peter Regitnig, Lukas Költringer & Gerhard A Holzapfel. *Biaxial mechanical properties of intact and layer-dissected*

human carotid arteries at physiological and supraphysiological loadings. American Journal of Physiology-Heart and Circulatory Physiology, vol. 298, no. 3, pages H898–H912, 2010.

[Stamenović 96] Dimitrije Stamenović, Jeffrey J Fredberg, Ning Wang, James P Butler & Donald E Ingber. *A microstructural approach to cytoskeletal mechanics based on tensegrity.* Journal of Theoretical Biology, vol. 181, no. 2, pages 125–136, 1996.

[Stamenovic 00] Dimitrije Stamenovic & Mark F Coughlin. *A quantitative model of cellular elasticity based on tensegrity.* Journal of Biomedical Engineering, vol. 122, no. 1, pages 39–43, 2000.

[Stoller 02] Patrick Stoller, Karen M Reiser, Peter M Celliers & Alexander M Rubenchik. *Polarization-modulated second harmonic generation in collagen.* Biophysical journal, vol. 82, no. 6, pages 3330–3342, 2002.

[Stylianopoulos 07] Triantafyllos Stylianopoulos & Victor H Barocas. *Multiscale, structure-based modeling for the elastic mechanical behavior of arterial walls.* Journal of Biomechanical Engineering, vol. 129, no. 4, pages 611–618, 2007.

[Sugita 17] Shukei Sugita & Takeo Matsumoto. *Multiphoton microscopy observations of 3D elastin and collagen fiber microstructure changes during pressurization in aortic media.* Biomechanics and Modeling in Mechanobiology, vol. 16, no. 3, pages 763–773, 2017.

[Sutton 08] MA Sutton, X Ke, SM Lessner, M Goldbach, M Yost, F Zhao & HW Schreier. *Strain field measurements on mouse carotid arteries using microscopic three-dimensional digital image correlation.* Journal of Biomedical Materials Research Part A, vol. 84, no. 1, pages 178–190, 2008.

[Tanaka 74] Toshiyuki T Tanaka & Yuan-Cheng Fung. *Elastic and inelastic properties of the canine aorta and their variation along the aortic tree.* Journal of Biomechanics, vol. 7, no. 4, pages 357–370, 1974.

[Taylor 09] Charles A Taylor & JD Humphrey. *Open problems in computational vascular biomechanics: hemodynamics and arterial wall mechanics.* Computer methods in applied mechanics and engineering, vol. 198, no. 45, pages 3514–3523, 2009.

[Teng 09] Zhongzhao Teng, Dalin Tang, Jie Zheng, Pamela K Woodard & Allen H Hoffman. *An experimental study on the ultimate strength*

of the adventitia and media of human atherosclerotic carotid arteries in circumferential and axial directions. Journal of Biomechanics, vol. 42, no. 15, pages 2535–2539, 2009.

[Thorpe 13] Chavaunne T Thorpe, Helen L Birch, Peter D Clegg & Hazel RC Screen. *The role of the non-collagenous matrix in tendon function.* International Journal of Experimental Pathology, vol. 94, no. 4, pages 248–259, 2013.

[Timmins 10] Lucas H Timmins, Qiaofeng Wu, Alvin T Yeh, James E Moore & Stephen E Greenwald. *Structural inhomogeneity and fiber orientation in the inner arterial media.* American Journal of Physiology-Heart and Circulatory Physiology, vol. 298, no. 5, pages H1537–H1545, 2010.

[Tonar 03] Zbyněk Tonar, Stanislav Nemecek, Radek Holota, Jitka Kocova, Vladislav Treska, Jiri Molacek, Tomáš Kohoutek & Sarka Hadravska. *Microscopic image analysis of elastin network in samples of normal, atherosclerotic and aneurysmatic abdominal aorta and its biomechanical implications.* J Appl Biomed, vol. 1, no. 3, pages 149–160, 2003.

[Tower 02] Theodore T. Tower, Michael R. Neidert & Robert T. Tranquillo. *Fiber alignment imaging during mechanical testing of soft tissues.* Annals of Biomedical Engineering, vol. 30, no. 10, pages 1221–1233, 2002.

[Tsamis 13] Alkiviadis Tsamis, Julie A Phillippi, Ryan G Koch, Salvatore Pasta, Antonio D Amore, Simon C Watkins, William R Wagner, Thomas G Gleason & David A Vorp. *Fiber micro-architecture in the longitudinal-radial and circumferential-radial planes of ascending thoracic aortic aneurysm media.* Journal of Biomechanics, vol. 46, no. 16, pages 2787–2794, 2013.

[Ushiki 02] Tatsuo Ushiki. *Collagen fibers, reticular fibers and elastic fibers. A comprehensive understanding from a morphological viewpoint.* Archives of histology and cytology, vol. 65, no. 2, pages 109–126, 2002.

[Vaishnav 87] Ramesh N Vaishnav & Jafar Vossoughi. *Residual stress and strain in aortic segments.* Journal of biomechanics, vol. 20, no. 3, pages 235239–237, 1987.

[Van Zandvoort 04] Marc Van Zandvoort, Wim Engels, Kim Douma, Linda Beckers, Mirjam Oude Egbrink, Mat Daemen & Dick W. Slaaf. *Two-Photon Microscopy for Imaging of the (Atherosclerotic) Vascular Wall: A Proof of Concept Study.* Journal of Vascular Research, vol. 41, no. 1, pages 54–63, 2004.

[Venkatasubramanian 06] Ramji T Venkatasubramanian, Erin D Grassl, Victor H Barocas, Daniel Lafontaine & John C Bischof. *Effects of freezing and cryopreservation on the mechanical properties of arteries.* Annals of Biomedical engineering, vol. 34, no. 5, pages 823–832, 2006.

[Vilanova 06] Anna Vilanova, Shangjian Zhang, Gordon Kindlmann & D Laidlaw. *An introduction to visualization of diffusion tensor imaging and its applications.* Visualization and Processing of Tensor Fields, pages 121–153, 2006.

[Voytik-Harbin 03] Sherry L. Voytik-Harbin, Blayne A. Roeder, Jennifer E. Sturgis, Klod Kokini & J. Paul Robinson. *Simultaneous mechanical loading and confocal reflection microscopy for three-dimensional microbiomechanical analysis of biomaterials and tissue constructs.* Microscopy and Microanalysis, vol. 9, pages 74–85, 2003.

[Wagner 52] R Wagner & E Kapal. *Über die elastischen Eigenschaften des Aortenwindkessels.* Journal of Molecular Medicine, vol. 30, no. 1, pages 1–8, 1952.

[Walker-Caprioglio 92] HM Walker-Caprioglio, JA Trotter, SA Little & LJ McGuffee. *Organization of cells and extracelluar matrix in mesenteric arteries of spontaneously hypertensive rats.* Cell and Tissue Research, vol. 269, no. 1, pages 141–149, 1992.

[Wan 12] William Wan, J Brandon Dixon & Rudolph L Gleason. *Constitutive modeling of mouse carotid arteries using experimentally measured microstructural parameters.* Biophysical Journal, vol. 102, no. 12, pages 2916–2925, 2012.

[Wang 93] Ning Wang, James P Butler & Donald E Ingber. *Mechanotransduction across the cell surface and through the cytoskeleton.* Science, pages 1124–1127, 1993.

[Wang 13] Ruoya Wang, Luke P. Brewster & Rudolph L. Gleason. *In-situ characterization of the uncrimping process of arterial collagen fibers using two-photon confocal microscopy and digital image correlation.* Journal of Biomechanics, vol. 46, no. 15, pages 2726–2729, 2013.

[Wasano 83] Kojiro Wasano & Torao Yamamota. *Tridimensional architecture of elastic tissue in the rat aorta and femoral arteryâĂŤa scanning electron microscope study.* Journal of Electron Microscopy, vol. 32, no. 1, pages 33–44, 1983.

[Weber 08] Christian Weber, Alma Zernecke & Peter Libby. *The multifaceted contributions of leukocyte subsets to atherosclerosis: lessons from mouse models.* Nature reviews. Immunology, vol. 8, no. 10, page 802, 2008.

[Weisbecker 12] Hannah Weisbecker, David M Pierce, Peter Regitnig & Gerhard A Holzapfel. *Layer-specific damage experiments and modeling of human thoracic and abdominal aortas with non-atherosclerotic intimal thickening.* Journal of the mechanical behavior of biomedical materials, vol. 12, pages 93–106, 2012.

[Weizsacker 88] Hans W Weizsacker & John G Pinto. *Isotropy and anisotropy of the arterial wall.* Journal of biomechanics, vol. 21, no. 6, pages 477–487, 1988.

[Wenger 07] Marco PE Wenger, Laurent Bozec, Michael A Horton & Patrick Mesquida. *Mechanical properties of collagen fibrils.* Biophysical Journal, vol. 93, no. 4, pages 1255–1263, 2007.

[Wertheim 47] Guillaume Wertheim. *Mémoire sur l'élasticité et la cohésion des principaux tissus du corps humain.* 1847.

[Westhoff 09] TH Westhoff, S Schmidt, R Meissner, W Zidek & M Van Der Giet. *The impact of pulse pressure on the accuracy of wrist blood pressure measurement.* Journal of human hypertension, vol. 23, no. 6, page 391, 2009.

[Wight 89] Thomas N Wight. *Cell biology of arterial proteoglycans.* Arteriosclerosis, Thrombosis, and Vascular Biology, vol. 9, no. 1, pages 1–20, 1989.

[Wolinsky 67] Harvey Wolinsky & Seymour Glagov. *A lamellar unit of aortic medial structure and function in mammals.* Circulation research, vol. 20, no. 1, pages 99–111, 1967.

[Wolinsky 70] H. Wolinsky & M. M. Daly. *A Method for the Isolation of Intima-Media Samples from Arteries.* Experimental Biology and Medicine, vol. 135, no. 2, pages 364–368, nov 1970.

[Yanagisawa 02] Hiromi Yanagisawa, Elaine C Davis, Barry C Starcher, Takashi Ouchi, Masashi Yanagisawa, James A Richardson & Eric N Olson. *Fibulin-5 is an elastin-binding protein essential for elastic fibre development in vivo.* Nature, vol. 415, no. 6868, pages 168–171, 2002.

[Young 08] Thomas Young. *The Croonian Lecture. On the Functions of the Heart and Arteries.* In Abstracts of the Papers Printed in the Philosophical Transactions of the Royal Society of London, volume 1, pages 314–316. The Royal Society, 1808.

[Zaoui 02] A. Zaoui. *Continuum micromechanics: Survey.* Journal of Engineering Mechanics, vol. 128, no. 8, pages 808–816, 2002.

[Zeinali-Davarani 15] Shahrokh Zeinali-Davarani, Yunjie Wang, Ming-Jay Chow, Raphaël Turcotte & Yanhang Zhang. *Contribution of collagen fiber undulation to regional biomechanical properties along porcine thoracic aorta.* Journal of Biomechanical Engineering, vol. 137, no. 5, page 051001, 2015.

[Zemánek 09] Miroslav Zemánek, Jiří Burša & Michal Děták. *Biaxial tension tests with soft tissues of arterial wall.* Engineering Mechanics, vol. 16, no. 1, pages 3–11, 2009.

[Zhang 13] L Zhang, SP Lake, VH Barocas, MS Shephard & RC Picu. *Cross-linked fiber network embedded in an elastic matrix.* Soft Matter, vol. 9, no. 28, pages 6398–6405, 2013.

[Zisserman 14] A. Zisserman. Image Analysis course - 2D Fourier transforms and applications. 2014.

[Zoumi 04] Aikaterini Zoumi, Xiao Lu, Ghassan S. Kassab & Bruce J. Tromberg. *Imaging Coronary Artery Microstructure Using Second-Harmonic and Two-Photon Fluorescence Microscopy.* Biophysical Journal, vol. 87, no. 4, pages 2778–2786, 2004.

[Zulliger 04] Martin A. Zulliger, Pierre Fridez, Kozaburo Hayashi & Nikos Stergiopulos. *A strain energy function for arteries accounting for wall composition and structure.* Journal of Biomechanics, vol. 37, no. 7, pages 989–1000, 2004.

Appendix - Experimental methodology

Résumé

Cette annexe est dédié à la présentation indépendante et détaillée des méthodes expérimentales conçues et mises en œuvre au cours du doctorat, concernant la réalisation d'expériences de traction uniaxiale ainsi que de traction-gonflement d'échantillons artériels, couplées à la microscopie multiphoton. Ainsi, elle fournit un complément d'information aux éléments de méthode présentés sous forme synthétique aux chapitres 3 et 4. Dans un premier temps, les outils mécaniques et d'imagerie sont décrits. Les équipements utilisés comprennent une machine de traction haute précision, une pompe à seringue équipée d'un capteur de pression, d'un appareil photo à objectif macro et d'un microscope multiphoton. Les étapes préparatoires aux essais expérimentaux sont ensuite décrites. Celles-ci consistent en (i) l'excision d'artères carotides sur des lapins New Zealand White, (ii) la mise en forme des échantillons et leur montage sur les dispositifs mécaniques, ainsi que (iii) la mesure des dimensions des échantillons, en utilisant des méthodes optiques spécifiques. Ces méthodes optiques consistent en la mesure de l'épaisseur des échantillons, et la mesure des diamètres variables de l'artère, pendant les expériences de gonflement. Deux protocoles de chargement mécanique sont par la suite détaillés : (i) la traction uniaxiale sur des échantillons artériels plans orientés selon diverses directions caractéristiques de l'artère et (ii) la traction-gonflement sur des échantillons cylindriques. Ces protocoles incluent le préconditionnement mécanique des échantillons et les cycles de chargement dédiés aux acquisitions de données et d'images de microscopie. Enfin, les procédures de post-traitement sont détaillées. Celles-ci incluent (i) la préparation des stack 3D d'images de microscopie multiphoton et (ii) la quantification et analyse des orientations des différents réseaux fibreux d'élastine et de collagène. En particulier, la méthodologie de quantification appliquée aux images de la microstructure acquises lors de la traction uniaxiale consiste en une analyse statistique des densités d'angles de fibres, basée sur l'intégration polaire des spectres de Fourier de l'image; tandis que la méthodologie de quantification appliquée aux images de la microstructure acquises lors des tests de traction-gonflement consiste en la comparaison de spectres de Fourier. Les deux méthodes permettent la comparaison des réorientations de fibres mesurées avec les réorientations de fibres prédites par la cinématique affine.

Abstract

This appendix constitutes a detailed, independant, presentation of the experimental methods designed and implemented during this doctoral work, dedicated to uniaxial tension and tension-inflation testing of arterial samples, coupled with multiphoton microscopy. A description of mechanical and imaging facilities is first provided. The equipment used includes a high precision tensile machine, a syringe pump equipped with a pressure transducer, a macroscopic camera and a multiphoton microscope. The preparatory steps to the experimental testings are then described, consisting in sample excision, sample shaping and mounting on the setups, as well as sample dimensions measurement, using optical methods that are also explained. Afterwards, two loading protocols are detailed, applied for (i) uniaxial tension on variously oriented flat arterial samples and (ii) tension-inflation on cylindrical samples. These protocols include the mechanical preconditioning of the samples and the loading cycles dedicated to data and microscopy image acquisitions. As a final methodological step from the experimental perspective, the post processing procedures are detailed, including the preparation of the 3D microscopy image stacks and the quantification algorithms for the analysis of fiber orientations. In particular, the quantification method applied to process microscopy images acquired during uniaxial tension consists in a commonly applied statistical analysis of fiber angle densities, based on the wedge-shape integration of the image's Fourier spectrum; while the quantification methodology applied to process microscopy images acquired during tension-inflation consists in an unprecedented method relying on the comparison of Fourier spectra. This novel method is hereafter presented. Both methods include the comparison of measured fiber reorientations with affine predicted fiber reorientations.

A.1 Introduction

In the course of this thesis, an experimental approach was applied, comprising the development of two mechanical setups enabling uniaxial tension and tension-inflation loadings on arterial samples with live imaging of the microstructure by means of multiphoton microscopy [Krasny 17a, Krasny 17b]. These developed methods are presented in the following Appendix, describing in the purpose of the experimental setups, the mechanical modalities, the imaging modalities, the arterial sample excision and preparation stages, the preliminary measurements, the loading protocols, and the post-processing methodologies and tools. The aim of this additional material is to provide self-sufficient, detailed methological information, which complement the summarized methods described in Chapters 3 and 4 (sections 3.2 and 4.2).

A.2 Mechanical loading modalities

As mentioned in section 2.2, in order to characterize the mechanical behavior of the arterial tissue, a common approach consists in imposing a mechanical deformation while analyzing both the microstructural and the macroscopic mechanical responses. The objective of the applied method was to design two mechanical testing setups which could test either variously oriented flat samples (under uniaxial tension) or cylindrical samples (under tension-inflation). These mechanical testing setups were meant to be coupled to multiphoton microscopy, while maintaining the arterial sample in a humid atmosphere (preventing the arterial sample from drying), which induced two important design constraints: geometrical compatibility and waterproof sealing of the sample testing region.

A.2.1 Tensile machine

A screw-driven high precision tensile machine (Deben® Microtest tensile/compression stage) was used for uniaxial tensile tests, with a 150 N capacity load cell (Figure 4(b) and 5(c)). The load cell signal provided a 0.01 N precision with satisfactory stability. For the tension-inflation tests, axial tension was also applied by this tensile machine. Given that the two heads of the machine moved in opposite directions, the operator could identify and keep track of a region of interest while the microscope was positioned at the center of the sample.

A.2.2 Inflation setup

A syringe pump (Figure 8(c)) (Harvard Apparatus®) was used for inflation purposes. It was equipped with a ± 300 mmHg pressure transducer (FISO® optic fiber) (Figure 9(a) and (c)) connected to the fluid network at the sample inlet (Figure 9(a), (d) and (f)), which infused phosphate-buffered saline (10x PBS, pH 7.1) at a constant ambient temperature of 20°C.

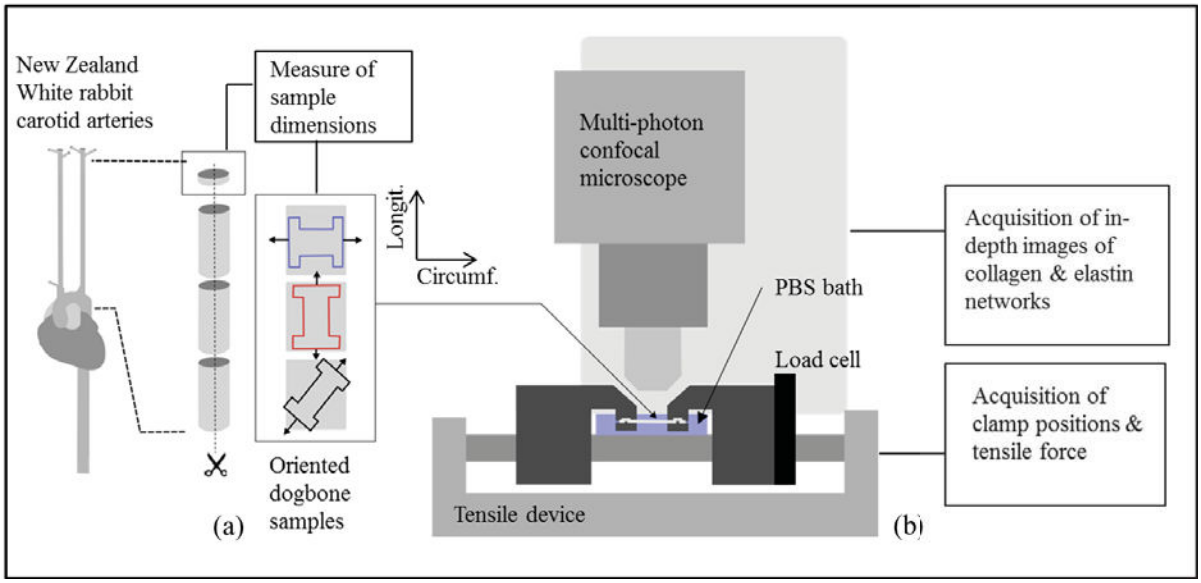

Figure 4 – (a) Schematic representation of the vascular tissue samples, prepared from cut-open cylindrical portions of New Zealand White rabbit carotid arteries; (b) schematic representation of the experimental setup composed of a tensile machine coupled to a multiphoton microscope.

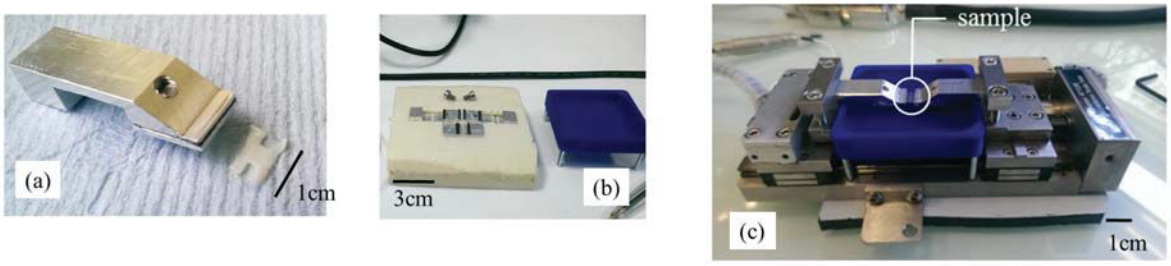

Figure 5 – (a) A clamp and a dogbone shaped arterial sample for uniaxial testing; (b) footprint reproducing the initial distance of the clamps, right: PBS bath; (c) uniaxial tension setup with a mounted sample (the shape of the clamps assures the immersion of the arterial sample in the PBS solution).

A.3 Imaging modalities

Coupled to the mechanical loading, the objective of the imaging modalities of the experimental setup consisted in the acquisition of (i) the macroscopic dimensions of the deforming sample (in particular the tissue's reference thickness and the diameter change under inflation loading) and (ii) the morphology of the microstructure of the deforming sample, for subsequent quantification. Macroscopic imaging was realized by a macroscopic camera, while microscopy was realized by means of a multiphoton microscope.

A.3.1 Macroscopic camera

A standard high definition optical camera (Nikon® D7200 equipped with Nikon® AF-S VR Micro-Nikkor optical 105 mm f/2.8G IF-ED lens) was used for sample geometry measurement.

A tripod and remote control ensured stability during the imaging procedure.

A.3.2 Multiphoton microscope

A multiphoton microscope (Nikon, A1R MP PLUS®) of the IVTV platform (Engineering and Ageing of Living Tissues Platform, ANR-10-EQPX-06-01) was used to image the collagen and elastin networks of the samples (Figure 9(f)). Setting the excitation wavelength to 870 nm [Hill 12] allowed collecting elastin autofluorescence and collagen second harmonic generation (SHG) signals through 500-550 nm and 400-492 nm band-pass filters respectively [Jayyosi 16], without any staining or fixation. The imaging resolution was set to 0.5 µm in all directions [Hill 12, Schrauwen 12], with a 512 μm^2 imaging window. This setting resulted in stacks of images characterized by 60-90 µm thicknesses, depending on the quality of the signal at in-depth focal position. In order to achieve an optimal compromise between image quality and acquisition time, the scan speed was set to 0.5 frames per second, with two-frame averaging. This setting resulted in acquisition times of approximately 20 to 30 minutes for a given configuration of loading. A period of 5 minutes was always observed after applying a load step to the arterial sample in order to stabilize the tissue before imaging it. However, this apparent creeping occurring after each load step did not change the microstructural morphology of the tissue, as observed by live imaging.

A.4 Arterial sample excision

Carotid arteries from New Zealand White rabbits were chosen as model for the experimental procedures. This choice was motivated by their straightness (available length of approximately 4-5 cm), the lack of bifurcations (favoring *in situ* inflation), ease of excision, and their characteristic dimensions. In fact the sample's diameter was sufficiently large to allow the preparation of longitudinally opened flat strips, and the sample's thickness was sufficiently small for the multiphoton microscope to penetrate as deep as 50% of their total thickness during imaging. The arteries (Figure 6) were harvested from healthy male New Zealand White rabbits, weighing 3 kg approximately. All excisions were realized at the Veterinary Campus of the Université de Lyon (VetAgro Sup, Marcy l'Etoile, FR). The rabbit cadavers, previously sacrificed under compliance with the NIH Guide for Care and Use of Laboratory Animals, were kindly provided by Centre Lago (Vonnas, FR).

The excisions consisted in accessing the animal's trachea after incision between the larynx and the lower sternum, in order to reach both carotid arteries (Figure 6(a) and (b)). The length of each carotid was measured *in vivo* and *ex vivo*, i.e. immediately after harvesting, in order to evaluate the *in vivo* pre-stretch condition (computed as the ratio of the *ex vivo* length to the *in vivo* length). The excised samples were immediately stored in phosphate-buffered saline (10x PBS, pH 7.1). This storing procedure is commonly applied in the context of *in situ* experimental procedures [Schrauwen 12, Keyes 11, Genovese 13]. Noticeably, a test was preliminarily performed on a fresh artery (i.e. tested 3 hours after the sacrifice of the animal, and 30 min

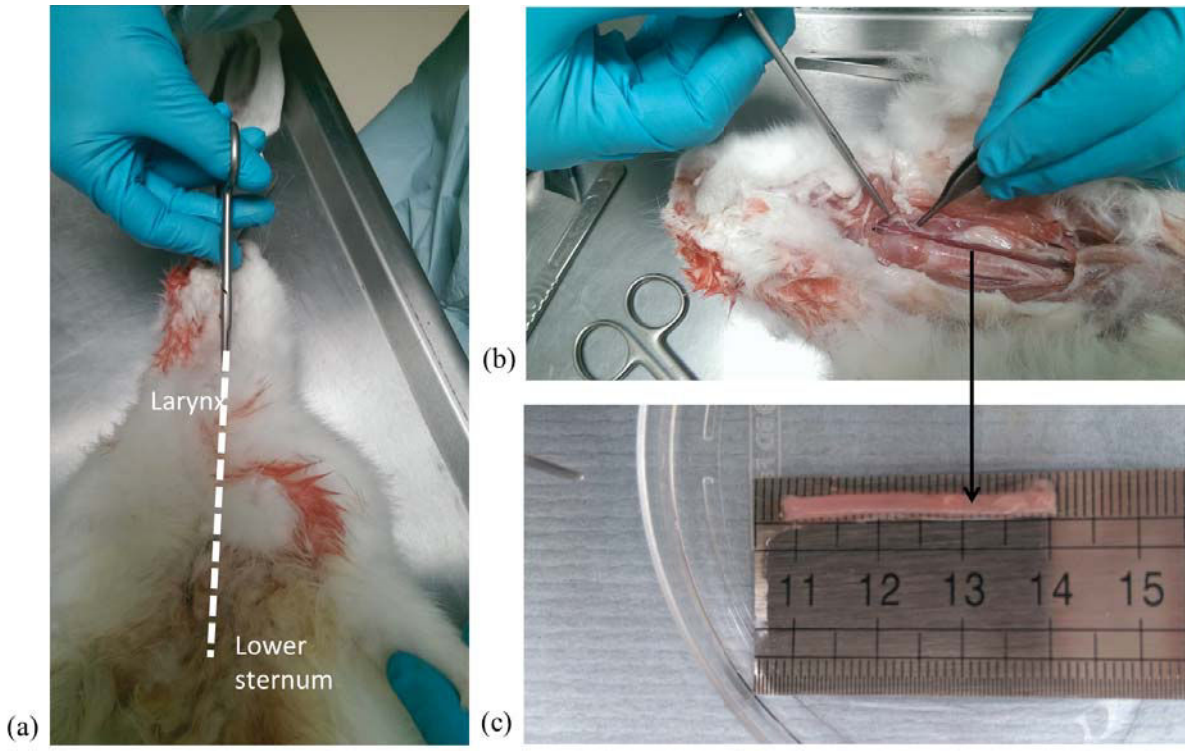

Figure 6 – (a) Incision locus allowing accessing to the rabbit's carotid arteries (from the larynx to the lower sternum); (b) carotid arteries (purple color) on both sides of the trachea; (c) carotid artery measured *ex vivo* immediately after excision.

after excision), and microscopy results revealed that the collagen and elastin morphology did not show significant discrepancies with samples unfrozen and stored overnight in PBS.

A.5 Preliminary preparations to the experimental procedures

A.5.1 Preparation to uniaxial tension

A.5.1.1 Sample preparation and fixation

After excision, the arteries were immediately frozen at -20°C until the day of the experimental tests and unfrozen in a bath of phosphate-buffered saline (10x PBS, pH 7.1) at ambient temperature (20°C). The samples dedicated to uniaxial tension were prepared as follows: 10 mm long cylindrical portions were withdrawn from the excised arteries and longitudinally cut open, with a resulting width of approximately 5 mm. For each artery, a 0.5 mm long ring (Figure 4(a), Figure 10(a1)) was also extracted for optical measurement of the arterial thickness. The rectangular strips were cut into dogbone shapes [Hill 12] (Figure 5(a)) aligned along the three following in-plane directions: circumferential, longitudinal, and an intermediate direction making a 45° angle with respect to the longitudinal direction (Figure 4(a) for a sketch of the sample preparation). This intermediate direction will be referred to as the diagonal direction. Ensuring a zero-strain state in the initial configuration before preconditioning was achieved by maximally constraining and controlling sample and clamp positions, upon fixation. The

procedure is described below:

- Upon sample fixation on the clamps of the tensile machine, the clamps were maintained motionless in a footprint (Figure 5(b)), reproducing their initial distance on the tensile machine before deformation, and which ensured that the inter-clamp distance was always the same for each sample (this distance measured 2 mm).
- The dogbone sample was then gently laid down on the clamps (a previously deposited drop of PBS on the clamp tips limited the risk of pre-stress before fixing that could be due to tissue-clamp friction);
- The sample was carefully tightened between clamps;
- The system clamps+sample was transferred from the footprint to the tensile machine, while its characteristic dimensions ensured both identical inter-clamp distance, and that no pre-strain was induced by sample fixation (Figure 5(c)).

The zero-stress initial configuration was achieved by resetting to 0 the load cell offset before mounting each sample, and by verifying the unchanged force readout after mounting the sample. This verification gave an a posteriori check that the fixation did not induce any pre-stress of the sample larger than the force threshold being detected by the sensor (i.e. 0.02 N, which corresponds to 30 kPa according to our sample's mean cross-sectional area).

A.5.1.2 Sample preconditioning

As explained in section 2.2.2.1, the arterial tissue is characterized by a transient response, inducing a hysteresis in the stress-strain relatinship. This hysteresis can be limited by performing several preconditioning cycles [Hill 12] on the sample. Whether unixaxial tension or tension-inflation is applied, the loading path and maximum load generally coincide with the further applied loading.

A.5.1.3 Geometrical measurements

The above mentioned zero stress and zero strain conditions are related to the initial configuration before preconditioning. However, as explained in section 2.2.2.1, preconditioning induces the accumulation of residual strains and possibly also internal stresses. It was decided not to account for this residual strain when plotting the stress-strain curves of the samples. Therefore, the reference length l_0 for strain calculation was taken as the post-preconditioning length of the unloaded sample, defined as the sum of the residual elongation l_{res} resulting from the 5 preconditioning cycles, and of the initial interclamp distance l^* (Figure 7(a1) and (a2)). This choice resulted in a zero initial strain. Besides, the preconditioning cycles always returned to a zero force, hence a zero total stress.
After preconditioning, four measures of the sample width L_i in the unloaded configuration were recorded using a caliper and averaged [Hill 12] (Figure 7(a2), red color). The measures

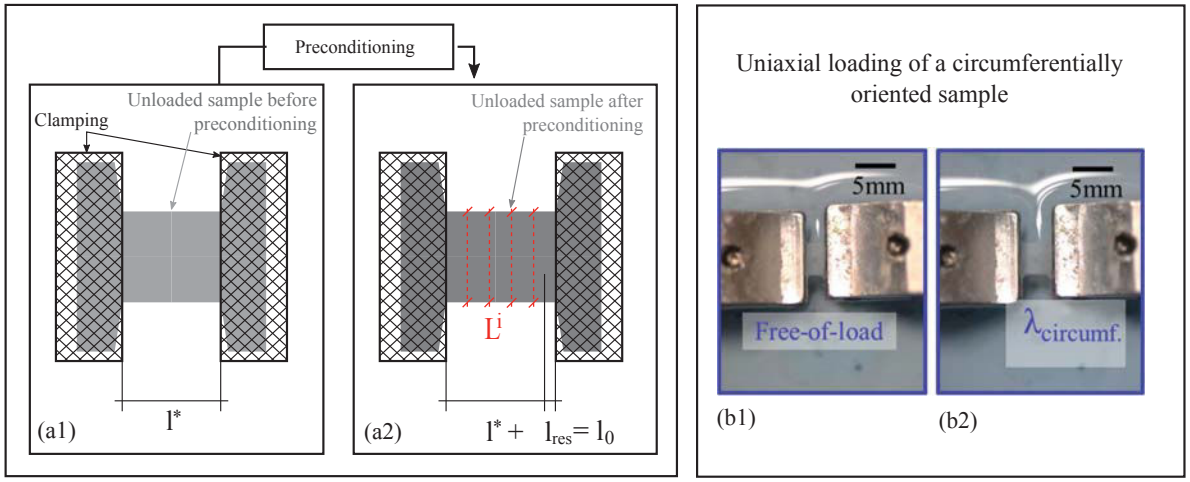

Figure 7 – (a1) Arterial sample (uniaxial tensile testing) before preconditioning, the length of the sample l^* is the initial inter-clamp distance; (a2) arterial sample after preconditioning, the reference length l_0 (used for stretch calculation) is the length of the unloaded sample, defined as the sum of the residual elongation l_{res} resulting from the 5 preconditioning cycles, and of the initial interclamp distance l^*; (b1) macroscopic picture of the arterial circumferentially oriented sample in laod-free state (uniaxial stretch λ=1); (b2) under circumferentially oriented tension.

of the sample width and thickness (Appendix A.3) allowed the computation of the reference cross-sectional area A_0 (under zero load, after preconditioning). The flat dogbone samples showed before testing a mean cross-sectional area of 0.5±0.1 mm^2. The first Piola-Kirchhoff stress (also called engineering stress) follows from [Hill 12]:

$$\sigma_{PK} = F/A_0, \tag{1}$$

where F is the displacement-dependent measure of the tensile force. The stretch was computed from the actual and reference length of the strip (l and l_0, respectively) as:

$$\lambda = l/l_0. \tag{2}$$

A.5.2 Preparation before tension-inflation tests

A.5.2.1 Sample preparation and fixation

Prior to tension-inflation tests and immediately after excision from the animal, the samples were stored in a bath of phosphate-buffered saline (10x PBS, pH 7.1) at 5°C and tested within 36 hours after harvesting. For each sample, a 15 mm long cylindrical segment was extracted as well as 0.5 mm long rings for optical measurement of the sample thickness (Figure 8(a), Figure 10(a1-a4)).

The sample tips were cannulated onto two needles using suture wire (Figure 8(a) and (f)), one needle becoming the infusion inlet, the other one becoming the infusion outlet. Two plastic rings previously fixed on the needles at the suture loci prevented slipping during axial tension and provided a waterproof sealing during inflation (Figure 8(f) and 9(b)). The force offset was

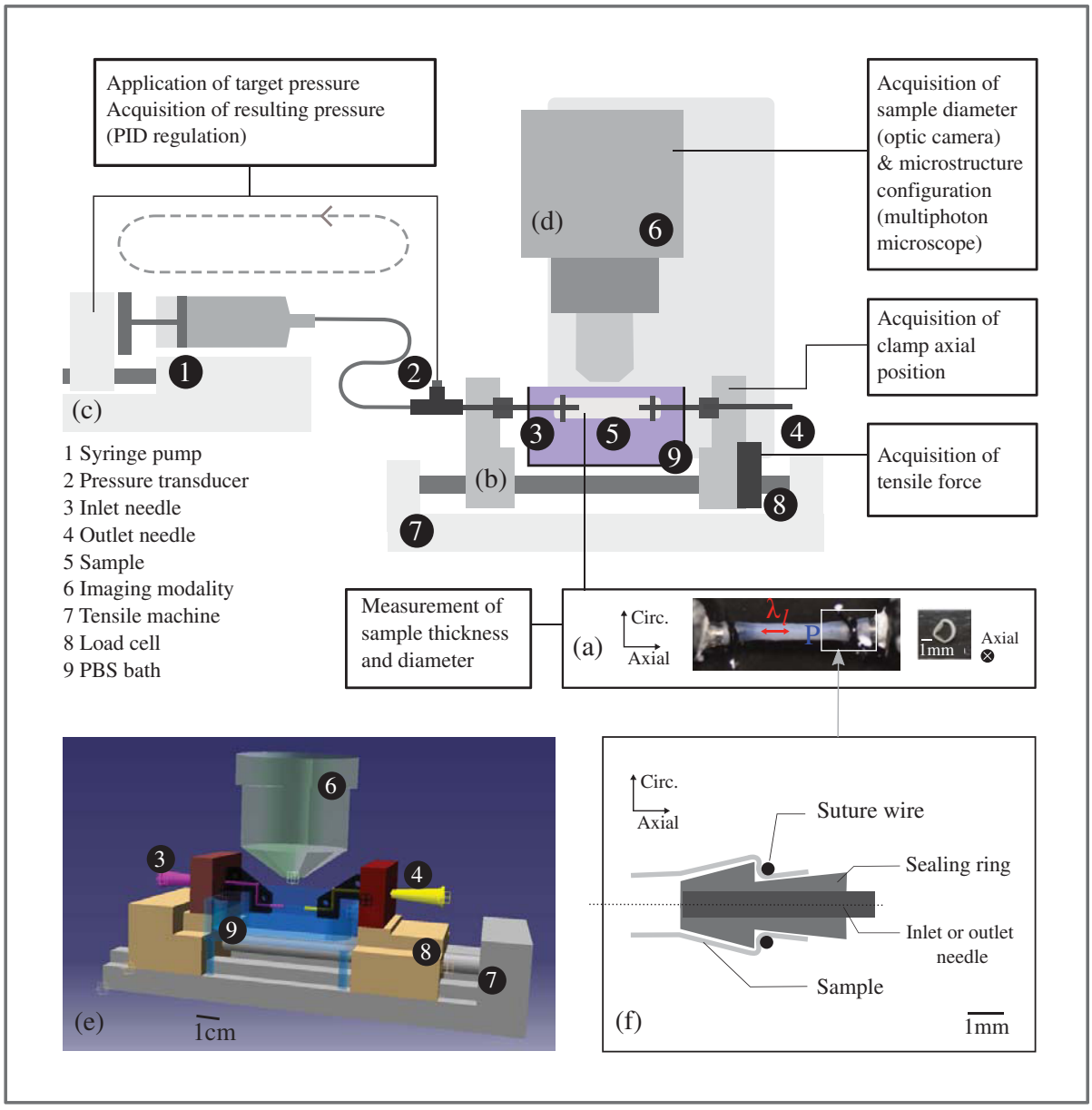

Figure 8 – Experimental tension-inflation setup showing (a) a sample cannulated on the needles and loaded, comprising (b) and (c) the mechanical loading devices (imposed axial load and pressure, respectively) and (d) imaging modalities (alternatively optical camera and multiphoton microscope); (e) schematic representation of the tension-inflation setup, showing the tensile stage, the PBS bath in blue transparency, needle stiffening casings in black transparency, the bended inlet (pink) and outlet (green) needles, and the multiphoton microscope's objective in grey (center); (f) section sketch of the cannulated arterial sample for tension-inflation testing, at the inlet tip of the artery.

zeroed prior to the fixation of the sample. Verifying that the axial force and sample length were unchanged after fixation allowed limiting the risk of potential pre-strain and pre-stress in the sample. The inlet and outlet needles were profiled and stiffened using polymere casings, in order to assure that the tissue remains immersed in the PBS bath during testing (humid atmosphere) (Figure 9(b)).

A.5.2.2 Preliminary settings and measurements

Applying a target pressure was made possible by the pump and pressure transducer communicating under closed loop control (PID mode). The settings of the proportional gain and integrator constant were iteratively adjusted in order to obtain a stable pressure step, characterized by a reasonable pressurizing time and limited overshooting. During the mechanical loading, the sample was continuously immersed in PBS at a constant ambient temperature of 20°C (Figure 8(b) and (e), Figure 9(d) and (f)). Also, the pressure readouts at inlet and outlet were compared to ensure that the pressure was uniformly distributed and did not vary due to friction forces in the needles during infusion.
The measurement of the sample length after preconditioning provided the reference length l_0 on the basis of which the macroscopic axial stretch was computed as:

$$\lambda_a = l/l_0. \tag{3}$$

Similarly to uniaxial tension, l refers to the current inter-clamp length of the sample. Also, the zero circumferential strain position was obtained from the measurement of the sample diameter after preconditioning, when the inflation system was opened, forcing the pressure to return to 0 mmHg in the sample. The measurement provided the reference diameter D_0 on the basis of which the macroscopic circumferential stretch was computed as:

$$\lambda_c = D/D_0. \tag{4}$$

D refers to the current diameter of the sample.

A.5.3 Optical measurement of sample thickness

For both samples dedicated to uniaxial tension or to tension-inflation, an image of the harvested ring of the artery was taken using the macro optical camera (Figure 8(a) and 9(e)). The caliper in 0.5 mm opening position was placed next to the sample ring in order to caliber the pixel size (Figure 10(a1)) and subsequently measure the thickness of the arterial wall by means of pixel intensity thresholding (Figure 10(a3) and (a4)) and multiple thickness evaluation (three measurement loci) in regions which showed the sharpest contrast between tissue and background (Fig 10(a4) - black dashed lines).

A.5.4 Optical measurement of sample diameter (tension-inflation)

The optical camera used for sample thickness measurement was also used to acquire images of the deforming artery under tension-inflation for subsequent analysis of sample diameter (Figure 8(d) and Figure 9(e)). A 1 mm wide rectangle was drawn on the background of the PBS bath in order to calibrate the pixel size before image processing (Figure 9(b1) - white mark in the center of the image). This led to a pixel size of 8±1 µm. Figure 10(b1)-(b4) show the image processing methodology that provides a measure of the artery's evolving diameter, namely:

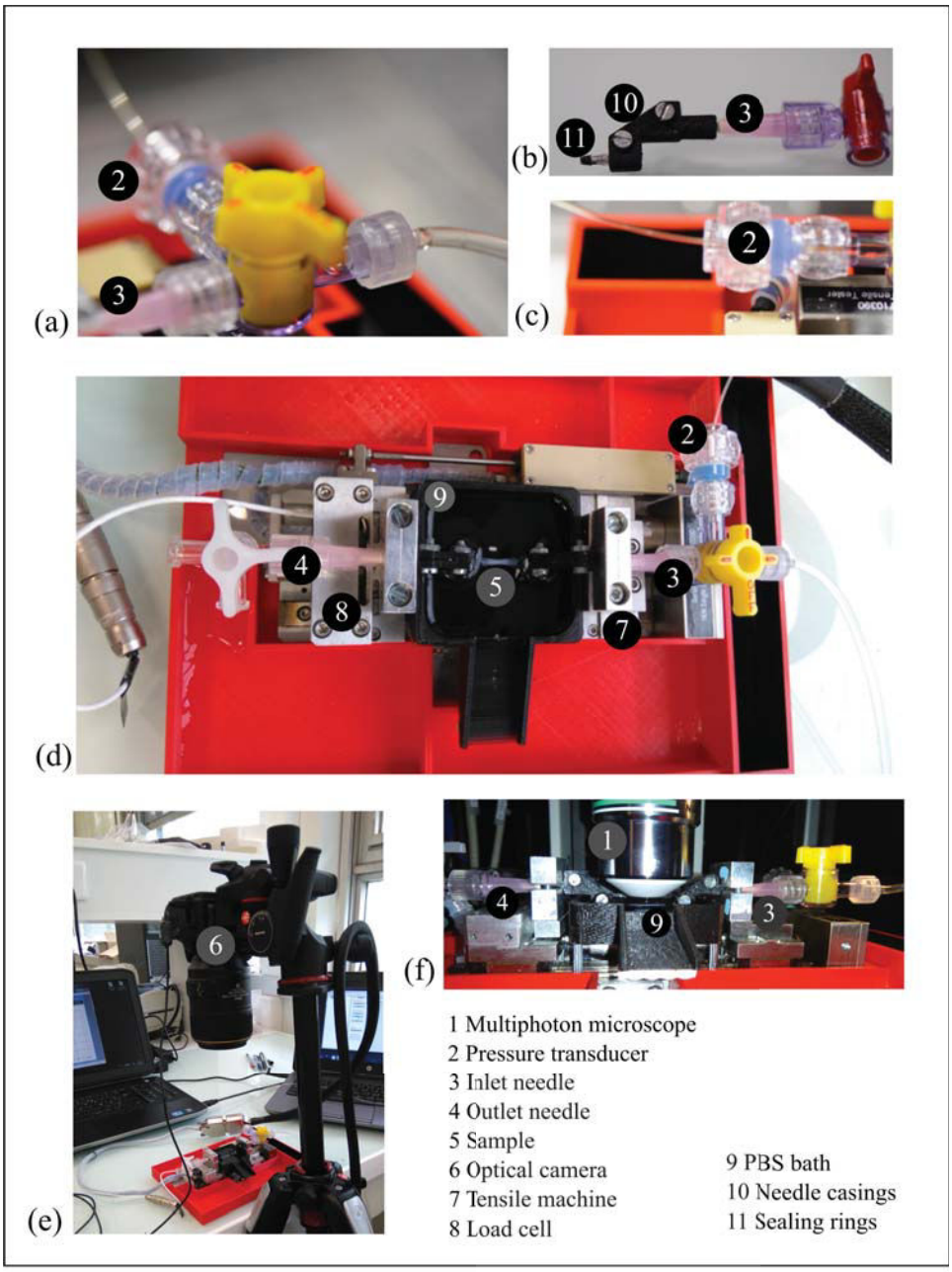

Figure 9 – (a) Inlet 3-way tap, connecting the infusion tube (right) with the pressure transducer (upper left) and the inlet needle (left); (b) customized needle for sample tip cannulation, showing polymere casings (black), extended with a 2-way tap (red); (c) optic fiber pressure transducer connected to the 3-way tap using a specific membrane sealing joint (blue color); (d) tension-inflation setup showing the inlet and pressure transducer system on the right hand side, and the outlet tap on the left hand side. The red frame provides multiple baths which could eventually recover the infused liquid when the network was open; (e) tension-inflation setup under macroscopic imaging modality (optical camera) enabling the analysis of the evolving sample diameter; (f) tension-inflation setup under the multiphoton microscope (the yellow inlet 3-way tap is noticeable on the right hand side).

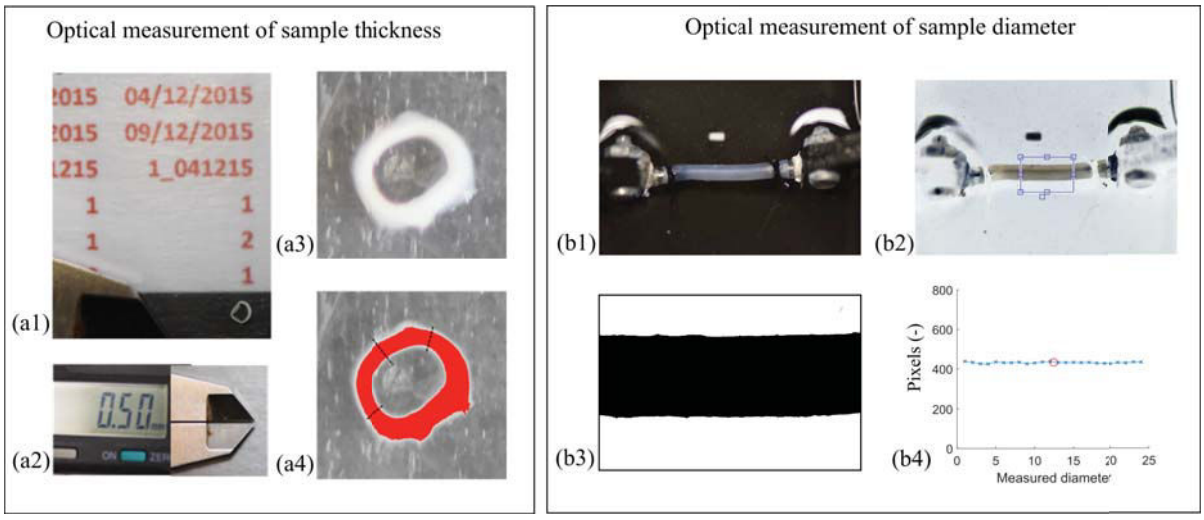

Figure 10 – (a1) Arterial ring cross-section imaged next to the caliper; (a2) caliper opened in 0.5 mm position for pixel calibration; (a3) zoom on the arterial ring before pixel intensity thresholding and (a4) after pixel intensity thresholding showing three thickness measurement loci (chosen where the borders were sharp); (b1) macroscopic picture of the deforming arterial sample showing in the center a 1 mm wide white rectangle, drawn on the background of the PBS bath and used to calibrate the pixel size; (b2) selection of a cropping region; (b3) pixel intensity thresholding of the selected region; (b4) evaluation of the artery's diameters, in pixels, across the length of the selected region and averaging of the overall diameter measurements.

- A cropping was performed in order to isolate a central region of the sample. This region was chosen sufficiently large in order to increase the number of diameter measurement points (subsequently averaged), but also sufficiently small in order to avoid optical artifacts during thresholding that would distort the diameter measurement (for example, diameter change at the vicinity of ligature points, optical light reflects, etc. (Figure 10(b2) - blue rectangle);

- A greyvalue threshold was defined that allows to separate the arterial wall from the background (Figure 10(b3));

- The number of pixels was evaluated across the width at different positions along the length of the cropped region (blue crosses), and averaged (red circle in the center of the image), providing an estimation of the artery's diameter in pixels (Figure 10(b4)).

Eventually, the post-processing of macroscopic images revealed a noticeable regularity of sample diameter, in both the reference loading configurations and the loaded configurations. Figure 11 shows the detailed measurements of Sample 2 thickness (chosen as representative), under two loading scenarii (see Appendix A.6.2), so as to visualize how variable diameter readings are along the length of the sample. We represent the mean arterial external diameter (averaged over 30 readings along the sample length) as the amplitude of the bar plots, with associated standard deviations. The standard deviations of the diameter measurement being about 2% (see table in Figure 11) illustrate the regularity of the diameter readings. It is in fact a very

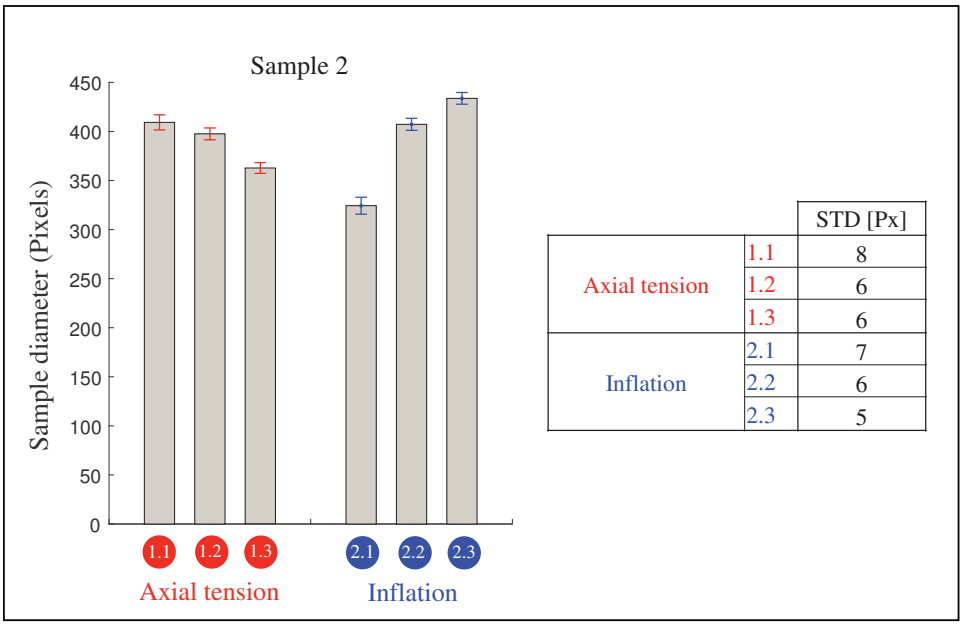

		STD [Px]
Axial tension	1.1	8
	1.2	6
	1.3	6
Inflation	2.1	7
	2.2	6
	2.3	5

Figure 11 – Statistical representations of the evolving diameter (example of Sample 2) under axial tension or inflation (see Appendix A.7.2), providing mean diameter values and associated standard deviations (left), with standard deviations of diameter readings along the length of the sample (right).

beneficial characteristic of the carotid artery, in the context of mechanical characterization: this artery presented a remarkable effective length, showing no bifurcations, no bending, but a constant diameter.

A.6 Loading scenarii

A.6.1 Uniaxial tension

The loading scenario chosen for uniaxial tension loadings consisted in submitting the circumferentially, diagonally, and longitudinally oriented, flat arterial samples to 3 gradually increasing tensile loading configurations after preconditioning. This loading scenario coupled to live imaging of the tissue's microstructure, allowed to test whether the well-known morphological changes of the vascular tissue under load (decrimping, realignment) are different depending on the direction of the load.

As a preliminary step, each sample underwent quasi static triangular preconditioning. According to the choice made by [Hill 12], a displacement-speed control was applied at a rate of 0.5 mm·min^{-1}, corresponding to a relative elongation speed of 0.2 min^{-1}, with fixed target tensile force equal to 1N. This elongation speed resulted in a total preconditioning time of approximately 30 min per sample. During the mechanical test, the sample was continuously immersed in PBS at a constant temperature of 20°C.

Each arterial tissue sample underwent two imaging sequences: one sequence with the adventi-

tial side facing the objective of the microscope after five preconditioning cycles [Hill 12]; and the other sequence with the intimal side facing the objective after two additional stabilizing preconditioning cycles. When the intima faced the objective or when the adventitial faced the objective, microscopy images were taken in the unloaded configuration and in three gradually loaded configurations, respectively at 0.2 N, 0.5 N, and 0.8 N.

A.6.2 Tension-inflation

The loading scenario chosen for tension-inflation loadings consisted in submitting the cylindrical samples either to (i) axial tension under constant internal pressure or to (ii) inflation under constant stretch. These loading scenarii coupled to live imaging of the tissue's microstructure allowed to test whether fiber kinematics are dependent on different biaxial loadings.

In agreement with well-established tension-inflation protocols for arteries [Keyes 11,Humphrey 10], the two loading scenarii were run as follows. Four carotids were used in the present study: carotid samples S1 and S2 were tested under both loading scenarii, while carotid samples S3 and S4 were tested under only one loading scenario, i.e. the axial tension and the inflation scenario, respectively. The loading scenarii, composed of three main loading steps, were run as follows:

- The sample underwent five preconditioning cycles (step 1), carried out in order to cancel the tissue's deformation history;
- The *in vivo* stretch, defined as the stretch resulting in unchanged axial reaction force during inflation [Humphrey 10] (section 2.2.2.2), was determined by adjusting the clamp position during the preconditioning cycles;
- The samples' reference cross-sectional areas A_0 were computed (Appendix A.5.3);
- In the case of the axial tension load scenario, the zero axial strain position was determined and the measurement of the sample length after preconditioning provided the reference length l_0 on the basis of which the macroscopic axial stretch was computed (Appendix A.5.2).
- Similarly, the reference diameter D_0 was determined, allowing the computation of the macroscopic circumferential stretch (Appendix A.5.4).
- After preconditioning, the gauge length of the samples (between suture) measured l_0 =12±2 mm, while the unloaded sample diameter measured D_0 =2.0±0.3 mm;
- Macroscopic images (step 2) of the samples were obtained every 20 mmHg during inflation and every 0.5 mm during axial tension, corresponding to 0.2±0.05 stretching steps approximately (see thick lines with ticks on Figure 12, showing macroscopic imaging);

– Microscopy images (Step 3) were obtained at 1.3±0.05, 1.6±0.05, and 1.8±0.05 stretches during axial tension (referenced as loading configurations 1.1, 1.2, and 1.3, respectively (Figure 12)), and at 20 mmHg, 100 mmHg, and 140 mmHg pressures during inflation (referenced as loading configurations 2.1, 2.2, and 2.3, respectively (Figure 12)).

As a result, on the one hand, three samples (S1, S2, and S3) underwent a total of seven axial tension cycles (with the two last cycles dedicated to data acquisition) between 0.1±0.02 and 0.8±0.02 N axial force, at an imposed velocity of 2 mm.min^{-1}, corresponding to an axial strain rate of 0.2 min^{-1}, with maintained pressure P = 100 mmHg. On the other hand, three samples (S1, S2, and S4) underwent a total of seven inflation cycles (with the two last cycles dedicated to data acquisition) between 20 and 140 mmHg, by steps of 20 mmHg imposed within 30 seconds, under a maintained *in vivo* axial stretch $\lambda_a = 1.6 \pm 0.05$.

The mechanical configurations 1.1 and 2.1 are referred to in the following as "reference configurations", while the mechanical configurations 1.3 and 2.3 are referred to as "loaded configurations". The intermediate loading configurations 1.2 and 2.2 were not used in the Fourier methodology enabling the characterization of fiber kinematics affinity but provided a refined insight at the evolution of the microstructure during the loading, and a verification of the right tracking of the same imaging windows.

The reference configurations included partial loading ($\lambda_a = 1.3$, P = 100 mmHg for scenario 1, $\lambda_a = 1.6$, P = 20 mmHg for scenario 2) for several reasons. First, we chose to post-process adventitial collagen images characterized by a sufficient degree of decrimping, hence avoiding imprecisions in the Fourier analysis of the global orientations of the fibers (at the bundle scale); second this choice prevented the potential buckling of the samples at high pressure and low axial stretch [Han 13], which could have impaired the analysis of macroscopic and microscopic kinematics.

A.7 Microscopy images pre-processing

The multiphoton imaging modality provided 3D image stacks, i.e. a sequence of bidimensional images of the microstructure in an interval of focal planes. Each of the image stacks could be reconstructed into a 3D visualization of the microstructure, allowing the access to three dimensional geometrical parameters, but rendering the analysis more complex and computationally very expensive. Moreover, previous studies have investigated the transmural angle (radial direction) of the fibers in the artery and showed that it is negligible in comparison to the in-plane angle [Roy 11, Rezakhaniha 12, Schrauwen 12]. They have also showed that the most relevant morphological changes in the microstructure occur in the circumferential and longitudinal directions. Subsequently, we focused in the following on the analysis of the in-plane angles of the fibrous networks. Hence, the image stacks were pre-processed so that they could represent the true tissue morphology on two-dimensional images while enabling reliable angle density

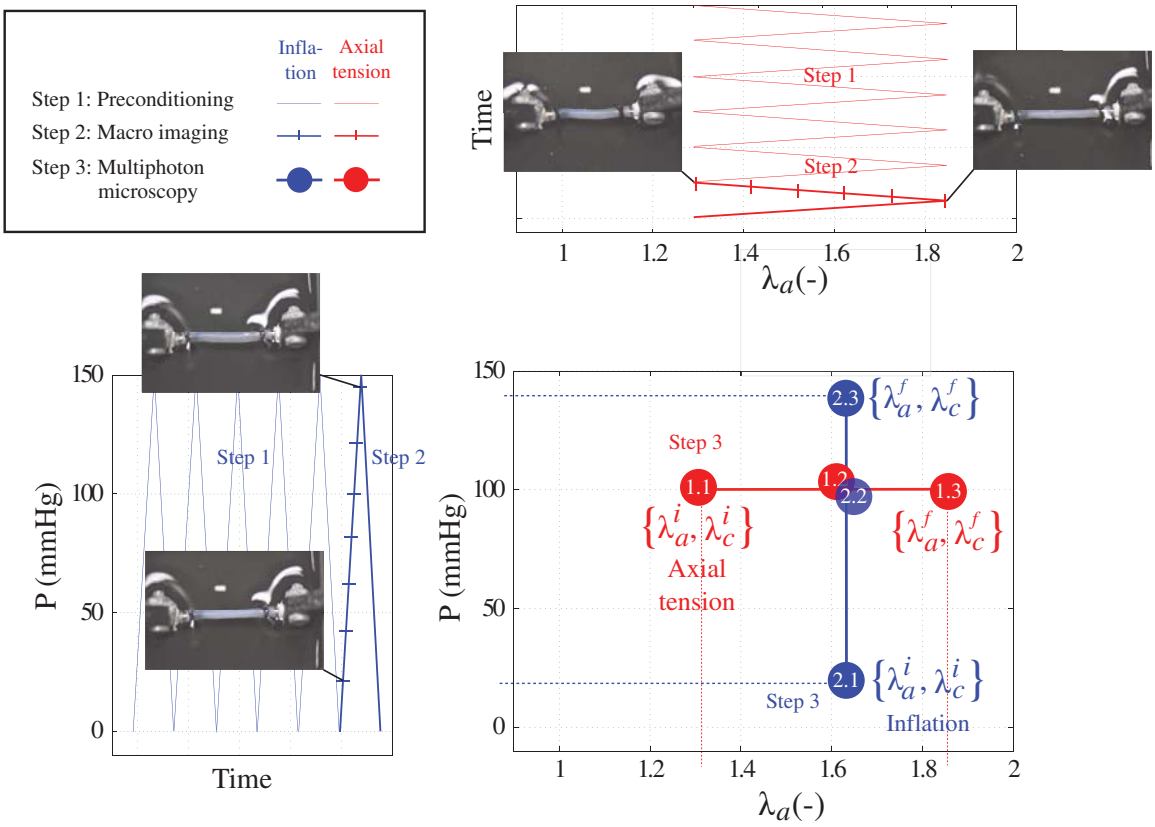

Figure 12 – Tension-inflation loading protocol, comprised of three loading steps for both axial tension and inflation scenario, namely (Step 1) preconditioning (thin line), (Step 2) macroscopic imaging sequence (thick line with ticks denoting macro images), and (Step 3) multiphoton microscopy sequence (thick line with circles denoting loading configurations in which the collagen morphology was acquired). The morphologies referring to load states 1.1, 1.3, 2.1, and 2.3 are used as inputs for subsequent image processing and fiber kinematics characterization (see Figure 10). The tensile loading scenario is represented in red, whereas the inflation loading scenario is represented in blue.

extraction.

For each uniaxial tension image stack, the part representing the adventitial layer of the vascular wall was subdivided into three equally thick sublayers (20-30 µm) and each sublayer was projected orthogonally onto a single image using a Maximum Intensity Projection (MIP) algorithm (Figure 14(a)). The choice of three sublayers allowed achieving an optimum between image pixel density and fiber transmural continuity (due to low but non-zero transmural angles which could cause bias in the angle density analysis). Pre-processing of the media stack consisted in a projection in the thickness of one representative lamella (5-10 µm), after verification of the equivalent morphologies of the different lamellae. The resulting set of 2D images used for the analysis of the fiber angle density consisted in three images of the adventitial collagen, three images of the adventitial elastin, one image of the medial collagen and one image of the medial elastin (Figure 14 - 1).

Concerning tension inflation microscopy, image stacks corresponding to the reference configurations 1.1 and 2.1, as well as image stacks corresponding to the loaded configurations 1.3 and 2.3 (Figure 12), were also processed using a Maximum Intensity Projection (MIP) algorithm (Figure 15 (a1) and (a2)), applied this time on the entire thickness of the adventitia and revealing optimal in-plane morphology. As a result, although the negligible transmurality information was lost, the fibers were represented with maximal effective length, strongly improving the interpretation of their in-plane orientation. Besides, a specific attention was preliminarily paid to the geometrical acceptability of applying a projection of slices of a cylinder into a 2D image: a geometrical evaluation of a "worst case error" was made in order to quantify the potential error or fiber orientation, as follows:

- Taking the imaging window of the multiphoton microscope (MPM) X_{MPM} and its imaging penetration depth Z_{MPM} as inputs, we extracted the maximal inclination angle ϕ of a fiber (we evaluate the angle of the tangent to the tissue surface at the periphery of the imaging window, Figure 13(a)) as:

$$\tan\frac{\phi}{2} = \frac{Z_{MPM}}{X_{MPM}} \tag{5}$$

- The orthogonal sketch of the imaged volume, in the $\{e_x, e_y\}$ frame, provides the expressions for the projected fiber angle, before (θ_i) and after (θ_f) the inclination of the fiber plane (Figure 13(b)):

$$\tan\theta_i = \frac{X}{Y} \tag{6}$$

$$\tan\theta_f = \frac{x}{Y} \tag{7}$$

  with

$$x = X\cos\phi \tag{8}$$

- We deduce then an estimation of the relative error on the orientation angle of a fiber, characterized by an inclination angle ϕ to the e_x axis, when this fiber in projected in the $\{e_x,e_y\}$ frame. This relative error reads as:

$$\epsilon(\%) = \frac{|\tan\theta_i - \tan\theta_f|}{|\tan\theta_i|} \tag{9}$$

The obtained inclination angle $\phi = 19°$ provided a maximal error of $\epsilon < 5\%$ on the orientation of peripheral fibers. For the sake of comparison, for the fibers which were located within 3/4 of the image window, this error drops to $\epsilon < 2\%$.

A.8 Quantitative characterization of the microstructure

After preprocessing the microscopy outputs, two distinct quantification routines were developed and applied in order to extract morphology parameters, enabling to:

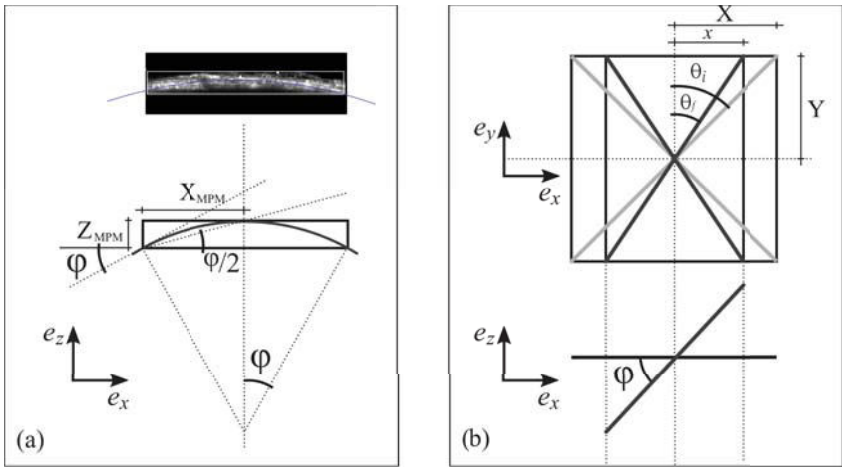

Figure 13 – (a) Sketch of the cylindrical sample, represented in the circumferential-radial plane, (b) sketches of an inclined fiber projected in the circumferential-longitudinal plane.

1. Evaluate fiber rotation magnitude when the tissue was loaded;

2. Compare this rotation with the one predicted by the affine rule;

in order to eventually quantify the affine prediction error with respect to actual (experimental) fiber kinematics.

A.8.1 Statistical angle density approach (uniaxial tension images)

A.8.1.1 Extraction of angle densities

After preprocessing the image stacks obtained under uniaxial loadings, the first step of the quantification routine consisted in the extraction of fiber angle densities. The latter were analyzed by combining wedge-shape integration of the Fourier power spectrum [Ayres 08, Schriefl 12, Schriefl 13] (section 2.4.1) and a custom method for the extraction of local density maxima with their associated dispersions. More precisely, this method consisted in applying an axisymmetry correction to the image before evaluating the power spectrum of the image (Figure 14-2), provided by the modulus of the 2D Fourier Transform of the image. A wedge-shape integration, with 1° angular stepping provided a raw segregation of orientations in the images, classified by the angle values. A standard smoothing algorithm was then applied in order to obtain a curve of relative orientation density in the analyzed image.

A.8.1.2 Extraction of local maxima and dispersions

Local density maxima were determined by a standard peak detection algorithm (Figure 14-3). The related dispersions were evaluated by first determining an arbitrary density threshold that represented a cumulative percentile of total fiber angles extracted from the image, and secondly by reading out angle values corresponding to this threshold.

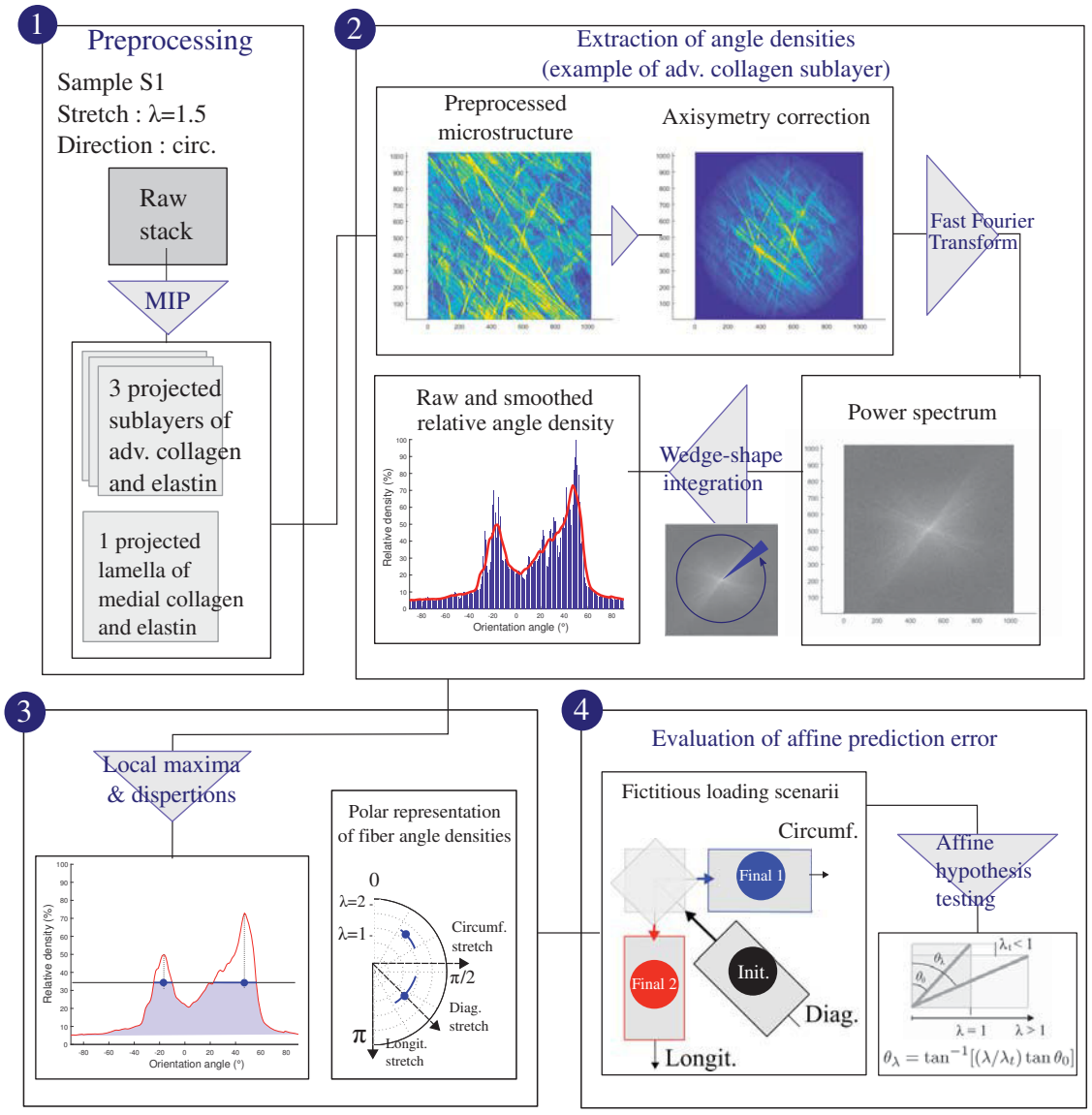

Figure 14 – Summary of the image analysis method applied to uniaxial tension microscopy images. (a) Partial Maximum Intensity Projections (MIP) of adventitial and medial microstructure image stacks; (b) Fast Fourier 2D transform of microstructure images providing the image's power spectrum; (c) wedge-shape integration of the power spectrum providing a raw and smoothed angle density; (d) local maxima detection and associated relative dispersions evaluation on smoothed fiber angles density function; (e) affine hypothesis testing for fiber kinematics, including the analytical computation of affine fiber reorientation and the prediction of fiber angles during a fictitious loading scenario.

Explicitly, let θ represent a local orientation angle, and $d(\theta)$ the angle density of the analyzed image; the angle density threshold p is the angle density below which the fraction $\alpha_p = 0.8$ of the total fibers is counted, i.e. the solution of the following equation:

$$\alpha_p = \frac{\int_0^\pi \min(d(\theta), p)d\theta}{\int_0^\pi d(\theta)d\theta} = 0.8. \tag{10}$$

We evaluated corresponding angles about each detected local maximum in order to extract

related relative dispersions (Figure 14-3). The resulting mean±dispersion "bar" representation was then converted into a polar plot format, with the radius parameter representing the mechanical stretch to which the analyzed microstructure is submitted. This representation of fiber orientation densities allows their comparison, in both load-free and loaded (multi directionally) configurations, providing a visual insight at fiber rotation amplitudes.

A.8.1.3 Affine hypothesis testing under a fictitious loading scenario

The assumption of affine reorientation considers that the fibers are continuously embedded in their surrounding matrix and are therefore constrained to the same deformation gradient as the matrix [Billiar 97, Chandran 06, Jayyosi 16]. For an uniaxial tensile loading, characterized by load-free conditions on the lateral boundaries of the sample, the assumptions are:

- the considered fiber shows an initial angle θ_0;
- a tensile stretch λ is externally applied;
- the resulting Poisson effect induces a compressive stretch λ_t that should be measured during the loading.

Hence the fiber orientations θ could be computed as (Figure 14-4):

$$\theta = \arctan\left(\frac{\lambda}{\lambda_t}\tan\theta_0\right). \tag{11}$$

The obtained angle values were compared to the experimentally measured angles in order to analyze to which extent this affine reorientation can predict true fiber network reorientations. The adventitial collagen bundles showed, in the load-free state, a dense crimped configuration for which it was difficult to extract global orientations using traditional image processing techniques. In order to avoid a subsequent imprecision of the analysis, a specific method was designed to isolate the global fiber rotation mechanism from the uncrimping mechanism, and to test the hypothesis of affine kinematics only on the global reorientation of the fibers. To this aim, we considered a deformation scenario which starts in the diagonally deformed state and reaches the circumferentially and longitudinally deformed states in two sequential steps: diagonal unloading followed by circumferential or longitudinal loading (Figure 14-4). Accordingly, only deformed configurations with straight collagen bundles needed to be processed for fiber angle analysis. Prediction errors were computed by dividing the difference between experimental and predicted fiber angles by the experimental fiber angle. To conclude the description of this quantification routine, the method allowed (i) to get rid of the crimped configuration with its imprecise extracted angles, as well as (ii) to only account for the global reorientation of the fiber bundles, since we consider only deformed configurations with straight collagen bundles.

A.8.2 Spectra comparison method (tension-inflation images)

After the preprocessing stages of the microstructure stacks obtained during tension-inflation tests (Figure 15(a1) and (a2)), a custom method was developed for the analysis of fiber rotations

and for testing the affine hypothesis applied to adventitial collagen fiber kinematics. The core of this novel quantification methodology consisted in simulating an affine transformation by numerically applying axial and circumferential deformations to the reference configurations. In more details:

- Loading scenario 1 (axial tension under constant pressure): a numerical axial stretch λ_a^* together with the corresponding measured transverse contraction (resulting from Poisson effect and applied proportionally) were gradually applied to the image of the unloaded configuration 1.1;
- Loading scenario 2 (inflation under constant axial stretch): a numerical circumferential stretch λ_c^* (corresponding to outer diameter change) was gradually applied to the image of the reference configuration 2.1.

The image resolution remained unchanged by the use of subpixel interpolation. Afterwards, the 2D Fourier spectrum moduli were extracted from the collagen morphologies for both the numerically deformed (Figure 15(c1)) and the experimentally loaded configurations (Figure 15(c2)). Use of the 2D Fourier transforms allowed removing the non-mechanical optical effects (such as contrast or brightness effects) as well as the artifacts (features occurring at short lengthscale, such as the decrimpring process), and the mismatch of imaged windows. Previous studies have proven the potential of the Fast Fourier transform (FFT 2D) for the analysis of biomedical images, and in particular the ability of the method to extract fiber angle densities or isotropy parameters (see Chapter 1). Here a special attention was paid to working with spectra being matrices of identical dimensions (Figure 15, red cropping square). A preliminary analysis allowed verifying that the locus of the cropping center in the image did not affect the results. Each spectrum was then multiplied by the Fourier transform of a Gaussian window whose size corresponded to the characteristic width of a collagen bundle (1/25 of the imaged window, equivalent to 20 µm), filtering undesirable small-length features in the images and highlighting meaningful morphological features (namely fiber orientations at the scale of the bundles) [Zisserman 14]. The obtained 2D Fourier spectrum moduli S^* and S (numerically and experimentally deformed microstructures, respectively) were finally compared using a relative norm-2 (Figure 15(e)).

We gradually increased the numerically applied affine deformation, eventually reaching a minimum in the relative difference between the two collagen morphologies (i.e. configurations 1.3 or 2.3 and the corresponding affine deformations of configurations 1.1 and 2.1, Figure 12). As a result, this minimum corresponded to the application of a fictitious stretch that should be applied to the reference microstructure in order to reach by affine deformation the most similar microstructure to the loaded experimental configuration. Eventually, this fictitious stretch was compared to the actual experimentally measured stretch. If the fictitious stretch and the actual stretch are equal, the kinematics at the scale of collagen fibers actually remained affine.

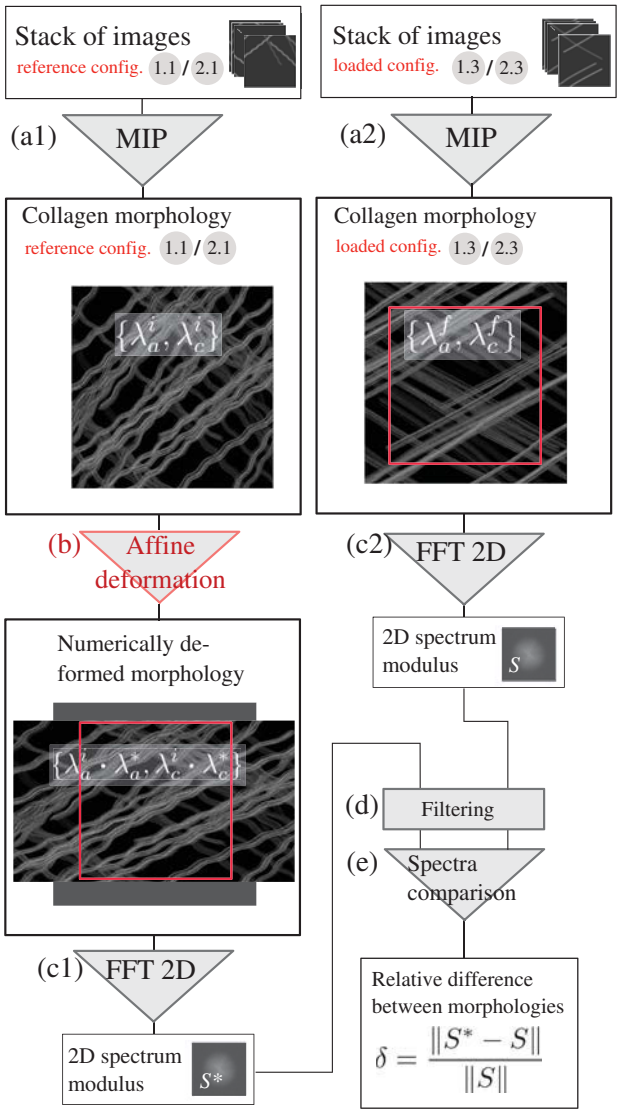

Figure 15 – Series of operations summarizing the image analysis and characterization methodology of fiber kinematics. The methodology consists in (i) analyzing the stacks of images in the reference (a1) and loaded (a2) configurations by means of a Maximum Intensity Projection (MIP); (ii) numerically applying a gradual affine deformation to the reference configurations (b); and (iii) comparing the microstructure configurations through their FFT spectra (c), so as to extract the affine deformation (applied numerically), which produces a microstructure with minimum relative difference between the experimental morphology and the numerically deformed one (d). For each loading scenario, the axial stretch ranges between λ_a^i (reference configuration) and λ_a^f (loaded configuration)(λ_a^i=λ_a^f in the case of the inflation loading), whereas the circumferential stretch ranges between λ_c^i (reference configuration) and λ_c^f (loaded configuration). In this figure, the used images are custom-drawn visual representations of collagen morphology, chosen for clarity and representativeness.

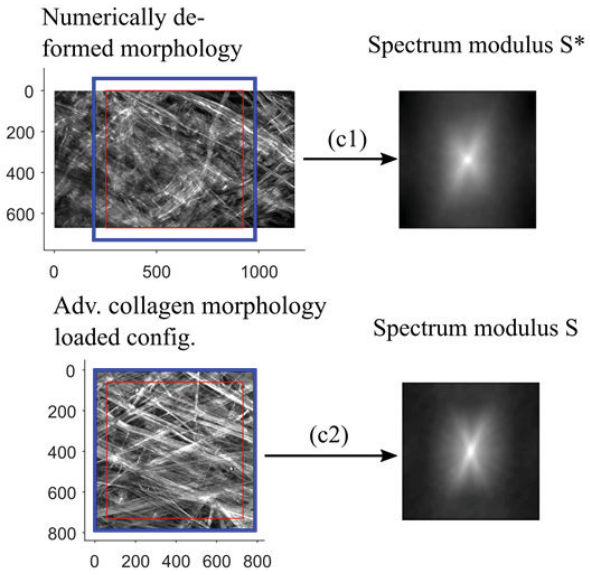

Figure 16 – Fourier spectrum $S*$ of a numerically deformed collagenous microstructure (affine deformation) (upper right) compared to the Fourier spectrum S of a deformed (experimental tension-inflation) configuration of collagenous microstructure.

École Nationale Supérieure des Mines
de Saint-Étienne

NNT : 2017LYSEM035

Witold KRASNY

MULTISCALE CHARACTERIZATION AND MODELING OF THE MECHANICAL BEHAVIOR OF THE ARTERY

Speciality: Mechanics and Engineering

Keywords: Microstructure, collagen, elastin, fiber kinematics

Abstract:

Improving the diagnosis and treatment of cardiovascular diseases relies on a better understanding of arterial biomechanics. In particular, the mechanical response of these tissues is highly dependent on the configuration of their microstructure. The objective of this doctoral work is on the one hand to characterize experimentally the arrangement of the different constituents within the microstructure of the artery during loading; and secondly to develop a micromechanical model capable of predicting (i) the change in morphology of fibrous networks; and (ii) the consequences of these morphological changes on the macroscopic mechanical response. To this aim, arterial samples were subjected to uniaxial and biaxial loadings while observing their microstructure by means of multiphoton microscopy. In particular, the evolution of the orientation of the various constituents during loading has been characterized. The results show that these rearrangements depend on the constituent, on the arterial layer which hosts the considered constituent, and on the loading scenario. Thus, the collagen network located in the outer layer of the artery can undergo significant morphological changes which do not obey the affine kinematics rule, while the overall organization of the elastin network remains unchanged and evolves following affine kinematics. The micromechanical model has allowed explaining the stiffening of the arterial tissue during its deformation by the progressive realignment of its constituent fibers, and suggests that the mechanical interactions between fibers and matrix as well as between fibers play a role in deformation mechanisms at the microscopic scale.

École Nationale Supérieure des Mines
de Saint-Étienne

NNT : 2017LYSEM035

Witold KRASNY

CARACTERISATION ET MODELISATION MULTI-ECHELLE DU COMPORTEMENT MECANIQUE DE L'ARTERE

Spécialité: Mécanique et Ingénierie

Mots clefs : Microstructure, collagène, élastine, cinématique de fibres

Résumé :

Améliorer le diagnostic et le traitement de pathologies cardio-vasculaires repose sur une meilleure compréhension de la biomécanique artérielle. En particulier, la réponse mécanique de ces tissus est fortement dépendante de la configuration de leur microstructure. L'objectif de ce travail doctoral est d'une part de caractériser expérimentalement l'arrangement des différents constituants au sein de la microstructure de l'artère lors du chargement ; et d'autre part de développer un modèle micromécanique permettant de prédire (i) le changement de morphologie des réseaux fibreux; et (ii) les conséquences de ces changements de morphologie sur la réponse mécanique macroscopique. Pour cela, des échantillons artériels ont été soumis à des chargements uniaxiaux et biaxiaux tout en observant leur microstructure par microscopie multi-photon. En particulier, l'évolution de l'orientation des différents constituants au cours du chargement a été caractérisée. Les résultats obtenus montrent que ces réarrangements sont variables selon le constituant, selon la couche de l'artère, et selon le scenario de chargement. Ainsi, le réseau de collagène situé dans la couche externe de l'artère peut subir des changements de morphologie importants n'obéissant pas à la règle de cinématique affine, tandis que l'organisation globale du réseau d'élastine ne change pas et évolue selon une cinématique affine. Le modèle micromécanique a quant à lui permis d'expliquer la rigidification du tissu artériel lors de sa déformation par le réalignement progressif de ses fibres constitutives, et suggère que les interactions mécaniques entre fibres et matrice ainsi qu'entre fibres jouent un rôle important dans les mécanismes de déformation à l'échelle microscopique.